

KAUNAS UNIVERSITY OF TECHNOLOGY

DALIUS GUDEIKA

**SYNTHESIS AND PROPERTIES OF ORGANIC
SEMICONDUCTORS CONTAINING 1,8-
NAPHTHALIMIDE, TRIPHENYLAMINE AND
FLUORENE MOIETIES**

Doctoral Dissertation
Technological sciences, Materials engineering (08T)

2014, Kaunas

The present work was carried out at Kaunas University of Technology, Faculty of Chemical Technology, Department of Organic Technology, now (Department of Polymer Chemistry and Technology) in the period of 2010–2014. The work was supported by The Research Council of Lithuania and State Studies Foundation.

Scientific supervisor:

Prof. habil. dr. Juozas Vidas GRAŽULEVIČIUS (Kaunas University of Technology, Technological Sciences, Materials Engineering – 08T).

Scientific adviser:

Dr. Ramūnas LYGAITIS (Kaunas University of Technology, Physical Sciences, Chemistry – 03P).

Reviewers:

Prof. habil. dr. Sigitas TAMULEVIČIUS (Kaunas University of Technology, Technological Sciences, Materials Engineering – 08T),

Prof. dr. Šarūnas MEŠKINIS (Kaunas University of Technology, Technological Sciences, Materials Engineering – 08T),

Doc. dr. Jolita OSTRauskaitė (Kaunas University of Technology, Technological Sciences, Materials Engineering – 08T).

KAUNO TECHNOLOGIJOS UNIVERSITETAS

DALIUS GUDEIKA

1,8-NAFTALIMIDO, TRIFENILAMINO IR
FLUORENO FRAGMENTUS TURINČIŲ
ORGANINIŲ PUSLAIDININKIŲ
SINTEZĖ IR SAVYBĖS

Daktaro disertacija
Technologijos mokslai, medžiagų inžinerija (08T)

2014, Kaunas

Disertacija parengta 2010–2014 metais Kauno technologijos universiteto Cheminės technologijos fakulteto Organinės technologijos katedroje (dabar – Polimerų chemijos ir technologijos katedra). Mokslinius tyrimus rėmė Lietuvos valstybinis mokslo ir studijų fondas, Lietuvos mokslo taryba.

Mokslinis vadovas:

Prof. habil. dr. Juozas Vidas GRAŽULEVIČIUS (Kauno technologijos universitetas, technologijos mokslai, medžiagų inžinerija – 08T).

Mokslinis konsultantas:

Dr. Ramūnas LYGAITIS (Kauno technologijos universitetas, fiziniai mokslai, chemija – 03P).

TABLE OF CONTENTS

LIST OF ABBREVIATIONS	12
1. INTRODUCTION	15
2. LITERATURE REVIEW	18
2.1. 1,8-Naphthalimide derivatives with aromatic substituents at the 4-position ..	18
2.1.1. 4-Aryl- and 4-aryloxy-substituted 1,8-naphthalimides	19
2.1.2. 4-Ethynyl- and 4-ethenyl-substituted 1,8-naphthalimides.....	26
2.1.3. 1,8-Naphthalimide moiety containing hydrazones and Schiff bases.....	31
2.1.4. 4-Heteroaromatic-substituted 1,8-naphthalimides.....	34
2.2. 1,8-Naphthalimide moieties containing polymers	44
2.3. Conclusions of literature review	51
3. EXPERIMENTAL	53
3.1. Instrumentation	53
3.2. Materials	58
4. RESULTS AND DISCUSSION.....	74
4.1. Bipolar compounds having 1,8-naphthalimide and triphenylamino moieties. 74	
4.1.1. Synthesis and properties of hydrazones containing 1,8-naphthalimide and triphenylamino moieties	74
4.1.2. Synthesis and properties of ambipolar organic compounds containing triphenylamino and 1,8-naphthalimide moieties linked via the single bonds.....	81
4.1.3. Synthesis and properties of glass-forming derivatives with triphenylamino and 1,8-naphthalimide moieties linked via ethenyl-containing linkages.....	102
4.1.4. Synthesis and properties of glass-forming derivatives with triphenylamino and 1,8-naphthalimide moieties linked via ethynyl-containing linkages	114
4.1.5. Comparison of properties of glass-forming derivatives with triphenylamino and 1,8-naphthalimide moieties.....	125
4.2. Synthesis and properties of electron-transporting derivatives of fluorene and 1,8-naphthalimide	128
5. THE MAIN RESULTS AND CONCLUSIONS	137
REFERENCES	140
LIST OF PUBLICATIONS.....	157
ACKNOWLEDGEMENTS	163
CURRICULUM VITAE	164

LIST OF TABLES

Table 2.1. Properties of diarylamine-substituted 1,8-naphthalimide derivatives.....	19
Table 2.2. Properties of 1,8-naphthalimide compounds	20
Table 2.3. Properties of benzene-based molecules with terminal 1,8-naphthalimide moieties.....	21
Table 2.4. Properties of carbazole derivative containing naphthalimide moiety	23
Table 2.5. Properties of 1,8-naphthalimide derivatives	24
Table 2.6. Properties of 1,8-naphthalimide derivatives	25
Table 2.7. Properties of <i>N</i> -alkyl-1,8-naphthalimide derivatives	27
Table 2.8. Electrochemical characteristics of compounds 1-55 – 1-62	29
Table 2.9. Properties of 1,8-naphthalimide derivatives	31
Table 2.10. Properties of 1,8-naphthalimide derivatives	32
Table 2.11. Properties of 1,8-naphthalimide derivatives	37
Table 2.12. Properties of 1,8-naphthalimide derivatives	38
Table 2.13. Properties of 1,8-naphthalimide derivatives	41
Table 2.14. Properties of 1,8-naphthalimide derivatives	45
Table 2.15. Properties of copolymers	48
Table 2.16. Properties of copolymers	49
Table 2.17. Properties of copolymers	50
Table 4.1. Temperatures of the thermal transitions of compounds 3-6	76
Table 4.2. Wavelengths of absorption and fluorescence maxima of compounds 3-6	77
Table 4.3. IP_{CV}/EA_{CV} , optical and electrochemical band-gap energies and IP_{EP} of bipolar hydrazones.....	79
Table 4.4. The crystal data for compound 7	83
Table 4.5. Thermal characteristics of compounds 7-10	85
Table 4.6. Fluorescence characteristics of the dilute cyclohexane solutions, solid films and 0.25 wt% solid solutions in PS of compounds 7-10	87
Table 4.7. Electrochemical, photoelectrical, and theoretical electronic characteristics of 7-10	94
Table 4.8. Hole and electron mobility data for the layers of compounds 7-10 and for the solid solution of 10 in PC-Z (50%).....	97
Table 4.9. Hole- and electron intramolecular reorganization energies for the model compounds M7-M10 computed at the B3LYP/6-31G(d,p) level.....	99
Table 4.10. Electronic couplings (t) and dissociation energies (E_D , corrected for BSSE and ZPE) for some selected dimers of model compounds M7 and M8 . The electronic couplings are calculated at the B3LYP/6-31G(d,p)//CPCM//wB97XD/6-31G(d,p) level. The dissociation energies are calculated at the CPCM/wB97XD/6-31G(d,p) level. Negative dissociation energies mean repulsive state (higher level calculations would slightly modify these values, however, the trends are expected to remain unchanged)	100
Table 4.11. Thermal characteristics of compounds 11-13	104
Table 4.12. Optical and fluorescence characteristics of 11-13	105

Table 4.13. IP _{CV} /EA _{CV} , optical and electrochemical band-gap energies and IP _{EP} of 11–13	109
Table 4.14. Thermal characteristics of compounds 14–16	116
Table 4.15. Optical and fluorescence characteristics of the solutions in the different solvents and of thin solid films of compounds 14–16	117
Table 4.16. Electrochemical characteristics of 14–16	122
Table 4.17. Properties of glass-forming derivatives 7–16	127
Table 4.18. Thermal characteristics of compounds 17–22	129
Table 4.19. Optical and fluorescence properties of the dilute cyclohexane solutions and solid films of compounds 17–22	130
Table 4.20. Fluorescence properties of the dilute solutions of compound 17 in the solvents of the different polarity	132
Table 4.21. Electrochemical characteristics of compounds 17–22	134

LIST OF SCHEMES

Scheme 4.1. Synthetic routes to hydrazones 3 and 4	75
Scheme 4.2. Synthesis of compounds 5 and 6	75
Scheme 4.3. The synthetic routes to 7–10	82
Scheme 4.4. Synthetic route to 11–13	103
Scheme 4.5. The synthetic routes to 14–16	115
Scheme 4.6. Synthesis of compounds 17–22 . Reagents and conditions: (a) Pd(Ph ₃) ₂ Cl ₂ , K ₂ CO ₃ , THF/H ₂ O, 80 °C, 12–16 h	128

LIST OF FIGURES

Figure 2.1	19
Figure 2.2	20
Figure 2.3	20
Figure 3.4	21
Figure 2.5	22
Figure 2.6	22
Figure 2.7	23
Figure 2.8	23
Figure 2.9	24
Figure 2.10	25
Figure 2.11	26
Figure 2.12	26
Figure 2.13	27
Figure 2.14	28
Figure 2.15	28
Figure 2.16	29
Figure 2.17	29
Figure 2.18	30

Figure 2.19	30
Figure 2.20	31
Figure 2.21	31
Figure 2.22	32
Figure 2.23	33
Figure 2.24	33
Figure 2.25	34
Figure 2.26	35
Figure 2.27	35
Figure 2.28	36
Figure 2.29	36
Figure 2.30	36
Figure 2.31	37
Figure 2.32	38
Figure 2.33	39
Figure 2.34	39
Figure 2.35	40
Figure 2.36	40
Figure 2.37	42
Figure 2.38	42
Figure 2.39	43
Figure 2.40	43
Figure 2.41	44
Figure 2.42	45
Figure 2.43	46
Figure 2.44	47
Figure 2.45	47
Figure 2.46	48
Figure 2.47	49
Figure 2.48	50
Figure 2.49	51
Figure 2.50	51
Figure 4.1. TGA curves of 4 and 6 recorded at the heating rate of 20 °C/min in N ₂ 76	
Figure 4.2. UV-Vis and FL spectra of dilute THF solutions (10 ⁻⁵ M) of hydrazones 3–6 . Absorption maxima wavelengths were used as excitation wavelengths	77
Figure 4.3. UV-Vis absorption spectra of thin films of hydrazones 3–6	77
Figure 4.4. CV curves of 1mM solutions in 1M Bu ₄ NBF ₄ DCM electrolyte of a) 5 ; b) 3 ; c) 6 ; d) 4	78
Figure 4.5. DPV curves of 1mM of solutions of compounds 3–6 in 1M Bu ₄ NBF ₄ DCM electrolyte.....	79
Figure 4.6. Electric field dependencies of hole-drift mobilities in the layers of hydrazones 5 , and 6 molecularly doped in PC-Z (50 wt.%).....	80
Figure 4.7. The molecular structure of 7	83
Figure 4.8. Optimized geometries of M7 (a), M8 (b), M9 (c), and M10 (d) model compounds, obtained at the B3LYP/6-31G(d,p) level. Some relevant bond-lengths	

(N-C bond-lengths in TPA core in Å) and dihedral angles (absolute values in degrees) are shown. The C-O bond-lengths for compound M8 in the neutral state are also indicated, along with the same distances in the cationic and anionic states (shorter and longer distances respectively in parentheses).....	84
Figure 4.9. Sketch of frontier orbitals for the model compounds M7–M10 . The encircled parts delimit the TPA moiety. The frontier orbitals for the three molecules (Fig. 4.9) look very similar for all compounds, being localized almost entirely on the TPA core for the HOMO or naphthalimide moiety for the LUMO. The presence of the π -donor methoxy groups in M8 is expected to destabilize the HOMO orbital [224] as compared to M7 , which can also be deduced from the anti-bonding contribution of the methoxy groups in the shape of the HOMO orbital of M8	84
Figure 4.10. DSC thermograms of compound 7 (scan rate of 10 °C/min, N ₂ atmosphere)	85
Figure 4.11. Absorption (dashed thin line) and normalized fluorescence spectra of the 10 ⁻⁶ M solutions of compounds 7–10 in cyclohexane (thick, solid line), of solid films (dashed grey line) and of molecular dispersions in polystyrene matrix at 0.25 wt% concentration (dotted line). Fluorescence quantum yields are indicated. Absorption maxima wavelengths were used as excitation wavelengths	86
Figure 4.12. Absorption spectra of the solutions of compounds 7–10 in cyclohexane (10 ⁻⁶ M) (thick, solid line), solid films (dashed line) and of the solid solutions in polystyrene at 0.25 wt% concentration (dotted line)	87
Figure 4.13. UV-Vis experimental (a) and theoretical spectra of M7–M10 model compounds (e, d, c, and b respectively) obtained by mean of TDDFT calculations at B3LYP/6-31G(d,p) level. The absorption bands are obtained by considering peak half-widths at half height of 0.2 eV. Some relevant MOs are also presented. The theoretical CT bands are red shifted with respect to the experimental ones. This is a known effect which is due to the bad performances of standard hybrid functionals (like B3LYP) in the description of CT excitations. For more details on this point see for example [225-229]	88
Figure 4.14. Dimers of different geometries optimized at the wB97XD/6-31G(d,p) level: a) and b) two different views of the same dimer for compound 7 , reported here as Dim- M7 -HH (head-to-head); c) dimer for compound 8 , reported here as Dim- M8 -HH; d) dimer for compound 8 , reported here as Dim- M8 -HT (head-to-tail); e) dimer for compound 8 , reported here as Dim- M8 -DA (donor-acceptor).....	89
Figure 4.15. Theoretical UV-Vis spectra of M7 and Dim- M7 -HH model compounds obtained by mean of TDDFT calculations at B3LYP/6-31G(d,p) level in THF. The absorption bands are obtained by considering peak half-widths at half height of 0.2 eV. Some relevant MOs are also presented. The geometry of Dim- M7 -HH is optimized at the wB97XD/6-31G(d,p) level by considering the effect of THF	90
Figure 4.16. Theoretical UV-Vis spectra of M8 and Dim- M8 -HH model compounds obtained by mean of TDDFT calculations at B3LYP/6-31G(d,p) level in THF. The absorption bands are obtained by considering peak half-widths at half height of 0.2 eV. The geometry of Dim- M8 model complexes are optimized at the wB97XD/6-31G(d,p) level by considering the effect of THF.....	91

Figure 4.17. Absorption and FL spectra of compounds 7 (a) and 8 (b) in dilute cyclohexane (solid line), toluene (dashed line), THF (dotted line), and acetonitrile (short dashed line) solutions (10^{-6} M, $\lambda_{\text{ex}} = 450$ nm)	92
Figure 4.18. Cyclic voltammograms of 7–10 (10^{-5} M solutions, scan rate of $50 \text{ mV}\cdot\text{s}^{-1}$ vs Ag/Ag ⁺) in 0.1 M solution of Bu ₄ NPF ₆ in DCM	94
Figure 4.19. Electron photoemission spectra of the neat layers of 7–10 recorded in air	95
Figure 4.20. Electric field dependencies of hole and electron drift mobilities for the layers of compounds 7–10 and for the layer the solid solution of 10 in PC-Z (50%)	96
Figure 4.21. XTOF transients of electrons for a solid film of 8	97
Figure 4.22. Optimized geometries of M11 (left), M12 (center), and M13 (right) model compounds, obtained at the B3LYP/6-31G(d,p) level. Some relevant dihedral angles (absolute values in degrees) are shown	103
Figure 4.23. Pictograms of frontier orbitals for the model compounds M11 , M12 , and M13 . The encircled parts delimit the TPA moiety	104
Figure 4.24. DSC thermograms of compound 12 (scan rate of $10 \text{ }^\circ\text{C}/\text{min}$, N ₂ atmosphere)	105
Figure 4.25. UV-Vis and FL ($\lambda_{\text{ex}} = 365$ nm) spectra of the dilute THF solutions (10^{-5} M) and of solid films of compounds 11–13	106
Figure 4.26. UV-Vis experimental (a) and theoretical spectra of M13 , M12 , and M11 model compounds (b, c, and d, respectively) obtained by mean of TDDFT calculations at B3LYP/6-31G(d,p) level. The absorption bands are obtained by considering peak half-widths at half height of 0.2 eV. Some relevant MOs are also presented (see Fig. 4.27 for more clear pictograms)	107
Figure 4.27. Pictograms of some relevant orbitals for the neutral model compounds M11–M13	108
Figure 4.28. Cyclic voltammograms of 11–13 (10^{-5} M solutions, scan rate of $50 \text{ mV}\cdot\text{s}^{-1}$ vs Ag/Ag ⁺) in 0.1 M solution of Bu ₄ NPF ₆ in DCM	110
Figure 4.29. Electron photoemission spectra of the layers of 11–13	111
Figure 4.30. Electric field dependencies of hole-drift mobilities in the layers of 11–13	112
Figure 4.31. Representative TOF transients of the layer of compound 11	112
Figure 4.32. DSC thermograms of compound 15 (scan rate of $10 \text{ }^\circ\text{C}/\text{min}$, N ₂ atmosphere)	116
Figure 4.33. UV-Vis (dashed thin line) spectra of 10^{-5} M solutions of compounds 14–16 and normalized FL spectra of the dilute solutions in toluene (thick, solid line), and of the solid films (solution spin-coated on quartz, dashed grey line). Fluorescence quantum yields are indicated. Absorption maxima wavelengths were used as excitation wavelengths	116
Figure 4.34. FL spectra of the solutions (10^{-5} M) of compounds 14 (a), 15 (b) and 16 (c) in dilute cyclohexane (solid line), toluene (dashed line), chloroform (dashed dot line), THF (dashed dot dot line), and acetonitrile (short dot line). Absorption maxima wavelengths were used as excitation wavelengths	118

Figure 4.35. (a) Dependences of Stokes shifts $\Delta\nu$ of compounds 14–16 ($c = 10^{-5}$ M) on the orientation polarizability Δf . Solid lines were obtained from the linear fits. (b) plots of the wavelengths of fluorescence intensity maxima of 14–16 versus the $E_T(30)$ polarity parameter of the different solvents. (c) fluorescence quantum yields of the solutions 14–16 versus the solvent polarity $\Delta f(\epsilon, n)$	119
Figure 4.36. Normalized prompt and delayed fluorescence spectra of the toluene solutions (10^{-5} M) of 14 (a) and 15 (b) and of the solid films of 14 (c) and 15 (d)	121
Figure 4.37. Cyclic voltammograms of 14–16 (10^{-5} M solutions, scan rate of $50 \text{ mV}\cdot\text{s}^{-1}$ vs Ag/Ag^+) in 0.1 M solution of Bu_4NPF_6 in CH_2Cl_2	122
Figure 4.38. Electron photoemission spectra of the films of compounds 14–16 ...	123
Figure 4.39. Dark CELIV and photo-CELIV curves for compound the layer of 14 as a function of an applied triangle-shaped voltage pulse with amplitude from 10 to 20 V. The maximum extraction time was marked in photo-CELIV curves when the maximum in the current transients was observed.....	124
Figure 4.40. Molecular structures of 7–16	125
Figure 4.41. DSC curves of compound 18 (heating/cooling rate $10 \text{ }^\circ\text{C}/\text{min}$, N_2)..	130
Figure 4.42. Absorption (thin solid line) and fluorescence spectra of the solutions (10^{-6} M) of 17–22 in cyclohexane (thick solid line) and of solid films (dashed grey line). Fluorescence quantum yields are indicated. Absorption maxima wavelengths were used as excitation wavelengths	131
Figure 4.43. Fluorescence spectra of the dilute cyclohexane, toluene, chloroform, dichloromethane, acetone, acetonitrile and dimethylsulfoxide solutions (10^{-6} M) of compound 17	132
Figure 4.44. a) FL quantum yield and b) FL decay time (triangles), radiative (circles) and non-radiative (squares) decay times versus dielectric constants of the solvents. Lines are showing the trends	133
Figure 4.45. Cyclic voltammograms of compounds 17–22	134
Figure 4.46. XTOF transients for the solid film of 21 . Arrow mark indicate transit time of electrons at the respective surface voltage	135
Figure 4.47. Electric field dependencies of electron-drift mobilities of the amorphous layers of 17 , 21 , 22 and of the molecular mixture of 18 with PC-Z (1:1)	135

LIST OF ABBREVIATIONS

α	Pool-Frenkel parameter
α, θ	orientation angles
β	stretched exponential fitting parameter
δ	chemical shift
ACN	acetonitrile
AlLi	aluminium-lithium
Alq ₃	tris(8-hydroxyquinoline)aluminium
Ar	aromatic(s), aryl
B3LYP	hybrid density functional theory
BePP ₂	bis[2-(2-hydroxyphenyl)-pyridine]beryllium
Bphen	bathophenanthroline
Bu ₄ NBF ₄	tetra- <i>N</i> -butylammonium hexafluoroborate
Bu ₄ NPF ₆	tetra- <i>N</i> -butylammonium hexafluorophosphate
CDCl ₃	deuterated chloroform
¹³ C NMR	carbon nuclear magnetic resonance
CELIV	charge extraction by linearly increasing voltage
CIE	commission Internationale de l'Eclairage
CT	charge-transfer
CuPc	copper(II)phthalocyanine
CV	cyclic voltammetry
(D-A)-D	(donor-acceptor)-donor
<i>d</i>	layer thickness
d	doublet
D	dipole moment
DCM	dichloromethane
dd	doublet of doublet
DFT	density functional theory
DMF	dimethylformamide
DMSO	dimethylsulfoxide
DPV	differential pulse voltammetry
DSC	differential scanning calorimetry
ϵ	molar extinction coefficient
EACV	electron affinity
EDOT	3,4-ethylenedioxy thiophene
E _g ^{elc}	electrochemical band gap
E _g ^{opt}	optical band gap
EL	electroluminescence
E _{onset} ^{ox}	onset oxidation potential
E _{onset} ^{red}	onset reduction potential
E _{ox}	oxidation potential
E _{red}	reduction potential
eV	electron volt
Φ_F	fluorescence quantum yield

Fc/Fc ⁺	ferrocene/ferrocenium
FL	fluorescence
FMO	frontier molecular orbital
FT-IR	Fourier transform IR
FWHM	full width at half maximum
g	gram
¹ H NMR	proton nuclear magnetic resonance
h	hour
HOMO	Highest Occupied Molecular Orbital
ICT	intramolecular charge transfer
IP _{CV}	ionization potential
IP _{EP}	solid state ionization potential
IR	infrared spectroscopy
ITO	indium tin oxide
<i>J</i>	coupling constant
<i>k_{ht}</i>	hole-transfer rate constant
LUMO	Lowest Unoccupied Molecular Orbital
λ _{abs}	maximum absorption wavelength
λ _e	reorganization energies for electron
λ _{em}	maximum emission wavelength
λ _h	reorganization energies for hole
λ _{ex}	excitation wavelength
λ _{edge}	onset value of absorption spectrum in long wave direction
λ _i	intramolecular reorganization energy
μ	charge carrier mobility
μ ₀	zero field mobility
m	multiplet
M	molar concentration (mol/l)
m.p.	melting point
<i>m/z</i>	mass/charge
MEH-PPV	poly(1-methoxy-4-(2-ethyl-hexyloxy)- <i>p</i> -phenylenevinylene)
MS	mass spectroscopy
NBS	<i>N</i> -bromosuccinimide
NPB	<i>N,N'</i> -bis(1-naphthyl)- <i>N,N'</i> -diphenyl-1,1'-biphenyl-4,4'-diamine
OLED	organic light emitting diode
P(o-tolyl) ₃	tri(o-tolyl)phosphine
PCBM	[6,6]-phenyl-C ₆₁ -butyric acid methyl ester
PCE	power conversion efficiencies
PC-Z	bisphenol Z polycarbonate
Pd(OAc) ₂	palladium(II) acetate
Pd(PPh ₃) ₂ Cl ₂	bis(triphenylphosphine)palladium(II) dichloride
PEDOT	poly(3,4-ethylenedioxythiophene)
PPh ₃	triphenylphosphine
ppm	parts per million

PS	polystyrene
PSS	poly(styrene sulfonic acid)
PTC	phase transfer catalyst
PVK	poly(<i>N</i> -vinylcarbazole)
q	quadruplet
s	singlet
τ	fluorescent decay time constant
τ_{NR}	non-radiative decay time constant
τ_R	radiative decay time constant
t	triplet
TBAF	tetrabutylammonium fluoride
T_{cr}	crystallization temperature
TDDFT	time dependent density functional theory method
TEA	triethylamine
T_g	glass transition temperature
TGA	thermogravimetric analysis
THF	tetrahydrofuran
T_{ID}	temperature of the onset of the thermal decomposition
$T_{ID-5\%}$	5% weight loss temperature
TiO ₂	titanium dioxide
TLC	thin layer chromatography
T_m	melting transition temperature
TMS	tetramethylsilane
TOF	time-of-flight
TPA	triphenylamine
TPBI	1,3,5-tris(<i>N</i> -phenylbenzimidazole-2-yl)benzene
TPD	<i>N,N'</i> -diphenyl- <i>N,N'</i> -bis(3-methylphenyl)-(1,1'-biphenyl)-4,4'-diamine
t_t	transit time
(UV-Vis)-NIR	(ultraviolet-visible)-near infrared light
U_0	surface potential at the moment of illumination
<i>vs</i>	<i>versus</i>
χ^2	parameter of goodness of fit
XRD	X-ray diffraction
XTOF	xerographic time-of-flight

1. INTRODUCTION

Organic compounds that emit in the UV-Vis region and whose fluorescence emission is sensitive to solvent polarity are of significant interest due to their versatile applications in optoelectronic devices. Considerable attempt has been expended in to shifting the fluorescence emission of organic compounds in to the visible region. The most employed strategy for the red shifting of the emission wavelength is to extend the conjugation of the derivatives with aryl, ethenyl or ethynyl groups. The addition of electron accepting and donating (A-D) groups to these conjugation extended molecules also helps in shifting the emission wavelengths in to the red region [1], therefore A-D type molecules are of considerable interest and importance. In this type of derivatives, the excited state is highly polar compared to the ground state, due to intramolecular charge transfer (ICT) from the donor to the acceptor moiety. This process leads to a large increase of the dipole moment in the excited state compared to that of the ground state and causes a large Stokes shift and a solvatochromic effect.

So far, the use of the concept of A-D system in 1,8-naphthalimide chemistry was rather limited. In the recent years the interest in the optical and fluorescence, electrochemical and photoelectrical properties of 1,8-naphthalimide derivatives has been steadily increasing [2–4]. Much attention has been paid to the design and synthesis of new 1,8-naphthalimide architectures as well as to the studies of the properties of the materials.

1,8-Naphthalimide derivatives possess several interesting properties: (a) they often combine intensive fluorescence with good charge transporting properties; (b) the oxidation and reduction potentials of naphthalimides can be tuned by substitution; (c) introduction of an electron-donating moiety at the C-4 position of 1,8-naphthalimide compounds generate ICT excited state [5,6] and leads to a large bathochromic shift in both absorption and emission spectra. The length of the shift depends on the strength of the electron donor. For example, introduction of alkylamino groups into C-4 position of naphthalimides results in bathochromic shifts up to 50 nm in absorption spectra and over 100 nm in emission [7].

Most of the ambipolar organic semiconductors are capable of transporting both holes and electrons when protected from air. However, until formulation of the aims of this work there had been less information regarding on the organic materials capable of transporting negative charges or both negative and positive charges with balanced hole and electron mobilities, which operate in air [8]. The investigation of the 4-substituted 1,8-naphthalimide derivatives demonstrate that many of these materials have charge transporting abilities and show film forming properties. These properties make naphthalimides the potential materials for the applications in optoelectronics. Moreover, the knowledge of the relationship of the structure and the characteristics such as ionization potential and electron affinity values, charge-mobilities of organic materials is important for the optimization of optoelectronic devices. By selection of appropriate electron-donating moieties the ionization potential values and thus the band gap can be controlled. On the other hand, the investigation of the fluorescence and charge transporting behavior of 1,8-

naphthalimide derivatives by the theoretical and experimental is important for design of the structures of new highly effective organic electroactive materials.

So, **the aim of this work:** synthesis, experimental and theoretical estimation of the structure-properties relationships of 1,8-naphthalimide-based organic compounds, containing triphenylamino and fluorenyl moieties, capable of transporting electrons or holes or both holes and electrons.

The tasks proposed for the achievement of the above stated aims were as follows:

1. Synthesis of hole-transporting hydrazones, having triphenylamino and 1,8-naphthalimide moieties. Investigation of their thermal, photoelectrical, electrochemical, and fluorescence properties.

2. Synthesis, experimental and theoretical studies of ambipolar organic materials containing triphenylamino and 1,8-naphthalimide moieties linked by single, double and triple bonds.

3. Synthesis and investigation of 1,8-naphthalimide-substituted derivatives of fluorene.

The main statements of the doctoral dissertation are:

1. Glass-forming triphenylamino-substituted naphthalimides are potential organic semiconducting materials for applications in optoelectronic devices, exhibiting high thermal and electrochemical stability, and high mobilities of positive, negative or both positive and negative charges.

2. 1,8-Naphthalimide-substituted derivatives of fluorene are solution processable materials, exhibiting high thermal and electrochemical stability, solvatochromic behavior, high fluorescence quantum yields, and high electron drift mobility.

Theoretical and practical value of this work

Several series of new potential n-, p-type or bipolar charge transporting organic semiconducting materials of 1,8-naphthalimide, containing triphenylamino and fluorenyl moieties were synthesized and investigated. Triphenylamino-substituted naphthalimides and naphthalimide-substituted derivatives of fluorene can be used as hole, electron or both charges transporting materials for application in optoelectronics. 4-(4'-(Di-(4'-methoxyphenyl)amino)phenyl)-N-(2-ethylhexyl)-1,8-naphthalimide is capable of transporting both negative and positive charges with balanced hole and electron mobilities.

Publication of the research results

The results of the doctoral dissertation work were presented at 7 international scientific conferences and 5 articles were published in the journals included into the Thomson Reuters Web of Knowledge database.

Contribution of the author

The author of the thesis performed the synthesis of all the compounds, made all the experiments of thermal, electrochemical characterization of all the

compounds and made the experiments of optical and fluorescence investigation of the compounds, analysed the data of the measurements. The author prepared manuscripts of most of the articles, and participated in the preparation of conference presentations. Part of the results was obtained in collaboration with other laboratories. The experiments of investigation of the optical and fluorescence properties of some compounds were performed in the laboratories of prof. S. A. Juršėnas (Vilnius University). The ionization potential measurements of the derivatives were performed in collaboration with habil. dr. V. Gaidelis. The charge drift mobility measurements were performed by dr. V. Jankauskas (Vilnius University). The theoretical calculations were performed in collaboration with dr. G. Sini (Cergy-Pontoise University, France).

Structure and contents of the dissertation

The dissertation consists of the introduction, literature survey, experimental part, results and discussion, conclusions, the lists of references and publications topic. The list of references includes 281 bibliographic sources. The doctoral dissertation consists of 164 pages, illustrated in 6 schemes, 38 tables and 97 figures.

2. LITERATURE REVIEW

1,8-Naphthalimides belong to a class of compounds with the interesting excited-state properties. 1,8-Naphthalimides moiety is one the most important building blocks for the synthesis of efficient fluorescent materials. Non-substituted 1,8-naphthalimides exhibit low fluorescence quantum yields. In contrast the substituted 1,8-naphthalimides have attracted much attention due to their high fluorescence quantum yields, good optical, thermal and chemical stabilities, and sizable Stokes shifts [9,10]. These derivatives also have high photoactivity [11] and make good photosensitizers because of their large extinction coefficients in the triplet and reduced states as well as their efficient intersystem crossings [12]. Furthermore, naphthalimide derivatives have high electron affinity due to the existence of an electron-deficient centre [13–15], and display good electron-transporting or hole-blocking capabilities that are appropriate for balanced carrier injection in OLEDs.

Mainly due to the unique fluorescence properties [16–19] 1,8-naphthalimide compounds have found applications in various areas [3], including coloration of polymers [20], laser active media [21], photosensitive biological units [22], fluorescent markers in biology [23], OLEDs [24], photoinduced electron transfer sensors [25], fluorescence switchers [26], electroluminescent materials [27], liquid crystal displays [28], strongly absorbing and colorful dyes [29], ion probes [30]. The attractive properties of the 1,8-naphthalimide chromophore have led to its incorporation into numerous polymeric [31] and dendritic [32–39] structures so as to tailor solubility, self-association, and molecular size to suit a particular application.

2.1. 1,8-Naphthalimide derivatives with aromatic substituents at the 4-position

Many studies were reported on 1,8-naphthalimide derivatives, however it is still meaningful to extend the research the derivatives, introducing new electron-donating and electron-accepting groups at the C4 position of 1,8-naphthalimides. The fluorescence properties of these derivatives can be changed by changing the nature of a substituent present on the aromatic ring [40]. Introduction of the substituents with different electron-donating capability, such as alkyl(aryl) amino [41], alkynyl/alkenyl [16,42], aryloxy or alkoxy groups [43] induces a polar CT excited state [5]. This ICT character leads to a large excited-state dipole and broad absorption and emission bands shifted at longer wavelengths. The ICT transition is highly solvent dependent. The optical and fluorescence properties of naphthalimides, such as the positions maxima of absorption and emission spectra, fluorescence quantum yields as well as fluorescence lifetimes, are all affected by the properties of solvents [44], and their fluorescence emission colour can be readily tuned from yellowish green to pure blue. 1,8-Naphthalimide derivatives with alkoxy groups constitute a very important class of compounds with intensive fluorescence and very good photo stability [45].

2.1.1. 4-Aryl- and 4-aryloxy-substituted 1,8-naphthalimides

Diarylamine-substituted naphthalimide derivatives **1-1** – **1-3** and the similar compounds consisting of 2-naphthalene-1-yl-benzo[de]isoquinoline-1,3-dione (**1-4**, **1-5**) and bulky diphenylamine or naphthylphenylamine substituted as a side moieties were reported [46,47] (Fig. 2.1).

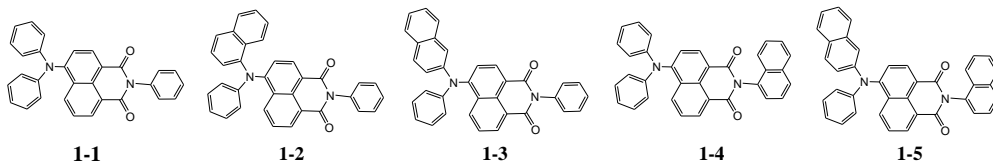


Figure 2.1

It was found, that the glass transition temperature (T_g) increased in the order 72 °C (**1-1**) < 95 °C (**1-3**) < 105 °C (**1-2**). For compounds **1-4** and **1-5**, T_g were observed at 128 °C and 148 °C, respectively. The higher T_g value of **1-5** can apparently be explained in terms of its higher molecular weight and higher intermolecular interaction. T_{ID} of **1-4** and **1-5** derivatives were at 368 °C and 407 °C, respectively. The high thermal stability indicate that **1-1** – **1-5** derivatives can form homogeneous and amorphous film through thermal evaporation. Increasing solvent polarity from *n*-hexane to DCM resulted in a 20 nm bathochromic shift of the λ_{abs} of compounds **1-1** – **1-3**. This shift suggested that the ground state of the molecules was significantly polar. For the compounds (**1-1** – **1-3**) red-shift was observed in the emission spectra of the solutions as the solvent polarity increased. The electron affinity values (EA_{CV}) of the compounds were found to be comparable: –3.06 eV for **1-4** and –3.04 eV for **1-5**. The CIE coordinates of the OLED device (ITO/DNTPD (60 nm)/NPD(20 nm)/Alq₃% dopant (20 nm)/Alq₃ (40 nm)/LiF/Al) were found to be (0.46, 0.52) for **1-4** and (0.48, 0.52) for **1-5** at 10 mA/cm². Luminance-efficiency were obtained 6.6 cd/A at the voltage of 5.9 V for OLED device containing **1-4** and 5.9 cd/A at the voltage of 6.3 V for OLED device containing **1-5**.

Table 2.1. Properties of diarylamine-substituted 1,8-naphthalimide derivatives

Material	T_g , (°C)	T_{ID} , (°C)	λ_{abs} , (nm) in <i>n</i> -hexane	λ_{abs} , (nm) in THF	λ_{abs} , (nm) in CH ₂ Cl ₂	EA_{CV} , (eV)	η_L , (cd/A)
1-1	72	NM	441	448	460	NM	NM
1-2	105	NM	430	438	450	NM	NM
1-3	95	NM	448	454	465	NM	NM
1-4	128	368	NM	NM	NM	-3.06	6.6
1-5	148	407	NM	NM	NM	-3.04	5.9

λ_{abs} – maximum absorption wavelength; T_g – glass-transition temperature; T_{ID} – temperature of the onset of the thermal decomposition; EA_{CV} – electron affinity; η_L – luminance-efficiency; NM – not measured.

Wang and co-workers [48] reported experimental and theoretical studies of similar naphthalimide compounds containing dimethylamino, diphenylamino groups (**1-6**, **1-7**), and different number of triphenylamino moieties (**1-8**, **1-9**, Fig. 2.2).

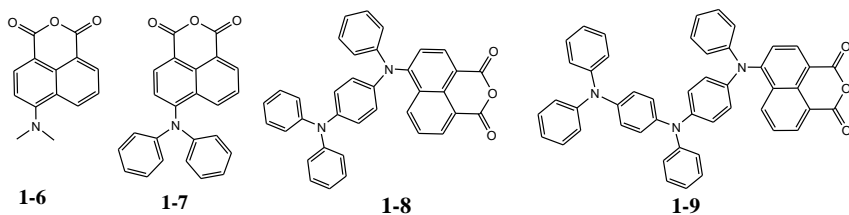


Figure 2.2

The replacement of dimethylamino group at C4 position of naphthalic ring with diphenylamino group led to a 38 nm red-shift of λ_{abs} (cf. λ_{abs} of **1-6** and **1-7**). When the number of aromatic amino groups in compounds **1-8** and **1-9** increased to two and three, respectively, λ_{abs} of these compounds red shifted for 31 and 9 nm, respectively compared to **1-7**. Small red shifts of λ_{abs} of the solutions of compounds **1-6** – **1-9** in polar solvents were identified relative to those observed for the solutions in non-polar solvents. Φ_{F} value of compound **1-7** ($\Phi_{\text{F}} = 0.057$) was much smaller than that of compound **1-6** ($\Phi_{\text{F}} = 1$) [49]. Φ_{F} of compounds **1-8** and **1-9** were very small ($\Phi_{\text{F}} = 0$ and $\Phi_{\text{F}} = 0.01$, respectively). The ionization potential values (IP_{CV}) increased for compounds **1-7** – **1-9** from 4.70 to 5.33 eV. The structures of compounds **1-6** – **1-9** were optimized using B3LYP/6-31G(d) method. It was established, that the naphthalic ring had a planar structure with a twisting angle of $\sim 90^\circ$ from the plane of directly connected amino group. IP_{CV} values increased along with the increase on the number of triphenylamino groups at C4 position and the $E_{\text{g}}^{\text{opt}}$ decreased following the order of **1-6** > **1-7** > **1-8** > **1-9**. The energy levels of HOMO-1 of compounds **1-6** – **1-9** increased along with the increase on the number of triphenylamino groups at 4-position.

Table 2.2. Properties of 1,8-naphthalimide compounds

Material	λ_{abs} , (nm)	Φ_{F}	IP_{CV} , (eV)	$E_{\text{g}}^{\text{opt}}$, (eV)
1-6	425	1	NM	NM
1-7	463	0.057	5.33	2.28
1-8	503	0	4.70	1.56
1-9	494	0.01	4.91	1.84

λ_{abs} – maximum absorption wavelength; Φ_{F} – fluorescence quantum yield; IP_{CV} – ionization potential; $E_{\text{g}}^{\text{opt}}$ – optical band gap; NM – not measured.

Several naphthalimide-based compounds containing differently substituted phenyl groups at C4 position (**1-10** – **1-12**) were reported [50] (Fig. 2.3).

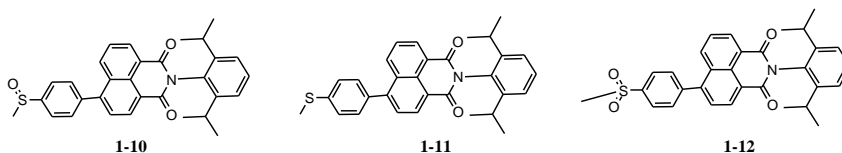


Figure 2.3

The absorbance and FL spectra of compound **1-10** revealed a strong absorption peak at 350 nm (*vs* $\lambda_{\text{abs}} = 370$ nm for compound **1-11**) and a high intensity emission

peak at 425 nm (*vs* $\lambda_{em} = 540$ nm for compound **1-11**) in dilute acetonitrile solutions. The strongest fluorescence was observed for the dilute solution of compound **1-10** in acetonitrile (ACN). At higher concentrations, reduction of the fluorescence signal intensity was observed. It was explained by self-quenching. Compound **1-12** exhibited a lower fluorescence intensity than the sulfoxide **1-10**, while the emission of **1-12** at $\lambda_{em} = 411$ nm closely overlapped the emission of **1-10** at $\lambda_{em} = 425$ nm.

A series of starburst benzene-based glass-forming molecules ((**1-13**)a-e) with terminal naphthalimide moieties for optoelectronic devices were reported [51] (Fig. 2.4).

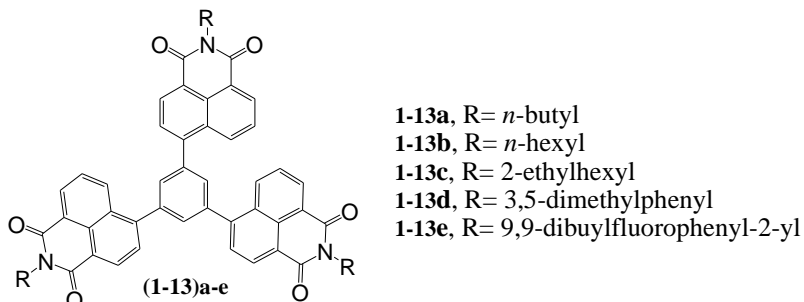


Figure 2.4

Glass transitions were observed for all compounds ((**1-13**)a-e). T_g reached as high as 254 °C for compound **1-13d** and 193 °C for **1-13e**. The compounds with more rigid moieties (**1-13d** and **1-13e**) exhibited higher T_g than those with flexible alkyl substituents ((**1-13**)a-e). T_g values dropped with increasing length of the alkyl chain. TGA experiments revealed that all these compounds exhibited high thermal stability with T_{ID} up to 489 °C. λ_{em} was observed in the range of 425–431 nm. Compound **1-13e** did not emit fluorescence under the ultraviolet excitation. Two organic electroluminescent devices ITO/MoO₃ (3 nm)/NPB (40 nm)/Alq₃ (20 nm)/Bphen (20 nm)/electron transporter (20 nm)/Cs₂CO₃ (1 nm)/Al (100 nm) were fabricated, where **1-13a** and Alq₃ were chosen as electron transporter. The **1-13a** based device showed the current density of 48.7 mA/cm², luminance of 985 cd/m² at 5 V, compared with 1 mA/cm² and 23 cd/m² observed for the Alq₃-based device.

Table 2.3. Properties of benzene-based molecules with terminal 1,8-naphthalimide moieties

Material	T_g , (°C)	T_{ID} , (°C)	λ_{em} , (nm)
1-13a	140	381	426
1-13b	91	489	430
1-13c	78	477	431
1-13d	254	488	425
1-13e	193	488	ND

T_g – glass-transition temperature; T_{ID} – temperature of the onset of the thermal decomposition; λ_{em} – maximum emission wavelength; ND – not detectable.

Two naphthalimide-based derivatives (**1-14**, **1-15**) containing electron donating moieties were reported [52] (Fig. 2.5).

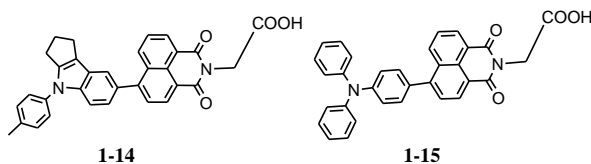


Figure 2.5

Indoline based **1-14** showed red shift ($\Delta\lambda_{\text{abs}} = 39$ nm) compared to the TPA based compound **1-15**. The absorption spectra of thin layers of **1-15** and **1-14** on TiO_2 showed blue shift by 2 and 21 nm, respectively compared to those of the solutions due to the indoline moiety has stronger electron-donating capability than that of TPA. The LUMO levels of **1-15** and **1-14** corresponding to the first reduction potentials (E_{red} vs the normal hydrogen electrode) were -1.42 V, -1.45 V, respectively. The HOMO level of **1-14** corresponding to the first oxidation potential (E_{ox} vs the normal hydrogen electrode) was more negative (0.79 V) than that of **1-15** (1.08 V). A solar energy to electricity conversion efficiencies of 1.10%, 1.18% were observed for dye-sensitized solar cells containing **1-15** and **1-14**, respectively.

Bipolar compounds containing naphthalimide and carbazole moieties (**1-16** – **1-21** and **1-22** – **1-24**) for organic electronic devices were reported [53] (Fig. 2.6).

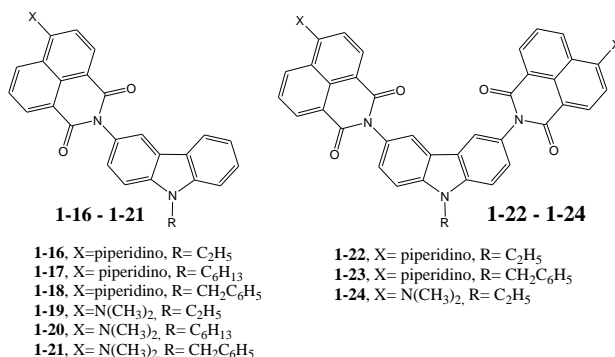


Figure 2.6

Two types of EL devices were fabricated. Device 1 had an architecture: ITO/compounds **1-16** – **1-21** or **1-22** – **1-24** (50–100 nm)/LiF (1 nm)/AlLi. Device 2 had the following structure: ITO/CuPc (10 nm)/TPD (10 nm)/compound **1-19** (30 nm)/BePP $_2$ (45 nm)/LiF (1 nm)/AlLi. To improve the performance of the two EL devices, a 1.0 nm LiF layer was inserted between the cathode and organic layer. The device 2 had maximum brightness of 110 cd/m^2 at a driving voltage of 21 V and a maximum current density of 240 mA/cm^2 . From the synthesized compounds **1-22** – **1-24** single-layer devices were prepared (ITO/**1-22** – **1-24** (50–100 nm)/LiF (1 nm)/AlLi). The devices containing triads (**1-22** – **1-24**) displayed higher brightness, lower turn-on voltage than those containing **1-16** – **1-21**. Due to improve the device efficiency the device 2 with additional electron-transporting layer (BePP $_2$) and hole-transporting layer (CuPc and TPD) were prepared. The maximum brightness of the device 2 reached 4800 cd/m^2 at the driving voltage of 21 V, the maximum current density increased up to 410 mA/cm^2 .

Koyuncu and co-workers [54] reported a donor-acceptor carbazole derivative (**1-27**) containing naphthalimide moiety at C4 position (Fig. 2.7).

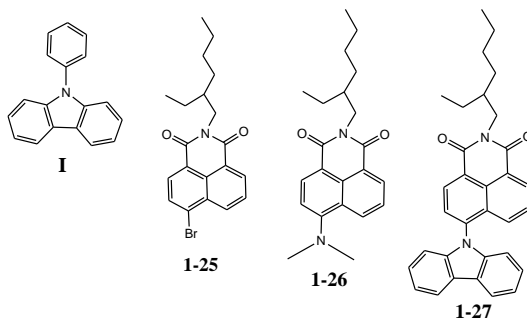


Figure 2.7

UV-Vis absorption spectra of **1-27** was red shifted in DCM [55] compared to the molecules **I** and **1-25** due to the direct attachment of carbazole moiety to naphthalimide moiety. A weak ICT band of **1-27** was observed at ~412 nm [56]. Fluorescence emission of compound **1-27** was quenched compared to that of compound **1-26** [57]. Φ_F value of **1-27** ($\Phi_F = 0.066$) was found ~10 times smaller than that of compound **1-26** ($\Phi_F = 0.686$) in DCM. The reduction half wave potential of compound **1-26** was observed at the more positive potential (-1.28 V) compared to that of derivative **1-25** (-1.31 V). E_{ox} of molecules **I** and **1-26** (1.29, 1.18 V, respectively) was observed at the lower potential than that of **1-27** (1.39 V).

Table 2.4. Properties of carbazole derivative containing naphthalimide moiety

Material	$\lambda_{abs.}$ (nm)	$\lambda_{em.}$ (nm)	Φ_F	$E_{ox.}$ (eV)	$E_{red.}$ (eV)
I	340	362	0.762	1.29	–
1-25	345	396	0.024	–	-1.31
1-26	422	512	0.686	1.18	-1.28
1-27	412	543	0.066	1.39	-1.22

λ_{abs} – maximum absorption wavelength; λ_{em} – maximum emission wavelength; Φ_F – fluorescence quantum yield; E_{ox} – oxidation potential; E_{red} – reduction potential.

Similar three naphthalimide derivatives **1-28** – **1-30** as candidates for optoelectronics, containing the same electron-donor moiety (carbazole), and electron-acceptor naphthalimide with the different substituents at N atom also were reported [55] (Fig. 2.8).

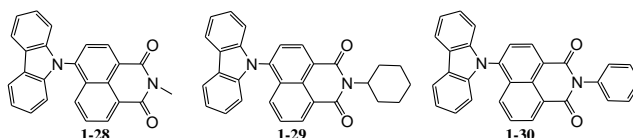


Figure 2.8

Increasing solvent polarity from *n*-hexane to DCM, λ_{em} of the solutions of compound **1-28** were red-shifted ($\Delta\lambda_{em} = 116$ nm). The similar trend was observed in other compounds **1-29** and **1-30**. The Stokes shifts of compounds **1-28** – **1-30** were

larger for the solutions in polar solvents as compared to those observed for the solutions in non-polar solvents [46]. From the slope of Lippert-Mataga plot, the difference of the dipole moment between the excited state and the ground state was estimated to be 15.83, 17.91 and 17.93 D for compounds **1-28** – **1-30**, respectively.

Blue light-emitting naphthalimide derivatives containing electron-donating phenoxy or *t*-butyl modified phenoxy groups (**1-32**, **1-33**)a) were reported [58] (Fig. 2.9).

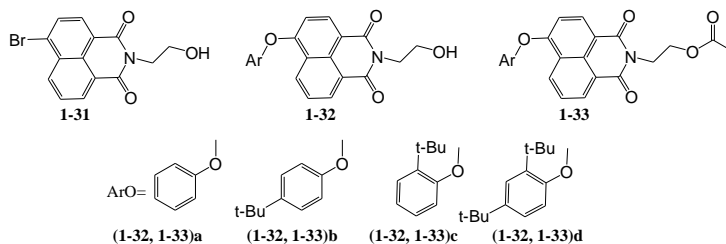


Figure 2.9

Compounds (**1-32**, **1-33**)d showed red-shift compared to **1-31** in solution, due to that *t*-butyl acts as weak electron-donating substituent. The fluorescence properties of the solid films differed from those of the solutions due to the aggregation. The dilute solutions of compounds (**1-32**, **1-33**)a in chloroform showed blue fluorescence with high Φ_F of 0.55 and 0.82 respectively. The solid films of the derivatives (**1-32**, **1-33**)a showed bathochromic shift ($\Delta\lambda_{em} = 50$ nm) with respect of those of the solutions. The films of compounds (**1-32**, **1-33**)a exhibited much lower Φ_F (<0.15) that those of compounds (**1-32**, **1-33**)b (0.27 and 0.46, respectively) [59]. Φ_F of the solutions of compounds (**1-32**, **1-33**)c were between 0.46–0.66, while those of the films were as low as 0.04. Compounds (**1-32**, **1-33**)d had much dropped Φ_F (<0.03) in solution, much improved Φ_F of >0.24 in the solid films. Derivatives (**1-32**, **1-33**)d had low E_{ACV} values ranging from -3.29 to -3.24 eV, and the IP_{CV} values ranging from 6.16 to 6.26 eV. Their E_g^{elc} were 2.92–3.01 eV, somewhat in good accordance with E_g^{opt} (3.03–3.08 eV).

Table 2.5. Properties of 1,8-naphthalimide derivatives

Material	λ_{abs} , (nm) in CHCl ₃ sol/solid film	λ_{em} , (nm) in CHCl ₃ sol/solid film	Φ_F sol/solid film	E_g^{opt} , (eV)	E_g^{elc} , (eV)	IP_{CV} , (eV)	E_{ACV} , (eV)
1-32a	366/369	429/478	0.55/0.14	NM	NM	NM	NM
1-32b	369/369	435/471	0.27/0.42	NM	NM	NM	NM
1-32c	369/369	432/448	0.66/0.04	NM	NM	NM	NM
1-32d	374/369	444/451	0.02/0.29	NM	NM	NM	NM
1-33a	365/367	425/473	0.82/0.15	3.08	2.96	6.25	-3.29
1-33b	367/368	429/475	0.46/0.11	3.06	3.01	6.26	-3.25
1-33c	364/366	427/438	0.46/0.04	3.08	2.92	6.16	-3.24
1-33d	372/370	442/441	0.03/0.24	3.03	2.95	6.19	-3.24

λ_{abs} – maximum absorption wavelength; λ_{em} – maximum emission wavelength; Φ_F – fluorescence quantum yield; IP_{CV} – ionization potential; E_{ACV} – electron affinity; E_g^{opt} – optical band gap; E_g^{elc} – electrochemical band gap; NM – not measured.

Similar series of naphthalimide derivatives by substituting electron-donating phenoxy, methylphenoxy and cyanophenoxy groups at the C4 position of naphthalimide also were synthesized (**1-34 – 1-35**)a-c [60] (Fig. 2.10).

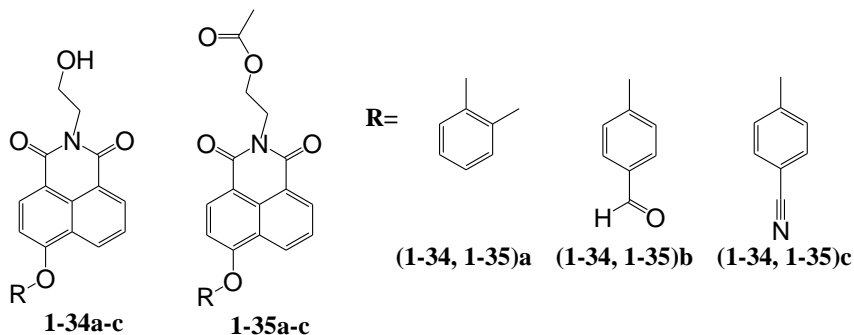


Figure 2.10

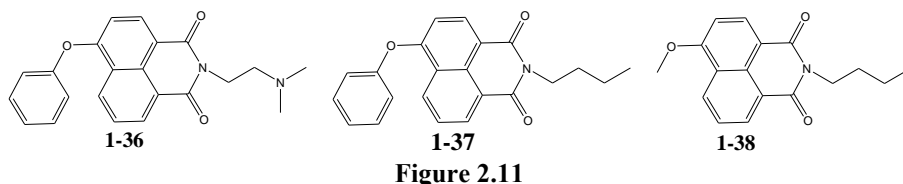
λ_{abs} of the films of derivatives (**1-34, 1-35**)a-c were red shifted relative to those of the dilute solutions. $E_{\text{g}}^{\text{opt}}$ for the derivatives (**1-35**)a-c varied from 3.06 eV to 3.14 eV. The values of $\log \varepsilon$ of the derivatives were high and ranged from 4.214 to 4.35. λ_{em} for the films of compounds (**1-35a-c**) were red shifted by 38–54 nm compared to those observed for the dilute solutions. The highest Φ_{F} value was found for the solution of compound **1-35c** ($\Phi_{\text{F}} = 0.37$) in chloroform. The calculated energy yields (E_{F}) of fluorescence were in the range of 0.09–0.311, which could be used instead of Φ_{F} ($E_{\text{F}} = \Phi_{\text{F}} \frac{\lambda_{\text{abs}}}{\lambda_{\text{em}}}$). T_{ID} corresponding to 5% and 10% weight losses were in the temperature range 260–275 °C and 278–308 °C, respectively for compounds (**1-34, 1-35**)a-c, and the T_{m} of the derivatives (**1-34, 1-35**)a-c were high and were in the range of 135–271 °C. IP_{CV} values of the molecules (**1-35**)a-c were in the range of 6.30–6.36 eV and $E_{\text{g}}^{\text{elc}}$ values were in the range of 2.93–3.0 eV. For this series of compounds (**1-35**)a-c IP_{CV} values were higher compared to earlier described HOMO energy level of compounds **1-31 – 1-33** [58].

Table 2.6. Properties of 1,8-naphthalimide derivatives

Material	T_{ID} , (°C)	T_{m} , (°C)	λ_{abs} , (nm) in CHCl_3 sol/solid film	λ_{em} , (nm) in CHCl_3 sol/solid film	Φ_{F} in CHCl_3 sol	E_{g}^{op} , (eV)	$E_{\text{g}}^{\text{elc}}$, (eV)	IP_{CV} , (eV)	E_{AC} , (eV)
1-34a	260 (278)	160	355 (365)	424 (462)	0.27	3.08	2.93	6.36	-3.43
1-34b	274 (293)	199	355 (368)	414 (468)	0.19	3.06	2.97	6.36	-3.39
1-34c	270 (308)	230	352 (368)	413 (463)	0.55	3.12	2.94	6.34	-3.40
1-35a	268 (287)	135	352 (363)	419 (457)	0.12	3.13	3.00	6.31	-3.31
1-35b	275 (293)	168	353 (364)	411 (465)	0.11	3.10	2.99	6.30	-3.31
1-35c	264 (294)	271	351 (368)	410 (460)	0.37	3.14	3.00	6.35	-3.35

T_{m} – melting transition temperature; T_{g} – glass-transition temperature; T_{ID} – decomposition temperatures at 5% and 10% (in parantheses) weight loss; λ_{abs} – maximum absorption wavelength; λ_{em} – maximum emission wavelength; Φ_{F} – fluorescence quantum yield; IP_{CV} – ionization potential; E_{AC} – electron affinity; $E_{\text{g}}^{\text{elc}}$ – electrochemical band gap; $E_{\text{g}}^{\text{opt}}$ – optical band gap.

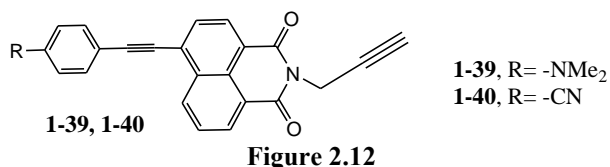
Marinova and co-workers [61] synthesized and studied three derivatives of 4-phenoxy- and 4-alkoxy-substituted 1,8-naphthalimides (**1-36** – **1-38**) (Fig. 2.11).



Compounds **1-36** – **1-38** showed the ϵ higher than 10000 l/mol·cm. Φ_F value of solvents with different polarity of compound **1-36** was lower those of the solutions of compounds **1-37** and **1-38**. Φ_F of compound **1-36** was low in toluene compared with that observed for the chloroform solution which is not consistent with the behaviour of other naphthalimides in organic solvents with different polarity. In polar organic solvents the Φ_F of naphthalimides were found to be lower ($\Phi_F = 0.003$ – 0.879) than those observed for the solutions in non-polar solvents ($\Phi_F = 0.004$ – 0.920). Compound **1-38** showed significantly less dependent on the solvent nature Φ_F compared to the compound **1-37**. The Stokes shift values of compounds **1-36** – **1-38** were in the range of 59–79 nm.

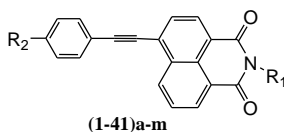
2.1.2. 4-Ethynyl- and 4-ethenyl-substituted 1,8-naphthalimides

The synthesis and fluorescence properties of donor-acceptor 4-ethynyl naphthalimides (**1-39** and **1-40**) were reported [62] (Fig. 2.12).



Increasing solvent polarity from hexane to DMSO, λ_{abs} of compounds **1-39** and **1-40** was red shifted (~ 14 – 24 nm). For compound **1-40**, a blue shift of ~ 17 nm of the absorption band was observed changing the solvent from dioxane to trifluoroethanol. As the solvent polarity increased a strong red shift of ca. 140 nm was observed in the FL spectra of compound **1-39** with the decrease in both the fluorescence intensity and Φ_F . No emission was observed when polarity of the solvent increased to that of methanol. The emission spectra of the solid films of compound **1-39** revealed a strong emission with a Stokes shift of 161 nm. The time resolved fluorescence of **1-39** in solid state showed a longer life time ($\tau = 5.59$ ns) compared to its solution state ($\tau = 1.38$ – 2.05 ns). The gas phase/solution phase E_g^{opt} (2.6–2.7 eV) remained very close to that of a band gap of an organic semiconductor [63]. For naphthalimide **1-40**, on changing the solvent polarity from cyclohexane to trifluoroethanol, both the intensity and Φ_F of emission increased with red shift of ~ 50 nm. For compound **1-39**, Φ_F value decreased with increase in solvent polarity. Time dependent DFT calculation [64] revealed that the emissive state of compound **1-39** was characterized with more significant electron redistribution.

Another series of *N*-alkyl-1,8-naphthalimide derivatives (**1-41**)**a-m** with phenylacetylene moiety at the C4 position were reported [16] (Fig. 2.13).



Comp.	1-41												
	a	b	c	d	e	f	g	h	i	j	k	l	m
R ₁	<i>n</i> -propyl	<i>n</i> -butyl	<i>n</i> -butyl	<i>n</i> -butyl	<i>n</i> -butyl	<i>n</i> -butyl	<i>n</i> -hexyl	<i>n</i> -hexyl	<i>n</i> -hexyl	<i>n</i> -hexyl	<i>n</i> -hexyl	(CH ₂) ₃ OCH ₃	(CH ₂) ₃ OCH ₃
R ₂	-H	-H	-OCH ₃	-OCH ₃	-Cl	-CN	-H	-CH ₃	-OCH ₃	-Cl	-CN	-H	-CH ₃

Figure 2.13

The same pattern was observed for compounds **1-41c**, **1-41h**, **1-41m**. The highest T_m was observed for the compounds having cyano group at the *p*-position of the phenylacetylene moiety (228 °C for **1-41f** and 193 °C for **1-41k**). For compounds **1-41d** and **1-41i**, the λ_{abs} was observed at the longest wavelengths (399 nm). Compounds containing chlorine atoms (**1-41e** and **1-41j**) or cyano group (**1-41f** and **1-41k**) at the *p*-position of the phenylacetylene moiety, showed blue-sifted absorption spectra with λ_{abs} at 374 nm and at 372 nm, respectively. Compounds **1-41d** and **1-41i** showed yellow fluorescence with the intensity maxima at 531–533 nm, and a great Stokes shifts (132 and 134 nm, respectively), while compounds **1-41f** and **1-41k** exhibited smaller Stokes shift (56 nm). Φ_F of (**1-41**)**a-m** in dilute DMF solutions were found to be from 0.25 to 0.75.

Table 2.7. Properties of *N*-alkyl-1,8-naphthalimide derivatives

Material	T_m , (°C)	λ_{abs} , (nm)	λ_{em} , (nm)	Φ_F	Stokes shift, (nm)
1-41a	166	374	447	0.70	73
1-41b	146	374	446	0.71	72
1-41c	170	380	462	0.75	82
1-41d	156	399	531	0.27	132
1-41e	160	374	446	0.72	72
1-41f	228	372	428	0.25	56
1-41g	121	375	446	0.70	71
1-41h	133	379	462	0.69	83
1-41i	134	399	533	0.37	134
1-41j	142	374	450	0.65	76
1-41k	193	372	428	0.25	56
1-41l	140	374	450	0.65	76
1-41m	139	378	462	0.67	84

λ_{abs} – maximum absorption wavelength; λ_{em} – maximum emission wavelength; Φ_F – fluorescence quantum yield.

A series of donor-spacer-acceptor compounds (**1-42** – **1-50**), and their fluorescence and electrochemical properties were reported [65] (Fig. 2.14).

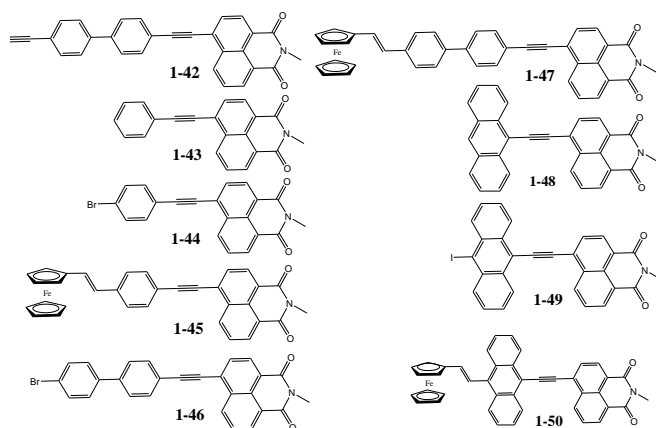


Figure 2.14

Compounds (**1-42 – 1-50**) showed reversible or quasi-reversible one-electron reduction processes in the CV experiments and they were in the range from -1.03 to -1.09 V. For compounds **1-42 – 1-50**, the broad absorption bands with λ_{abs} being in the ranges of $280\text{--}370$ nm and of $375\text{--}477$ nm were assigned to $\pi\text{--}\pi^*$ transitions of the *p*-band of the aryl group and the naphthalimide, respectively [66]. The absorption of ferrocenyl-containing compound **1-45** was stronger and red-shifted compared to that of compounds **1-44**, **1-46** and **1-47**. Φ_{F} values in DCM obtained for compounds **1-45**, **1-47** and **1-50** were low ($\Phi_{\text{F}} < 0.01$). In all cases, attachment of a ferrocenyl moiety to compounds **1-45**, **1-47**, **1-50** resulted in significant intramolecular quenching of the fluorescence [67].

By variation of the linking topology at the phenyl groups, four naphthalimide compounds (**1-51 – 1-54**) with 0, 1, and 2 *meta* linkages were reported [68] (Fig. 2.15).

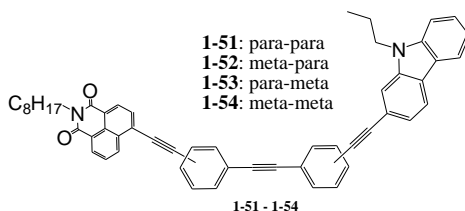


Figure 2.15

As the number of *meta* linkages in the phenylacetylene moiety increased from 0 to 2, the two-photon cross section decreased by almost 1 order of magnitude. Each additional *meta* linkage reduced the two-photon cross section by about a factor of 3, mainly due to the decreased ability of the ground-state bridge to support charge transfer between the donor and acceptor moieties. In all the molecules, the absorption was red-shifted relative to the absorptions of the donor carbazole (365 nm) and the acceptor naphthalimide (345 nm). The toluene solutions of compounds **1-51 – 1-54** exhibited small Stokes shifts and the FL spectra exhibited vibronic features. As the solvent became more polar, the emission broadened and shifted to the longer wavelength. Φ_{F} of **1-51 – 1-54** in dilute toluene solutions were found to 28

be from 0.14 to 1.00. In more polar solvents the Φ_F dropped, suggesting that the fluorescence was being quenched by an intramolecular electron transfer which became more favorable in polar solvents.

Jin *et al.* [69] reported a series of naphthalimide derivatives (**1-55** – **1-62**) and their theoretical properties were investigated (Fig. 2.16).

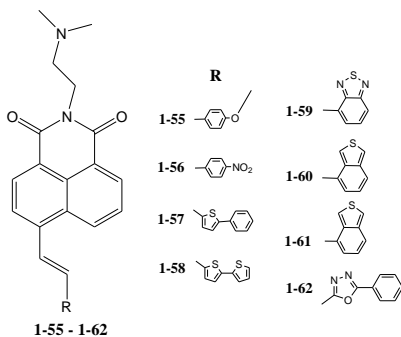


Figure 2.16

Table 2.8. Electrochemical characteristics of compounds **1-55** – **1-62**

Compound	IP _{CV} , eV	EA _{CV} , eV	E _g ^{opt} , eV
1-55	6.899	-1.279	5.610
1-56	7.305	-1.815	5.490
1-57	6.832	-1.439	5.393
1-58	6.753	-1.476	5.277
1-59	7.217	-1.696	5.521
1-60	6.605	-1.360	5.244
1-61	7.273	-1.898	5.374
1-62	7.258	-1.645	5.613

The theoretical values of IP_{CV} values for compounds **1-57**, **1-58**, and **1-60** increased, while EA_{CV} values decreased compared with those of compound **1-55** (Table 2.8). E_g^{opt} values of derivatives **1-55** – **1-62** decreased compared with that of compound **1-55**. The results were all in agreement with experimental results [70], with the maximum deviation being less than 33 and 120 nm. The HOMO→LUMO excitations dominated in compounds **1-55** and **1-57** – **1-60**, while the HOMO-1→LUMO excitations dominated in compounds **1-56**, **1-61**, and **1-62**. λ_{abs} values of compounds **1-57** – **1-61** had bathochromic shifts of 7–30 nm, while compounds **1-56** and **1-62** showed hypsochromic shifts of 8 and 7 nm referring to the spectrum of **1-55**, respectively. λ_{em} values of compounds **1-57** – **1-61** showed bathochromic shifts 49, 64, 24, 40, and 64 nm, while the values of derivatives **1-56** and **1-62** showed hypsochromic shifts 9 and 11 nm, respectively compared with that of compound **1-55**.

Two compounds with the donor-acceptor structure **1-63** and **1-64** [56] for memory devices were reported [72] (Fig. 2.17).

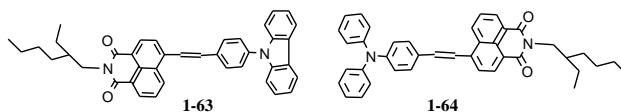


Figure 2.17

Both compounds exhibited high thermal stability with T_{ID} of 323 °C (for **1-63**) and 407 °C (for **1-64**). The ICT absorption peaks of the films were red-shifted ($\Delta\lambda_{\text{abs}} = 13$ nm for **1-63**, and $\Delta\lambda_{\text{abs}} = 10$ nm for **1-64**) compared with the absorption spectra of the solutions of the same compounds. E_g^{opt} of the films of compounds **1-63** and **1-64** was 2.51 and 2.19 eV, respectively. IP_{CV} and EA_{CV} values were determined to be 5.66 eV (or 5.22 eV) and -3.15 eV (or -2.54 eV) for the **1-63** (or **1-64**). IP_{CV} values of **1-63** and **1-64** were higher compared to other donor-acceptor structures **1-55** – **1-62** [69]. The memory device based on **1-63** exhibited much better characteristics

than that based on **1-64** due to the presence of rigid carbazole moiety in favor of improving the surface morphology, which was revealed by atomic force microscopy measurement.

Mikroyannidis and co-workers [73] reported two linear divinylenes **1-65** and **1-66** that contained fluorene and phenylene, as central unit and naphthalimide moieties as the terminal groups (Fig. 2.18).

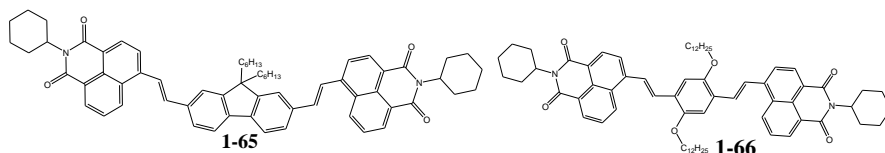


Figure 2.18

The values of T_{ID} **1-65** and **1-66** were 362 and 410 °C, respectively, and T_g followed the trend **1-65** (45 °C) > **1-66** (42 °C). E_g^{opt} values of **1-65** (2.55 eV) and **1-66** (2.48 eV) were comparable with that of poly(9,9-dioctylfluorene-2,7-vinylene) [74] (2.6 eV) and higher than that of MEH-PPV [74] (2.21 eV). **1-65**, **1-66** showed close Φ_F values (0.10–0.15). IP_{CV} values were 5.37 and 5.54 eV, and EA_{CV} values were –2.89 and –2.99 eV, respectively. Double-layer electroluminescent devices with the configuration of ITO/PEDOT:PSS (30 nm)/PVK:(25%)emitter (75 nm)/TPBI (25 nm)/LiF (0.5 nm)/Al (200 nm) were fabricated. The devices based on **1-65** and **1-66** showed the similar current efficiency of 0.15–0.10 cd/A. For the device based on **1-65**, the maximum luminance of 143 cd/m² are comparable to that of 124 cd/m² based on **1-66**.

Green host compounds (**1-67** – **1-69**) containing the naphthalimide moieties were reported [75] (Fig. 2.19).

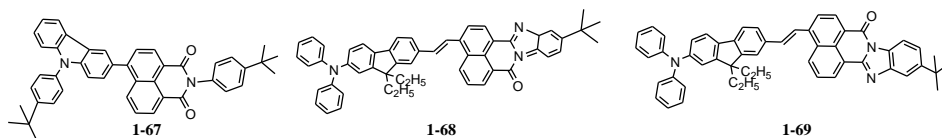


Figure 2.19

λ_{abs} of dilute DCM solution of compound **1-68** was red-shifted by 10 nm compared with the absorption spectra of the solution of compound **1-69**. Although **1-68** and **1-69** exhibited the similar fluorescence properties with respect to both emission color and Φ_F of dilute solutions, Φ_F of their solid films were differed. The value of Φ_F of compound **1-69** was by ca. 10 times higher than that of **1-68** [76]. The solid films of **1-69** also displayed higher Φ_F than those of **1-68**. Both compounds exhibited high T_{ID} (higher than 400 °C). T_g of the two compounds was not identified, however high melting points (>290 °C) were observed. IP_{CV} values of **1-69** and **1-67** were calculated to be 5.38 eV and 5.67 eV, respectively. EA_{CV} values of –3.14 eV and –2.99 eV were deduced for **1-69** and **1-67**, respectively. T_{ID} , IP_{CV} and EA_{CV} values of compounds **1-67**, **1-69** were comparable with compounds **1-63** – **1-66** [75,77]. OLEDs employing **1-69/1-67** as the guest/host pair were fabricated. The configuration of the devices were: ITO/NPB (30 nm)/CBP (2 nm)/**1-67:1-69** (x

wt%) (20 nm)/Bphen (40 nm)/Mg:Ag (200 nm), *N,N'*-diphenyl-*N,N'*-bis(1-naphthyl)-(1,10-biphenyl)-4,4'-diamine (NPB), Bphen, **1-69/1-67**, Mg/Ag, 4,4'-bis(9*H*-carbazol-9-yl)biphenyl. Devices I and II represented OLEDs with **1-69** blending ratio of 3 wt% and 6 wt%, respectively. The turn-on voltages of device I and II were 5.2 V and 4.1 V, respectively. Device II showed higher current at the similar driving voltages (<13 V) relative to device I.

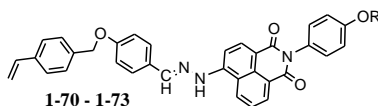
Table 2.9. Properties of 1,8-naphthalimide derivatives

Material	T _{ID} , (°C)	λ _{abs} , (nm)	λ _{em} , (nm)	Φ _F in sol/solid film	IP _{CV} , (eV)	EA _{CV} , (eV)
1-67	419	NM	NM	NM	5.67	-2.99
1-68	NM	477	477	0.004/0.016	NM	NM
1-69	423	468	466	0.005/0.153	5.38	-3.14

λ_{abs} – maximum absorption wavelength; λ_{em} – maximum emission wavelength; Φ_F – fluorescence quantum yield; IP_{CV} – ionization potential; EA_{CV} – electron affinity.

2.1.3. 1,8-Naphthalimide moiety containing hydrazones and Schiff bases

Four naphthalimides (**1-70** – **1-73**) containing hydrazone moieties were synthesized and investigated [78] (Fig. 2.20).

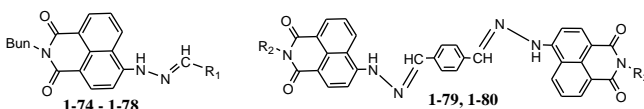


Compound	1-70	1-71	1-72	1-73
R	-C ₃ H ₇	-C ₆ H ₁₃	-C ₉ H ₁₉	-C ₁₂ H ₂₅

Figure 2.20

The emission bands of **1-70** – **1-73** were similar and red shifted by ca. 20 nm in comparison with that of naphthalimide group. Meanwhile, the intensity of fluorescence was enhanced compared with naphthalimide group and this was assigned to the significant ICT and larger conjugation due to the presence hydrazone moiety. These compounds possessed the similar non-linear optical properties because of their similar structure. E_g^{opt} of compounds **1-70** – **1-73** were similar, ranging from 3.182 to 3.184 eV. In the HOMO of **1-70** – **1-73**, the electrons were distributed throughout the whole molecule, while in the LUMO, the electrons were mainly concentrated on naphthalimide moiety.

Gan and co-workers [79] reported naphthalimide derivatives containing Schiff base moiety (Fig. 2.21).



Comp.	1-74	1-75	1-76	1-77	1-78	1-79	1-80
R ₁	-CH ₃	-phenyl	4-methoxyphenyl	-anthracenyl	4-dimethylaminophenyl	–	–
R ₂	–	–	–	–	–	<i>n</i> -butyl	<i>n</i> -C ₁₂ H ₂₅

Figure 2.21

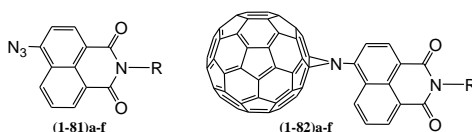
By extending the conjugation length, the fluorescent lifetimes of the solutions of **1-75** and **1-77** in THF decreased to 4.71 and 0.29 ns, respectively, in comparison with that of **1-74** (7.4 ns). The similar trend was evident for compounds **1-76** and **1-78**. λ_{abs} of **1-75** – **1-80** in acetonitrile were red-shifted by 10, 22, 33, 46, 54, and 55 nm, respectively with respect of that of **1-74**. λ_{em} of the solid films of compounds **1-76** – **1-80** were shifted to longer wavelengths with respect of that of **1-75**. When a methoxyl group was attached to the *para* position of the benzene ring, the λ_{em} of the solid film of **1-76** was red shifted. The emission of the film of compound **1-77** showed a red-shift of more than 110 nm compared to that of **1-74**. IP_{CV} values of naphthalimides **1-75** – **1-80** were in the range of 6.9–7.3 eV. OLEDs with the structure ITO/CuPc (12 nm)/(NPB 30 nm)/**1-77**/sodium stearate (2 nm)/Al (100 nm) were prepared. The device with a 45 nm thick **1-77** film had maximum luminance of 15.5 cd/m² and a maximum current density of 2.9 mA/cm² at an applied voltage of 22 V. Turn-on voltage of this EL device was 14 V. In the same device structure, the organic photovoltaic properties containing **1-77** with a 1.1 V voltage and a 5 $\mu\text{A}/\text{cm}^2$ current density were observed, when the device was irradiated by the quartz light at 50 W.

Table 2.10. Properties of 1,8-naphthalimide derivatives

Material	τ , (ns)	λ_{abs} , (nm)	λ_{em} , (nm) in sol/solid film
1-74	7.40	431	521/545
1-75	4.71	441	527/558
1-76	4.21	453	546/643
1-77	0.29	464	564/661
1-78	0.23	477	659/ND
1-79	1.91	485	536/618
1-80	1.94	486	517/620

λ_{abs} – maximum absorption wavelength; λ_{em} – maximum emission wavelength; τ – fluorescent decay time constant; ND – not detectable.

A series of 4-aziridino[C₆₀]fullerene-1,8-naphthalimide compounds ((**1-81** – **1-82**)**a-f**) and their spectroscopic properties were reported [80] (Fig. 2.22).



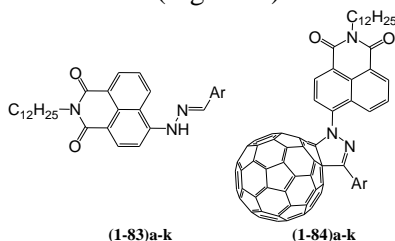
Comp.	(1-81 , 1-82)a	(1-81 , 1-82)b	(1-81 , 1-82)c	(1-81 , 1-82)d	(1-81 , 1-82)e	(1-81 , 1-82)f
R	-C ₈ H ₁₇	-C ₁₂ H ₂₅	-C ₁₆ H ₃₃	-C ₂ H ₅ OC ₆ H ₄	-CH ₃ C ₆ H ₄	-C ₆ H ₅

Figure 2.22

Geometrical optimization was performed with semiempirical methods using PM3 parametrization with Hyperchem 7.5. The alkyl group was found to be the tail of the planar naphthalimide core (**1-82**)**a-f**, but the phenyl group was nearly perpendicular to the planar naphthalimide core, minimizing steric hindrance between phenyl group and the imide functionality. The plane of the phenyl spacer was oriented out of the naphthalimide plane. The absorption of dilute solutions of

compound **1-82d** was much stronger than that of **1-82b**, which indicated that the substituent (**R**) on the naphthalimide moiety has an obvious influence on the absorption feature. The fluorescence of the solution of compound **(1-82)d-f** was subjected to a strong quenching relative to that of the derivative **1-81d**.

The same scientific group [81] also reported the synthesis of 4-aziridino[C₆₀]fullerene-1,8-naphthalimide under microwave irradiation [80] and the first comparative study of the fluorescence properties of pyrazolo- and aziridino-fullerene (**1-83 – 1-84**)a-k derivatives (Fig. 2.23).

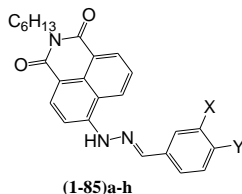


Ar	-C ₆ H ₅	-C ₆ F ₅	4-NO ₂ C ₆ H ₄	4-Me ₂ NC ₆ H ₄	4-EtOC ₆ H ₄	4-FC ₆ H ₄	4-CIC ₆ H ₄	4-BrC ₆ H ₄	2,4-2FC ₆ H ₃	2,4-2FC ₆ H ₃	4-CNC ₆ H ₄
C ₆₀	(1-83, 1-84)a	(1-83, 1-84)b	(1-83, 1-84)c	(1-83, 1-84)d	(1-83, 1-84)e	(1-83, 1-84)f	(1-83, 1-84)g	(1-83, 1-84)h	(1-83, 1-84)i	(1-83, 1-84)j	(1-83, 1-84)k

Figure 2.23

The UV-Vis spectra of compounds **(1-84)a,b,e** and **1-82b** [65] had two main λ_{abs} appearing at ~254 and 326 nm. λ_{em} for compounds **(1-84)a,b,e** were blue-shifted by 60–100 nm relative to the hydrazones **(1-83)a-k**, and the fluorescence of **(1-84)a-k** was quenched. DFT framework calculations were performed at the B3LYP/6-31G level. The electron density of the HOMO level of hydrazone **1-84a** and **1-84b** was found to be delocalized among the naphthalimide moiety and pyrazole ring, whereas the electron density of the LUMO level was located in the C₆₀ cage [82]. IP_{CV} values of **(1-84)a-k** were higher in energy relative to C₆₀ (9.48 eV). EA_{CV} values of compounds **(1-84)a-k** were lower than that of C₆₀ (–2.88 eV). The natural bonding orbitals of compounds **(1-84)a,b** were calculated and it was found that the sp₃ nitrogen atom in the pyrazole ring plays a key role in the charge transfer process.

Ivanov *et al.* [83] reported a series of aryl-substituted hydrazones (**(1-85)a-h**, Fig. 2.24).



Comp.	1-85a	1-85b	1-85c	1-85d	1-85e	1-85f	1-85g	1-85h
X	-N(OCH ₃) ₂	-OCH ₃	-CH ₃	H	-Cl	-CN	-NO ₂	-OCH ₃
Y	-H	-H	-H	-H	-H	-H	-H	-OCH ₃

Figure 2.24

For compound **1-85a** intensive red fluorescence was observed, while the *p*-nitro substituted compound **1-85g** did not fluorescence. For the solid samples the spectral shapes of aryl-substituted hydrazones (**1-85a-h**) were similar to each other. The emission band of **1-85a** was situated in the red light area. The *p*-cyano substituted compound **1-85f** showed a small (7 nm) hypsochromic shift. FL spectra of the films of compounds (**1-85a-h**) were red-shifted by 33–76 nm compared to those of the solutions.

2.1.4. 4-Heteroaromatic-substituted 1,8-naphthalimides

A series of naphthalimides with different electron-donating, electron-withdrawing, or aromatic substituent groups (**1-86 – 1-94**) were reported [84] (Fig. 2.25).

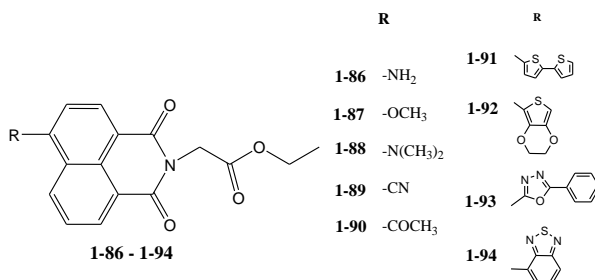


Figure 2.25

TDB3LYP calculated λ_{abs} and λ_{em} values of **1-86** were in agreement with experimental results, with the deviations being 17 and 2 nm, respectively. Stokes shift of compound **1-86** was 82 nm, which is comparable to the experimental one (63 nm). λ_{em} values of derivatives **1-86** and **1-87 – 1-94** (ranged from 0.361 to 0.525 eV) were larger than that of Alq₃ [85] (0.276 eV). The calculated reorganization energies for hole (λ_{h}) values of **1-86** (0.455 eV) and compounds **1-87**, **1-88**, **1-90 – 1-92**, and **1-94** (ranged from 0.341 to 0.636 eV) were larger than that of TPD, which is a typical hole transport material ($\lambda_{\text{h}} = 0.290$ eV) [86]. λ_{h} value of compound **1-89** (0.202 eV) was smaller than that of TPD, while the value of **1-93** (0.295 eV) was almost equal to that of TPD. It indicates that the hole transfer rate of **1-93** may be higher than that of TPD and the hole transfer rate of **1-93** may equal to that of TPD. Derivatives **1-87 – 1-94** had nearly equal values of absolute hardness (η , ranging from 2.695 to 3.365), being almost equal to that of **1-86** ($\eta = 3.208$). These results revealed that the different substituent groups did not affect the stability of these molecules.

The similar derivatives of *N*-butyl-1,8-naphthalimides for organic optoelectronics (**1-95 – 1-103**) also were reported [87] (Fig. 2.26).

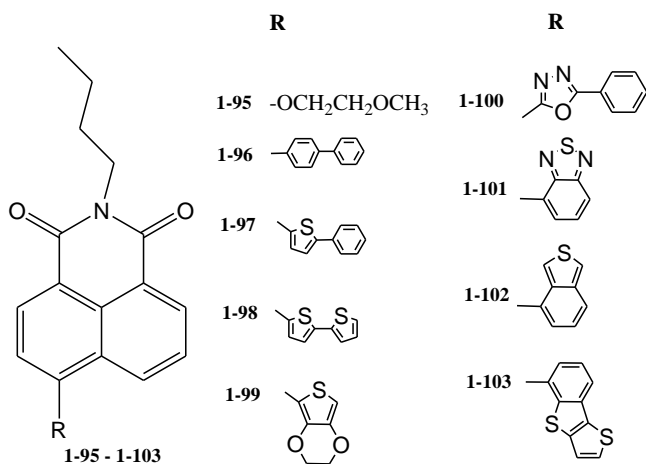


Figure 2.26

The values of λ_{abs} and λ_{em} of **1-96** – **1-103** showed bathochromic shift compared with that of the compound **1-95** having aliphatic substituent at nitrogen atom. The Stokes shifts of compounds **1-96** – **1-103** were 82, 114, 120, 95, 68, 97, 90, and 72 nm, respectively. The values of reorganization energies for electron (λ_{e}) and λ_{h} of the molecules were predicted from the single point energy at the B3LYP/6-31G(d,p) level based on the CAM-B3LYP/6-31G(d,p) optimized neutral, cationic, and anionic geometries. λ_{e} values of **1-95** (0.365 eV) and compounds **1-96** – **1-103** (ranged from 0.361 to 0.415 eV) were larger than that of Alq₃ ($\lambda_{\text{e}} = 0.276$ eV). The calculated λ_{h} values of **1-95** and **1-96** – **1-101** (ranged from 0.327 to 0.527 eV) were comparable with compounds **1-86** – **1-94** [84] and were larger than that of TPD ($\lambda_{\text{h}} = 0.290$ eV). λ_{h} values of derivatives **1-102** and **1-103** (0.268 and 0.222 eV) were smaller than that of TPD (0.364). This observation indicated that the hole transfer rates of **1-95** and **1-96** – **1-101** might lower while the corresponding characteristic of compounds **1-102** ($\lambda_{\text{h}} = 0.268$) and **1-103** ($\lambda_{\text{h}} = 0.222$) might higher than that of TPD.

Zhengen *et al.* [88] reported a series of *N*-alkyl-1,8-naphthalimides ((**1-104**)a-k) with a thiophene rings at C4 position (Fig. 2.27).

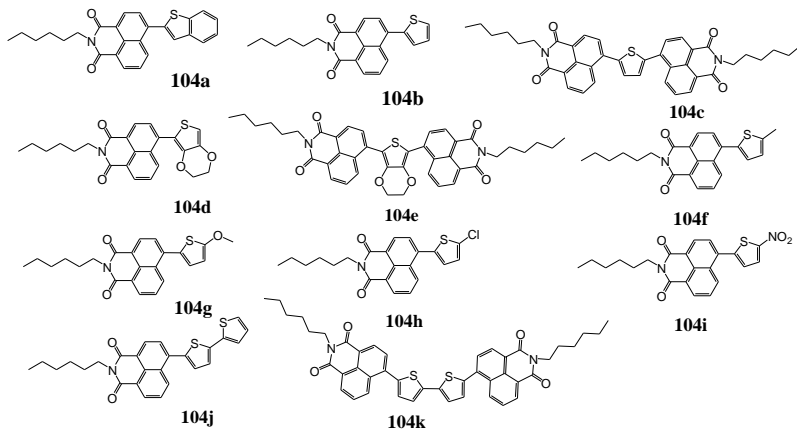


Figure 2.27

The value of λ_{abs} of compounds **(1-104)c,e,k** were bathochromically shifted for ca. 10–30 nm [16] compared with those of compounds **(1-104)b,d,j**. Due to the strong electron-accepting ability of nitro group on the thiophene ring, compound **1-104i** exhibited no fluorescence. λ_{em} values of compound **1-104a** and compound **1-104j** were red shifted ~ 7 nm and 69 nm, respectively compared with that of compound **1-104b**. Compound **1-104k** exhibited a yellow fluorescence with the λ_{em} at 542 nm. Among all the compounds, **(1-104)d,f,g** in dilute chloroform solutions had relatively longer fluorescence lifetime 3891, 5571 and 3885 ps, respectively.

Three compounds containing naphthalimide acceptor and *N*-aryl donors (**1-105** – **1-107**) were reported [89] (Fig. 2.28).

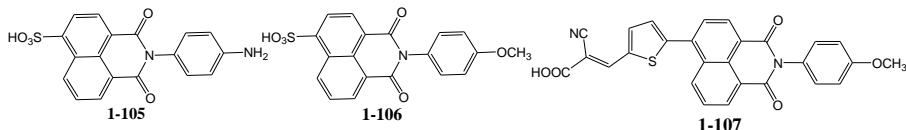


Figure 2.28

Compounds **1-105** and **1-106** exhibited two major absorption bands at 350 and 450 nm, and compound **1-107** exhibited red-shifted absorption maxima at 439 nm and 672 nm, respectively. EA_{CV} (-3.67 – -3.19 eV) and IP_{CV} values (6.01–6.43 eV) of compounds **1-105** – **1-107** were obtained.

Xiao and co-workers [90] reported derivatives of naphthalimide and spirobifluorene (**1-108**, **1-109**, Fig. 2.29).

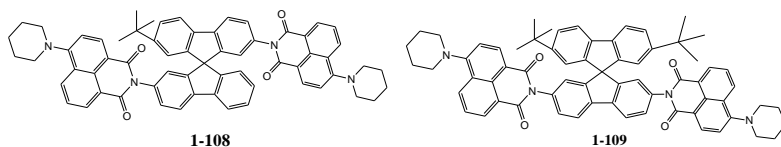


Figure 2.29

FL spectra of **1-108** and **1-109** showed red-shifts going from low-polarity to high-polarity solvents along with the decreased fluorescence intensity. **1-108** and **1-109** were highly stable as they only started to decompose around 451, 430 °C, respectively [91]. $E_{\text{g}}^{\text{opt}}$ (2.48, 2.49 eV), and IP_{CV} (5.81, 5.85 eV) and EA_{CV} values (-3.36 , -3.34 eV) of derivatives **1-108** and **1-109** were obtained.

The same scientific group [92] reported a series of naphthalimide derivatives containing thiophene and pyrazole moieties (**(1-110 – 1-111)a-d**, Fig. 2.30).

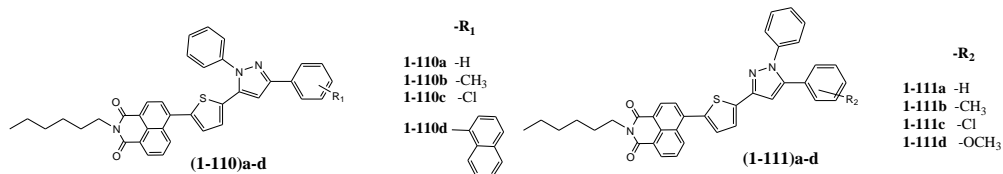


Figure 2.30

Compounds **(1-111)a-d** have a maximum absorption bathochromic shift of ~ 12 – 20 nm in DCM solution compared with **(1-110)a-d**. **(1-111)a-d** exhibited a bathochromic shift of nearly 2–6 nm relative to that of **(1-110)a-d**. λ_{em} of

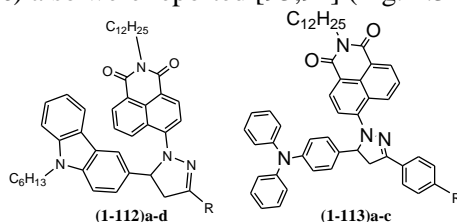
compounds **(1-111)a-d** showed a bathochromic shift of ~7–18 nm compared with those of **(1-110)a-d**. Compounds **(1-110)a-d** showed Φ_F values in solutions ranging from 0.15 to 0.18, and **(1-111)a-d** had Φ_F ranging from 0.33 to 0.38. For compounds **1-110a** and **1-111a** both UV-Vis absorption and emission spectra were red-shifted with the increase of solvent polarity. EA_{CV} and IP_{CV} values were -3.30 eV, 5.85 eV for **1-111a** and -3.34 eV, 5.81 eV for **1-111a**. For other compounds, EA_{CV} values ranged from -3.29 eV to -3.49 eV, and IP_{CV} values ranged from 5.34 eV to 5.94 eV. The ground-state geometry of the compounds was optimized by hybrid density functional theory (B3LYP) with 6-31G* basis set in the Gaussian 03 program package [64]. The HOMOs for **1-110a** and **1-111a** were localized at the thiophene-containing pyrazole moiety, the LUMOs were mainly located at the naphthalimide moiety.

Table 2.11. Properties of 1,8-naphthalimide derivatives

Material	λ_{abs} , (nm)	λ_{em} , (nm)	Φ_F	IP_{CV} , (eV)	EA_{CV} , (eV)
1-110a	388	517	0.16	5.85	-3.30
1-110b	389	519	0.18	5.94	-3.40
1-110c	389	519	0.15	6.04	-3.49
1-110d	389	515	0.16	5.81	-3.29
1-111a	400	519	0.35	5.81	-3.34
1-111b	402	521	0.36	5.94	-3.41
1-111c	402	517	0.33	5.79	-3.34
1-111d	403	521	0.38	5.85	-3.39

λ_{abs} – maximum absorption wavelength; λ_{em} – maximum emission wavelength; Φ_F – fluorescence quantum yield; IP_{CV} – ionization potential; EA_{CV} – electron affinity.

Several compounds containing naphthalimide and the pyrazoline moieties (**(1-112)a-d** and **(1-113)a-c**) also were reported [93,94] (Fig. 2.31).



Comp.	1-112				1-113		
	a	b	c	d	a	b	c
R	-phenyl	4-methoxyphenyl	4-nitrophenyl	-thiophenyl	-H	-OCH ₃	-Cl

Figure 2.31

Compounds **(1-112)a-d** and **(1-113)a-c** exhibited two prominent bands in the chloroform solution, appearing at 280–352 nm and 464–615 nm, respectively. λ_{abs} at 280–352 nm were attributed to the absorption of the carbazole moiety; λ_{abs} at 464–615 nm was attributed to naphthalimide moiety. The absorption and FL spectra of the solid films of these compounds were similar to the corresponding spectra of the solutions. For compound **1-112c**, the position of λ_{em} in the THF solution was red-shifted from 505 nm to 530 nm when the NO_2 functional group with the electron-

accepting ability was introduced [95]. Φ_F value of 0.96 was observed for the chloroform solution of derivative **1-113a**, which was higher than that of the other compounds. Φ_F of the other compounds were in the range of 0.40–0.41. This difference of Φ_F might be due to the change of the molecular size and the change of the electronic push-pull substitution of the conjugated part in the molecules [96]. Compounds (**1-113a-c**) showed distinct T_g at 133, 133 and 130 °C, respectively. Compounds showed high thermal stabilities with T_{ID} from 400 to 450 °C. IP_{CV} values of compounds (**1-112a-d**) and (**1-113a-c**) ranged from 4.95 to 5.88 eV, and the EA_{CV} values ranged from –2.65 to –1.83 eV, which were in agreement with the calculated values (from 5.07 to 5.62 eV for IP_{CV} , and from –2.65 to –2.05 eV for EA_{CV} values of compounds (**1-112a-d**) and (**1-113a-c**) and were comparable with earlier described compounds (**1-110a-d**, (**1-111a-d**) [92]. The ground-state geometry of the compounds were optimized by B3LYP with 6-31G* basis set in the Gaussian 03 program package [64]. For compound **1-113a**, the HOMO level was a p orbital concentrated on the central triphenylamino moiety, and the LUMO level was of p^* character distributed on the pyrazoline ring and naphthalimide ring.

Table 2.12. Properties of 1,8-naphthalimide derivatives

Material	T_{ID} , (°C)	T_g , (°C)	λ_{abs} , (nm) in sol/solid film	λ_{em} , (nm) in sol/solid film	Φ_F	IP_{CV} , (eV)	EA_{CV} , (eV)
1-112a	NM	NM	465	505	0.15	5.31	–2.13
1-112b	NM	NM	475	516	0.026	5.12	–2.05
1-112c	NM	NM	476	548	0.021	5.62	–2.65
1-112d	NM	NM	472	516	0.040	5.23	–2.14
1-113a	400	133	613/466	535/600	0.96	4.95	–1.83
1-113b	410	133	615/475	543/561	0.40	5.02	–2.07
1-113c	450	130	581/462	519/622	0.41	4.97	–1.85

T_{ID} – temperature of the onset of the thermal decomposition; T_g – glass-transition temperature; λ_{abs} – maximum absorption wavelength; λ_{em} – maximum emission wavelength; Φ_F – fluorescence quantum yield; IP_{CV} – ionization potential; EA_{CV} – electron affinity; NM – not measured.

Marinova *et al.* [97] reported on the synthesis of compounds **1-114** – **1-116** based on naphthalimide moieties (Fig. 2.32).

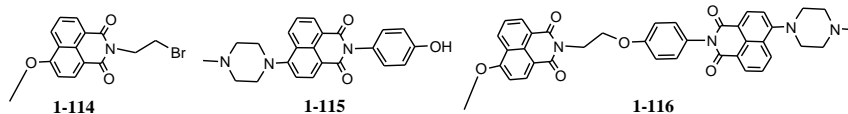


Figure 2.32

All of the compounds showed ϵ higher than 132 nm. In different solvents the Stokes shift values of compound **1-114** were between 64 nm and 117 nm. The DMF, chloroform and methanol solutions of compounds **1-115** and **1-116** exhibited low Φ_F values compared to 4-amino-1,8-naphthalimides [98]. Φ_F of methylpiperazinyl substituted naphthalimide **1-115** was highly solvent dependent. In polar media Φ_F of

1-114 – 1-116 was low ($\Phi_F = 0.005\text{--}0.012$), while in non-polar media Φ_F was higher ($\Phi_F = 0.185$).

A series of *N*-heteroaryl-1,8-naphthalimides ((**1-117**)**a-c**) were prepared and studied [99] (Fig. 2.33).

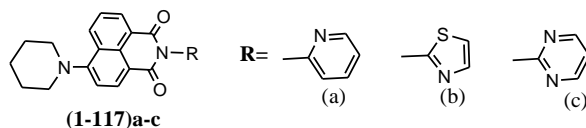


Figure 2.33

Changing of the solvents from cyclohexane to methanol led to the red shift of λ_{em} of compound **1-117c** by 75 nm. The Stokes shifts increased with increasing solvent polarity and Φ_F decreased [100]. The calculated λ_{abs} of compound **1-117c** in the gas phase (387 nm) correlated well with the experimental λ_{abs} in cyclohexane which had quite a low polarity (389 nm). The calculated λ_{em} was blue shifted, because the computations were performed without corrections for solvent effects. For compound **1-117c**, the dipole moment in the ground state was 4.31 D and the difference between the dipole moments of the first excited state and the ground states was 1.61 D.

Panchenko and co-workers [101] reported 4-amino- and 4-(acetyl)amino-*N*-aryl-1,8-naphthalimides containing aza-15-crown-5 ether moieties in the *N*-aryl fragment and at C-4 of the naphthalimide ((**1-118 – 1-120**)**a-c**, Fig. 2.34).

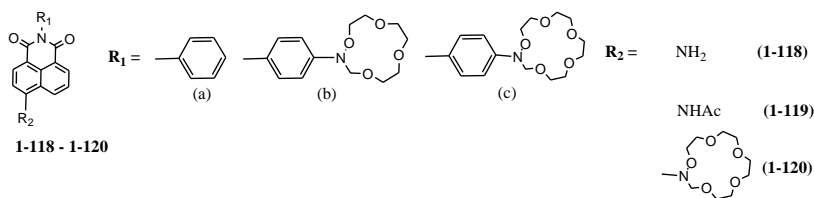


Figure 2.34

Substitution of amino hydrogen in (**1-118**)**a,b** by the acetyl group to produce (**1-119**)**a,b** caused a blue shift of λ_{abs} and λ_{em} with the changes in Φ_F . The introduction of aza-15-crown-5 ether substituent at C-4 of the naphthalene ring enhanced ICT interaction in the molecule and in the absorption spectra bathochromic shift (3 nm) was observed. As compared with compound **1-118a**, λ_{em} of **1-120a** was 22 nm red-shifted and the emission intensity decreased [100]. The relatively low Φ_F of compound **1-120a** in dilute acetonitrile with respect to that of **1-118a** was a result of conformational changes at the 4-amino moiety. The effect of decrease in emission intensity of compounds **1-118b** and **1-119b** could be explained in terms of photoinduced electron transfer quenching mechanism [102].

Another series of fluorescent naphthalimide compounds **1-121 – 1-123** with amines, alkoxides and thiols under microwave irradiation were reported [103] (Fig. 2.35).

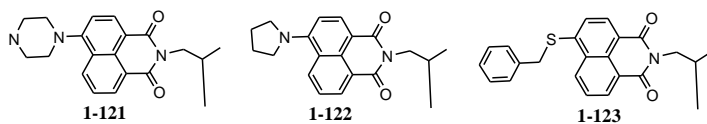


Figure 2.35

λ_{em} of **1-122** shifted from 490 nm to 524 nm as the solvent was changed from toluene to acetonitrile. The major difference that distinct **1-121** from **1-122**, was the presence of 5 member ring of pyrrolidine in **1-122** instead of 6 member ring of morpholine containing an oxygen atom. The aforementioned differences were the origin of some observations: ϵ of the **1-122** was greater than **1-121** in all of the examined solvents. While λ_{em} spectra of **1-121** and **1-122** were in the same range in different solvents, the absorption spectra showed a red-shifted for **1-122** compared to **1-121** in examined solvents. Φ_F of the solutions of compounds in ethyl acetate **1-121** – **1-123** was estimated experimentally 0.66, 0.74 and 0.71, respectively.

Ding and co-workers [9] also reported a series of naphthalimide derivatives containing a benzoazole moiety (**1-124** – **1-126**, Fig. 2.36).

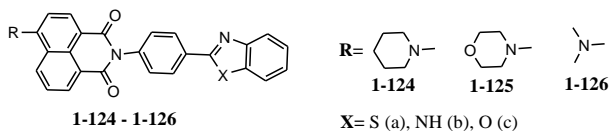


Figure 2.36

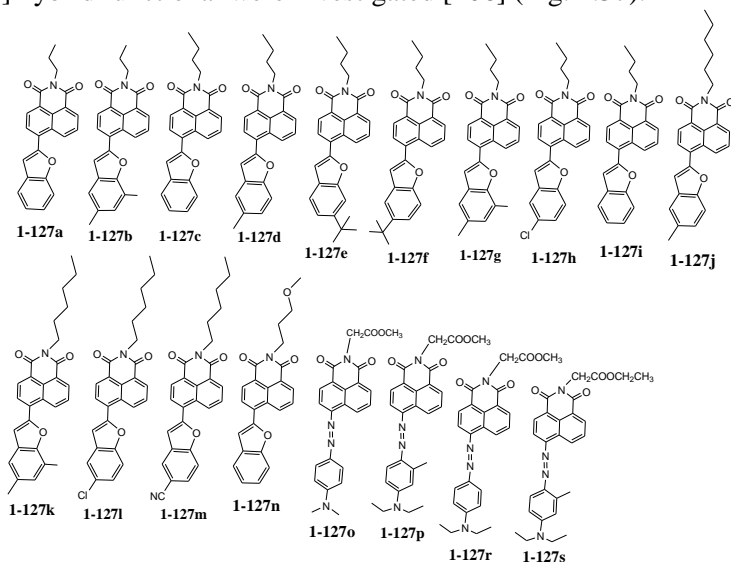
In chloroform solutions all compounds displayed strong fluorescence emission with λ_{em} of 511–521 nm. The optimized molecular structures of the compounds calculated using the MOPAC AM1 or PM 3 method showed that the benzoazole unit was twisted by the steric hindrance of carbonyl group of naphthalimide, with the dihedral angle between the plane of benzothiazole benzoazole and naphthalimide moieties. These compounds exhibited high Φ_F in solutions ranging from 0.4 to 0.8. IP_{CV} (5.51–5.68 eV) and EA_{CV} values (–3.12 – –2.61 eV) of the compounds were calculated. T_g of compound **1-125b** was found 150 °C. The electroluminescent devices ITO/NPB (75 nm)/emissive layer (65 nm)/Mg:Ag/Ag (100 nm) were fabricated. Compounds **1-124a**, **1-124b**, and **1-126a** were used as both emissive materials and electron transporters. The best performance was observed for the device based on **1-124a** with a maximum luminance of 4500 cd/m² (at 19 V) and a turn-on voltage of 10 V. Maximum luminance values of 1100 cd/m² (at 16 V) and 2119 cd/m² (at 17 V) were obtained for the devices containing **1-124b** and **1-126a**, respectively. The power efficiency of the device based on **1-124b** (0.26 lm/W) was the highest among the three devices, and power efficiency of **1-124a** and **1-126a** was identical (0.12 lm/W). The order of the current efficiency was as follows: **1-124b** (0.94 cd/A) > **1-124a** (0.65 cd/A) > **1-126a** (0.56 cd/A).

Table 2.13. Properties of 1,8-naphthalimide derivatives

Material	1-124a	1-124b	1-124c	1-125a	1-125b	1-125c	1-126a	1-126b	1-126c
T _m , (°C)	NM	355	NM	345	355	NM	NM	NM	329
T _g , (°C)	NM	NM	NM	NM	150	NM	NM	NM	177
λ _{em} , (nm)	521	518	521	513	513	511	512	513	512
Φ _F	0.80	0.7	0.71	0.74	0.71	0.75	0.53	0.48	0.54
IP _{CV} , (eV)	5.60	5.55	5.57	5.68	5.63	5.64	5.51	5.5	5.51
E _{ACV} , (eV)	-2.87	-2.61	-2.78	-2.63	-2.92	-2.89	-2.87	-3.26	-3.12
Maximum luminance (at 120 mA/cm ²)	4500	2119	NM	NM	NM	NM	1100	NM	NM
Turn-on voltage (V) (at 1 mA/cm ²)	10	7	NM	NM	NM	NM	6	NM	NM
Current efficiency (cd/A) (at 5 mA/cm ²)	0.65	0.94	NM	NM	NM	NM	0.56	NM	NM
Power efficiency (lm/W) (at 5 mA/cm ²)	0.12	0.26	NM	NM	NM	NM	0.12	NM	NM

λ_{abs} – maximum absorption wavelength; λ_{em} – maximum emission wavelength; Φ_F – fluorescence quantum yield; T_g – glass-transition temperature; IP_{CV} – ionization potential; E_{ACV} – electron affinity; E_g^{opt} – optical band gap; E_g^{elc} – electrochemical band gap; NM – not measured.

N-substituted 1,8-naphthalimide derivatives ((**1-127a-s**) and ((**1-128a-p**) by TDDFT and polarizable continuum TDDFT (PCM-TDDFT) with B3LYP [104] and PBE0 [105] hybrid functional were investigated [106] (Fig. 2.37).



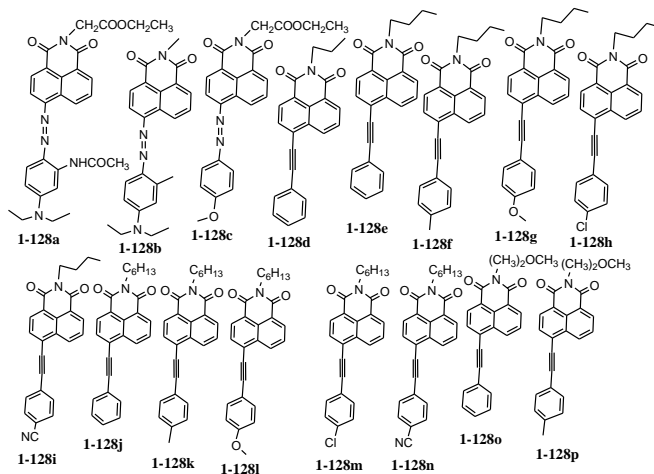
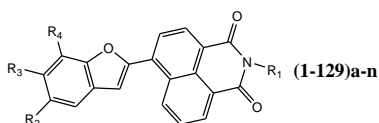


Figure 2.37

When the hydrogen atom at C-4 position was replaced by a benzofuran group, λ_{abs} of compounds (**1-127**)**a-n** was red-shifted. For compounds (**1-128**)**c-p**, the introduction of 4-arylacetylene group resulted in ~ 40 nm bathochromic shift. When the hydrogen atom was replaced by a monoazo phenyl group, λ_{abs} of compounds **1-127o** – **1-128c** was shifted to 530–550 nm. Theoretical values of TD-B3LYP (3.68–3.70 eV), PCM-TD-B3LYP (3.56–3.62 eV), PCM-TD-PBE0 (3.67–3.71 eV) were in good agreement with those observed in the experimental spectra (3.60–3.67 eV). The mean absolute error was 0.21 eV compared with the experimental spectra data. The theoretical excitation energies of compounds (**1-127**)**a-n** and (**1-128**)**d-p** were lower than those observed experimentally. For compounds **1-127o** – **1-128c**, the excitation energies calculated under cyclohexane or chloroform solvent environment was in good agreement with the experimental results.

Yang *et al.* [42] also reported on naphthalimides ((**1-129**)**a-n**) with a larger *p*-conjugated group at the C-4 position of the naphthalene moiety (Fig. 2.38).

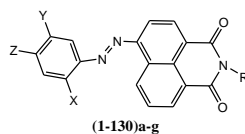


Co mp.	1-129													
	a	b	c	d	e	f	g	h	i	j	k	l	m	n
R₁	<i>n</i> -propyl	<i>n</i> -propyl	<i>n</i> -butyl	<i>n</i> -butyl	<i>n</i> -butyl	<i>n</i> -butyl	<i>n</i> -butyl	<i>n</i> -butyl	<i>n</i> -hexyl	<i>n</i> -hexyl	<i>n</i> -hexyl	<i>n</i> -hexyl	<i>n</i> -hexyl	$-(\text{CH}_2)_5\text{OCH}_3$
R₂		-CH ₃	-H	-CH ₃	<i>t</i> -butyl	-H	-CH ₃	-Cl	-H	-CH ₃	-CH ₃	-Cl	-CN	-H
R₃		-H	-H	-CH ₃	-H	<i>t</i> -butyl	-H	-H	-H	-H	-H	-H	-H	-H
R₄		-CH ₃	-H	-H	-H	-H	-CH ₃	-H	-H	-H	-CH ₃	-H	-H	-H

Figure 2.38

The largest bathochromic shift in the UV-Vis absorption spectra occurred when a *t*-butyl was at the C-6 position (**R**₃) of the benzofuran ring (**1-129f**). Compounds (**1-129a-g**), (**1-129i-k**) and **1-129n** exhibited a strong yellow-green fluorescence, and Stokes shifts of 107–115 nm. Compound **1-129f** showed the greatest red shift (519 nm) and greatest Stokes shift (115 nm) compared to λ_{em} of the other derivatives. Compound **1-129m** with a cyano group at the benzofuran ring showed blue fluorescence and the smallest Stokes shift (92 nm). All these compounds in dilute DMF showed Φ_F in the range of 0.52–0.75. Φ_F of compounds **1-129h** and **1-129m** were higher ($\Phi_F = 0.52$ – 0.75) compared with those of compounds **1-129d**, **1-129j** ($\Phi_F = 0.52$ – 0.56).

A series of monoazo compounds based on *N*-ester-1,8-naphthalimides ((**1-130a-g**)) were reported [18] (Fig. 2.39).



Compound	R	X	Y	Z
1-130a	-CH ₃ COOCH ₃	-H	-H	-N(CH ₂ CH ₃) ₂
1-130b	-CH ₃ COOCH ₃	-CH ₃	-H	-N(CH ₂ CH ₃) ₂
1-130c	-CH ₃ COOC ₂ H ₅	-H	-H	-N(CH ₂ CH ₃) ₂
1-130d	-CH ₃ COOC ₂ H ₅	-CH ₃	-H	-N(CH ₂ CH ₃) ₂
1-130e	-CH ₃ COOC ₂ H ₅	-NHCOCH ₃	-H	-N(CH ₂ CH ₃) ₂
1-130f	-CH ₃	-CH ₃	-H	-N(CH ₂ CH ₃) ₂
1-130g	-CH ₃ COOC ₂ H ₅	-NH ₂	-COCH ₃	-H

Figure 2.39

The strong hypsochromic effect of compound **1-130g** ($\Delta\lambda_{abs} = 102$ nm) was obtained containing *p*-aminoacetophenone moiety in comparison with the corresponding *N,N*-diethylaniline derivative (**1-130c**) [107]. λ_{abs} of compound **1-130e** was characterized by significant bathochromic shifts compared to its *N,N*-diethylaniline analogues ($\Delta\lambda_{abs} = 26$ nm) due to the possession of -NHCOCH₃ group. By changing the solvent polarity from toluene to DMF, the positive solvatochromism was observed ($\Delta\lambda_{abs} = 5$ – 31 nm). ϵ maxima of this series compounds in chloroform were in the range of 33196–49080 l/mol·cm.

Another series of bipolar molecules with TPA and naphthalimide moieties with the different π -conjugated bridges (**1-131** – **1-140**) were reported [108] (Fig. 2.40).

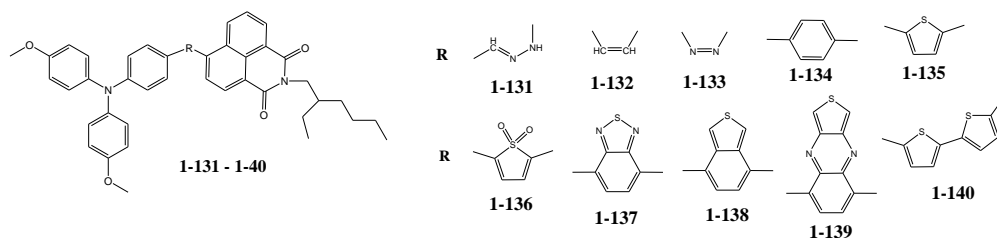


Figure 2.40

The geometries of compounds in the ground states and the first excited singlet state were optimized using the CAM-B3LYP and TD-CAM-B3LYP functionals. λ_{abs} value of compound **1-131** in gas phase was in agreement with the experimental result recorded for the solid films [109]. λ_{abs} value of **1-131** in THF showed larger deviation from the experimental data (the deviation was 77 nm) than in the gas phase. λ_{em} values of compound **1-131** both in THF and toluene solvents also showed larger deviations from the experimental data than those in gas phase. The deviations were 37 and 64 nm, respectively. λ_{abs} of compounds **1-132** – **1-139** exhibited strong bathochromic shifts compared with that of the compound **1-131**. The fluorescence of derivatives **1-131** – **1-139** were assigned to the $S_0 \leftarrow S_1$ electronic transitions and LUMOs \leftarrow HOMO excitations played a dominant role.

2.2. 1,8-Naphthalimide moieties containing polymers

It was shown that when *N*-aryl-1,8-naphthalimide derivatives were incorporated into polymer chains, the resulting materials show interesting fluorescent and electroluminescent properties [110,111]. If *N*-arylnaphthalimide or 1,8-naphthoilenearylimidazole derivatives have different electron-accepting (or donating) groups and different coplanar degree of molecular structures, these groups can change the optical properties shift the fluorescence wavelengths, change the emission quantum yields [112]. By controlling the electron-donating property of the substituent at the C-4 position of 1,8-naphthalimide moiety, the emission color of the resulting polymer can be tunable within a large range. Moreover, highly efficient and nearly pure white electroluminescence can be achieved using such polymers.

Simas *et al.* [113] reported polyfluorene containing *N*-(2-benzothiazole)-1,8-naphthalimide (**1-141**) moieties as the end groups (Fig. 2.41).

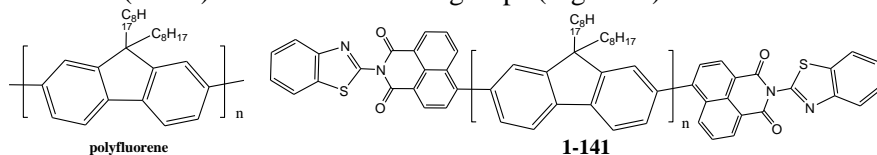


Figure 2.41

The absorption spectra of **1-141** in all solvents was similar that of polyfluorene, and it was characterized by a broad π - π^* absorption band of the polyfluorene backbone entered at ~ 380 nm. The content of end groups in the polymer was low, its absorption band overlapped with the intense absorption of polyfluorene. Φ_F of **1-141** (0.58–0.68) was lower than that of polyfluorene (0.74–0.78) in all the solvents investigated. The analysis of frontier molecular orbitals showed that HOMO and LUMO electron densities of **1-141** molecule were distributed over the π -orbitals of the benzothiazole and naphthalimide moieties, respectively, revealing a charge transfer character for the HOMO–LUMO transition. The fluorescence life time of **1-141** in dilute solution were found in the ranges 26–87 ps (τ_1), 438–472 ps (τ_2), and 1.3–3.4 ns (τ_3).

Several green light emitting polyfluorenes containing *N*-arylnaphthalimide and 1,8-naphthoilenearyl-imidazole as end caps ((**1-142** – **1-146**)P) for optoelectronics were reported [114] (Fig. 2.42).

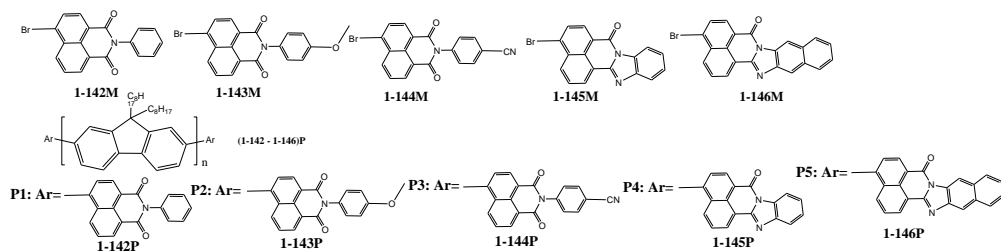


Figure 2.42

T_{ID} of the polymers ranged from 416 to 424 °C and T_g was in the range of 110–113 °C. Φ_F of compounds (**1-142** – **1-146**)M were in the range of 0.01–0.82. FL spectra of the films of these polymers showed green emission. It was due to the effective energy transfer from the fluorene segments to the vicinity of the moieties (**1-142** – **1-146**)M in the films. The energy levels of the polymers were in the range of 5.62–5.70 eV (for IP_{CV}), and –2.36 – –2.12 eV (for EA_{CV}), and these energy levels of the polymers had slightly different than those of polyfluorene [114]. The devices were fabricated in the configuration of ITO/PEDOT:PSS/PVK/emission layer/Ca/Ag. EL spectra of (**1-142** – **1-144**)P also exhibited a blue peak of fluorene ($\lambda_{max} = 433$ nm), because of the incomplete energy transfer from fluorene segments to (**1-142** – **1-144**)M units. The turn-on voltage, maximum brightness, and maximum luminance of the devices containing polymers were: (11 V, 930 cd/m², 0.19 cd/A) for the device containing **1-142P**, (10 V, 2890 cd/m², 0.28 cd/A) for the device with the emission layer of **1-143P**, (11 V, 772 cd/m², 0.15 cd/A) for the device with **1-144P**, (6 V, 11500 cd/m², 0.83 cd/A) for the device with **1-145P**, and (7 V, 6534 cd/m², 0.56 cd/A) for the device with **1-146P**. The devices based on (**1-142** – **1-144**)P had higher turn-on voltages and lower current density. The device with **1-145P** emitted pure green light, and exhibited maximum brightness of 11500 cd/m² at 12 V.

Table 2.14. Properties of 1,8-naphthalimide derivatives

Material	T_{ID} , (°C)	T_g , (°C)	IP_{CV} , (eV)	EA_{CV} , (eV)	Turn-on voltage, (V)	Brightness max, (cd/m ²)	Luminous efficiency max, (cd/A)
1-142P	420	110	5.62	–2.14	22	930	0.19
1-143P	424	112	5.67	–2.12	20	2890	0.28
1-144P	421	110	5.68	–2.15	22	772	0.15
1-145P	417	113	5.67	–2.24	6	11500	0.83
1-146P	416	110	5.70	–2.36	7	6354	0.56

T_{ID} – temperature of the onset of the thermal decomposition; T_g – glass-transition temperature λ_{abs} – maximum absorption wavelength; λ_{em} – maximum emission wavelength; Φ_F – fluorescence quantum yield; IP_{CV} – ionization potential; EA_{CV} – electron affinity; E_g^{opt} – optical band gap; E_g^{elc} – electrochemical band gap.

Tu and co-workers [115] reported copolymers (**1-150** – **1-152**) with naphthalimide chromophores chemically doped into the polyfluorene backbones (Fig. 2.43).

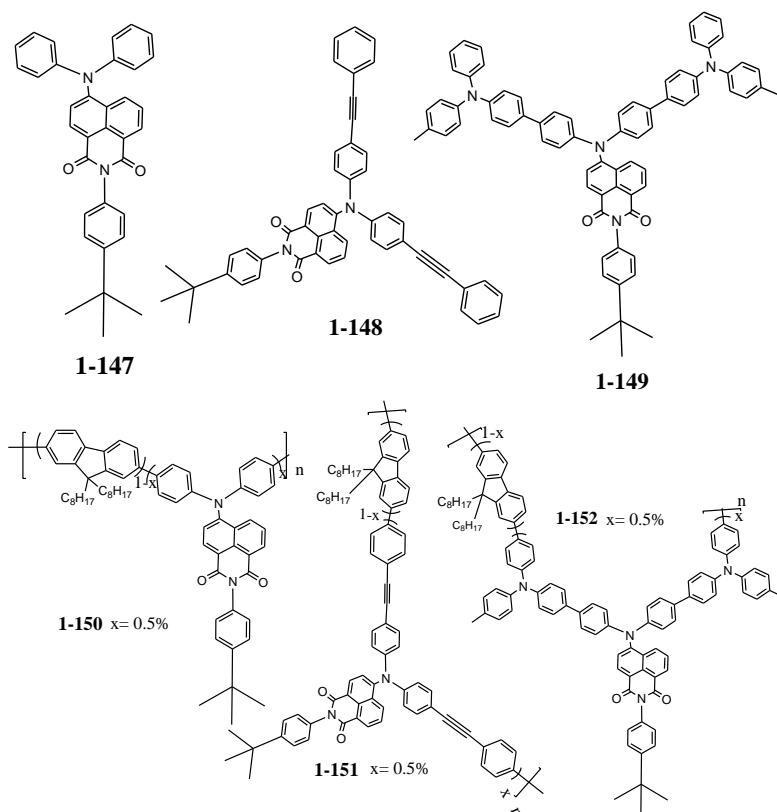


Figure 2.43

The films of the compounds **1-148**, **1-149** showed red fluorescence with Φ_F of 0.30 and 0.25, respectively. Their IP_{CV} and EA_{CV} values were determined to be (5.60 eV, -3.30 eV) for **1-147**, (5.24 eV, -3.26 eV) for **1-148**, and (5.26 eV, -3.31 eV) for **1-149**. The electroluminescent devices with a configuration of indium tin oxide (ITO)/(PEDOT; 50 nm)/copolymer(80 nm)/Ca(10 nm)/Al(100 nm) were fabricated by spin coating the polymer solution onto PEDOT-modified ITO glass under ambient conditions. The device made from **1-152** showed the best performance, with a maximum brightness of 11 900 cd/m^2 , a luminance efficiency of 3.8 cd/A , a power efficiency of 2.0 lm/W , and external quantum efficiency of 1.50%. In the case of **1-152**, when a driving voltages of 8, 10, 12, and 14 V were applied the CIE coordinates under the different voltages were (0.32, 0.36), (0.32, 0.36), (0.31, 0.35), and (0.31, 0.35), respectively, corresponding to maximum brightnesses of 144, 997, 3026, and 5560 cd/m^2 , respectively.

Poly(fluorene-alt-phenylene) containing pendant naphthalimide-based moieties (**1-153** – **1-157**) were reported [116] (Fig. 2.44).

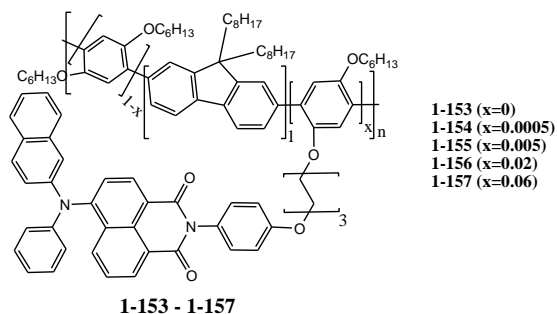


Figure 2.44

The cyclic voltammograms of copolymers **1-154** – **1-157** showed the similar redox behaviour as **1-153**. It exhibited a relatively broad quasi-reversible wave with an onset oxidation potential at around 0.53 V. The absorption spectra of the films of **1-154** – **1-157** and **1-153** were similar to those observed for the solutions. With respect to the emission of the films, **1-153** emission spectra exhibited the same shape as the spectrum of the solution, with the small red shift. The fluorescence life times of copolymers **1-155** – **1-157** were close, slightly increasing with the naphthalimide concentration (13.4, 14.5 and 14.9 ns, respectively). Copolymer **1-157** exhibited a significant emission at 600 nm with with the life time of 14.4 ns, similar to that observed at 530 nm. The introduction of the naphthalimide moiety diminished the emission efficiency from 0.89 for **1-153** to 0.39, 0.17, 0.41, 0.38 and 0.40 for **1-154** – **1-157**. OLED structures were fabricated with configuration: ITO/PEDOT:PSS (50 nm)/copolymer (90–125 nm)/Ba/Al (200 nm). The highest efficiency (47.11 cd/A) was obtained for the device containing **1-156**.

A series of highly efficient blue electroluminescent copolymers containing pendant naphthalimide species were reported [10] (Fig. 2.45).

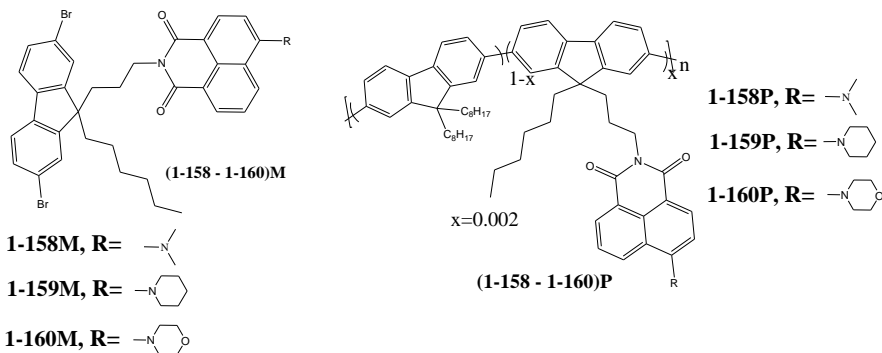


Figure 2.45

E_{Acv} and I_{Pcv} values of polymers **1-158P**, **1-159P** and **1-160P** were estimated to be -2.12 eV and 5.80 eV, respectively. The absorption spectrum of monomer **1-160M** was blue shifted by ~ 12 nm compared to those of **1-158M** and **1-159M**. FL spectrum of **1-159M** was red shifted by 5 nm relative to those of **1-158M** and **1-160M**. The toluene solutions of all three copolymers exhibited high Φ_{F} values (0.74–0.91). Single-layer electroluminescent devices were fabricated with the

configuration of ITO/(PEDOT:PSS) (40 nm)/copolymer (90 nm)/Ca (10 nm)/Al (100 nm). The devices containing the layers of **1-158P**, **1-159P** and **1-160P** exhibited turn on voltages of 3.5 V, luminous efficiencies of 2.20–5.22 cd/A and power efficiency of 1.53–3.28 lm/W.

Table 2.15. Properties of copolymers

Material	λ_{abs} , (nm)	λ_{em} , (nm)	Φ_{F}	Turn-on voltage, (V)	Maximum luminous efficiency, (cd/A)	Maximum power efficiency, (lm/W)	IP _{CV} , (eV)	EA _{CV} , (eV)
1-158M	411	490	0.77	–	–	–	5.49	–3.05
1-159M	410	495	0.91	–	–	–	5.51	–3.04
1-160M	398	490	0.74	–	–	–	5.62	–3.07
1-158P^a	–	–	NM	3.5	4.41	2.34	NM	NM
1-159P^a	–	–	NM	3.5	5.22	3.28	NM	NM
1-160P^a	–	–	NM	3.5	2.20	1.53	NM	NM
1-158P^b	–	–	NM	3.5	5.71	3.35	NM	NM
1-159P^b	–	–	NM	3.5	6.84	4.28	NM	NM
1-160P^b	–	–	NM	3.5	2.89	2.01	NM	NM

λ_{abs} – maximum absorption wavelength; λ_{em} – maximum emission wavelength; Φ_{F} – fluorescence quantum yield; IP_{CV} – ionization potential; EA_{CV} – electron affinity; ^a the device without thermal treatment; ^b the device with thermal annealing; NM – not measured.

Mei and co-workers [117] reported a series of low-band-gap copolymers containing 1,8-naphthalimide moieties (**1-161** – **1-164**, Fig. 2.46).

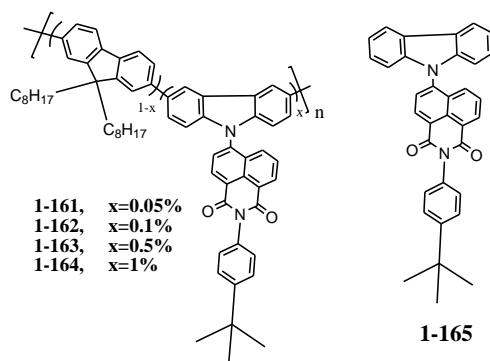


Figure 2.46

T_g **1-161** – **1-164** were in the range of 70–82 °C. All the polymers showed the similar values of T_{ID} around 415 °C. They showed the similar electrochemical behavior to that of polyfluorene rather than to that of **1-165**. Slight down-shifts of redox potentials were observed for **1-161** – **1-164** (0.08 and 0.09 V for the oxidation and reduction potentials of **1-163**, respectively in relative to those of polyfluorene, whereas a large difference (1.2 V down-shift of the reduction potential for **1-163**) was revealed when compared to the redox properties of **1-165**. The single-layer electroluminescent devices with the configuration of ITO/PEDOT/copolymer/-Ca/Al were fabricated. The turn-on voltages increased with the increase of **1-165** content

and were in the range of 3.5–4.9 V. At a **1-165** content of 0.1 mol%, the **1-162**-based device showed the best performance with a brightness of 9104 cd/m² at 18 V, the maximum luminous efficiency of 2.74 cd/A and a power efficiency of 1.51 lm/W. In order to further improve the device performances, the electron and hole trapping at the low-band-gap unit should be balanced.

The same group of authors synthesized a new 1,8-naphthalimide containing copolymer [117] (**1-166**, Fig. 2.47).

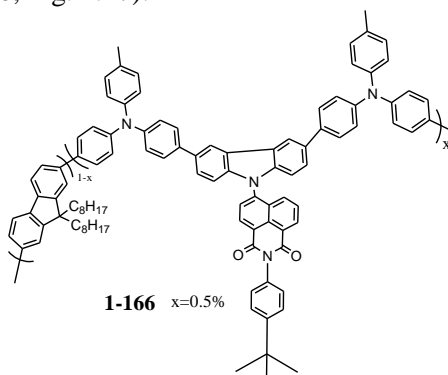


Figure 2.47

The device based on **1-166** exhibited much better performance than the devices based on **1-163**. The maximum brightness was as high as 14228 cd/m² at 23 V, the maximum luminous efficiency was 4.53 cd/A and power efficiency was 1.57 lm/W.

Table 2.16. Properties of copolymers

Material	T _{ID} , (°C)	T _g , (°C)	Turn-on voltage (V)	Brightness max, (cd/m ²)	Maximum luminous efficiency, (cd/A)	Maximum power efficiency, (lm/W)	E _{ox} , (eV)	E _{red} , (eV)
1-161	418	76	3.5	7095	2.51	1.41	NM	NM
1-162	420	70	4.2	9104	2.74	1.51	NM	NM
1-163	415	75	4.4	8189	2.17	0.90	1.37	-2.30
1-164	412	77	4.9	6648	1.15	0.34	NM	NM
1-165	NM	NM	NM	NM	NM	NM	1.41	-1.13
1-166	411	82	4.9	14228	4.53	1.57	1.42	-2.25

T_{ID} – temperature of the onset of the thermal decomposition; T_g – glass-transition temperature; E_{ox} – oxidation potential; E_{red} – reduction potential; NM – not measured.

Wang *et al.* [115] developed several series of copolymers with pendant 1,8-naphthalimide moieties (**1-167** – **1-169**) for single-layer white OLEDs (Fig. 2.48).

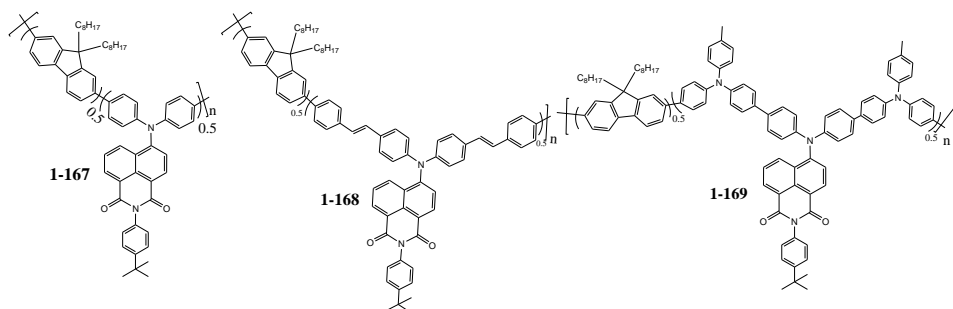


Figure 2.48

Among **1-167** – **1-169** the best performance with a maximum luminance of 11 900 cd/m², a peak external quantum efficiency of 1.5%, a luminance efficiency of 3.8 cd/A, and a power efficiency of 2.0 lm/W in the device configuration of ITO/PEDOT:PSS (50 nm)/ **1-169** (80 nm)/Ca (10 nm)/Al (100 nm) showed **1-169**. OLED with **1-169** showed stable white electroluminescence spectra in a wide driving voltage range from 8 V to 14 V. In the voltage range corresponding to the maximum brightness from 144 cd/m² to 5560 cd/m², the CIE coordinates remained relatively stable ($\Delta x = 0.01$, $\Delta y = 0.01$) with CIE (0.32, 0.36) at 8 V and (0.31, 0.35) at 14 V.

Table 2.17. Properties of copolymers

Material	Turn-on voltage, (V)	Brightness max, (cd/m ²)	Maximum luminous efficiency, (cd/A)	Maximum power efficiency, (lm/W)	External quantum efficiency, (%)	CIE 1931 co-ordinates (x,y)
1-167	5.8	18300	3.8	1.2	1.15	0.34, 0.49
1-168	4.8	12400	2.7	0.81	0.72	0.29, 0.33
1-169	6.6	11900	3.8	2.0	1.50	0.32, 0.36

The external quantum efficiencies were measured at 100 mA·cm⁻²; the CIE coordinates were measured at 8 V.

Another series of white light-emitting copolymers (**1-170**, **1-171**) with pendant naphthalimide moieties also were reported [118,119] (Fig. 2.49).

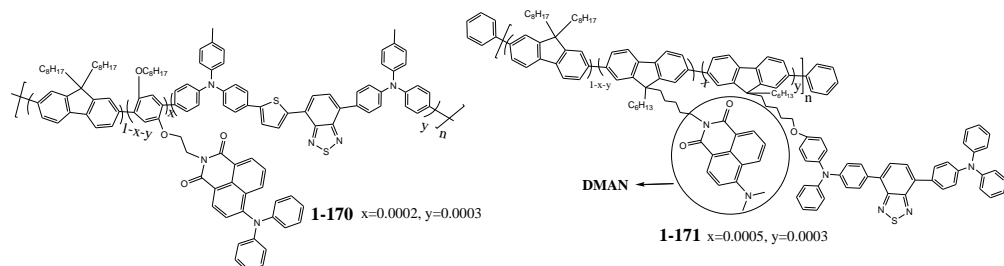


Figure 2.49

Although the device based on **1-170** could not give attractive EL efficiencies (luminance efficiency of 1.59 cd/A and power efficiency of 0.83 lm/W), it showed very good white light color quality with CIE coordinates at (0.31, 0.34) and stable

EL spectra from 8 V to 12 V. White-emitting terpolymer **1-171** with bluish-green emitting chromophore 4-dimethylamino-1,8-naphthalimide (DMAN) OLED with the configuration of ITO/PEDOT:PSS (40 nm)/copolymer (90 nm)/Ca (10 nm)/Al (100 nm) showed EL with luminance efficiency of 12.8 cd/A, external quantum efficiency of 5.4% and power efficiency of 8.5 lm/W. OLED with **1-171** emitted white light of high quality with CIE coordinates of (0.31, 0.36) and nearly invariant EL spectra from 6 V to 10 V.

Lee and co-workers [120] reported low-band-gap copolymer of fluorene and diphenylamine with the derivatives of naphthalimide as the pendants and the end caps (**1-172**, Fig. 2.50).

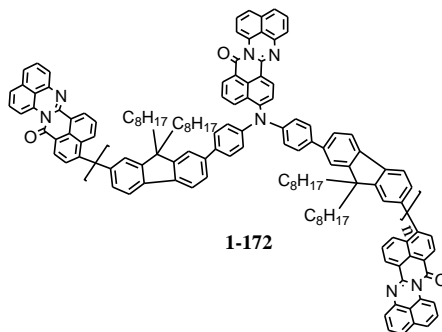


Figure 2.50

T_{ID} of **1-172** was observed at 423 °C and E_g^{opt} of **1-172** was found to be 1.82 eV. The maximum of absorption of the films **1-172** was red-shifted by ~18 nm relative to that of the solution, which suggested more efficient p-stacking and stronger intermolecular interactions in the film than in dilute solution [121]. The fluorescence of the films of **1-172** was quenched relative to that of polyfluorene due to the electron-withdrawing side chain. IP_{CV} and EA_{CV} values of **1-172** were 5.21 and -3.32 eV, respectively. E_g^{elc} of **1-172** was 1.89 eV, and E_g^{elc} was larger than E_g^{opt} (1.82 eV), due to the interface barrier for charge injection [122]. The bulk heterojunction solar cell were fabricated with a structure of ITO/PEDOT:PSS (50 nm)/ **1-172**:PCBM (110 nm)/LiF (0.5 nm)/Al (80 nm). The power conversion efficiencies of solar cells based on **1-172**:PCBM (1:3) and **1-172**:PCBM (1:4) were 0.61% and 0.67%, respectively, under the illumination of AM1.5 G, 100 mW/cm². The solar cell fabricated from **1-172**:PCBM (1:4) exhibited open-circuit voltage (0.55 V) and a higher short-circuit current (4.46 mA/cm²), which resulted in a higher power conversion efficiencies of 0.67%. The maximum external quantum efficiency value of **1-172**/PCBM (1:4) device was 30.9% at 535 nm.

2.3. Conclusions of literature review

The literature review shows that wide possibilities of changing the thermal, electrochemical, optical, fluorescence, electroluminescent, and photoelectrical properties of 1,8-naphthalimide derivatives can be materialized by introducing different electron-donating or electron-accepting substituents at the C-4 position in the 1,8-naphthalimide moiety, including aryl/aryloxy, alkynyl/alkenyl groups. 1,8-

Naphthalimide-based compounds display a wide range of interesting fluorescence properties, including high fluorescence quantum yields in solutions and solid films, good optical properties, high thermal (up to 489 °C) and chemical stabilities. Most of the low-molar-mass charge transporting materials are not capable of forming thin, neat, homogenous layers, and must be used in combination with polymeric hosts. The presence of a large proportion of polymer host in the compositions, leads to considerable decrease of charge carrier mobility. Many 4-substituted 1,8-naphthalimide derivatives were capable to form glasses (up to 254 °C) with good morphological stability. Moreover, some of them displayed relatively good charge-transporting capabilities that were appropriated for balanced carrier injection in organic light-emitting diodes. At the same time, derivatives 1,8-naphthalimide have found application in other optoelectronic devices, such as organic solar cells as well as in memory devices. The attractive properties of the 1,8-naphthalimide chromophore have led to its incorporation into numerous polymeric structures in order to tailor solubility, self-association, and molecular size to suit a particular application. To conclude, the synthesis and investigation of the derivatives of 1,8-naphthalimides is still a comparatively new area of research of new effective materials for practical application with similar or better thermal, fluorescence, photoelectrical and electrochemical properties. The design of stable molecular glasses must include combining of rigid moieties together with flexible units. Searching for new effective charge transporting materials for optoelectronic devices it is of interest to synthesize and study 1,8-naphthalimide derivatives with desirable hole, electron or ambipolar charge mobility values of an order of 10^{-5} – 10^{-3} cm²/V·s. Such derivatives as potential organic semiconductors showing ambipolar behavior should have low lying ionization potential (slightly lower than –5.0 eV) and electron affinity (below –3.9 eV with respect to the vacuum level) values. Some of organic ambipolar materials are hardly soluble and for this reason difficult to be used in organic optoelectronics. In this viewpoint, solution processable ambipolar organic materials are of great interest.

3. EXPERIMENTAL

3.1. Instrumentation

Nuclear magnetic resonance (NMR) spectroscopy. ^1H NMR and ^{13}C NMR spectra were obtained using a Varrian Unity Inova (300 MHz (^1H), 75.4 MHz (^{13}C)). The samples were prepared by dissolving 20–30 mg of the material in ~1 ml of deuterated chloroform (CDCl_3) with an inner standard, tetramethylsilane (TMS). Hydrogen nuclei (^1H) were excited using the frequency of 300 MHz, and carbon nuclei (^{13}C) were excited with the 75 MHz frequency. Spectrum scale is divided into parts per million (ppm). The presented chemical shifts (δ) are relative to TMS, the δ of which is attributed to zero ($\delta_{\text{TMS}} = 0$).

Mass spectrometry (MS). Mass spectra were recorded either on a Waters ZQ 2000 or on a Bruker Maxis 4G analytical system. The system is comprised of high-performance liquid chromatograph (HPLC) and mass spectrometer. The samples were prepared as diluted solutions (of ppm order) of the materials. The particles were ionized using atmospheric pressure chemical ionization method (APCI).

Fourier–transform infrared (FT–IR) spectroscopy. IR spectra in the range of 400–4000 inverse centimeters (cm^{-1}) were recorded on a Perkin-Elmer Spectrum GX II FT–IR System spectrometer. The samples were semi-transparent pellets of potassium bromide (KBr) containing ~1% of the analyzed material. FT–IR spectra are presented as a function of transparency (T) expressed in percent against wavenumber (ν) expressed in cm^{-1} .

Elemental analysis was performed with an Exeter Analytical CE-440 Elemental Analyzer. A weighed sample of a material (1–3 mg) is combusted at *ca.* 1100 °C in pure oxygen. The combustion products are carried through the analytical system using inert argon gas. Components of the sample gas are separated by absorption traps. Concentrations of the components are detected using thermal conductivity cells by comparing the output signal to a reference cell through which pure argon flows. Acetanilide ($\text{C}_8\text{H}_9\text{NO}$) is used as a standard for calibration.

Single crystal X-ray diffraction data of the selected compounds was performed on a Rigaku XtaLAB mini diffractometer using graphite monochromated Mo- $\text{K}\alpha$ radiation. The crystal-to-detector distance was 50.05 mm. The primary X-rays were made to fall on the sample substance. Because of its wave nature, it got diffracted to a certain angle. This angle of diffraction, which differs from that of the incident beam, gave the information regarding the crystal nature of the substance. Data were collected and processed using CrystalClear 2.0 program. All calculations were performed using the CrystalStructure 4.0 crystallographic software package except for refinement, which was performed using SHELXS97 and expanding using Fourier techniques.

Melting point (m.p.) of the compounds were determined using Electrothermal Mel-Temp apparatus.

Differential scanning calorimetry (DSC). Thermal transition data of synthesized compounds was collected using a Q100 TA DSC, Perkin-Elmer DSC-7 series thermal analyzer. Samples of 3–6 mg as obtained from the synthesis were heated in 40 μL pans at a scan rate of 10 $^{\circ}\text{C}/\text{min}$ under nitrogen flow. An empty pan was used for a reference. Baseline calibration was performed with sapphire disks. Temperature calibration was performed with indium standard.

Thermogravimetric analysis (TGA) was carried out using a Mettler TGA/SDTA851e/LF/1100, Mettler Toledo TGA/SDTA 851e. The samples were open alumina (Al_2O_3) crucibles loaded with a 3–6 mg milligrams of investigated material. The equipment was calibrated with indium and aluminum standards. All measurements were performed under nitrogen flow (75 cm^3/min) in a temperature range from -30 to 800 $^{\circ}\text{C}$ at a heating rate of 20 $^{\circ}\text{C}/\text{min}$.

Absorption spectra of the dilute solutions of concentration of 10^{-5} M were recorded by Perkin-Elmer Lambda 35 spectrophotometer and Hitachi U-3000 spectrometer, UV-Vis-NIR spectrophotometer Lambda 950 (Perkin Elmer). The absorption spectra of thin films prepared by vacuum deposition on quartz plates. The spectra were recorded under ambient conditions. Molar absorption (extinction) coefficients for solutions (ϵ) were estimated according to Beer-Lambert law: $A = \epsilon \cdot c \cdot l$, where c is molar concentration of a material in solution (in M), and l is the path length (in cm) which light travels through a sample (the thickness of cuvette was 0.99 cm).

Fluorescence (FL) spectroscopy. Fluorescence spectra of dilute solutions, solid solutions in PS matrix and of the solid films were measured using back-thinned CCD spectrophotometer PMA-11 (Hamamatsu), Hitachi MPF-4 or Perkin-Elmer LS55 fluorescence spectrometer at ambient conditions. The slit widths may be varied to give resolutions between 2.5 nm to 15 nm for the excitation monochromator and between 2.5 nm to 20 nm for the emission measurements in increments of 0.1 nm. The value of 0 can also be selected for both the excitation and emission slit and this gives a resolution of <2 nm. For these measurements, the dilute solutions of the investigated compounds were prepared by dissolving them in a spectral grade solvent at 10^{-6} – 10^{-5} M concentration. The PS films with the molecularly dispersed compounds with the concentration of 0.25 wt% were prepared by mixing the dissolved compounds and PS in THF and casting the solutions on quartz substrates in an ambient air. The drop-casting from THF solutions (1×10^{-3} M) was employed to prepare the solid films of the compounds. Fluorescence quantum yield (Φ_F) of the solutions and solid films were estimated by using integrated sphere (Sphere Optics) coupled to the CCD spectrometer [123]. FL transients of the samples were recorded using a time-correlated single photon counting system PicoHarp 300 (PicoQuant) utilizing semiconductor diode laser (repetition rate 1 MHz, pulse duration 70 ps, emission wavelength 375 nm) as an excitation source.

The spectra of the prompt and delayed luminescence were recorded at room temperature using spectrometer FS980 with microsecond gated detector.

Electron photoemission measurements (IP_{EP}). IP_{EP} were established by electron photoemission technique in air. The samples were prepared by the earlier reported procedure [124]. They were obtained by casting THF solutions of the materials on aluminium foil coated with the adhesive layer of methylmetacrylate and metacrylic acid copolymer. The samples before measurements were dried at 80 °C in air for 1 hour. The samples were illuminated with monochromatic UV radiation of the energy range of 4.5–6.3 eV. The negative voltage of an order of -10^2 V was applied to the sample substrate. The counter electrode with the slit for illumination was placed at a few millimeters of distance from the sample surface. The counter electrode was connected to an electrometer working in an open input regime for the photocurrent measurement. The charge formed under illumination was accumulated at a capacitor and the rate of the potential change (dU/dt) was measured. The photocurrent (which is attributed to dU/dt) is dependent on the incident light photon energy ($h\nu$). The IP_{EP} were estimated as the intersection points of the extrapolated linear part of the dependence $(dU/dt)^{1/2} = f(h\nu)$ and the $h\nu$ axis (*i.e.* $h\nu$ value at zero photocurrent) [125]. Standard error in the mean to 95% confidence for values of ionization potential was up to 0.04 eV.

Charge drift mobility was measured by xerographic time of flight (XTOF) method [126,127]. The samples for the measurements were prepared by the earlier reported procedure [128]. The charge-transporting layers were cast from the solutions of the compounds synthesized or from solutions of the mixtures of these compounds with polymer host PC-Z at mass proportion 1:1 in THF. The substrates were polyester film with Al layer. After coating the samples were heated at 80 °C for 1 h. Charge drift mobility was measured in electrophotographic regime. Electric field was created by positive (for hole drift mobility measurements) and negative (for electron drift mobility measurements) corona charging. The charge carriers were generated at the layer surface by illumination with pulses of nitrogen laser (pulse duration was 2 ns, wavelength 337 nm, pulse energy was $(6-7)\times 10^{-6}$ J). The layer surface potential decrease as a result of pulse illumination was up to 1–5% of initial potential before illumination. The capacitance probe that was connected to the wide frequency band electrometer measured the rate of the surface potential decrease dU/dt . The transit time t_t was determined from the kink on the curve of the dU/dt transient in log–log scale. The drift mobility was calculated by the formula $\mu_{hi} = d^2 / U_0 t_t$. The thickness contained a ~10% error and therefore contributed an error of $\pm 20\%$ in the mobility calculation. The field typically carries an error of $\pm 10\%$, arising from the 10% error in the thickness, and 0% negligible error in the voltage from the power supply. Because of this, a $\pm 20\%$ mobility error bar was included in the Poole-Frenkel plots.

Charge drift mobility measurements were also performed using charge extraction by linearly increasing voltage (CELIV) method [129,130]. For the CELIV measurements the samples in configuration ITO/compound/Al with the thickness of layers organic compound of 100–200 nm and an active area of 7 mm² were prepared. The layers from 10 mg/ml THF solutions of the compounds were spin coated onto glass/ITO substrates at 1000 rpm. Glass/ITO substrates were sonicated in acetone, deionized water, and isopropanol for 10 minutes before use. Al electrode

of 60 nm of was thermally evaporated at 10 Å/s at a pressure below 5×10^{-5} mbar using a mask, t_p obtain three top contact pixels. The light pulse was used to photogenerate the charge carriers by exciting layers of compounds through the ITO layer. The charge carriers were generated by illumination with pulses of Nd:YAG laser (pulse duration was 25 ps, wavelength 355 nm). The experimental setup consisted of a delay generator Tektronix AFG 3011 and a digital storage oscilloscope Tektronix DPO 4032. Transient currents were determined averaging over 10^3 laser pulses and statistical error of measurement was estimated by triplicating each transient current experiment.

Electrochemical investigations (CV) were carried out in a dry argon atmosphere on an Autolab potentiostat (PGSTAT20) or μ -Autolab Type III (EcoChemie, Netherlands) potentiostat. The data were collected using GPES (General Purpose Electrochemical System) software. The electrolyte medium consisted of the studied semiconducting compounds dissolved in 0.1 M $\text{Bu}_4\text{NBF}_4/\text{DCM}$ or $\text{Bu}_4\text{NPF}_6/\text{DCM}$ electrolyte. For cyclic voltammetry, following two kinds of three electrode systems were used: i) platinum working electrode of surface area of 3 mm², platinum wire counter electrode and Ag/AgCl reference electrode (used also for differential pulse voltammetry) and ii) glassy carbon working electrode (0.12 cm² surface), platinum wire counter electrode and Ag/0.1 M $\text{AgNO}_3/\text{CH}_3\text{CN}$ reference electrode. Ionization potential (IP_{CV}) and electron affinity (EA_{CV}) values were calculated from the first onsets of oxidation and reduction potentials, respectively, on the basis of the reference energy standard of ferrocene/ferrocenium redox couple. IP_{CV} value for Fc with respect to zero vacuum level was determined as 4.8 eV [131].

Computational methodology. The theoretical study was carried out in the frame of density functional theory (DFT) [132] employing the Becke, 3-parameter, Lee-Yang-Parr (B3LYP) [133,134] functional in conjunction with the 6-31G(d,p) basis set. All the geometry optimizations were followed by frequency calculations to assure that real minima were obtained. The geometry optimizations of the cationic radical species were performed at the unrestricted open shell level.

Time-dependent density functional theory (TDDFT) [135–139] was used for the study of the spectroscopic properties of the molecules. Up to 40 excited states were calculated and the theoretical absorption bands were obtained by considering a band half-width of 0.2 eV at half-height (Gaussview 5 software).

The vertical ionization potentials (I_p) were calculated at the B3LYP/6-31G(d,p) level as energy difference between neutral and radical cation species at the neutral state geometry. In order to check for any methodology influence on these values, other functionals (M052X [140], BMK [141], wB97X-D [142], wB97X [143]) and different basis sets (6-31G(d,p), 6-311+G(2d,p)) were considered.

The values of hole-transfer constants (k_{HT}) were calculated on the basis of the Marcus-Levich-Jortner equation:

$$k_{\text{CT}} = \frac{4\pi^2}{h} \frac{1}{\sqrt{4\pi\lambda_s k_B T}} t^2 \sum_{n=0}^{\infty} \exp(-S) \frac{S^n}{n!} \exp\left[-\frac{(\Delta G^0 + \lambda_s + n\hbar\omega_i)^2}{4\lambda_s k_B T}\right], \quad (3.1)$$

where t is the electronic coupling between two adjacent molecules; ΔG° is the charge-transfer (CT) reaction free energy (which is set to zero in the case of hole transfer between identical molecules); λ_s is the medium (outer) reorganization energy (set to 0.3 eV), representing the contribution from the medium polarization energy; $S_i = \lambda_i/h\omega_i$ is the Huang-Rhys factor characterizing the strength of the electron-vibration coupling for the internal mode i (in the products). λ_i represents the energetic effort due to the intramolecular geometric relaxations related to the CT between two adjacent molecules.

In this calculation, the vibration mode $h\omega_i$ has been set equal to 0.2 eV, which is a typical value for the energy of a carbon-carbon bond stretch in a conjugated system.

The internal reorganization energy (λ_i) values of model compounds were calculated at the B3LYP/6-31G(d,p) level according to the following equation [144]:

$$\lambda_i = \lambda_i^1 + \lambda_i^2 = (E_M^{Geom(M^+)} - E_M^{Geom(M)}) + (E_{M^*}^{Geom(M)} - E_{M^*}^{Geom(M^+)}) \quad (3.2)$$

where the quantity E_M for instance corresponds to the energy of the neutral molecule (M) in the geometry of the cationic species (M^+). The calculation of the electronic couplings was based on the following approximations: (I) despite the irregular packing between adjacent molecules in the amorphous materials, dimers of different geometries can be established which are supposed to adopt local minima geometries; (II) the hole is localized in only one molecule; (III) electronic coupling between the HOMO orbitals of adjacent monomers, also known as the “direct calculation” or “two state model” is considered instead of the coupling between states.

The simplest but the more limited method for calculation of transfer integrals is based on the Koopmans’ theorem, in which the transfer integrals are determined as half of the energy splitting between the HOMO–1 (LUMO–1) and HOMO (LUMO) orbitals in the dimer. As this method is applicable only if the dimer possesses a perfect symmetry, the “direct calculation” of the transfer integrals in the frame of a “two state” model is commonly employed.

The transfer integrals between frontier orbitals of two monomers in a dimer were calculated on the basis of the equation:

$$t_{12} = \frac{\tilde{t}_{12} - \frac{1}{2}(\tilde{\varepsilon}_1 + \tilde{\varepsilon}_2)S_{12}}{1 - S_{12}^2} \quad (3.3)$$

The parameters involved in eq. 3.3 were calculated as follows (for example in the case of the transfer integral between the HOMO orbitals of two monomers, noted here as $M1$ and $M2$):

$$\tilde{t}_{12} = \langle \psi_{HOMO}^{M1} | \hat{H}_{dimer} | \psi_{HOMO}^{M2} \rangle \quad (3.4)$$

$$\tilde{\varepsilon}_{1(2)} = \langle \psi_{HOMO}^{M1(M2)} | \hat{H}_{dimer} | \psi_{HOMO}^{M1(M2)} \rangle \quad (3.5)$$

$$S_{12} = \langle \psi_{HOMO}^{M1} | \psi_{HOMO}^{M2} \rangle \quad (3.6)$$

$\psi_{HOMO}^{M1(M2)}$ in eq. 3.4–3.6 represent the wave functions corresponding to $HOMO_{M1}$ and $HOMO_{M2}$ as calculated from the isolated monomers, whereas \hat{H}_{dimer} is the Hamiltonian in a given geometry of the dimer $M1 \cdots M2$. The necessary matrices for these calculations (S_{12} and \tilde{t}_{12}) are produced by Gaussian09 program [145].

A general method evaluating the electronic coupling between electronic states (instead of frontier orbitals) has been proposed. The “two state” model making use of the frontier orbitals for the calculation of the transfer integrals has been employed.

In order to correctly describe the π -stacking interactions, the geometries of the dimers formed by two identical molecules have been optimized by employing the ω B97X-D functional at the 6-31G** basis set. The electronic couplings between the HOMO orbitals of two adjacent molecules have been calculated at the same level (ω B97X-D/6-31G**) with the corresponding matrix elements evaluated with Gaussian 09 program.

The interaction energies of some optimized dimers were calculated with respect to the isolated monomers with the 6-311++G(3df,3pd) basis set and were corrected for the basis set superposition error (BSSE) by the counterpoise correction method. The zero point energy (ZPE) correction has been also taken into account by using the value obtained at the 6-31G** basis set.

3.2. Materials

4-Bromo-1,8-naphthalic anhydride (98%), 1-iodoethane (99%), hydrazine hydrate (99%), triphenylamine (TPA, 98%), 1-iodo-4-methoxybenzene (97%), tris(4-bromophenyl)amine (99%), 4-(diphenylamino)phenylboronic acid (97%), *n*-BuLi (2.5 mol·L⁻¹ in hexane), 2-isopropoxy-4,4,5,5-tetramethyl-1,3,2-dioxaborolane (98%), bis(triphenylphosphine)palladium(II) (Pd(PPh₃)₂Cl₂, 98%), *N*-bromosuccinimide (NBS, 98%), 1,10-phenanthroline (99%), 18-crown-6 (99%), triethylamine (TEA, 99.5%), tri(*o*-tolyl)phosphine (P(*o*-tolyl)₃, 98%), palladium(II) acetate (Pd(OAc)₂, 97%), ethynyltrimethylsilane (98%), diisopropylamine (99.5%), tetrabutylammonium fluoride solution 1.0 M in THF (TBAF), triphenylphosphine (PPh₃, 98%), 2-bromofluorene (99%), 2,7-dibromofluorene (99%), [9,9-bis(2-ethylhexyl)-9*H*-fluorene-2,7-diyl]bisboronic acid (98%), 9,9-(2-ethylhexyl)-9*H*-fluorene-2-yl-boronic acid (97%), 1-bromooctane (99%), *n*-octylamine (99%), tetrabutylammonium hydrogen sulphate (97%) were purchased from Aldrich and used as received. 2-Ethylhexylamine (98%) and 4-bromoaniline (98%) were purchased from TCI Europe. Diphenylamine (99%) was purchased from Reakchim. Potassium hydroxide (KOH, >85%), tetrabutylammonium bromide (99%), magnesium sulfate (MgSO₄, >97%), copper iodide (CuI, 99%), potassium *tert*-butoxide (*t*-BuOK, 99%), methyltriphenylphosphonium bromide (CH₃PPh₃, 99%), potassium carbonate (K₂CO₃, 99%), tetrabutylammonium tetrafluoroborate (Bu₄NBF₄, 99%) and tetrabutylammonium hexafluorophosphate (Bu₄NBF₆, 99%) were purchased from Aldrich as reagent grade chemicals and used as received. The solvents, i.e. toluene, 2-methoxy ethanol (Aldrich); chloroform, ethylacetate, *n*-

hexane, diethyl ether and methanol (Penta) and other solvents were purified and dried using the standard procedures [146]. Dimethylformamide (DMF, Lachema) was dried by distillation over calcium (II) hydride. Tetrahydrofuran (THF) was dried and distilled over sodium and benzophenone. Dichloromethane (DCM, POCH), ethyl acetate and *n*-hexane (Penta), TEA were purified by distillation over KOH.

4-(Di(4-methoxyphenyl)amine)benzaldehyde (a) (yellow crystals, m.p. = 92–93 °C) was prepared by the reported procedure [147].

4,4'-Diformyl-4''-methoxyphenylamine (b) (yellow crystals, m.p. = 83–84 °C, lit. [148] m.p. = 80 °C) was prepared by the reported procedure as described in literature [148].

***N,N*-diphenyl-4-bromoaniline (1a)** (white crystals, m.p. = 106–107 °C, lit. [149] m.p. = 101–103 °C) was prepared by the reported procedure [150].

(4-Bromo-phenyl)-di-(4-methoxyphenyl)-amine (2b) (grey crystals, m.p. = 92–93 °C, lit. [151] m.p. = 96–98 °C) was prepared by the reported procedure as described in literature [152].

Bis(4-bromophenyl)phenylamine (2c) (colorless oil) was prepared by the reported procedure [153].

4-(4,4,5,5-Tetramethyl-(1,3,2)dioxaborolan-2-yl)-phenyl)-di-(4-methoxyphenyl)-amine (3b) (white crystals, m.p. = 122–123 °C) was prepared by the reported procedure [152].

Bis(4-(4,4,5,5-tetramethyl-(1,3,2)dioxaborolan-2-yl)-phenyl)phenylamine (3c) (white crystals, m.p. = 228–230 °C (lit. [154] m.p. = 229–230 °C) was prepared by the reported procedure [154].

Tris(4-(4,4,5,5-tetramethyl-(1,3,2)dioxaborolan-2-yl)-phenyl)phenylamine (3d) (white crystals, m.p. 327–330 °C, lit. [155] m.p. = 334–335 °C) was prepared by the reported procedure as described in literature [154].

4-(Diphenylamino)benzaldehyde (2') (yellow crystals, m.p. = 120–121 °C, lit. [156] m.p. = 120–121 °C) was prepared by the reported procedure [157].

4,4'-Diformyl triphenylamine (3') (yellow crystals, m.p. = 143–144 °C, lit. [158] m.p. = 142–145 °C) was prepared by the reported procedure as described in literature [159].

Tris-(4-formyl-phenyl)amine (4') (yellow crystals, m.p. = 245–247 °C) was prepared by the reported procedure as described in literature [160].

4-Vinyltriphenylamine (5') (yellowish crystals, m.p. = 90–91 °C, lit. [161] m.p. = 91–92 °C) was prepared by the reported procedure [162].

4,4'-Vivinyltriphenylamine (6') (yellowish crystals, m.p. = 62–63 °C, lit. [163] m.p. = 64.5 °C) was prepared by the reported procedure as described in literature [164].

Tris-(4-vinyl-phenyl)amine (7'') (yellowish crystals, m.p. = 77–78 °C) was prepared by the reported procedure [165].

***N,N*-Diphenyl-4-((trimethylsilyl)ethynyl)benzenamine (2a')** (yellow oil) was prepared by the reported procedure as described in literature [166].

***N*-Phenyl-4-((trimethylsilyl)ethynyl)-*N*-(4-((trimethylsilyl)ethynyl)phenyl)aniline (2b')** (yellow oil) was prepared by the reported procedure [167].

Tris((*p*-trimethylsilyl)ethynyl)phenyl)aniline (2c') (yellow crystals, m.p. = 171–174 °C, lit. [168] m.p. = 172–175 °C) was prepared by the reported procedure as described in literature [169].

4-Ethynylphenyldiphenylamine (3a') (yellow oil) was prepared by the reported procedure [166].

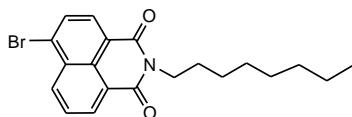
4-Ethynyl-*N*-(4-ethynylphenyl)-*N*-phenylbenzenamine (3b') (viscous oil) was prepared by the reported procedure as described in literature [167].

Tris[*p*-ethynylphenyl]amine (3c') (yellow crystals, m.p. = 107–108 °C, lit. [168] m.p. = 113–114 °C) was prepared by the reported procedure [169].

9,9-Diethylfluorene-2-boronic acid (2a'') (white crystals, m.p. = 113–114 °C, lit. [170] m.p. = 118–120 °C) was prepared by the reported procedure.

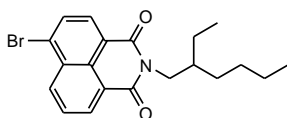
9,9-Dioctylfluorene-2-boronic acid (2c'') (white crystals, m.p. = 72–74 °C, lit. [171] m.p. = 70.1–77.3 °C) was prepared by the reported procedure as described in literature.

9,9-Dioctylfluorene-2,7-diboronic acid (3c'') (white crystals, m.p. = >400 °C, lit. [172] m.p. >400 °C) was prepared by the reported procedure.

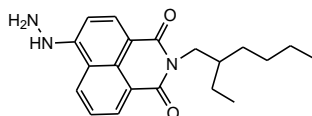


4-Bromo-*N*-octyl-1,8-naphthalimide (1a'). A solution of 4-bromo-1,8-naphthalic anhydride (1 g, 3.61 mmol) in 25 ml of DMF was added to a 100 mL three neck round bottom flask equipped with a reflux condenser and a magnetic stirrer. Then *n*-octylamine (0.60 g, 3.61 mmol) was added drop-wise and the reaction mixture was heated up to 120 °C and stirred under nitrogen for 24 h. The reaction mixture was concentrated using rotary evaporator and then the product was precipitated out into 1N HCl solution, filtered off and washed with 1N HCl solution. The crude product was purified by silica gel column chromatography using hexane/ethylacetate, 8:1 as an eluent. Yield: 1.03 g (74%) of white crystals; m.p. = 74–75 °C. ¹H NMR spectrum (300 MHz, CDCl₃, δ, ppm): 8.67 (d, 1H, *J* = 8.4 Hz, –H_{Naphthalene}), 8.57 (d, 1H, *J* = 7.5 Hz, –H_{Naphthalene}), 8.43 (d, 1H, *J* = 7.9 Hz, –H_{Naphthalene}), 8.05 (d, 1H, *J* = 7.9 Hz, –H_{Naphthalene}), 7.87 (t, 1H, *J*₁ = 7.3 Hz, *J*₂ = 15.8 Hz, –H_{Naphthalene}), 4.21–4.13 (m, 2H, –CH₂, –H_{aliphatic}), 1.80–1.69 (m, 2H, CH₂, –

H_{aliphatic}), 1.51–1.18 (m, 10H, CH₂, –H_{aliphatic}), 0.89 (t, 3H, $J_1 = 6.7$ Hz, $J_2 = 13.7$ Hz, CH₃, –H_{aliphatic}). IR (KBr, ν cm⁻¹): (arene C–H) 3068; (aliphatic C–H) 2958, 2927, 2871, 2852; (imide C=O) 1699; (Ar C=C) 1585, 1512, 1458; (imide C–N) 1351, 1234; (C–Br) 665, 560. ¹³C NMR spectrum (75.5 MHz, CDCl₃, δ , ppm): 163.6, 133.2, 132.0, 131.2, 131.0, 130.6, 130.1, 129.0, 128.0, 123.1, 122.3, 40.6, 31.8, 29.2, 28.1, 27.1, 22.6, 14.1. Anal. Calcd. for C₂₀H₂₂BrNO₂: C, 61.86; H, 5.71; Br, 20.58; N, 3.61; O, 8.24%. Found: C, 61.78; H, 5.77; N, 3.59%. MS (APCI⁺, 20 V), m/z : 389 ([M+H]⁺).

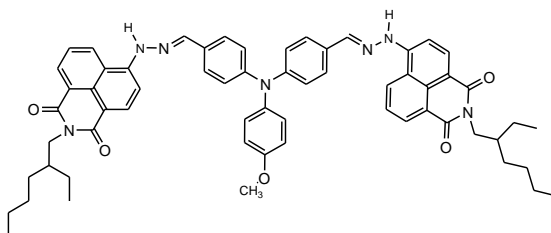


4-Bromo-*N*-(2-ethylhexyl)-1,8-naphthalimide (1). Compound **1** was prepared by the reported procedure [173]. The procedure followed in this work for the synthesis is slightly different. A solution of 4-bromo-1,8-naphthalic anhydride (1 g, 3.61 mmol) in 25 ml of DMF was added to a 100 ml three neck round bottom flask equipped with a reflux condenser and a magnetic stirrer. Then 2-ethylhexylamine (0.47 g, 3.61 mmol) was added drop-wise and the reaction mixture was heated up to 110 °C and stirred under nitrogen for 1.5 h. The end of the reaction was detected by thin-layer chromatography (TLC) (eluent: toluene/ether, 6:1). The reaction mixture was concentrated using rotary evaporator and then the product was precipitated out into 1N HCl, filtered off and washed with 1N HCl. The crude product was purified by silica gel column chromatography using acetone and hexane mixture (vol. ratio 1:1.5) as an eluent. Yield: 0.86 g (62%) of yellow crystals. M.p. = 82–83 °C. ¹H NMR spectrum (300 MHz, CDCl₃, δ , ppm): 8.70 (dd, 1H, $J_1 = 1.1$ Hz, $J_2 = 7.3$ Hz, –H_{Naphthalene}), 8.61 (dd, 1H, $J_1 = 1.1$ Hz, $J_2 = 8.5$ Hz, –H_{Naphthalene}), 8.45 (d, 1H, $J = 7.8$ Hz, –H_{Naphthalene}), 8.08 (d, 1H, $J = 7.8$ Hz, –H_{Naphthalene}), 7.89 (t, 1H, $J_1 = 7.3$ Hz, $J_2 = 8.5$ Hz, –H_{Naphthalene}), 4.18–4.11 (m, 1H, –CH, –H_{aliphatic}), 1.60–1.34 (m, 10H, 5×CH₂, –H_{aliphatic}), 0.99–0.90 (m, 6H, 2×CH₃, –H_{aliphatic}). IR, (in KBr), cm⁻¹: 3070 ν (CH_{ar}); 2959, 2926, 2871, 2855 ν (CH_{aliphatic}); 1702 ν (C=O_{anhydride}); 1653, 1590, 1504, 1459 ν (C=C_{ar}); 1344, 1231 ν (C–N); 783 γ (CH_{ar}); 664, 563 ν (C–Br). ¹³C NMR spectrum (300 MHz, CDCl₃, δ , ppm): 164.2, 133.4, 132.3, 131.5, 131.3, 130.8, 130.3, 129.3, 128.3, 123.4, 122.5, 44.5, 38.1, 31.0, 28.9, 24.3, 23.3, 14.3, 10.9. MS (APCI⁺, 20 V), m/z : 388 ([M+H]⁺). Anal. Calcd. for C₂₀H₂₂BrNO₂: C, 61.86; H, 5.71; Br, 20.58; N, 3.61; O, 8.24%. Found: C, 61.79; H, 5.75; Br, 20.62; N, 3.58%.



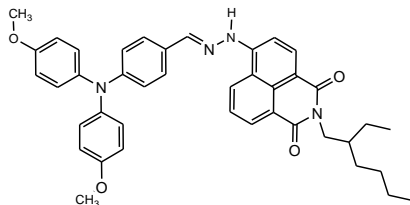
4-Hydrazino-*N*-(2-ethylhexyl)-1,8-naphthalimide (2). 4-Bromo-*N*-(2-ethylhexyl)-1,8-naphthalimide (**1**) (1.5 g, 3.86 mmol) and hydrazine hydrate (0.38 ml, 7.73 mmol) were dissolved in 40 ml of 2-methoxy ethanol and placed into an oven-dried, 150 ml two-necked round-bottomed flask equipped with a magnetic stir bar under an nitrogen atmosphere. The reaction mixture was refluxed at the

room temperature for 1.5 h. The end of the reaction was detected by TLC (eluent: acetone/*n*-hexane, 1:1.5). The reaction mixture was concentrated using rotary evaporator and then the product was precipitated out into 1N HCl, filtered off and washed with 1N HCl. The crude product was purified by silica gel column chromatography using acetone and hexane mixture (vol. ratio 1:1.5) as an eluent. Yield: 0.67 g (52%) of yellow crystals. M.p. = 81–82 °C. ¹H NMR spectrum (300 MHz, CDCl₃, δ, ppm): 8.64 (dd, 1H, *J*₁ = 1.0 Hz, *J*₂ = 7.3 Hz, –H_{Naphthalene}), 8.58 (d, 1H, *J* = 8.3 Hz, –H_{Naphthalene}), 8.09 (d, 1H, *J* = 1.0 Hz, –H_{Naphthalene}), 8.06 (d, 1H, *J* = 1.0 Hz, –H_{Naphthalene}), 7.69 (d, 1H, *J* = 1.0 Hz, –H_{Naphthalene}), 6.61 (s, 1H, –NH), 4.15–4.12 (m, 1H, CH_{aliphatic}), 3.88 (s, 2H, –NH₂), 1.60–1.32 (m, 10H, 5×CH₂, –H_{aliphatic}), 1.01–0.87 (m, 6H, 2×CH₃, –H_{aliphatic}). IR, (in KBr), cm⁻¹: 3341, 3310 ν (NH₂); 3295 ν (NH); 3073 ν (CH_{ar}); 2950, 2924, 2868 ν (CH_{aliphatic}); 1693 ν (C=O_{anhydride}); 1642, 1616, 1581, 1543 ν (C=C_{ar}); 1392, 1358 ν (C–N); 778 γ (CH_{ar}); ¹³C NMR spectrum (300 MHz, CDCl₃, δ, ppm): 133.7, 133.1, 132.7, 132.1, 131.6, 131.3, 131.0, 130.9, 127.1, 125.1, 113.6, 54.1, 53.8, 47.3, 45.0, 32.6, 29.2, 27.9, 27.5. MS (APCI⁺, 20 V), *m/z*: 339 ([M+H]⁺). Anal. Calcd. for C₂₀H₂₅N₃O₂: C, 70.77; H, 7.42; N, 12.38; O, 9.43%. Found: C, 70.81; H, 7.39; N, 12.33%.

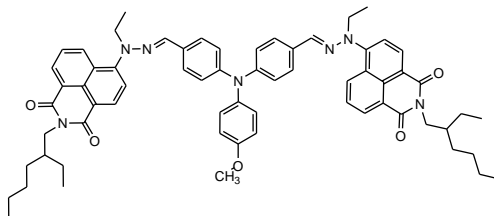


4,4'-Diformyl-4''-methoxyphenylamine bis(*N*-(2-ethylhexyl)-1,8-naphthalimide hydrazone) (3). 4,4'-Diformyl-4''-methoxyphenylamine (**b**) (0.1 g, 0.03 mmol) and 25 ml of methanol were placed into 250 ml 2-neck round bottom flask equipped with reflux condenser and mechanical stirrer and heated at 60 °C until the homogeneous solution was obtained. Then the solution of 4-hydrazino-*N*-(2-ethylhexyl)-1,8-naphthalimide (**2**) (0.026 g, 0.08 mmol) in 15 ml of methanol was added drop-wise. The mixture was refluxed until the dialdehyde (**b**) fully reacted (1.5 h, TLC control: eluent acetone/*n*-hexane 1:3). After the reaction, the mixture was slowly cooled to the room temperature. Crystals formed upon standing were filtered off, washed with methanol and dried to obtain 0.02 g (70%) of compound **3**. M.p. = 158–159 °C. ¹H NMR spectrum (300 MHz, CDCl₃, δ, ppm): 8.80 (s, 2H, 2×N–CH), 8.61 (q, 6H, *J*₁ = 7.7 Hz, *J*₂ = 17.5 Hz, –H_{Naphthalene}), 8.25 (d, 2H, *J* = 8.5 Hz, –H_{Naphthalene}), 8.07 (d, 2H, *J* = 4.2 Hz, –H_{Naphthalene}), 7.81–7.59 (m, 10H, –Ar), 7.54 (q, 2H, *J*₁ = 3.3 Hz, *J*₂ = 5.7 Hz, –Ar), 4.09 (p, 4H, *J*₁ = 6.5 Hz, *J*₂ = 13.4 Hz, 2×N–CH₂, –H_{aliphatic}), 3.84 (s, 3H, –OCH₃), 3.49 (s, 2H, 2×NH), 1.44–1.32 (m, 16H, 8×CH₂, –H_{aliphatic}), 0.98–0.85 (m, 12H, 4×CH₃, –H_{aliphatic}). IR, (in KBr), cm⁻¹: 3284 ν (NH); 3060 ν (CH_{ar}); 2954, 2926, 2856 ν (CH_{aliphatic}); 1691 ν (C=O_{anhydride}); 1651, 1614, 1578, 1504 ν (C=C_{ar}); 1460, 1427 γ (OCH₃); 1387, 1352 ν (C–N); 827, 774 γ (CH_{ar}); ¹³C NMR spectrum (300 MHz, CDCl₃, δ, ppm): 165.1, 164.7, 152.4, 151.3, 149.0, 145.4, 134.1, 131.6, 131.5, 131.4, 129.8, 128.8, 128.4, 125.8, 120.0, 118.9,

115.5, 115.4, 55.8, 44.3, 38.2, 31.0, 29.0, 24.3, 23.3, 14.3, 10.9. MS (APCI⁺, 20 V), m/z: 973 ([M+H]⁺). Anal. Calcd. for C₁₆H₆₃N₇O₅: C, 75.21; H, 6.52; N, 10.06; O, 8.21%. Found: C, 75.30; H, 6.56; N, 10.12%.

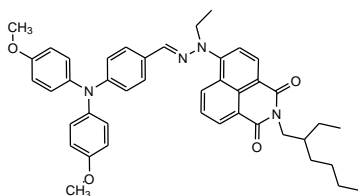


4-(Di(4-methoxyphenyl)amine)benzaldehyde *N*-(2-ethylhexyl)-1,8-naphthalimide hydrazone (**4**). Compound **4** was synthesized by the same procedure as compound **3**, only 4-(di(4-methoxyphenyl)amine)benzaldehyde (**a**) was used instead of compound (**b**). The yield of red crystals of **4** was 0.09 g (56%). M.p. = 125–126 °C. ¹H NMR spectrum (300 MHz, CDCl₃, δ, ppm): 8.59 (d, 1H, *J* = 7.7 Hz, –H_{Naphthalene}), 8.53 (d, 1H, *J* = 8.3 Hz, –H_{Naphthalene}), 8.21 (d, 2H, *J* = 8.4 Hz, –H_{Naphthalene}), 7.74 (d, 1H, *J* = 8.3 Hz, –H_{Naphthalene}), 7.55 (d, 2H, *J* = 8.7 Hz, –Ar), 7.18–7.09 (m, 4H, –Ar), 6.96–6.84 (m, 6H, –Ar), 4.12–4.08 (m, 2H, *J*₁ = 5.4 Hz, *J*₂ = 12.9 Hz, N–CH₂, –H_{aliphatic}), 3.82 (s, 6H, 2×OCH₃), 3.49 (s, 1H, –NH), 1.43–1.29 (m, 8H, 4×CH₂, –H_{aliphatic}), 0.96–0.84 (m, 6H, 2×CH₃, –H_{aliphatic}). IR, (in KBr), cm⁻¹: 3282 ν (NH); 3038, 2994 ν (CH_{ar}); 2953, 2926, 2836 ν (CH_{aliphatic}); 1688 ν (C=O_{anhydride}); 1647, 1575, 1503 ν (C=C_{ar}); 1462, 1440, 1427 γ (OCH₃); 1387, 1370, 1352 ν (C–N); 822, 775 γ (CH_{ar}); ¹³C NMR spectrum (300 MHz, CDCl₃, δ, ppm): 165.1, 164.7, 161.6, 156.8, 140.1, 134.4, 131.8, 131.7, 128.4, 128.3, 127.5, 125.6, 125.3, 123.5, 119.3, 116.9, 115.3, 115.1, 55.7, 44.2, 38.2, 31.0, 29.0, 24.3, 23.3, 14.3, 10.9. MS (APCI⁺, 20 V), m/z: 655 ([M+H]⁺). Anal. Calcd. for C₄₁H₄₂N₄O₄: C, 75.20; H, 6.47; N, 8.56; O, 9.77%. Found: C, 75.15; H, 6.42; N, 8.63%.

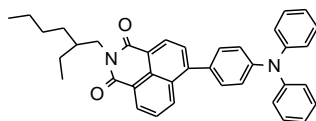


4,4'-Diformyl-4''-methoxyphenylamine bis(*N*-ethyl-*N*-(2-ethylhexyl)-1,8-naphthalimide hydrazone (**5**). Compound **3** (0.5 g, 0.51 mmol) and 30 ml of acetone were placed into a 100 ml 3-neck round bottom flask equipped with reflux condenser, thermometer and mechanical stirrer. The mixture was stirred vigorously at 50–60 °C for 10 min, and powdered KOH (0.072 g, 1.29 mmol), 1-iodoethane (0.094 g, 1.18 mmol) and tetrabutylammonium bromide (0.01 g, 0.032 mmol) were added. After 30 min the reaction mixture was filtered, and the solvent was evaporated. The crude product was purified by silica gel column chromatography using the mixture of acetone and *n*-hexane (vol. ratio 1:3) as an eluent. Yield: 0.38 g (53%) of red crystals. M.p. = 94–95 °C. ¹H NMR spectrum (300 MHz, CDCl₃, δ, ppm): 8.67–8.58 (m, 5H, H_{Naphthalene}), 7.72 (dd, 3H, *J*₁ = 7.3 Hz, *J*₂ = 8.5 Hz, –

$H_{\text{Naphthalene}}$), 7.65 (s, 2H, $-H_{\text{naphthalene}}$), 7.53 (dd, 6H, $J_1 = 2.3$ Hz, $J_2 = 8.4$ Hz, $-Ar$), 7.13–7.07 (m, 4H, $-Ar$), 6.92–6.88 (m, 2H, $-Ar$), 4.18–4.16 (m, 4H, $2 \times N-CH_2$, $-H_{\text{aliphatic}}$), 3.85 (s, 3H, $-OCH_3$), 2.04–1.95 (m, 2H, $2 \times CH$, $-H_{\text{aliphatic}}$), 1.46–1.36 (m, 20H, $10 \times CH_2$, $-H_{\text{aliphatic}}$), 1.13–0.74 (m, 18H, $6 \times CH_3$, $-H_{\text{aliphatic}}$). IR, (in KBr), cm^{-1} : 3063 ν (CH_{ar}); 2955, 2926, 2856 ν ($CH_{\text{aliphatic}}$); 1691 ν ($C=O_{\text{anhydride}}$); 1696, 1656, 1585, 1505 ν ($C=C_{\text{ar}}$); 1465, 1426 γ ($-OCH_3$); 1386, 1352 ν ($C-N$); 828, 779 γ (CH_{ar}); ^{13}C NMR spectrum (300 MHz, $CDCl_3$, δ , ppm): 165.0, 164.5, 150.9, 148.3, 139.9, 137.7, 132.2, 131.7, 131.6, 130.2, 129.7, 128.0, 127.5, 127.4, 126.1, 119.6, 118.4, 115.2, 55.7, 47.0, 44.3, 38.2, 31.0, 29.0, 24.3, 23.3, 14.3, 11.2, 10.9. MS (APCI $^+$, 20 V), m/z : 1030 ($[M+H]^+$). Anal. Calcd. for $C_{65}H_{71}N_7O_5$: C, 75.77; H, 6.95; N, 9.52; O, 7.76%. Found: C, 75.68; H, 6.88; N, 9.59%.

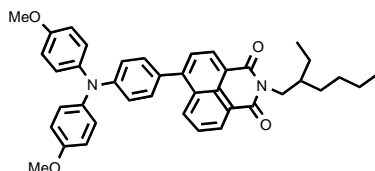


4-(Di(4-methoxyphenyl)amine)benzaldehyde *N*-ethyl-*N*-(2-ethylhexyl)-1,8-naphthalimide hydrazone (6). Compound **6** was synthesized by the same procedure as compound **5**, only compound **4** was used instead of compound **3**. The yield of red crystals was 0.2 g (80%). M.p. = 67–68 °C. 1H NMR spectrum (300 MHz, $CDCl_3$, δ , ppm): 7.71 (d, 2H, $J = 1.2$ Hz, $-H_{\text{Naphthalene}}$), 7.68 (d, 1H, $J = 4.1$ Hz, $-H_{\text{Naphthalene}}$), 7.53 (s, 1H, $-H_{\text{naphthalene}}$), 7.49 (d, 1H, $J = 4.1$ Hz, $-H_{\text{naphthalene}}$), 7.16–7.07 (m, 4H, $-Ar$), 7.02–6.81 (m, 8H, $-Ar$), 4.18–4.13 (m, 2H, $N-CH_2$, $-H_{\text{aliphatic}}$), 3.83 (s, 6H, $2 \times OCH_3$), 2.02–1.94 (m, 1H, $N-CH$, $-H_{\text{aliphatic}}$), 1.47–1.33 (m, 10H, $5 \times CH_2$, $-H_{\text{aliphatic}}$), 1.01–0.86 (m, 9H, $3 \times CH_3$, $-H_{\text{aliphatic}}$). IR, (in KBr), cm^{-1} : 3037 ν (CH_{ar}); 2954, 2927, 2856 ν ($CH_{\text{aliphatic}}$); 1695 ν ($C=O_{\text{anhydride}}$); 1655, 1585, 1504 ν ($C=C_{\text{ar}}$); 1464, 1441, 1427 γ (OCH_3); 1400 1385, 1353 ν ($C-N$); 826, 779 γ (CH_{ar}); ^{13}C NMR spectrum (300 MHz, $CDCl_3$, δ , ppm): 165.1, 164.5, 156.4, 151.3, 149.6, 140.6, 138.8, 132.2, 131.9, 131.5, 127.5, 127.4, 127.1, 126.0, 120.1, 119.2, 118.0, 115.0, 55.7, 44.2, 38.2, 31.0, 29.0, 24.3, 23.3, 14.3, 10.9. MS (APCI $^+$, 20 V), m/z : 683 ($[M+H]^+$). Anal. Calcd. for $C_{43}H_{46}N_4O_4$: C, 75.63; H, 6.79; N, 8.20; O, 9.37%. Found: C, 75.58; H, 6.83; N, 8.15%.

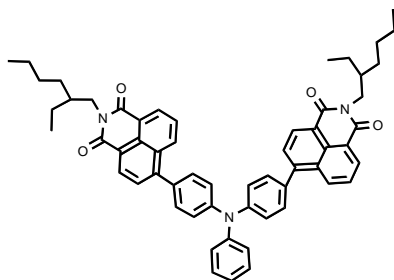


4-(4'-Diphenylaminophenyl)-*N*-ethylhexyl-1,8-naphthalimide (7). The solution of 4-bromo-1,8-naphthalimide (**1**) (0.5 g, 1.29 mmol) and $Pd(PPh_3)_2Cl_2$ (0.03 g, 0.04 mmol) in THF (15 mL) was purged with nitrogen, and the solution of 4-(diphenylamino)phenylboronic acid (0.37 g, 1.28 mmol) in THF (3 mL) and aqueous K_2CO_3 solution (1.70 g, 12.32 mmol) in H_2O (2 mL) were added with a syringe. The reaction mixture was stirred at 80 °C for 24 h. After cooling down, the product was extracted with CH_2Cl_2 , washed with water and dried over $MgSO_4$. The

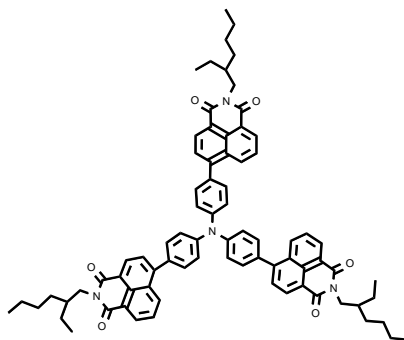
solvent was evaporated to afford a crude product. After column chromatography on silica gel with the eluent mixture of ethyl acetate and hexane (1:8, V:V), compound **7** was obtained as yellow powder with the yield of 0.55 g (78%), m.p. = 127–128 °C; ¹H NMR (300 MHz, CDCl₃, δ, ppm): 8.67 (d, 1H, *J* = 7.3 Hz, –H_{Naphthalene}), 8.66 (d, 1H, *J* = 8.5 Hz, –H_{Naphthalene}), 8.46 (d, 1H, *J* = 1.1 Hz, –H_{Naphthalene}), 8.43 (d, 1H, *J* = 1.1 Hz, –H_{Naphthalene}), 7.75 (t, 1H, *J* = 7.5 Hz, –H_{Naphthalene}), 7.44–7.31 (m, 7H, –Ar), 7.27–7.09 (m, 9H, –Ar), 4.26–4.11 (m, 2H, –CH₂, –H_{aliphatic}), 2.06–1.95 (m, 1H, –CH, –H_{aliphatic}), 1.48–1.31 (m, 8H, 4×CH₂, –H_{aliphatic}), 1.01–0.89 (m, 6H, 2×CH₃, –H_{aliphatic}). ¹³C NMR (75.4 MHz, CDCl₃, δ, ppm): 167.4, 147.7, 146.7, 146.1, 132.8, 131.9, 131.4, 131.2, 130.3, 130.0, 129.3, 128.4, 127.9, 126.7, 125.7, 124.7, 123.8, 121.6, 43.8, 38.1, 31.7, 28.8, 24.5, 23.4, 14.4, 10.8. IR, (KBr), cm⁻¹: 3060 ν (CH_{ar}); 2954, 2925, 2858 ν (CH_{aliphatic}); 1697 ν (C=O_{anhydride}); 1656, 1584, 1505, 1486 ν (C=C_{ar}); 1350, 1279 ν (C–N); 784, 759, 695 γ (CH_{ar}). MS (APCI⁺, 20 V), *m/z*: 552 ([M+H]⁺). Elemental analysis for C₃₈H₃₆N₂O₂: calcd. C, 82.58; H, 6.57, N, 5.07; O, 5.79%. Found: C, 82.63; H, 6.60; N, 5.08%.



4-(4'-(Di-(4'-methoxyphenyl)amino)phenyl)-N-(2-ethylhexyl)-1,8-naphthalimide (8) was prepared by the similar procedure as **7** using 4-(4,4,5,5-tetramethyl-(1,3,2)dioxaborolan-2-yl)-phenyl-di-(4-methoxyphenyl)-amine (**3b**) (0.58 g, 1.42 mmol), **1** (0.5 g, 1.29 mmol), Pd(PPh₃)₂Cl₂ (0.03 g, 0.039 mmol), K₂CO₃ (1.78 g, 12.89 mmol). The crude product was purified by silica gel column chromatography using the mixture of ethyl acetate and hexane (1:8, V:V) as an eluent to obtain **8** as amorphous material with the yield of 0.59 g (75%); ¹H NMR (300 MHz, CDCl₃, δ, ppm): 8.66 (d, 1H, *J* = 7.3 Hz, –H_{Naphthalene}), 8.64 (d, 1H, *J* = 7.4 Hz, –H_{Naphthalene}), 8.45 (d, 1H, *J* = 1.1 Hz, –H_{Naphthalene}), 8.44 (d, 1H, *J* = 1.1 Hz, –H_{Naphthalene}), 7.73 (t, 1H, *J* = 7.6 Hz, –H_{Naphthalene}), 7.35 (d, 2H, *J* = 8.8 Hz, –Ar), 7.20 (d, 4H, *J* = 9.1 Hz, –Ar), 7.08 (d, 2H, *J* = 8.8 Hz, –Ar), 6.92 (d, 4H, *J* = 9.1 Hz, –Ar), 4.24–4.12 (m, 2H, –CH₂, –H_{aliphatic}), 3.85 (s, 6H, 2×OCH₃), 2.04–1.94 (m, 1H, –CH, –H_{aliphatic}), 1.48–1.30 (m, 8H, 4×CH₂, –H_{aliphatic}), 1.01–0.90 (m, 6H, 2×CH₃, –H_{aliphatic}). ¹³C NMR (75.4 MHz, CDCl₃, δ, ppm): 164.9, 156.7, 149.4, 147.2, 140.4, 133.2, 131.3, 130.8, 130.0, 127.8, 127.7, 127.3, 126.8, 123.1, 121.2, 119.6, 115.1, 55.7, 44.3, 38.1, 30.9, 28.9, 24.3, 23.3, 14.3, 10.8. IR, (KBr), cm⁻¹: 3037 ν (CH_{ar}); 2955, 2927, 2856 ν (CH_{aliphatic}); 1698 ν (C=O_{anhydride}); 1657, 1586, 1504, 1463 ν (C=C_{ar}); 1440, 1425 γ (OCH₃); 1354, 1282 ν (C–N); 784, 758, 656 γ (CH_{ar}). MS (APCI⁺, 20 V), *m/z*: 612 ([M+H]⁺). Elemental analysis for C₄₀H₄₀N₂O₄: calcd. C, 78.40; H, 6.58; N, 4.57; O, 10.44%. Found: C, 78.45; H, 6.65; N, 4.52%.

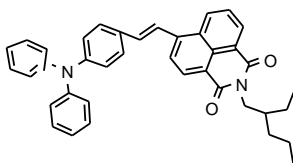


4,4'-(Di(*N*-(2-ethylhexyl)-1,8-naphthalimide-4-yl)phenyl)benzenamine (9) was prepared by the similar procedure as **7** using bis(4-(4,4,5,5-tetramethyl-(1,3,2)dioxaborolan-2-yl)-phenyl)phenylamine (**3c**) (0.28 g, 0.59 mmol), **1** (0.5 g, 1.29 mmol), (PPh₃)₂Cl₂ (0.02 g, 0.035 mmol), K₂CO₃ (1.21 g, 8.79 mmol). The crude product was purified by silica gel column chromatography using the mixture of ethyl acetate and hexane (1:8, V:V) as an eluent to obtain **9** as a red crystals with the yield of 0.32 g (64%), m.p. = 131–132 °C; ¹H NMR (300 MHz, CDCl₃, δ, ppm): 8.68 (d, 4H, *J* = 7.5 Hz, -H_{Naphthalene}), 8.46 (d, 2H, *J* = 8.4 Hz, -H_{Naphthalene}), 7.84–7.71 (m, 4H, -H_{Naphthalene}), 7.56–7.34 (m, 11H, -Ar), 7.27–7.20 (m, 1H, -Ar), 4.25–4.12 (m, 4H, 2×CH₂, -H_{aliphatic}), 2.05–1.97 (m, 2H, 2×CH, -H_{aliphatic}), 1.53–1.29 (m, 16H, 8×CH₂, -H_{aliphatic}), 1.06–0.85 (m, 12H, 4×CH₃, -H_{aliphatic}). ¹³C NMR (75.4 MHz, CDCl₃, δ, ppm): 164.7, 148.0, 147.2, 146.6, 133.2, 132.8, 131.5, 131.2, 130.2, 130.0, 129.0, 128.0, 127.0, 126.0, 124.5, 123.8, 123.2, 121.7, 44.4, 38.2, 31.0, 29.0, 24.3, 23.3, 14.3, 10.9. IR, (KBr), cm⁻¹: 3032 ν (CH_{ar}); 2955, 2926, 2856 ν (CH_{aliphatic}); 1701 ν (C=O_{anhydride}); 1659, 1587, 1504, 1464 ν (C=C_{ar}); 1353, 1284 ν (C–N); 783, 758, 697 γ (CH_{ar}). MS (APCI⁺, 20 V), *m/z*: 859 ([M+H]⁺). Elemental analysis for C₅₈H₅₇N₃O₄: calcd. C, 80.99; H, 6.68; N, 4.89; O, 7.44%. Found: C, 81.06; H, 6.65; N, 4.92%.

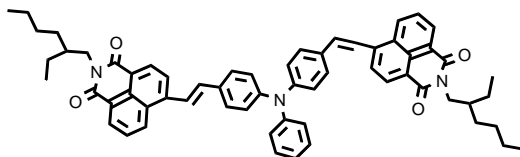


4,4',4''-(Tris(*N*-(2-ethylhexyl)-1,8-naphthalimide-4-yl)phenyl)benzenamine (10) was prepared by the similar procedure as **7** using tris(4-(4,4,5,5-tetramethyl-(1,3,2)dioxaborolan-2-yl)-phenyl)phenylamine (**3d**) (0.23 g, 0.39 mmol), **1** (0.5 g, 1.29 mmol), (PPh₃)₂Cl₂ (0.02 g, 0.035 mmol), K₂CO₃ (1.08 g, 7.81 mmol). The crude product was purified by silica gel column chromatography using the eluent mixture of ethyl acetate and hexane (1:8, V:V) to obtain **10** as a yellow crystals with the yield of 0.15 g (34%), m.p. = 133–134 °C; ¹H NMR (300 MHz, CDCl₃, δ, ppm): 8.71 (d, 3H, *J* = 2.7 Hz, -H_{Naphthalene}), 8.69 (d, 3H, *J* = 2.5 Hz,

$-\text{H}_{\text{Naphthalene}}$), 8.47 (dd, 3H, $J_1 = 0.8$ Hz, $J_2 = 8.6$ Hz, $-\text{H}_{\text{Naphthalene}}$) 7.76 (t, 6H, $J = 7.7$ Hz, $-\text{H}_{\text{Naphthalene}}$), 7.58 (d, 6H, $J = 8.6$ Hz, $-\text{Ar}$), 7.51 (d, 6H, $J = 8.69$ Hz, $-\text{Ar}$), 4.26–4.12 (m, 6H, $3 \times \text{CH}_2$, $-\text{H}_{\text{aliphatic}}$), 2.04–1.96 (m, 3H, $3 \times \text{CH}$, $-\text{H}_{\text{aliphatic}}$), 1.48–1.32 (m, 24H, $12 \times \text{CH}_2$, $-\text{H}_{\text{aliphatic}}$), 1.00–0.91 (m, 18H, $6 \times \text{CH}_3$, $-\text{H}_{\text{aliphatic}}$). ^{13}C NMR (75.4 MHz, CDCl_3 , δ , ppm): 162.5, 145.3, 146.4, 133.3, 133.8, 132.5, 132.2, 129.7, 129.1, 127.8, 127.1, 125.9, 125.1, 123.7, 123.2, 121.8, 44.4, 38.3, 31.1, 28.9, 24.2, 23.2, 14.3, 11.0. IR, (KBr), cm^{-1} : 3063 ν (CH_{ar}); 2956, 2927, 2857 ν ($\text{CH}_{\text{aliphatic}}$); 1700 ν ($\text{C}=\text{O}_{\text{anhydride}}$); 1659, 1586, 1504, 1464 ν ($\text{C}=\text{C}_{\text{ar}}$); 1354, 1281 ν ($\text{C}-\text{N}$); 783, 758, 696 γ (CH_{ar}). MS (APCI $^+$, 20 V), m/z : 1166 ($[\text{M}+\text{H}]^+$). Elemental analysis for $\text{C}_{78}\text{H}_{78}\text{N}_4\text{O}_6$: calcd C, 80.24; H, 6.73; N, 4.80; O, 8.22%. Found: C, 80.29; H, 6.79; N, 4.85%.

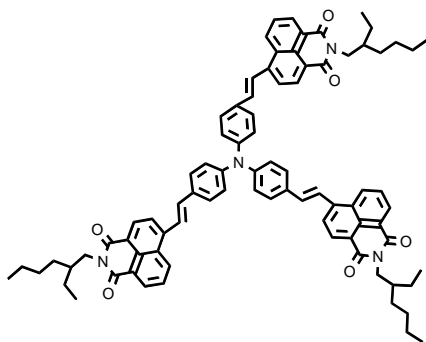


4-((E)-2-(N-(2-ethylhexyl)-1,8-naphthalimid-4-yl)vinyl)phenyl)benzenamine (11). A flask was charged with a mixture of **1** (0.50 g, 1.29 mmol), 4-vinyltriphenylamine (**5'**) (0.42 g, 1.55 mmol), $\text{Pd}(\text{OAc})_2$ (5 mg, 0.016 mmol), $\text{P}(o\text{-tolyl})_3$ (16 mg, 0.071 mmol), DMF (10 mL) and TEA (3 mL). The flask was degassed and purged with N_2 . The mixture was heated at 90 °C for 24 h under N_2 . Then, it was filtered and the filtrate was poured into methanol. The orange precipitate was filtered and washed with methanol. The crude product was purified by dissolving it in THF and precipitating into methanol (0.35 g, 47%). It was recrystallized from methanol. M.p. = 156–157 °C. ^1H NMR spectrum (300 MHz, CDCl_3 , δ , ppm): 8.67 (dd, 1H, $J_1 = 1.1$ Hz, $J_2 = 7.3$ Hz, $-\text{H}_{\text{Naphthalene}}$), 8.64–8.61 (m, 2H, $-\text{H}_{\text{Naphthalene}}$), 8.03 (d, 1H, $J = 7.9$ Hz, $-\text{H}_{\text{Naphthalene}}$), 7.85–7.78 (m, 2H, $-\text{H}_{\text{Naphthalene}}$, $=\text{CH}-$), 7.56–7.53 (m, 2H, $-\text{Ar}$), 7.38–7.29 (m, 7H, $-\text{Ar}$, $-\text{CH}=\text{CH}$), 7.21–7.11 (m, 6H, $-\text{Ar}$), 4.18–4.11 (m, 2H, $\text{N}-\text{CH}_2$), 2.02–1.97 (m, 1H, $-\text{CH}$), 1.49–1.29 (m, 8H, $-\text{CH}_2$), 1.00–0.88 (m, 6H, $-\text{CH}_3$). IR, (in KBr), cm^{-1} : 3033 ν (CH_{ar}); 2956, 2924, 2855 ν ($\text{CH}_{\text{aliphatic}}$); 1695 ν ($\text{C}=\text{O}_{\text{anhydride}}$); 1655, 1584, 1508, 1491 ν ($\text{C}=\text{C}_{\text{ar}}$); 1354, 1231 ν ($\text{C}-\text{N}$); 965 γ (*trans*, $-\text{CH}=\text{CH}$); 778, 751, 695 γ (CH_{ar}). ^{13}C NMR spectrum (75.4 MHz, CDCl_3 , δ , ppm): 143.4, 142.6, 140.7, 136.1, 132.7, 130.9, 130.4, 130.4, 129.3, 128.3, 128.3, 127.4, 126.9, 125.5, 125.3, 124.5, 122.8, 122.3, 122.2, 112.8, 54.7, 45.7, 38.6, 36.4, 33.1, 28.0, 27.8, 23.5, 15.3, 10.9. MS (APCI $^+$, 20 V), m/z : 578 ($[\text{M}+\text{H}]^+$). Anal. Calcd. for $\text{C}_{40}\text{H}_{38}\text{N}_2\text{O}_2$: C, 83.01; H, 6.62; N, 4.84. Found: C, 82.90; H, 6.67; N, 4.92%.



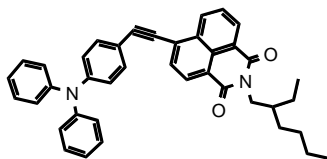
4-((E)-2-(N-(2-ethylhexyl)-1,8-naphthalimid-4-yl)vinyl)-N-(4-((E)-2-(N-(2-ethylhexyl)-1,8-naphthalimid-4-yl)vinyl)phenyl)benzenamine (12). A flask was

charged with a mixture of **1** (1.08 g, 2.78 mmol), 4,4'-vivinyltriphenylamine (**6'**) (0.30 g, 1.01 mmol), Pd(OAc)₂ (3.1 mg, 0.010 mmol), P(*o*-tolyl)₃ (9.2 mg, 0.041 mmol), DMF (20 mL) and TEA (6 mL). The flask was degassed and purged with N₂. The reaction mixture was heated at 90 °C for 24 h under N₂. Then, it was filtered and the filtrate was poured into methanol. The red precipitate was filtered and washed with methanol and then dissolved in methylene chloride. After evaporation of the solvent, the crude product was purified by silica gel column chromatography using the mixture of ethyl acetate and *n*-hexane (vol. ratio 1:4) as an eluent and by recrystallization from methanol to obtain 0.60 g of red crystals of **12** with a yield of 65%. M.p. = 179–180 °C. ¹H NMR spectrum (300 MHz, CDCl₃, δ, ppm): 8.69 (dd, 2H, *J*₁ = 1.0 Hz, *J*₂ = 7.2 Hz, -H_{Naphthalene}), 8.64–8.61 (m, 4H, -H_{Naphthalene}, -H_{Naphthalene}), 8.03 (d, 2H, *J* = 7.7 Hz, -H_{Naphthalene}), 7.88–7.79 (m, 4H, -H_{Naphthalene}, =CH-), 7.60 (d, 4H, *J* = 8.6 Hz, -Ar), 7.41–7.33 (m, 5H, -Ar, =CH-), 7.26–7.19 (m, 6H, -Ar), 4.19–4.15 (m, 4H, N-CH₂), 2.08–1.92 (m, 2H, -CH), 1.52–1.25 (m, 16H, -CH₂), 1.02–0.86 (m, 12H, -CH₃). IR, (in KBr), cm⁻¹: 3032 ν (CH_{ar}); 2956, 2924, 2855 ν (CH_{aliphatic}); 1695 ν (C=O_{anhydride}); 1657, 1583, 1506, 1490 ν (C=C_{ar}); 1355, 1231 ν (C-N); 961 γ (*trans*, -CH=CH); 781, 753, 696 γ (CH_{ar}). ¹³C NMR spectrum (75.4 MHz, CDCl₃, δ, ppm): 165.0, 164.6, 148.1, 147.0, 141.8, 134.8, 131.4, 130.2, 129.8, 129.7, 129.0, 128.4, 126.8, 125.7, 124.0, 123.8, 123.3, 123.3, 122.1, 121.4, 44.3, 38.2, 31.0, 29.0, 24.2, 23.3, 14.4, 10.9. MS (APCI⁺, 20 V), *m/z*: 911 ([M+H]⁺). Anal. Calcd. for C₆₂H₆₁N₃O₄: C, 81.64; H, 6.74; N, 4.61; O, 7.02. Found: C, 81.51; H, 6.80; N, 4.68%.

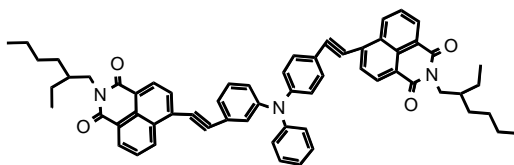


4-((E)-2-(N-(2-ethylhexyl)-1,8-naphthalimid-4-yl)vinyl)-N-(4-((E)-2-(N-(2-ethylhexyl)-1,8-naphthalimid-4-yl)vinyl)phenyl)benzenamine (13**)**. A flask was charged with a mixture of **1** (1.27 g, 3.27 mmol), tris-(4-vinyl-phenyl)amine (**7'**) (0.25 g, 0.77 mmol), Pd(OAc)₂ (2.6 mg, 0.084 mmol), P(*o*-tolyl)₃ (7 mg, 0.031 mmol), DMF (30 mL) and TEA (9 mL). The flask was degassed and purged with N₂. The reaction mixture was heated at 90 °C for 24 h under N₂. Then, it was filtered and the filtrate was poured into methanol. The red precipitate was filtered and washed with methanol and dissolved in methylene chloride. After evaporation of the solvent, the crude product was purified by silica gel column chromatography using the mixture of ethyl acetate and *n*-hexane (vol. ratio 1:8) as an eluent and by recrystallization from methanol to obtain 0.42 g of red crystals of **13** with a yield of 44%. M.p. = 209–210

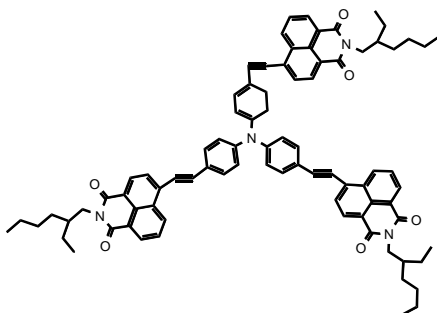
°C. ^1H NMR spectrum (300 MHz, CDCl_3 , δ , ppm): 8.67 (dd, 3H, $J_1 = 0.9$ Hz, $J_2 = 7.2$ Hz, $-\text{H}_{\text{Naphthalene}}$), 8.64–8.61 (m, 3H, $-\text{H}_{\text{Naphthalene}}$), 8.04 (d, 3H, $J = 7.8$ Hz, $-\text{H}_{\text{Naphthalene}}$), 7.91–7.79 (m, 6H, $-\text{H}_{\text{Naphthalene}}$, $-\text{vinylic}$), 7.65–7.54 (m, 6H, $-\text{Ar}$), 7.41–7.27 (m, 9H, $-\text{Ar}$, $=\text{CH}-$), 4.18–4.16 (m, 6H, $\text{N}-\text{CH}_2$), 2.07–1.95 (m, 3H, $-\text{CH}$), 1.47–1.31 (m, 24H, $-\text{CH}_2$), 1.00–0.91 (m, 18H, $-\text{CH}_3$). IR, (in KBr), cm^{-1} : 3032 ν (CH_{ar}); 2954, 2925, 2856 ν ($\text{CH}_{\text{aliphatic}}$); 1698 ν ($\text{C}=\text{O}_{\text{anhydride}}$); 1656, 1583, 1504, 1461 ν ($\text{C}=\text{C}_{\text{ar}}$); 1354, 1231 ν ($\text{C}-\text{N}$); 956 γ (*trans*, $-\text{CH}=\text{CH}$); 778, 753, 724 γ (CH_{ar}). ^{13}C NMR spectrum (75.4 MHz, CDCl_3 , δ , ppm): 164.9, 164.7, 147.6, 141.6, 134.7, 132.2, 131.5, 131.5, 131.4, 130.0, 129.7, 129.0, 128.6, 126.9, 124.7, 123.9, 123.4, 122.6, 122.4, 121.4, 44.4, 38.2, 30.9, 29.0, 24.3, 23.3, 14.4, 10.9. MS (APCI $^+$, 20 V), m/z : 1244 ($[\text{M}+\text{H}]^+$). Anal. Calcd. for $\text{C}_{84}\text{H}_{84}\text{N}_4\text{O}_6$: C, 81.00; H, 6.80; N, 4.50. Found: C, 79.75; H, 6.85; N, 4.48%.



4-((4'-Diphenylaminophenyl)ethynyl)-N-(2-ethylhexyl)-1,8-naphthalimide (14). To a mixture of 4-ethynylphenyldiphenylamine (**3a'**) (0.38 g, 1.42 mmol), $\text{PdCl}_2(\text{PPh}_3)_2$ (0.036 g, 0.052 mmol), CuI (0.003 g, 0.017 mmol), 4-bromo-*N*-(2-ethylhexyl)-1,8-naphthalimide (**1**) (0.5 g, 1.29 mmol) in diisopropylamine (20 mL) was purged with nitrogen and stirred at room temperature for 24 h. After removing the solvent under vacuum, the residue was eluted through a silica gel column using gradient solvents from pure hexane, a mixture of *n*-hexane:ethylacetate (12:1), *n*-hexane:ethylacetate (8:1) and *n*-hexane:ethylacetate (4:1) to give the pure product **14** (0.31 g; 42%) as an orange crystals, m.p. = 177–178 °C; ^1H NMR (300 MHz, CDCl_3 , δ , ppm): 8.78–8.73 (m, 1H, $\text{H}_{\text{Naphthalene}}$), 8.69 (dd, 1H, $J_1 = 4.6$ Hz, $J_2 = 1.25$ Hz, $\text{H}_{\text{Naphthalene}}$), 8.68–8.66 (m, 1H, $\text{H}_{\text{Naphthalene}}$), 8.58 (dd, 1H, $J_1 = 7.7$ Hz, $J_2 = 1.0$ Hz, $\text{H}_{\text{Naphthalene}}$), 8.47 (dd, 1H, $J_1 = 8.4$ Hz, $J_2 = 1.1$ Hz, $\text{H}_{\text{Naphthalene}}$), 7.96 (dd, 1H, $J_1 = 7.7$ Hz, $J_2 = 1.7$ Hz, $-\text{Ar}$), 7.90–7.82 (m, 1H, $-\text{Ar}$), 7.75–7.66 (m, 2H, $-\text{Ar}$), 7.60–7.43 (m, 5H, $-\text{Ar}$), 7.14–7.00 (m, 5H, $-\text{Ar}$), 4.22–4.09 (m, 2H, $-\text{H}_{\text{aliphatic}}$), 1.98 (s, 1H, $-\text{H}_{\text{aliphatic}}$), 1.43–1.21 (m, 8H, $-\text{H}_{\text{aliphatic}}$), 1.01–0.87 (m, 6H, $-\text{H}_{\text{aliphatic}}$). ^{13}C NMR (75.4 MHz, CDCl_3 , δ , ppm): 159.3, 150.7, 141.3, 137.3, 137.2, 137.2, 135.9, 133.3, 133.2, 131.3, 129.7, 129.7, 129.2, 128.7, 125.8, 125.0, 123.3, 123.2, 122.3, 122.3, 122.2, 122.2, 117.2, 92.2, 44.7, 37.0, 31.5, 29.4, 25.8, 23.2, 14.8. IR, (KBr), cm^{-1} : 3034 ν (CH_{ar}); 2957, 2934, 2855 ν ($\text{CH}_{\text{aliphatic}}$); 1698 ν ($\text{C}=\text{O}_{\text{anhydride}}$); 1654, 1588, 1501, 1486 ν ($\text{C}=\text{C}_{\text{ar}}$); 1323, 1312, 1273 ν ($\text{C}-\text{N}$); 779, 752, 691 γ (CH_{ar}). MS (APCI $^+$, 20 V), m/z : 577 ($[\text{M}+\text{H}]^+$). Elemental analysis for $\text{C}_{40}\text{H}_{36}\text{N}_2\text{O}_2$: calcd. C, 83.30; H, 6.29; N, 4.86; O, 5.55. Found: C, 83.36; H, 6.25; N, 4.82%.



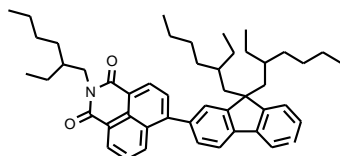
4,4'-(Di(*N*-(2-ethylhexyl)-1,8-naphthalimide-4-yl)phenyl)ethynyl)benzenamine (15) was prepared by the similar procedure as **14** using 4-ethynyl-*N*-(4-ethynylphenyl)-*N*-phenylbenzenamine (**3b^c**) (0.5 g, 3.35 mmol), **1** (1.72 g, 4.44 mmol), (PPh₃)₂Cl₂ (0.11 g, 0.16 mmol), CuI (0.02 g, 0.1 mmol). The crude product was purified by silica gel column chromatography using gradient solvents from pure hexane, a mixture of *n*-hexane:ethylacetate (12:1), *n*-hexane:ethylacetate (7:1) and *n*-hexane:ethylacetate (3:1) to obtain **15** as a red crystals with the yield of 0.48 g (31%), m.p. = 202–203 °C; ¹H NMR (300 MHz, CDCl₃, δ, ppm): 8.76 (dd, 2H, *J*₁ = 8.4 Hz, *J*₂ = 1.0 Hz, H_{Naphthalene}), 8.67 (dd, 2H, *J*₁ = 7.3 Hz, *J*₂ = 1.0 Hz, H_{Naphthalene}), 8.58 (d, 2H, *J* = 7.7 Hz, H_{Naphthalene}), 7.96 (d, 2H, *J* = 7.7 Hz, H_{Naphthalene}), 7.86 (dd, 2H, *J*₁ = 8.2 Hz, *J*₂ = 7.52 Hz, H_{Naphthalene}), 7.60 (d, 4H, *J* = 8.7 Hz, –Ar), 7.45–7.36 (m, 2H, –Ar), 7.21 (dd, 7H, *J*₁ = 17.8 Hz, *J*₂ = 7.9 Hz, –Ar), 4.23–4.08 (m, 4H, –H_{aliphatic}), 2.04–1.89 (m, 2H, –H_{aliphatic}), 1.50–1.25 (m, 16H, –H_{aliphatic}), 0.93 (m, 12H, –H_{aliphatic}). ¹³C NMR (75.4 MHz, CDCl₃, δ, ppm): 159.3, 141.3, 140.2, 137.8, 137.7, 137.2, 135.8, 135.2, 133.7, 133.0, 131.7, 131.3, 129.3, 128.7, 125.7, 125.6, 125.3, 123.6, 122.8, 122.6, 122.3, 117.4, 92.4, 44.2, 37.8, 31.2, 29.3, 25.6, 23.9, 14.2, 11.4. IR, (KBr), cm⁻¹: 3040 ν (CH_{ar}); 2957, 2927, 2857 ν (CH_{aliphatic}); 1699 ν (C=O_{anhydride}); 1657, 1585, 1509, 1492 ν (C=C_{ar}); 1355, 1316, 1284 ν (C–N); 784, 755, 695 γ (CH_{ar}). MS (APCI⁺, 20 V), *m/z*: 909 ([M+H]⁺). Elemental analysis for C₆₂H₅₇N₃O₄: calcd. C, 82.00; H, 6.33; N, 4.63; O, 7.05. Found: C, 82.03; H, 6.36; N, 4.64%.



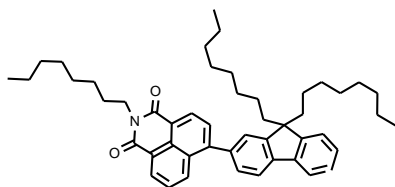
4,4',4'''-(Tris(*N*-(2-ethylhexyl)-1,8-naphthalimide-4-yl)phenyl)ethynyl)benzenamine (16) was prepared by the similar procedure as **14** using tri[*p*-ethynylphenyl]amine (**3c^c**) (0.5 g, 1.58 mmol), **1** (2.08 g, 5.36 mmol), (PPh₃)₂Cl₂ (0.12 g, 0.17 mmol), CuI (0.03 g, 0.19 mmol). The crude product was purified by silica gel column chromatography using gradient solvents from pure hexane, a mixture of *n*-hexane:ethylacetate (12:1), *n*-hexane:ethylacetate (6:1) and *n*-hexane:ethylacetate (2:1) to obtain **16** as a red crystals with the yield of 0.45 g (23%), m.p. = 213–215 °C; ¹H NMR (300 MHz, CDCl₃, δ, ppm): 9.19 (dd, 5H, *J*₁ = 19.3 Hz, *J*₂ = 10.1 Hz, H_{Naphthalene}), 8.39 (d, 4H, *J* = 6.8 Hz, H_{Naphthalene}), 7.99 (t, 3H, *J*

= 6.1 Hz, H_{Naphthalene}), 7.85–7.76 (m, 3H, H_{Naphthalene}), 7.46–7.41 (m, 6H, –Ar), 7.15–7.11 (m, 6H, –Ar), 4.17–4.04 (m, 6H, –H_{aliphatic}), 1.98–1.84 (m, 3H, –H_{aliphatic}), 1.45–1.22 (m, 24H, –H_{aliphatic}), 1.03–0.76 (m, 18H, –H_{aliphatic}). ¹³C NMR (75.4 MHz, CDCl₃, δ, ppm): 159.4, 140.5, 137.8, 137.5, 137.2, 135.2, 133.5, 133.4, 133.4, 131.4, 128.6, 125.8, 125.6, 124.8, 122.4, 117.8, 92.4, 44.6, 37.8, 31.4, 29.4, 25.2, 23.1, 14.6, 11.5. IR, (KBr), cm⁻¹: 3051 ν (CH_{ar}); 2956, 2929, 2853 ν (CH_{aliphatic}); 1700 ν (C=O_{anhydride}); 1654, 1585, 1510, 1489 ν (C=C_{ar}); 1356, 1317, 1284 ν (C–N); 774, 765, 698 γ (CH_{ar}). MS (APCI⁺, 20 V), m/z: 1242 ([M+H]⁺). Elemental analysis for C₈₄H₈₀N₄O₆: calcd. C, 81.26; H, 6.49; N, 4.51; O, 7.73. Found: C, 81.22; H, 6.54; N, 4.48%.

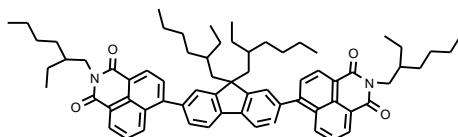
2-((N-(2-ethylhexyl)-1,8-naphthalimide)-4-yl)-9,9-diethyl-9H-fluorene (17) and **2,7-di((N-(2-ethylhexyl)-1,8-naphthalimide)-4-yl)-9,9-diethyl-9H-fluorene (20)** were prepared according to the published procedure [174].



2-((N-(2-ethylhexyl)-1,8-naphthalimide)-4-yl)-9,9-di(2-ethylhexyl)-9H-fluorene (18). 4-Bromo-*N*-2-ethylhexyl-1,8-naphthalimide (**1**) (300 mg, 0.77 mmol) and 9,9-di(2-ethylhexyl)-2-(4,4,5,5-tetramethyl-1,3,2-dioxaborolane-2-yl)-9H-fluorene (0.85 mmol) were taken in a 100 mL Schlenk flask. A solvent mixture of 20 mL of THF and 2 mL of water and powdered K₂CO₃ (2.7 mmol) was added. The reaction mixture was purged with nitrogen for 5 min. The reaction flask was degassed and then again purged with nitrogen for 2 min. Pd(PPh₃)₂Cl₂ (0.04 mmol) was added into it and stirred for 12–16 hrs at 80 °C under nitrogen. The reaction mixture was allowed to cool down to the room temperature, diluted with water and extracted using ethyl acetate. The organic layers were dried over sodium sulfate and evaporated at reduced pressure. The product was purified by column chromatography using an eluent mixture of *n*-hexane and ethyl acetate in a volume ratio of 8:1. Yield = 78% (180 mg); Yellow crystals (FW = 698.03 g/mol); m.p. = 55–56 °C. ¹H NMR (300 MHz, CDCl₃, δ, ppm): 8.74–8.66 (m, 2H), 8.45 (d, *J* = 7.9 Hz, 1H), 8.37 (dd, *J*₁ = 1.1 Hz, *J*₂ = 8.5 Hz, 1H), 7.94–7.88 (m, 1H), 7.85–7.81 (m, 2H), 7.79–7.72 (m, 1H), 7.54–7.49 (m, 2H), 7.47–7.40 (m, 2H), 4.26–4.13 (m, 2H, NCH₂), 3.56–3.47 (m, 1H, CH), 2.18–2.07 (m, 4H, CH₂Fluorene), 2.05–1.93 (m, 2H, CH_{Naphthalimide}), 1.55–1.27 (m, 24H, CH₂Naphthalimide, CH₂Fluorene), 1.07–0.80 (m, 12H, CH₃Naphthalimide, CH₃Fluorene), 0.47 (t, *J* = 7.3 Hz, 6H, CH₃Fluorene). ¹³C NMR (75.5 MHz, CDCl₃, δ, ppm): 164.9, 164.3, 150.8, 150.4, 147.6, 142.2, 141.0, 137.8, 133.4, 132.9, 132.3, 131.5, 131.2, 130.4, 129.1, 128.1, 127.9, 127.3, 127.1, 124.7, 123.3, 121.8, 120.2, 119.8, 56.5, 44.5, 44.4, 38.2, 38.2, 33.0, 31.1, 29.0, 24.4, 23.5, 23.3, 14.4, 11.0, 10.9, 8.9. IR (KBr, ν cm⁻¹): (arene C–H) 3063; (aliphatic C–H) 2960, 2927, 2855; (imide C=O) 1699; (Ar C=C) 1658, 1588; (imide C–N) 1354, 1231. Anal. Calc. for C₄₉H₆₃NO₂: C, 84.31; H, 9.10; N, 2.01; O, 4.58%. Found: C, 84.37; H, 9.14; N, 2.03%. MS (APCI⁺, 20 V), m/z: 698 [M+H]⁺.

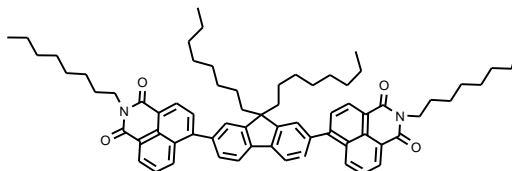


2-((*N*-(octyl)-1,8-naphthalimide)-4-yl)-9,9-dioctyl-9*H*-fluorene (19) was prepared by the similar procedure as **18** using 4-bromo-*N*-octyl-1,8-naphthalimide (**1a'**) (300 mg, 0.77 mmol), 9,9-dioctyl-2-(4,4,5,5-tetramethyl-1,3,2-dioxaborolane-2-yl)-9*H*-fluorene (0.85 mmol), K_2CO_3 (2.7 mmol), $Pd(PPh_3)_2Cl_2$ (0.04 mmol). The product was purified by column chromatography using an eluent mixture of *n*-hexane and ethyl acetate in a volume ratio of 8:1 to yield the viscous solid. Yield = 71% (134 mg); (FW = 698.03 g/mol). 1H NMR (300 MHz, $CDCl_3$, δ ppm): 8.76–8.65 (m, 2H), 8.36 (dd, $J_1 = 1.1$ Hz, $J_2 = 8.5$ Hz, 1H), 7.90 (d, $J = 8.5$ Hz, 1H), 7.86–7.79 (m, 2H), 7.72 (m, 2H), 7.52 (dd, $J_1 = 1.5$ Hz, $J_2 = 7.0$ Hz, 2H), 7.46–7.39 (m, 2H), 4.30–4.22 (m, 2H, NCH_2), 2.11–1.98 (m, 4H, CH_2 Fluorene), 1.87–1.74 (m, 2H, NCH_2CH_2), 1.41–0.94 (m, 22H, CH_2 Naphthlimide, CH_2 Fluorene), 0.94–0.82 (m, 11H, CH_2 , CH_3 Fluorene, CH_3 Naphthlimide). ^{13}C NMR (75.5 MHz, $CDCl_3$, δ ppm): 164.6, 164.4, 151.5, 151.3, 147.8, 141.8, 140.6, 137.6, 132.9, 131.4, 131.1, 130.5, 129.0, 128.1, 127.9, 127.3, 127.0, 124.8, 123.2, 121.9, 120.3, 120.1, 119.9, 55.6, 40.8, 40.5, 32.0, 30.3, 29.7, 29.5, 28.4, 27.5, 24.2, 22.9, 14.3. IR (KBr, ν cm^{-1}): (arene C–H) 3061; (aliphatic C–H) 2958, 2923, 2845; (imide C=O) 1698; (Ar C=C) 1655, 1585; (imide C–N) 1353, 1234. Anal. Calc. for $C_{49}H_{63}NO_2$: C, 84.31; H, 9.10; N, 2.01; O, 4.58%. Found: C, 84.35; H 9.15; N, 2.07%. MS (APCI⁺, 20 V), m/z : 698 [M+H]⁺.



2,7-Di((*N*-(2-ethylhexyl)-1,8-naphthalimide)-4-yl)-9,9-di(2-ethylhexyl)-9*H*-fluorene (21) was prepared by the similar procedure as **18** using 4-bromo-*N*-2-ethylhexyl-1,8-naphthalimide (**1**) (300 mg, 1.54 mmol), 9,9-di(2-ethylhexyl)-2,7-di(4,4,5,5-tetramethyl-1,3,2-dioxaborolane-2-yl)-9*H*-fluorene (0.38 mmol), K_2CO_3 (5.4 mmol), $Pd(PPh_3)_2Cl_2$ (0.08 mmol). The product was purified by silica gel column chromatography using an eluent mixture of *n*-hexane and ethyl acetate in a volume ratio of 8:1. Yield = 72% (145 mg); Yellow crystals (FW = 1005.42 g/mol); m.p. = 118–119 °C. 1H NMR (300 MHz, $CDCl_3$, δ ppm): 8.75–8.67 (m, 4H), 8.40–8.30 (m, 2H), 8.00 (d, $J = 7.7$ Hz, 2H), 7.80–7.71 (m, 4H), 7.63–7.53 (m, 4H), 4.28–4.14 (m, 4H, NCH_2), 2.19–2.09 (q, $J = 7.1$ Hz, 4H, CH_2 Fluorene), 2.08–1.93 (m, 4H, CH Naphthlimide), 1.51–1.31 (m, 16H, CH_2 Naphthlimide), 1.07–0.76 (m, 28H, CH_2 Naphthlimide, CH_3 Naphthlimide), 0.75–0.58 (m, 12H, CH_3 Fluorene). ^{13}C NMR (75.5 MHz, $CDCl_3$, δ ppm): 165.1, 164.8, 151.6, 151.6, 151.5, 147.5, 141.2, 137.9, 132.8, 131.7, 131.4, 130.6, 129.4, 128.0, 127.0, 125.9, 123.3, 122.1, 120.5, 55.9, 44.9, 44.5, 38.2, 35.2, 34.3, 31.1, 29.0, 28.9, 27.3, 24.4, 23.2, 14.3, 11.0, 10.5. IR (KBr, ν cm^{-1}): (arene C–H) 3062; (aliphatic C–H) 2957, 2925, 2856; (imide C=O) 1702; (Ar C=C) 1660,

1588; (imide C–N) 1353, 1233. Anal. Calc. for C₆₉H₈₄N₂O₄: C, 82.43; H, 8.42, N, 2.79, O, 6.37%. Found: C, 82.51; H, 8.49; N, 2.71%. MS (APCI⁺, 20 V), *m/z*: 1004 [M]⁺.



2,7-Di((*N*-(octyl)-1,8-naphthalimide)-4-yl)-9,9-dioctyl-9*H*-fluorene (22) was prepared by the similar procedure as **18** using 4-bromo-*N*-octyl-1,8-naphthalimide (**1**) (300 mg, 1.54 mmol), 9,9-dioctyl-2,7-di(4,4,5,5-tetramethyl-1,3,2-dioxaborolane-2-yl)-9*H*-fluorene (0.38 mmol), K₂CO₃ (5.4 mmol), Pd(PPh₃)₂Cl₂ (0.08 mmol). The product was purified by column chromatography using silica gel as stationary phase and an eluent mixture of *n*-hexane and ethyl acetate in a volume ratio of 8:1. Yield = 65% (112 mg); Yellow crystals (FW = 1005.42 g/mol); m.p. = 161–162 °C. ¹H NMR (300 MHz, CDCl₃, δ ppm): 8.78–8.66 (m, 4H), 8.38 (dd, *J*₁ = 1.0 Hz, *J*₂ = 8.5 Hz, 2H), 8.00 (d, *J* = 7.5 Hz, 2H), 7.85 (d, *J* = 7.5 Hz, 2H), 7.75 (dd, *J*₁ = 7.3 Hz, *J*₂ = 8.5 Hz, 2H), 7.63–7.52 (m, 4H, CH₂Fluorene), 4.32–4.20 (m, 4H, NCH₂), 2.18–2.02 (m, 4H, CH₂Fluorene), 1.86–1.74 (m, 4H, CH₂Naphthalimide), 1.49–1.11 (m, 32H, CH₂Naphthalimide, CH₂Fluorene), 0.96–0.80 (m, 12H, CH₃Fluorene, CH₃Naphthalimide). ¹³C NMR (75.5 MHz, CDCl₃, δ ppm): 164.6, 164.4, 151.8, 147.4, 141.0, 138.3, 132.9, 131.5, 131.1, 130.4, 129.4, 129.1, 128.2, 127.1, 124.9, 123.3, 122.0, 120.5, 55.8, 40.9, 40.5, 32.0, 30.2, 29.7, 29.5, 28.4, 27.5, 24.3, 22.9, 14.4. IR (KBr, ν cm⁻¹): (arene C–H) 3060; (aliphatic C–H) 2956, 2926, 2856; (imide C=O) 1701; (Ar C=C) 1658, 1589; (imide C–N) 1354, 1232. Anal. Calc. for C₆₉H₈₄N₂O₄: C, 82.43; H, 8.42, N, 2.79, O, 6.37%. Found: C, 82.49; H, 8.46; N, 2.78%. MS (APCI⁺, 20 V), *m/z*: 1004 [M]⁺.

4. RESULTS AND DISCUSSION

4.1. Bipolar compounds having 1,8-naphthalimide and triphenylamino moieties

Naphthalimide derivatives represent an attractive class of electron-deficient organic materials with high electron affinities (~ -3 eV) [13], due to the existence of an electron-deficient centre [13] and display good electron-transporting or hole-blocking capabilities. They have wide energy gaps ($\sim 2.2-3$ eV) [175] and low reduction potentials ($\sim -1.8-2$ V) [176]. They also exhibit good photochemical stability [177,178] and high luminescence quantum yields [13–15,179]. Wide possibility of functionalization via imide moiety [180] and carbocyclic core using non-chromophore or chromophore substituents in order to improve the processability or electronic properties have also driven research interest extensively on naphthalimides and their derivatives [178,181]. The substitutions at the C-4 position of 1,8-naphthalimide derivatives [16,41,43], may change glass transition temperatures, shift fluorescence wavelengths, change fluorescence quantum yields, shift redox potentials and/or improve photoelectrical characteristics [71,109,182,183].

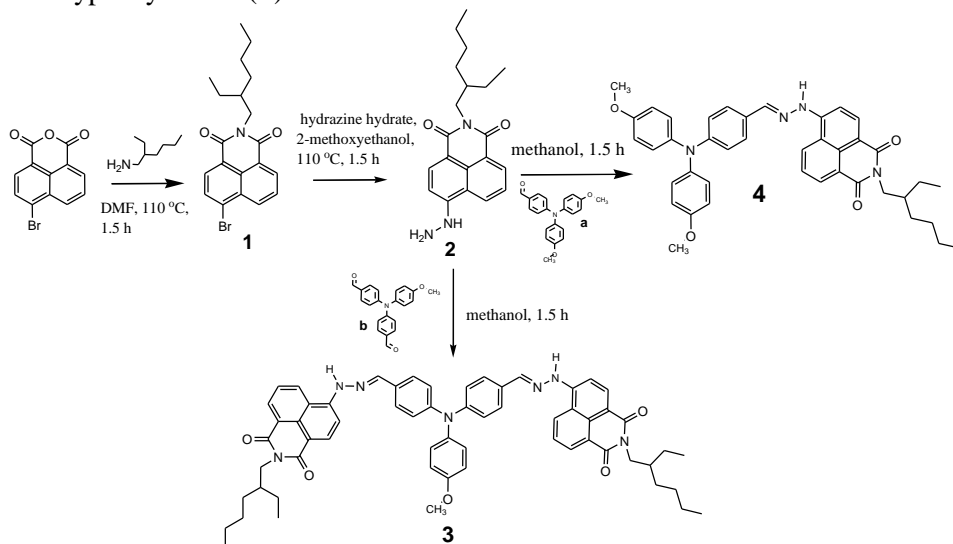
Compounds bearing TPA moiety are widely investigated mainly as hole-transporting materials, and their properties were described in a number of papers and reviews [8,184–186]. TPA and its derivatives, with excellent solubility, good stability, and high photoluminescent efficiency, have been extensively used in optoelectronic devices [187]. Electron-rich TPA derivatives have been typically used as hole-transporting materials and/or blue light emitting materials [188–190] due to the easy oxidizability of the nitrogen center and the ability to transport positive charges via the radical-cation species. These properties are related to the presence of nitrogen atom linked to three electron rich phenyl groups in a three-dimensional propeller-like shape [191], which benefits the amorphous structure and solution-processability of the compounds containing it.

4.1.1. Synthesis and properties of hydrazones containing 1,8-naphthalimide and triphenylamino moieties

Bipolar molecular glasses are of interest for the applications in optoelectronic devices such as organic light-emitting diodes. Recently materials showing bipolar charge transport properties have been reported by several groups [192–194]. To achieve a good balance of holes and electrons, both hole and electron-transporting functions should be incorporated into a single bipolar material [195,196]. One promising strategy is to develop bipolar compounds bearing both electron-donating and electron-accepting moieties capable of matching for charge carrier injection and acceptance of both holes and electrons [189,197,198]. In this chapter, the synthesis and a systematic investigation of hydrazones containing both donor (triphenylamino) and acceptor (1,8-naphthalimide) moieties are reported.

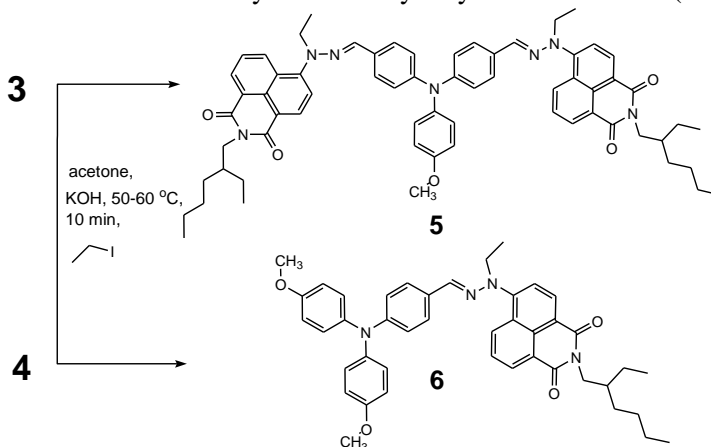
Synthesis and characterization

Compounds **3** and **4** were synthesized by the synthetic route, shown in Scheme 4.1. The first step was condensation of 4-bromo-1,8-naphthalic anhydride with 2-ethylhexylamine to obtain 4-bromo-*N*-(2-ethylhexyl)-1,8-naphthalimide (**1**). Compounds **3** and **4** were obtained by condensation of compound **2** with an excess of 4-(di(4-methoxyphenyl)amino)benzaldehyde (**a**) and 4,4'-diformyl-4''-methoxyphenylamine (**b**).



Scheme 4.1. Synthetic routes to hydrazones **3** and **4**

Compounds **5** and **6** were synthesized by alkylation of **3** and **4** (Scheme 4.2).



Scheme 4.2. Synthesis of compounds **5** and **6**

The chemical structures of the newly synthesized compounds (**1–6**) were confirmed by ^1H NMR, ^{13}C NMR, IR, and mass spectrometries. Hydrazones **3–6** were found to be soluble in common organic solvents such as chloroform, acetone, THF.

Thermal properties

The behaviour under heating of compounds **3–6** was studied by DSC and TGA under a nitrogen atmosphere. The values of T_g and 5% weight loss temperatures ($T_{ID-5\%}$) are summarized in Table 4.1.

Table 4.1. Temperatures of the thermal transitions of compounds **3–6**

Compound	T_g ($^{\circ}\text{C}$) (2 nd heating)	$T_{ID-5\%}$ ($^{\circ}\text{C}$)
3	142	275
4	87	348
5	73	268
6	46	303

Compounds **3–6** demonstrated thermal stability similar to that of other hydrazones [199]. The $T_{ID-5\%}$ ranging from 268 $^{\circ}\text{C}$ to 348 $^{\circ}\text{C}$ we recorded by TGA with a heating rate of 20 $^{\circ}\text{C}/\text{min}$. Alkyl substituted derivatives **5** and **6** exhibited lower thermal stability than the corresponding unsubstituted compounds (**3** and **4**). The attachment of ethyl group at the nitrogen atom of hydrazone moiety lead to the change of the mechanism of thermal degradation. While the degradation of unsubstituted compounds (**3** and **4**) occurred in one stage, the alkyl-substituted derivatives (**5** and **6**) showed two-step thermal degradation. Fig. 4.1 showing TGA curves of compounds **4** and **6** illustrates this statement.

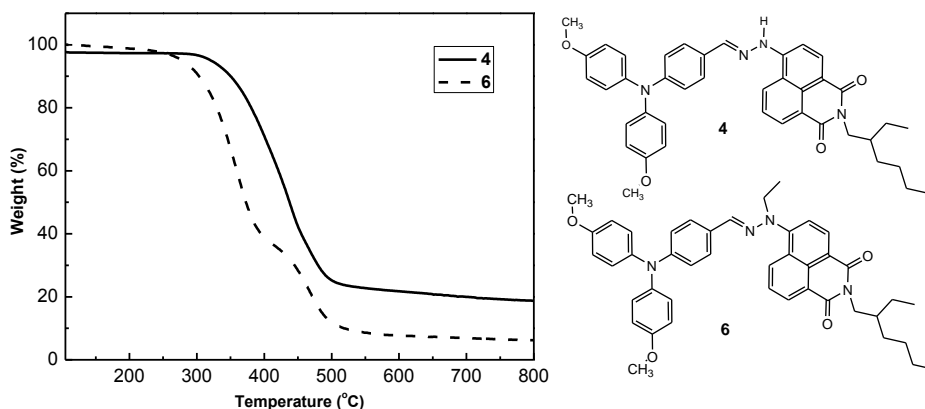


Figure 4.1. TGA curves of **4** and **6** recorded at the heating rate of 20 $^{\circ}\text{C}/\text{min}$ in N_2

The compounds synthesized can exist in the glassy state. Their T_g range from 46 to 142 $^{\circ}\text{C}$. The comparison T_g of compounds **3** and **4** having secondary amino group with those of alkyl substituted hydrazones **5** and **6** revealed considerably higher T_g of **3** and **4**. This observation can apparently be explained by the hydrogen bonding in the glasses of **3** and **4**.

Optical and fluorescence properties

Fig. 4.2 and Fig. 4.3 show UV and FL spectra of dilute solutions and thin films of compounds **3–6**. The wavelengths of absorption and emission maxima are summarized in Table 4.2.

Table 4.2. Wavelengths of absorption and fluorescence maxima of compounds **3–6**

Compound	UV: λ_{max} , (nm) ^a	UV: λ_{max} , (nm) ^b	FL: λ_{max} , (nm) ^a
3	476	499	562
4	478	511	585
5	471	485	N.d
6	475	491	N.d

^a Solution in THF with the concentration of 10^{-5} M. ^b Measured for thin films on the fused quartz plates. N.d – fluorescence not detectable.

The absorption spectra of compounds **3**, **4** and **5**, **6** are similar. The lowest energy absorption bands of monohydrazones **4** and **6** are slightly red-shifted with respect of those of dihydrazones **3** and **5**. This observation can apparently be explained by the presence of two methoxy groups in the triphenylamino moieties of monohydrazones. The FL spectra of compounds **3** and **4** are also similar. The spectrum of monohydrazone **4** shows bathochromic shift with respect to the spectrum of dihydrazone **3**. This observation is consistent with the UV spectrometry data. Absorbance spectra of the films are similar to those of the dilute solutions, however the lowest energy absorption bands of the films are red-shifted with respect to those of the solutions, apparently due to enhanced intermolecular interactions in the solid state. Bathochromic shifts of the spectra of the films with respect of the spectra of the solutions are more evident for compounds **3** and **4** relative to compounds **5** and **6**. The intermolecular interaction in the films of unsubstituted hydrazones is apparently stronger due to hydrogen bonding. We did not manage to record FL from the films of compounds **5** and **6**. This was apparently due to the intermolecular quenching.

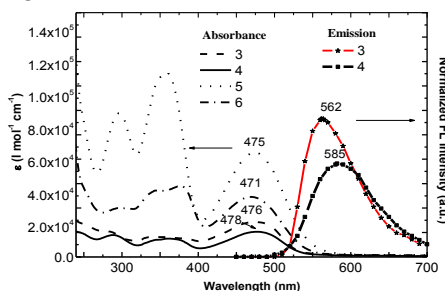


Figure 4.2. UV-Vis and FL spectra of dilute THF solutions (10^{-5} M) of hydrazones **3–6**. Absorption maxima wavelengths were used as excitation wavelengths

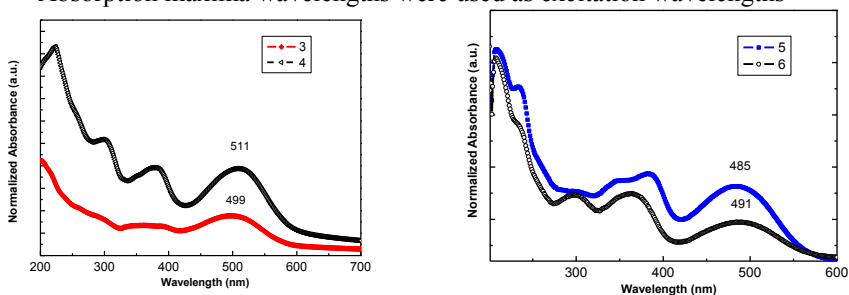


Figure 4.3. UV-Vis absorption spectra of thin films of hydrazones **3–6**

Electrochemical properties

Electrochemical investigation of DCM solutions of compounds showed that oxidation starts at the same potential of 0.09 V as shown in Fig. 4.4a-d. The first oxidation potential of compounds occurs at 0.30 V for **3** and at 0.25 V for **4**. Oxidation of **3** and **4** is a reversible redox process (Fig. 4.4) but the reduction process is reversible only for **5** and **6** (Fig. 4.4a,c). The first reduction potential occurred at -1.86 V, -1.84 V for compounds with alkyl chain (**5**, **6**) and at -1.97 V, -1.99 V for compounds with unsubstituted hydrazine moiety (**3**, **4**).

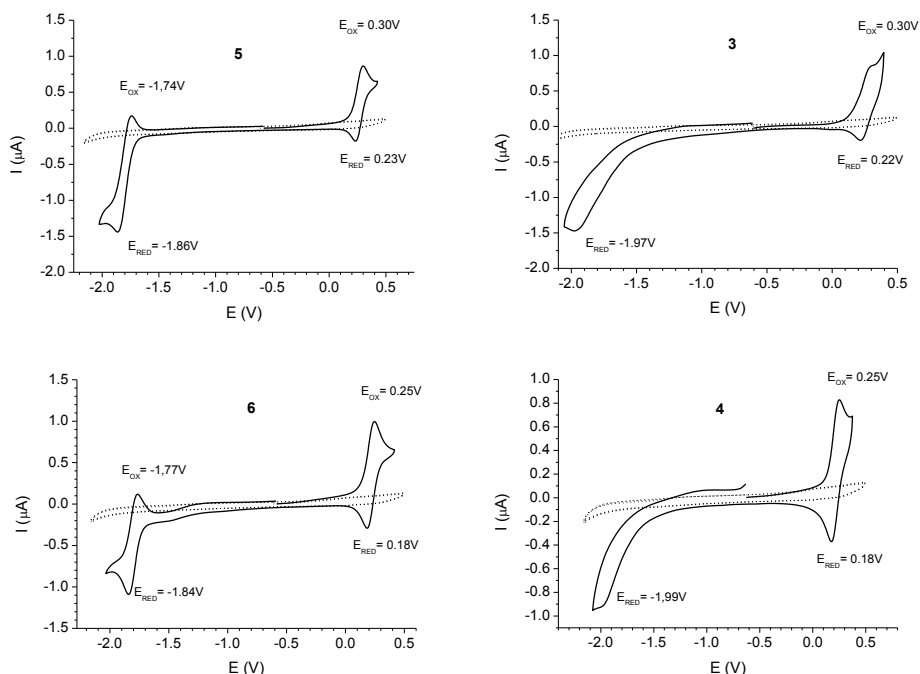


Figure 4.4. CV¹ curves of 1mM solutions in 1M Bu₄NBF₄ DCM electrolyte of a) **5**; b) **3**; c) **6**; d) **4**

CV curves of monohydrazones **4**, **6** are shifted to the left as compared to the curves of dihydrazones **3**, **5**. The shapes of CV curves are similar for alkyl substituted compounds **5** and **6** (cf. curves 4.4a,c). They are also similar for unsubstituted derivatives (**3** and **4**) (cf. curves 4.4b,d). However the considerable distinctions are observed between CV curves of alkyl substituted (**5**, **6**) and unsubstituted (**3**, **4**) compounds (cf. curves 4.4a,b). Free hydrogen at hydrazine nitrogen is apparently involved in side reactions of electrochemical process and because of that reduction process is not reversible. Oxidation part of CV curves is related to the oxidation of triphenylamino group and reduction part is related to the reduction of imido group.

¹ Electrochemical measurements were carried out at the Faculty of Chemistry, Silesian University of Technology by dr. P. Data.

DPV spectra (Fig. 4.5) show absolute peaks of oxidation and reduction processes. In correlation to the molecular band, oxidation peak is related to IP_{CV} and reduction peak is related to EA_{CV} values. E_g^{elc} value is in the range between those peaks. Oxidation potential peaks are similar for monohydrazones **4** and **6** (0.21 V) and dihydrazones **3** and **5** (0.16 V). For the reduction potential peaks the opposite correlation is observed: the potentials are similar for compounds with alkyl groups **5**, **6** (-1.80 V) or without them **3**, **4** (-1.89 V).

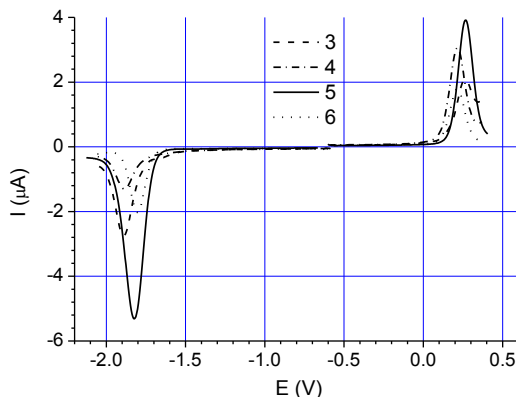


Figure 4.5. DPV curves of 1mM of solutions of compounds **3–6** in 1M Bu_4NBF_4 DCM electrolyte

The band-gap value is one of the most useful characteristic for materials used in optoelectronic devices. E_g^{elc} is usually slightly lower than the E_g^{opt} one. The band gap value for the alkyl-substituted hydrazones **5**, **6** are lower than those of unsubstituted hydrazones **3** and **4**. Alkyl-substituted hydrazones **5**, **6** show lower of EA_{CV} values than their unsubstituted counterparts. Compounds **4** and **6** having two methoxy groups in triphenylamino moiety show increased IP_{CV} (see Table 4.3).

Table 4.3. IP_{CV}/EA_{CV} , optical and electrochemical band-gap energies and IP_{EP} of bipolar hydrazones

Compound	IP_{CV} , (eV) ^a	EA_{CV} , (eV) ^b	E_g^{elc} , (eV) ^c	E_g^{opt} , (eV) ^d	IP_{EP} , (eV) ^e
3	5.06	-2.91	2.15	2.27	–
4	5.01	-2.91	2.10	2.27	–
5	5.06	-3.00	2.06	2.24	5.45
6	5.01	-3.00	2.01	2.25	5.45

^a Ionization potentials and electron affinities estimated according to $IP_{CV} = (E_{onset}^{ox} + 4.8)$ (eV). $EA_{CV} = -(E_{onset}^{red} + 4.8)$ (eV). ^b $EA_{CV} = -(|IP_{CV}| - E_g^{opt})$. ^c $E_g^{elc} = |IP_{CV}| - |EA_{CV}|$. ^d The optical band gap estimated from the onset wavelength of optical absorption according to the empirical formula: $E_g^{opt} = 1240/\lambda_{edge}$. ^e Established from electron photoemission in air spectra².

² IP_{EP} was measured at the Department of Solid State Electronics, Vilnius University.

The IP_{EP} values determined by cyclic voltammetry do not represent any absolute solid-state or gas-phase ionization energies, they can be used only for the comparison of different compounds. It was therefore of interest to estimate the ionization potentials of the amorphous layers of the synthesized compounds by electron photoemission technique. The values of IP_{EP} of compounds **5** and **6** are given in Table 4.3. It seems that the presence of electron accepting 1,8-naphthalimide species has minor effect on the ionization potentials of these compounds. They are close to the ionization potentials of earlier reported triphenylamine-based hydrazones [200,201]. The IP_{EP} values of the synthesized compounds are rather close and comparable to IP_{EP} of classical hole transporting material TPD (5.3–5.5 eV) [202].

Photoelectrical properties

Xerographic time of flight measurements were used to characterize the magnitudes of hole drift mobility (μ_h) for the solid solutions of compounds **5** and **6** in the host polymer bisphenol Z polycarbonate (PC-Z). For the layers of the solid solutions of compounds **5** and **6** in PC-Z the room temperature μ_h shows the linear dependencies on the square root of the electric field (Fig. 4.6). This characteristic dependence is observed for the majority of amorphous organic systems and can be attributed to the effects of disorder on charge transport [203]. The layers of the solid solutions of compounds **5** and **6** in PC-Z (50%) showed μ_h exceeding $10^{-5} \text{ cm}^2 \cdot \text{V}^{-1} \cdot \text{s}^{-1}$ at high electric fields at 25 °C, these results indicate that such compounds are suitable for practical applications in the solid-state dye-sensitized solar cells [204]. The hole drift mobility values of the synthesized hydrazones are comparable to those of the other derivatives of hydrazones [205,206].

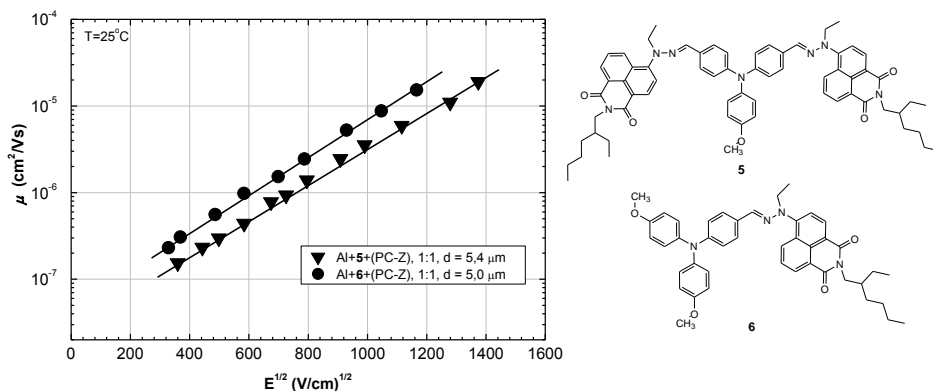


Figure 4.6. Electric field dependencies of hole-drift mobilities³ in the layers of hydrazones **5**, and **6** molecularly doped in PC-Z (50 wt.%)

In conclusion, four new hydrazones containing both acceptor and donor moieties were synthesized and their thermal, optical, electrochemical and photoelectrical properties were investigated. The hydrazones exhibit 5% weight loss

³ Hole mobilities were measured at the Department of Solid State Electronics, Vilnius University by dr. V. Jankauskas.

temperatures in the range of 268–348 °C and can form glasses with glass transition temperatures in the range of 46–142 °C. Room temperature time-of-flight hole mobilities in the solid solutions of the derivatives in the polymeric host bisphenol-Z polycarbonate (50%) exceeded 10^{-5} cm²/V·s at high applied electric fields.

4.1.2. Synthesis and properties of ambipolar organic compounds containing triphenylamino and 1,8-naphthalimide moieties linked via the single bonds

In the last decades many kinds of organic hole-transporting amorphous molecular materials were reported [8]. Lesser assortment is available of glass-forming electron-transporting organic molecular materials especially those capable of working in air [207–210]. Even smaller amount of amorphous organic molecular materials capable of effectively transporting both holes and electrons were reported. Such materials recently attract much attention [211–213]. Ambipolar charge-transporting materials are of interest for the applications in organic light emitting diodes (OLED) [214,215] and in particular in electrophosphorescent devices [216]. Materials capable of transporting both negative and positive charges at ambient conditions are of particular interest [217,218].

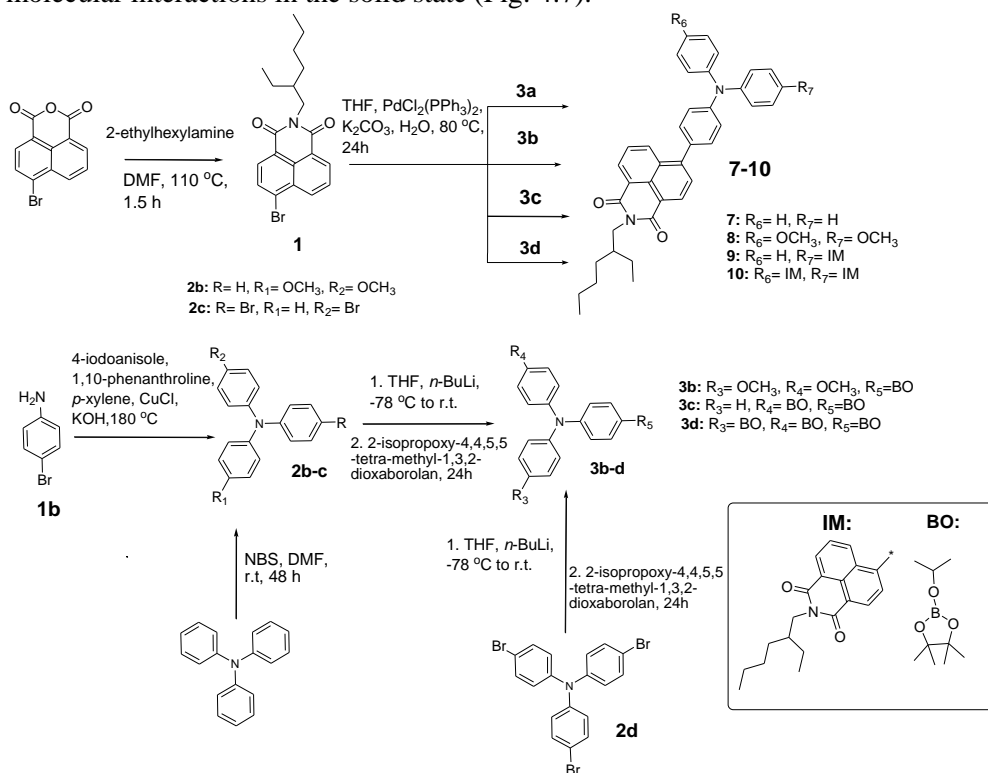
In this chapter, the synthesis and properties of compounds consisting of 1,8-naphthalimide and TPA moieties capable of effectively transporting both holes and electrons in air are reported. Hydrazones containing 1,8-naphthalimide and triphenylamino moieties (see Chapter 4.1.1) were found to be capable of transporting only positive charges in air. To our knowledge no studies demonstrating ambipolar charge transport in the derivatives of 1,8-naphthalimide and TPA were yet reported.

By applying a joint experimental and theoretical approaches, the aim of this study is twofold: (i) report on the synthesis of four new derivatives of TPA containing direct linkages with a different number of naphthalimide moieties (ii) characterization of the four new compounds for better understanding of the structure-property relationships. The hole-transport properties of these amorphous compounds are discussed in the frame of Marcus theory [219–222].

Synthesis and characterization

Scheme 4.3 shows the synthetic routes to compounds **7–10**. The first step was condensation of 4-bromo-1,8-naphthalic anhydride with 2-ethylhexylamine in DMF which gave 4-bromo-*N*-(2-ethylhexyl)-1,8-naphthalimide (**1**). Compound **2b** was obtained by Ullmann coupling of 4-bromoaniline (**1b**) with 1-iodo-4-methoxybenzene [223]. Compound **2c** was prepared by bromination of TPA with NBS. Compounds **3b–d** were obtained by the reactions of **2b**, **2c** and commercially available tris(4-bromophenyl)amine (**2d**) with *n*-BuLi at –78 °C and the following quenching with 2-isopropoxy-4,4,5,5-tetramethyl-1,3,2-dioxaborolane. 4-(4'-Diphenylaminophenyl)-*N*-ethylhexyl-1,8-naphthalimide (**7**) was synthesized by Suzuki coupling of 4-bromo-*N*-(2-ethylhexyl)-1,8-naphthalimide (**1**) with 4-(diphenylamino)phenylboronic acid (**3a**). Compounds **8–10**, were also synthesized by the Suzuki coupling reactions between compounds **3b–d** and compound **1** under

nitrogen atmosphere. All the derivatives were characterized by ^1H and ^{13}C NMR, mass spectrometries and elemental analysis, and additionally. The crystal structure of compound **7** was identified by X-ray analysis which helped to understand the molecular interactions in the solid state (Fig. 4.7).



Scheme 4.3. The synthetic routes to **7–10**

The target compounds (**7–10**) are soluble in common organic solvents such as DCM, chloroform, THF, chlorobenzene and toluene.

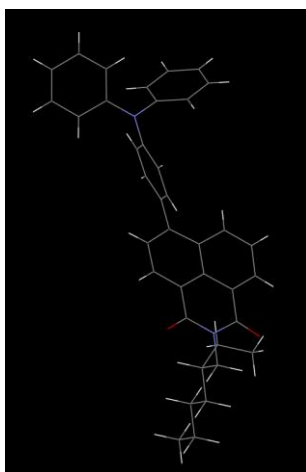
X-ray structure analysis⁴

Single crystals of **7** suitable for the XRD analysis were obtained by slow evaporation of the solvent mixture from chloroform and hexane. Compound **7** was packed in a monoclinic crystal lattice; the crystal data are summarized in Table 4.4. The steric interactions of the phenyl ring of TPA impart a propeller-like conformation stemming from the trigonal nitrogen center (Fig. 4.7).

⁴ X-ray structure analysis have done at the Department of Polymer Chemistry and Technology, Kaunas University of Technology by dr. G. Bagdziunas.

Table 4.4. The crystal data for compound **7**

Empirical formula	C ₃₈ H ₃₆ N ₂ O ₂
Formula weight	552.71
Crystal color, habit	colorless, prism
Crystal dimensions	0.520 × 0.260 × 0.120 mm
Crystal system	monoclinic
Lattice type	primitive
Lattice parameters	a = 12.54(2) Å b = 8.378(9) Å c = 28.27(3) Å β = 92.58(2) ° V = 2967(6) Å ³
Space group	P2 ₁ /n (#14)
Z value	4
D _{calc}	1.237 g/cm ³
F ₀₀₀	1176.00
μ (MoKα)	0.759 cm ⁻¹
Temperature	20.0 °C
Refinement method	Full-matrix least-squares on F ²
Goodness of Fit Indicator	1.096
Largest difference peak and hole, e·Å ⁻³	0.48 e ⁻ /Å ³ and -0.38 e ⁻ /Å ³
Maximum and minimum transmission	from 0.152 to 0.991

**Figure 4.7.** The molecular structure of **7**

DFT calculations, geometries and frontier orbitals

The geometries of model compounds **M7–M10**, (containing methyl groups instead of the experimental alkyl groups) are presented in Fig. 4.8, along with some relevant geometrical parameters.

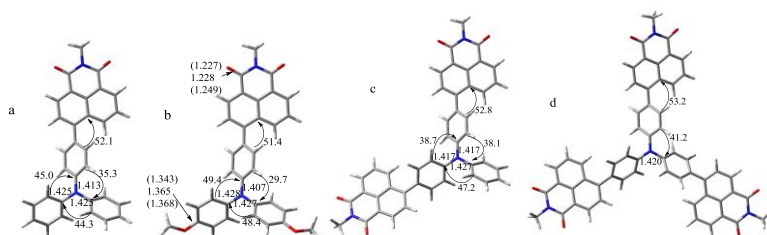


Figure 4.8. Optimized geometries of **M7** (a), **M8** (b), **M9** (c), and **M10** (d) model compounds, obtained at the B3LYP/6-31G(d,p) level. Some relevant bond-lengths (N-C bond-lengths in TPA core in Å) and dihedral angles (absolute values in degrees) are shown. The C-O bond-lengths for compound **M8** in the neutral state are also indicated, along with the same distances in the cationic and anionic states (shorter and longer distances respectively in parentheses)⁵

The TPA N atom of each compound and the three appended carbon atoms form a plane (reported hereafter as “N-plane”), due to the π -conjugation between the phenyl groups and the lone pair of the central N atom. In the case of **M8**, only one conformer is presented. Other conformers of similar energy can be assumed, with the methoxy groups combined in different orientations. Compared to the model compound **M7**, the geometry around the N(TPA) atom in **M5** has more quinoidal character, which is due to the π -donor effect of the methoxy groups. The same observation can be done when comparing **M8** with **M9** and **M10**. The frontier orbitals for the three molecules are given in Fig. 4.9.

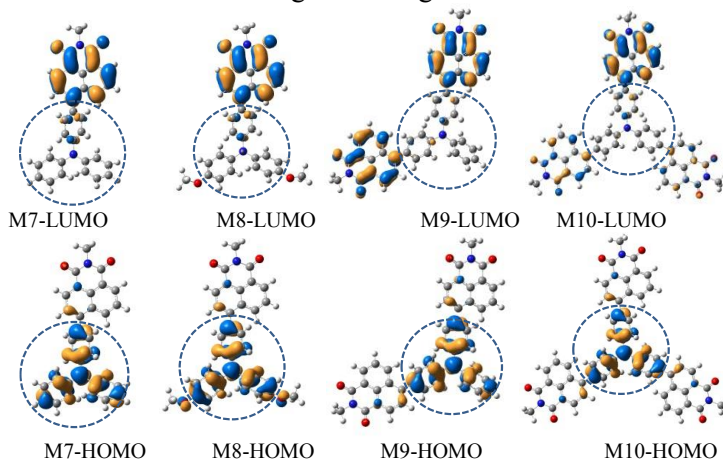


Figure 4.9. Sketch of frontier orbitals for the model compounds **M7**–**M10**. The encircled parts delimit the TPA moiety. The frontier orbitals for the three molecules (Fig. 4.9) look very similar for all compounds, being localized almost entirely on the TPA core for the HOMO or naphthalimide moiety for the LUMO. The presence of the π -donor methoxy groups in **M8** is expected to destabilize the HOMO orbital [224] as compared to **M7**, which can also be deduced from the anti-bonding contribution of the methoxy groups in the shape of the HOMO orbital of **M8**

⁵ DFT calculations have done at the Laboratoire de Physicochimie des Polymères et des Interfaces, Université de Cergy-Pontoise by dr. G. Sini.

Thermal properties

The thermal properties of **7–10** were examined by DSC and TGA under a nitrogen atmosphere. The values of T_g , T_m and 5% weight loss temperatures ($T_{ID-5\%}$) are summarized in Table 4.5.

Table 4.5. Thermal characteristics of compounds **7–10**

Compound	T_g (°C) (2 nd heating)	T_m (°C)	$T_{ID-5\%}$ (°C)
7	47	134	437
8	45	–	429
9	76	136	448
10	84	141	483

TGA revealed that all the target compounds exhibit excellent thermal stabilities. Their $T_{ID-5\%}$ range from 429 to 483 °C. These temperatures are close to 5% weight loss temperatures of methoxy-substituted derivatives of TPA [224]. Increase of the number of 1,8-naphthalimide moieties leads to the increase of the thermal stability of the derivatives. Molecules **9**, **10** having two and three 1,8-naphthalimide moieties showed higher 5% weight loss temperatures than molecules **7** and **8** containing one 1,8-naphthalimide moiety.

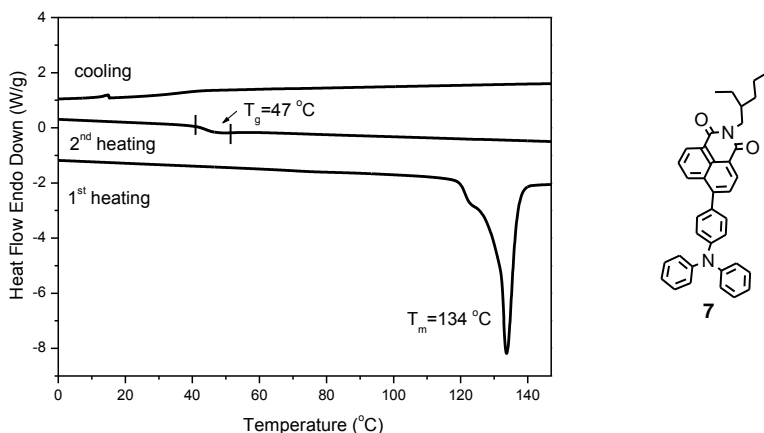


Figure 4.10. DSC thermograms of compound **7** (scan rate of 10 °C/min, N_2 atmosphere)

Compounds **7**, **9** and **10** were obtained as crystalline materials. Their first DSC heating scans revealed melting in the range of 134–148 °C. Their second DSC heating scans revealed the T_g in the range of 45–93 °C and no peaks due to crystallization appeared. The values of T_g of molecular glasses of **7–10** are affected by the number of naphthalimide moieties in the para positions of triphenylamino moiety and increase in the order $7 < 9 < 10$. The lower T_g values of **7** and **8** can apparently be explained in terms of their lower molecular weight and lower intermolecular interaction. The DSC traces of **5** did not display transition associated with melting even during repeated scans. The absence of melting confirms the amorphous character of **8**. This observation can apparently be attributed to the presence of methoxy groups at the triphenylamino moiety which increase the disorder in the molecule packing. Previously it has been suggested that C-H... π short

contacts can be established between the methoxy groups and the phenyl groups [224]. C-H... π short contacts of different interaction energies may thus be present in the films of compound **8**, which might be responsible for the absence of a well-defined melting temperature. The amorphous nature of compound **8** is also reflected in its enhanced solubility. Fig. 4.10 shows DSC thermograms of compound **7**. During the first heating scan of the sample of **7** the endothermal melting signal at 134 °C was observed. After re-cooling, the following second heating scan revealed glass transition at 47 °C and no crystallization signal was observed. This observation shows that the material can exist in solid amorphous state and can be considered as molecular glass.

Optical and fluorescence properties

UV-Vis absorption spectra and fluorescence spectra of the dilute solutions in nonpolar cyclohexane, of dilute solid solutions in PS matrixes, and of solid films of the investigated TPA and naphthalimide derivatives are shown in Fig. 4.11 and Fig. 4.12). The fluorescence characteristics of the compounds are summarized in Table 4.6.

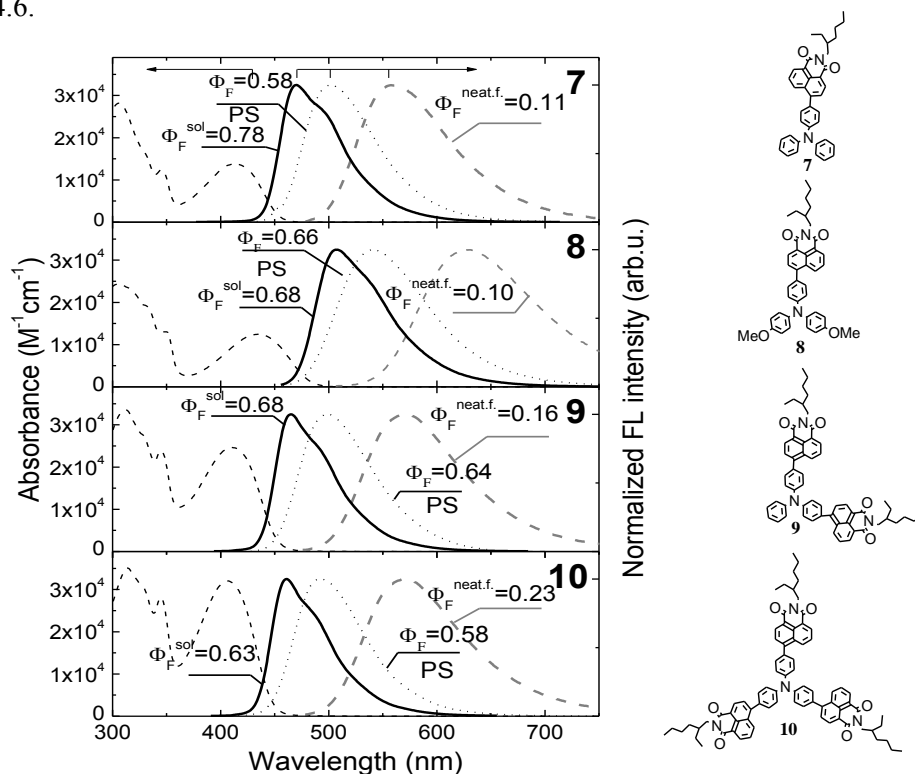


Figure 4.11. Absorption (dashed thin line) and normalized fluorescence spectra of the 10^{-6} M solutions of compounds **7–10** in cyclohexane (thick, solid line), of solid films (dashed grey line) and of molecular dispersions in polystyrene matrix at 0.25 wt% concentration (dotted line). Fluorescence quantum yields are indicated. Absorption maxima wavelengths were used as excitation wavelengths

Table 4.6. Fluorescence characteristics⁶ of the dilute cyclohexane solutions, solid films and 0.25 wt% solid solutions in PS of compounds **7–10**

Compound	Solution in cyclohexane							Solid film				In PS			
	$\lambda_{\text{abs.}}$ (nm) (ϵ^a , L mol ⁻¹ cm ⁻¹)	$\lambda_{\text{em.}}$ (nm)	Φ_{F}	τ (ns)	$\tau_{\text{R}}^{\text{b}}$ (ns)	$\tau_{\text{NR}}^{\text{b}}$ (ns)	$\lambda_{\text{teor}}^{\text{c}}$ (nm)	$\lambda_{\text{abs.}}$ (nm)	$\lambda_{\text{em.}}$ (nm)	Φ_{F}	$\tau_{\text{avg.}}$ (ns)	$\lambda_{\text{abs.}}$ (nm)	$\lambda_{\text{em.}}$ (nm)	Φ_{F}	$\tau_{\text{avg.}}$ (ns)
7	413 (13821)	470	0.78	3.2	4.1	14.5	488	425	557	0.11	13.1	430	501	0.58	5
8	434 (12459)	506	0.68	4.7	6.9	14.7	532	448	630	0.10	10.8	452	541	0.66	7.2
9	410 (24658)	465	0.68	2.6	3.8	8.1	482	426	569	0.16	9.2	426	498	0.64	2.8
10	407 (32025)	461	0.63	2.2	3.5	5.9	470	425	570	0.23	13.3	426	493	0.58	3.8

^a Molar extinction coefficient. ^b Radiative and non-radiative decay time constants calculated as τ/η and $\tau/(1-\eta)$, respectively. ^c The theoretical $S_0 \rightarrow S_1$ values calculated at the TDB3LYP/6-31G(d,p) level.

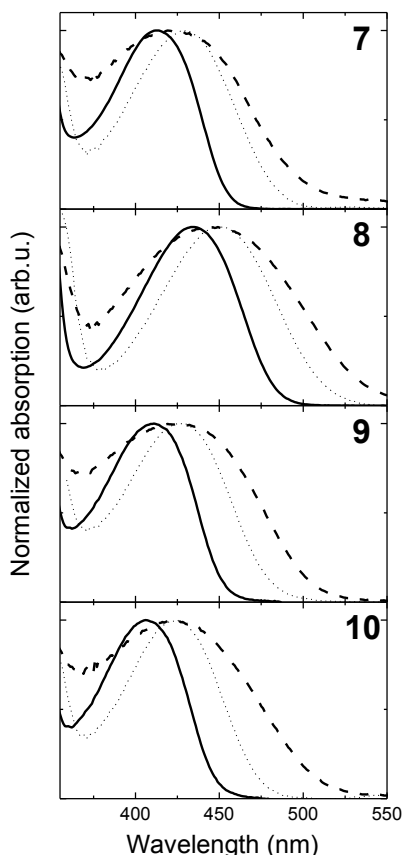


Figure 4.12. Absorption spectra of the solutions of compounds **7–10** in cyclohexane (10^{-6} M) (thick, solid line), solid films (dashed line) and of the solid solutions in polystyrene at 0.25 wt% concentration (dotted line)

⁶ Optical and fluorescence properties were obtained at the Institute of Applied Research, Vilnius University by dr. A. Miasojedovas.

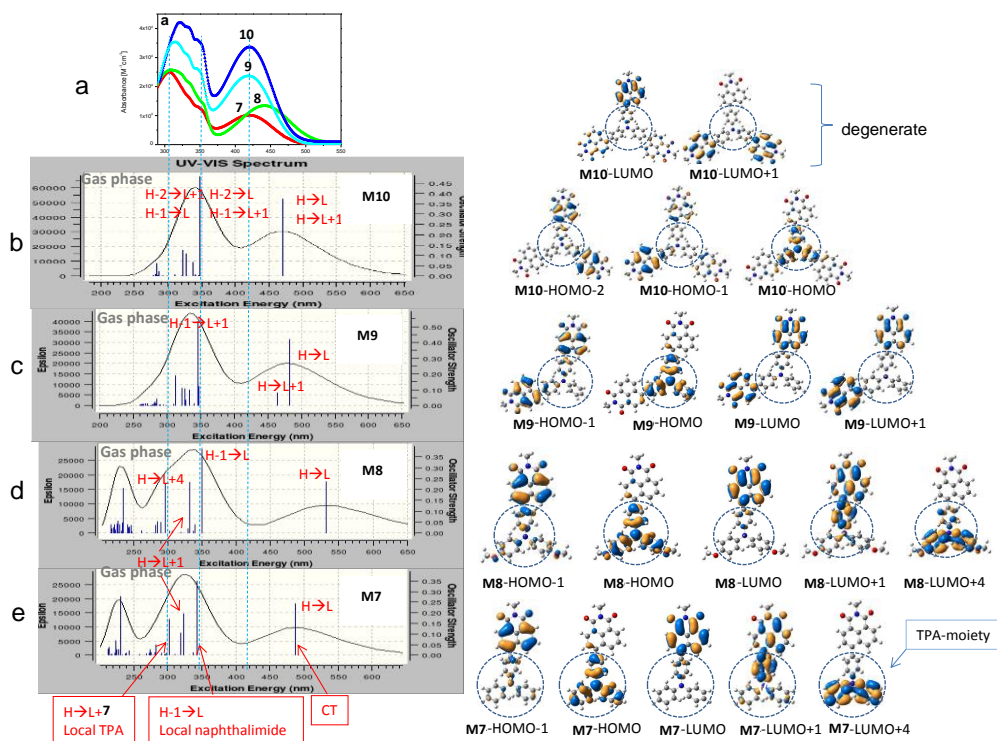


Figure 4.13. UV-Vis experimental (a) and theoretical spectra of **M7–M10** model compounds (e, d, c, and b respectively) obtained by mean of TDDFT calculations⁷ at B3LYP/6-31G(d,p) level. The absorption bands are obtained by considering peak half-widths at half height of 0.2 eV. Some relevant MOs are also presented. The theoretical CT bands are red shifted with respect to the experimental ones. This is a known effect which is due to the bad performances of standard hybrid functionals (like B3LYP) in the description of CT excitations. For more details on this point see for example [225–229]

The theoretical UV-Vis spectra for the model compounds **M7–M10** (Fig. 4.13) suggest that the absorption bands peaking at about 320 nm and 350 nm (Fig. 4.11) correspond to the local $\pi-\pi^*$ electron transitions of the triphenylamino moieties and naphthalimide fragments [230], respectively. Absorption peaks which appear in the range of 406–436 nm correspond to HOMO \rightarrow LUMO electronic transition, with HOMO and LUMO orbitals being almost exclusively localized on the donor and acceptor moieties, respectively (Fig. 4.9). These broad unstructured bands correspond consequently to the intramolecular charge-transfer transitions between the TPA donor moieties and the naphthalimide acceptor moieties. In the case of compounds **M9** and **M10**, a second CT excitation ($S_0\rightarrow S_2$) is present in the CT band (Fig. 4.13). The $S_0\rightarrow S_1$ and $S_0\rightarrow S_2$ excitations correspond to HOMO \rightarrow LUMO and HOMO \rightarrow LUMO+1 electronic transitions, both virtual orbitals being exclusively localized on the naphthalimide arms (see Fig. 4.13 for the pictograms of the

⁷ DFT calculations have done at the Laboratoire de Physicochimie des Polymères et des Interfaces, Université de Cergy-Pontoise by dr. G. Sini.

LUMO+1 orbitals of **M9** and **M10**). In the case of compound **M9**, the oscillator strength of $S_0 \rightarrow S_2$ transition is smaller as compared to $S_0 \rightarrow S_1$ (0.079 and 0.419 respectively). As for compound **M10**, the two CT electronic transitions, HOMO \rightarrow LUMO and HOMO \rightarrow LUMO+1, are degenerate, (identical oscillator strengths values of 0.373). The increasing intensity of the charge transfer bands from **7** to **10** (Fig. 4.11 and Fig. 4.13) is thus related to the presence of a second CT transition of increasing intensity in the order **M9** < **M10**.

The lowest energy absorption band of **8** is red shifted by ca. 20 nm in comparison with those of **7**, **9** and **10**. This effect is due to the electron donating ability of methoxy groups in the triphenylamino moiety of **8**, (see also the anti-bonding contribution of the methoxy groups in the shape of the HOMO orbital of **M8**, Fig. 4.9). By using the onset wavelengths of the absorption bands it was possible to roughly estimate the E_g^{opt} of the molecules which ranged from 2.40 to 2.58 eV (Table 4.7). The E_g^{opt} of compound **8** containing methoxy groups in the para positions of triphenylamino moiety is evaluated at 2.40 eV, which is by 0.15 eV lower than that of the corresponding derivative (**7**) containing no methoxy substituents (2.55 eV).

The absorption spectra of solid films of **7–10** and those of molecular dispersions in PS matrixes are presented in Fig. 4.12. The low energy absorption bands of the films are broader and slightly red shifted with respect to those of the dilute solutions. It is presumed that the red shifts of the absorption spectra of films as compared to those of solutions may be due to smaller dihedral angles in solid state, thus giving rise to more efficient π -conjugation and decreased HOMO–LUMO gap, but can also be due to more efficient π -stacking and stronger intermolecular interactions in the films than in dilute solutions [231]. Some degree of aggregation in the ground state may also be suspected to influence the absorption spectra of the films of these compounds. As a means to confirm this assumption, we have optimized dimers of different geometries for compounds **7** and **8** (Fig. 4.14).

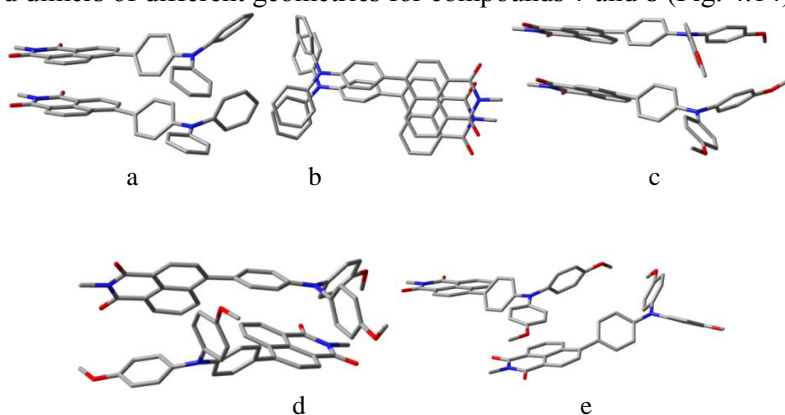


Figure 4.14. Dimers of different geometries optimized at the wB97XD/6-31G(d,p) level: a) and b) two different views of the same dimer for compound **7**, reported here as Dim-**M7**-HH (head-to-head); c) dimer for compound **8**, reported here as Dim-**M8**-HH; d) dimer for compound **8**, reported here as Dim-**M8**-HT (head-to-tail); e) dimer for compound **8**, reported here as Dim-**M8**-DA (donor-acceptor)

The theoretical UV-Vis spectra corresponding to some of these dimers are presented in Fig. 4.15 and Fig. 4.16, showing the appearance of new transitions in the proximity of the HOMO \rightarrow LUMO transition. Depending on the aggregation pattern, a blue or red shift of roughly 20–30 nm (0.12 eV) can be observed between the band maxima of dimer and monomer species (Fig. 4.15 and Fig. 4.16), which seem to be due to the contribution of these new slightly higher energy transitions.

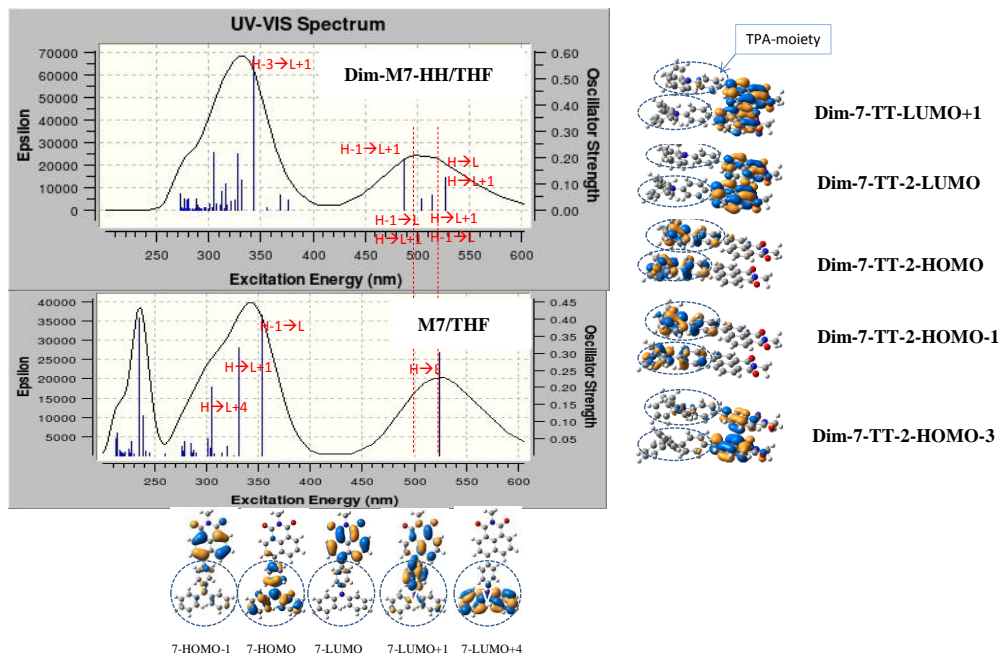


Figure 4.15. Theoretical UV-Vis spectra of **M7** and **Dim-M7-HH** model compounds obtained by mean of TDDFT calculations at B3LYP/6-31G(d,p) level in THF. The absorption bands are obtained by considering peak half-widths at half height of 0.2 eV. Some relevant MOs are also presented. The geometry of **Dim-M7-HH** is optimized at the wB97XD/6-31G(d,p) level by considering the effect of THF

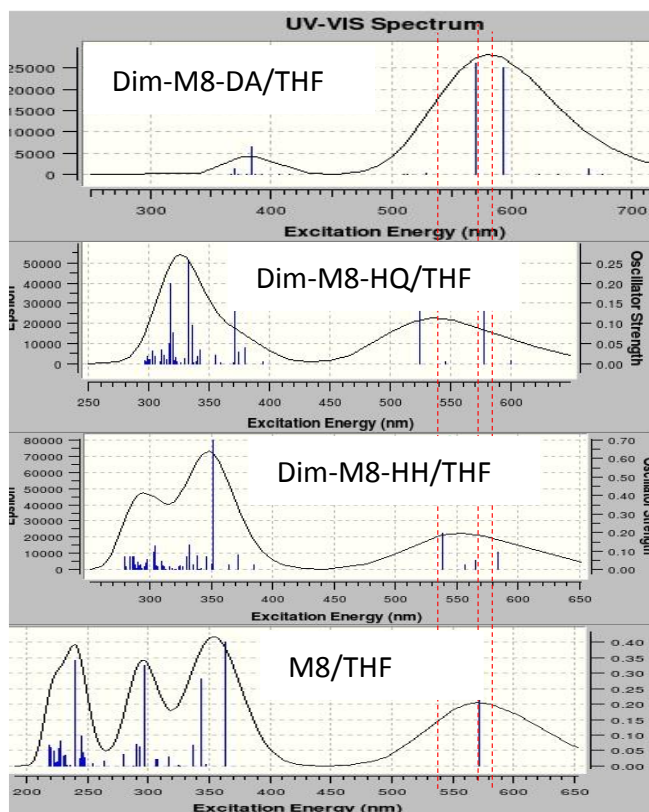


Figure 4.16. Theoretical UV-Vis spectra of **M8** and Dim-**M8**-HH model compounds obtained by mean of TDDFT calculations at B3LYP/6-31G(d,p) level in THF. The absorption bands are obtained by considering peak half-widths at half height of 0.2 eV. The geometry of Dim-**M8** model complexes are optimized at the wb97XD/6-31G(d,p) level by considering the effect of THF

FL spectra of the dilute solutions of the synthesized compounds in nonpolar cyclohexane (10^{-6} mol·L $^{-1}$), in PS and of solid films are shown in Fig. 4.17. FL spectra of compounds **7**, **9**, **10** dissolved in nonpolar cyclohexane exhibit efficient molecular emission with Φ_F of 0.63–0.78. The spectra show vibronic progression and pronounced Stokes-shift of ca. 55 nm. The Stokes-shift of compound **8** is of 72 nm. This observation indicates more polar nature of the excited states, but can also be due to the additional relaxations in the C-OMe bonds in compound **8** as compared to **7**. These bonds exhibit anti-bonding and non-bonding contributions at the HOMO and LUMO orbitals respectively (Fig. 4.9). After the HOMO→LUMO transition, the anti-bonding character vanishes, resulting in decreased C-O bond-lengths and non-negligible contribution in the relaxation energy (see also C-OMe bond-lengths in the neutral, cationic states, Fig. 4.8). After HOMO→LUMO transition, a somewhat zwitterionic structure is created, with positive charge in the TPA core and the negative one in the naphthalimide core. Calculations on the cationic and anionic compounds **7** and **8** confirm this assumption. The difference in the C-OMe bond-lengths between neutral and cationic state in **8** is roughly 0.02 Å (THF/B3LYP/6-

31(d,p) level. The charge-transfer origin of the lowest transitions is revealed by the spectral properties of the compounds dissolved in solvents of various polarities. As it is evidenced in Fig. 4.17 the studied derivatives of TPA and 1,8-naphthalimide exhibit pronounced positive solvatochromic behavior.

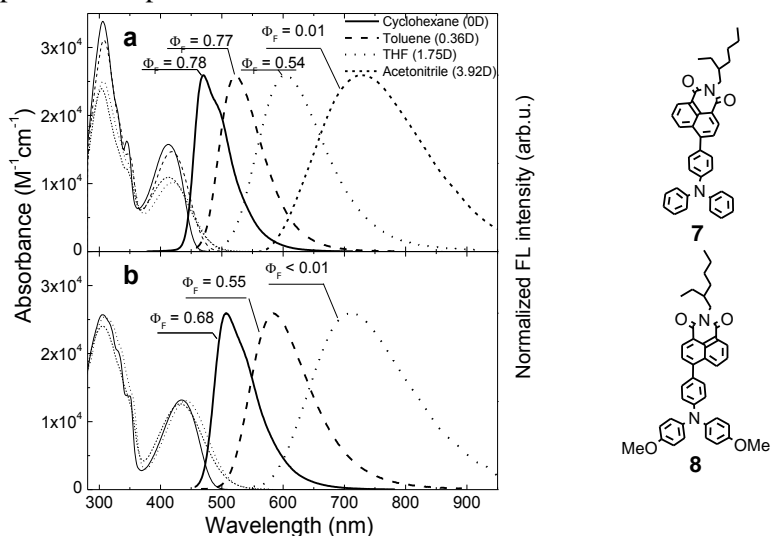


Figure 4.17. Absorption and FL spectra of compounds **7** (a) and **8** (b) in dilute cyclohexane (solid line), toluene (dashed line), THF (dotted line), and acetonitrile (short dashed line) solutions (10^{-6} M, $\lambda_{ex} = 450$ nm)

In the case of the solution of compound **8** in acetonitrile, the FL band is expected to be at about 850–950 nm and is undetectable.

Compound **7** is emitting at 470 nm in nonpolar cyclohexane and shows remarkable bathochromic shift of the fluorescence in THF (of 134 nm with respect to cyclohexane) and even larger red shift (of 258 nm with respect to cyclohexane) in acetonitrile. Φ_F of **7** is reduced down to 0.54 in THF and to 0.01 in acetonitrile. At the same time, the absorption spectra are only weakly shifted (by ca. 6 nm). Such solvatochromic behavior is typical for compounds with significantly enhanced dipole moment in the excited state. Solvation effect is even more pronounced for compound **8** possessing polar methoxy groups in the donor triphenylamino moiety. The bathochromic shift of the fluorescence in THF is significantly larger (of 204 nm with respect to cyclohexane), while Φ_F is found to be below 0.01 (see Fig. 4.17b). The solvation-shift of fluorescence bands decreases with increase of the number of naphthalimide side arms, which is in line with the reduced polarity of the excited state. The dependence of the optical properties of the naphthalimide derivatives on the solvent polarity has been reported [232–235]. The fluorescence quenching in the most polar solvents was accounted for the exciplex or cluster formation [232]. Solvatochromic behaviour of TPA and naphthalimide derivatives seems to be different. It is very weak in absorbance, while it is much stronger in fluorescence particularly for compound **8**, possessing polar methoxy groups. Such behavior is typical for the compounds with enhanced polarity in the excited state, what is in line with the DFT calculations. The theoretical dipole moments in the

ground state are 7.7D, 7.9D, 7.2D, and ~ 1D for compounds **M7–M10** respectively (B3LYP/6-31G** level, in THF. The value of **M7** does not correspond to the C3 geometry). Test single point calculations of **M7** and **M8** in the lowest triplet state (geometry of the singlet ground state, with the excited electron localized on the acceptor core) result in dipole moments of 24.5D and 29.8D respectively, thus giving a rough idea on the evolution of the dipole moments after charge separation in the excited state. Although the spectral behavior of TPA and naphthalimide compounds dissolved in solvents of various polarity seems to be systematic and could be accounted to the solute and solvent interaction, the specific solute-solvent interactions in most polar solvents THF and acetonitrile, leading to the pronounced decrease in fluorescence intensity, can not be excluded.

The largest Φ_F of 0.78 is found for the monosubstituted derivative of TPA (**7**) in nonpolar surrounding and it is steadily decreasing for compounds **9** and **10** down to 0.68 and 0.63, respectively. This is in contradiction with the enhanced oscillator strength of the lowest transition of the compounds possessing one, two and three side arms (see Fig. 4.15) and thus less pronounced charge transfer character of the lowest excited states. Indeed, the radiative decay time systematically decreases in the order 3.2 ns, 2.6 ns and 2.2 ns for compounds **7**, **9**, **10**, respectively. However increase in the number of the singly bonded naphthalimide arms results in almost threefold increase in the rate of nonradiative recombination. Nonradiative decay time decreases in the order 14.5 ns, 8.1 ns and 5.6 ns for compounds **7**, **9**, **10**, respectively. Incorporation of the polar methoxy groups for compound **8** results in more expressed charge transfer character of the excited states and, thus enhanced excited state lifetime of 4.7 ns and decreased radiative decay rate with 6.9 ns radiative decay constant. Meanwhile, the nonradiative decay constant is almost the same for both mono 1,8-naphthalimide-4-yl substituted compounds **7** and **8**.

FL spectra of the compounds molecularly dispersed in a rigid PS matrix are similar to those observed for the dilute solutions in nonpolar solvents. A systematic red shift of fluorescence spectra of about 20–30 nm is due to the slightly different polarity of the media. Since in the case of solid dispersion the intramolecular motion is suppressed, few peculiarities of the emission are evident. FL spectra are broader and non-structured, the emission efficiency is slightly decreased and the fluorescence transients are non-exponential. This observation can be explained by “freezing” of the initial molecular geometry in the ground state [236,237]. However, the impact of restriction of intramolecular twisting is not strong. The largest decrease in Φ_F (from 0.78 to 0.58) is observed for compound **7**.

Intramolecular interaction seems to have pronounced impact on the optical properties, particularly on emission properties of the solid films of compounds **7–10**. FL spectra are broad, unstructured and significantly red shifted. The Stokes shift is of 132 nm, 143 nm and 145 nm, and is weakly increasing with the number of naphthalimide arms, for compounds **7**, **9** and **10** respectively. It is strongly dependent on the polarity of the excited state and increases up to 182 nm for compound **8**, possessing polar methoxy groups. Such behavior can be rationalized in the frame of the model of self-trapped excitons [238,239]. Non-exponential fluorescence decay and decreased fluorescence quantum yields indicate on the

impact of exciton migration. Interestingly, Φ_F increases in the order 0.11, 0.16 and 0.23 for compounds **7**, **9** and **10**, respectively. This can be accounted for the enhanced oscillator strength and the reduced intramolecular vibrations.

Electrochemical and photoelectrical properties

In order to gain information on the charge injection capabilities, the electrochemical behavior of compounds **7–10** were estimated by CV at room temperature in DCM solutions. Table 4.7 outlines the onset oxidation and reduction potentials of **7–10**. Fig. 4.18 shows CV curves of the compounds.

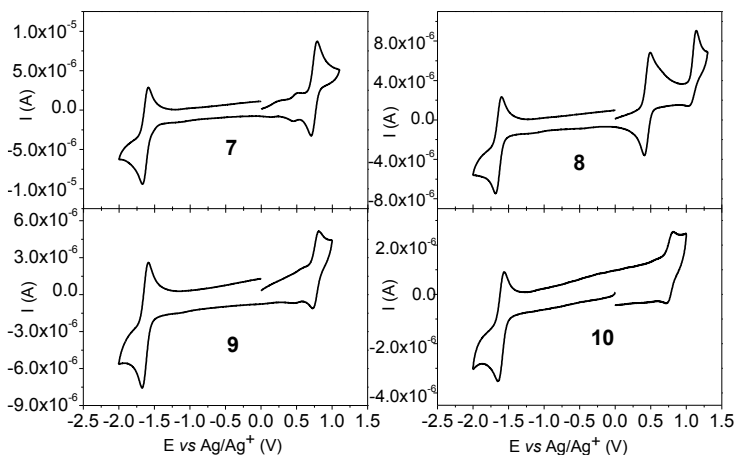


Figure 4.18. Cyclic voltammograms of **7–10** (10^{-5} M solutions, scan rate of $50 \text{ mV} \cdot \text{s}^{-1}$ vs Ag/Ag^+) in 0.1 M solution of Bu_4NPF_6 in DCM

Table 4.7. Electrochemical, photoelectrical, and theoretical electronic characteristics of **7–10**

Compound	$E_{\text{onset}}^{\text{ox}}$ vs Fc/V	$E_{\text{onset}}^{\text{red}}$ vs Fc/V	IP_{CV} , (eV) ^a	EA_{CV} , (eV) ^a	E_g^{opt} (eV)	ϵ_{H} , (eV) ^b	ϵ_{L} , (eV) ^b	IP_{EP} , (eV) ^c
7	0.54	-1.83	5.34	-2.97	2.55	-5.28	-2.34	5.79 (6.39)
8	0.25	-1.84	5.05	-2.96	2.40	-4.96	-2.26	5.57 (5.97)
9	0.57	-1.84	5.37	-2.96	2.57	-5.48	-2.49	5.93 (6.45)
10	0.58	-1.80	5.38	-3.00	2.58	-5.68	-2.60	6.01 (6.51)

^a Calculated with reference to ferrocene (4.8 eV). Ionization potentials and electron affinities estimated according to $\text{IP}_{\text{CV}} = (E_{\text{onset}}^{\text{ox}} + 4.8)$ (eV). $\text{EA}_{\text{CV}} = -(E_{\text{onset}}^{\text{red}} + 4.8)$ (eV) [240]. $E_{\text{onset}}^{\text{ox}}$ and $E_{\text{onset}}^{\text{red}}$ of Fc/Fc^+ measured in DCM solution containing 0.1 M Bu_4NPF_6 was 0.204 V vs. ferrocene/ferrocenium). ^b HOMO and LUMO energies corresponding to the isolated model compounds **M7–M10**, calculated at the B3LYP/6-31G(d,p) level. ^c Established from electron photoemission in air spectra. The values in parentheses correspond to the adiabatic IP of isolated model compounds **M7–M10**, calculated at the B3LYP/6-31G(d,p) level.

Compounds **7–10** displayed one reversible reduction peak, which might be due to the electron withdrawing nature of naphthalimide moieties, as well as one reversible oxidation peak, which can be attributed to the electron donating nature of TPA segment [241–243], suggesting that these compounds possess excellent electrochemical stability. The reduction current of **9** and **10** is obviously higher than that of the oxidation current in the cyclic voltammograms, suggesting that **9** and **10** can be classified as electron-accepting materials in organic electronics. The oxidative processes of **7–10** started at 0.54, 0.25, 0.57 and 0.58 V, respectively, and the reduction processes started at -1.83 , -1.84 , -1.84 and -1.80 V, respectively.

In the anodic scan regime of the cyclic voltammogram of **8**, reversible oxidation peak at 0.49 V is observed which can be ascribed to oxidation of the electron-rich nitrogen atom in the TPA core. The irreversible oxidation peak at 1.14 V can be attributed to oxidation of methoxy groups, causing radical recombination and formation of a quinoid structure [244]. This observation is attributed to two-electron stepwise oxidation process.

An important characteristic of electronically active compounds intended for the application in optoelectronic devices is IP_{EP} , which characterizes the electron releasing work under illumination. Except for compound **8**, the IP_{CV} values deduced from the onset redox potentials range in a very small window (5.34–5.38 eV) and are in agreement with those of naphthalimide containing hydrazones [109]. The IP_{EP} values of the solid samples of compounds **7–10** were also estimated by electron photoemission spectrometry (Fig. 4.19) and the results are collected in Table 4.7.

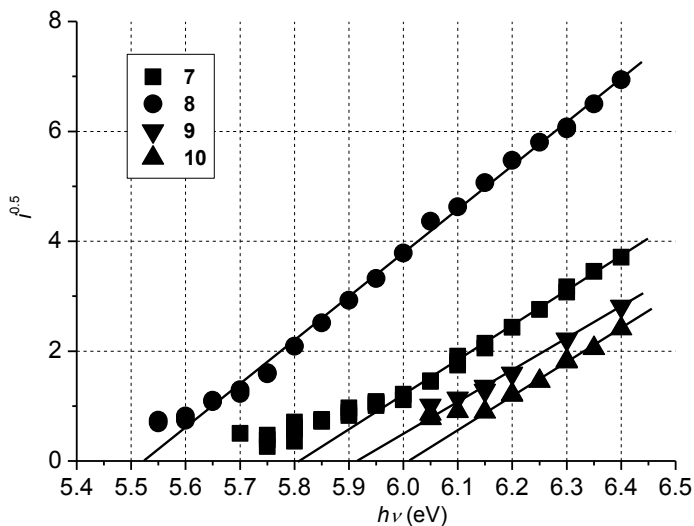


Figure 4.19. Electron photoemission spectra⁸ of the neat layers of **7–10** recorded in air

The values of IP_{EP} of amorphous layers of the compounds **7**, **9**, and **10** range from 5.79 to 6.01 eV, indicating good air stability for these materials. Compounds **9** and **10** with two and three 1,8-naphthalimide moieties, respectively, demonstrated a

⁸ IP_{EP} was measured at the Department of Solid State Electronics, Vilnius University.

little higher IP_{EP} values with respect to those of **7** and **8** with one 1,8-naphthalimide moiety. While the range of the electrochemical IP_{EP} values is smaller than those obtained by electron photoemission spectrometry, both methods provide similar trends, with the IP_{EP} values for **8** being smaller by 0.2–0.3 eV as compared to those of **7**.

The trend in the theoretical IP_{EP} values (Table 4.7) is in agreement with the experimental ones. In the frame of Koopmans' theorem (relating in this case the first IP_{EP} values to the HOMO energies) these trends can be explained by the similar evolution of the HOMO energies in these compounds (Table 4.7). The evolution in the HOMO energies in the order $7 > 9 > 10$ is related to the electron withdrawing nature of 1,8-naphthalimide arms, whereas the small experimental and theoretical ranges of the IP_{EP} values of compounds **7**, **9**, and **10** are due to the similar nature of their HOMO orbitals (Fig. 4.9). As for compound **8**, the higher HOMO energy (and smaller IP_{EP}) as compared to that of **7** (by roughly 0.2–0.3 eV) is due to the strong π -donor effect of the methoxy groups, which can be observed in the anti-bonding contribution of this group in the HOMO orbital (Fig. 4.9).

Charge-transporting properties of the synthesized compounds were estimated by xerographic time-of-flight technique. Fig. 4.20 shows electric field dependencies of hole and electron drift mobilities for the molecular glasses of **7–10** and for the solid solution (50%) of compound **10** in bisphenol Z polycarbonate ((PC-Z), 1:1). Charge drift mobility values are summarized in Table 4.8.

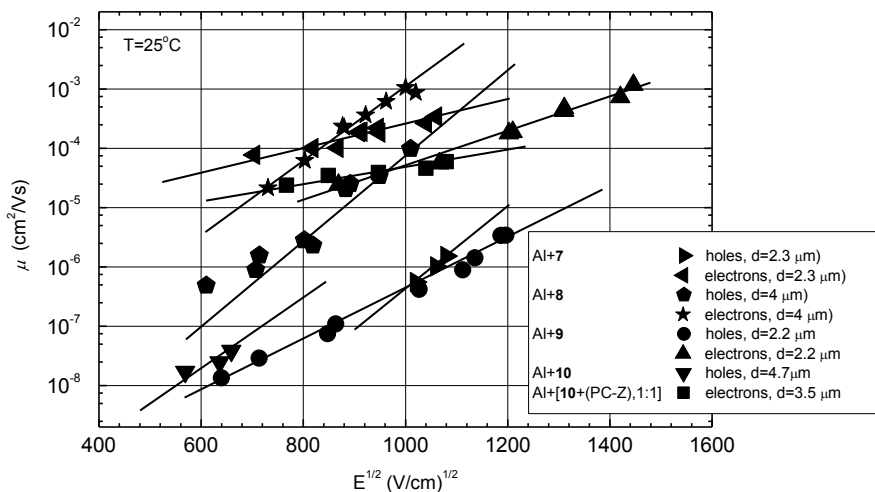


Figure 4.20. Electric field dependencies of hole and electron drift mobilities⁹ for the layers of compounds **7–10** and for the layer the solid solution of **10** in PC-Z (50%)

⁹ Electron and hole mobilities were measured at the Department of Solid State Electronics, Vilnius University by dr. V. Jankauskas.

Table 4.8. Hole and electron mobility data for the layers of compounds **7–10** and for the solid solution of **10** in PC-Z (50%)

Transport material, host polymer	Electron mobility μ_e , (cm ² /V·s) ^a	Hole mobility μ_h , (cm ² /V·s) ^a	d , μm	α , (cm ^{1/2} V ^{-1/2})
Al+ 7	2.3×10^{-4}	3.7×10^{-7}	2.3	–
Al+ 8	7.5×10^{-4}	1.1×10^{-4}	4.0	0.013 ^[c] , 0.014 ^[d]
Al+ 9	4.7×10^{-5}	4×10^{-7}	2.2	~ 0.0068 ^[c] , 0.0097 ^[d]
Al+ 10	–	2×10^{-8} ^[b]	7.0	~ 0.008 ^[d]
Al+[10 +(PC-Z), 1:1]	4.2×10^{-5}	–	3.5	~ 0.0025 ^[c]

^a Hole and electron drift mobility values at electric field 1×10^6 V/cm. ^b Hole drift mobility value at electric field 3.6×10^5 V/cm. ^c Pool-Frenkel parameter for electrons. ^d Pool-Frenkel parameter for holes.

All the compounds (**7–10**) are capable of transporting both holes and electrons. Their amorphous layers demonstrated μ_h values reaching 10^{-8} – 10^{-7} cm²/V·s at an electric field of 1×10^6 V/cm at room temperature and electron mobilities reaching 10^{-5} – 10^{-4} cm²/V·s at the same electric field. Compound **8** showed the best ambipolar charge-transporting properties. This hole and electron mobility value is comparable to that of other ambipolar compounds [187,245]. Its amorphous layers showed the highest values of both hole and electron mobilities (Table 4.8). We did not manage to estimate electron mobilities in the layers of **10**. In order to confirm the ability of the compound to transport negative charges we estimated electron mobilities in the 50 wt% solid solutions of **10** in bisphenol Z polycarbonate and observed relatively high mobilities reaching 4.2×10^{-5} cm²/V·s at an electric field 1×10^6 V/cm (Fig. 4.21). The dU/dt transients of electrons for the layer of neat **8** are shown in Fig. 4.21.

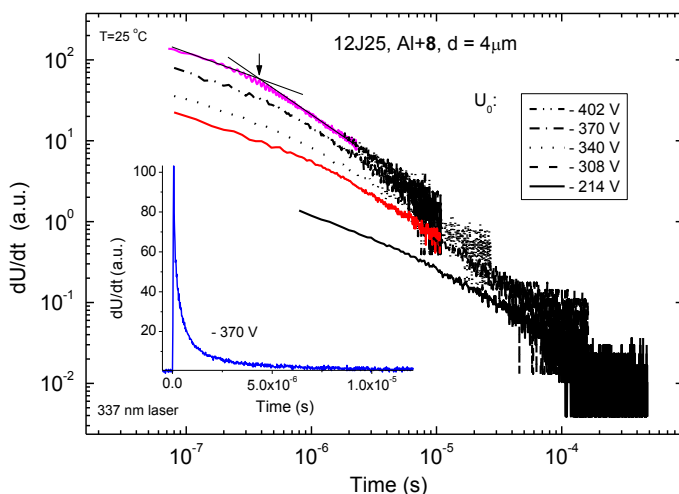


Figure 4.21. XTOF transients of electrons for a solid film of **8**

The layer of compound **8** exhibited dispersive electron transport, which, along with the strong electric-field mobility dependence may suggest trap-dominant

charge transport in this material. The t_i needed for the estimation of electron mobilities were established from the intersection points of two asymptotes from the double logarithmic plots. Dispersive charge transport was also observed for the other compounds studied in this work.

It is interesting to point out that, except of compound **8**, the electron mobilities are by 2–3 orders of magnitude higher as compared to the hole mobilities. Related to this observation, the ambipolar CT character of **8** is intriguing. Moreover, the larger hole mobility of compound **8** as compared to that of the parent compound **7** (by ~ 3 orders of magnitude) seems quite different from the results reported by Borsenberger *et al.* [246] and Maldonado *et al.* [247], in which, the lower hole mobilities for the substituted compounds were related to the role of the increase of the dipole moments (and the disorder) induced by the substitutions. The calculated dipole moment for compounds **7** and **8** are 6.2 D and 6.5 D respectively, which, in line with the results of Borsenberger *et al.* [246], suggests negligible role of this factor.

In order to obtain more insight in these questions, we present a qualitative discussion of charge-transfer rate-constants (k_{CT}) based on the Marcus theory [219–222]. In the frame of Marcus’ “hopping” mechanism, the rate-constant of a charge-transfer reaction between two adjacent molecules in amorphous materials can be calculated by means of the following equation:

$$k_{CT} = \frac{4\pi^2}{h} \frac{1}{\sqrt{4\pi\lambda k_B T}} t^2 \exp\left[\frac{-(\Delta G^\circ + \lambda)^2}{4k_B \lambda T}\right], \quad (4.1)$$

In this equation, t is the electronic coupling between two adjacent molecules, ΔG° is the free energy of the charge-transfer reaction (approximated to zero in the case of charge hopping between identical molecules in the absence of electric field), and λ is the reorganization energy. This last parameter is the sum of two terms: (i) λ_s , containing the contribution from the medium polarization energy. (ii) λ_i , representing the energetic effort due to the intra-molecular geometric relaxations related to the charge transfer between two adjacent molecules. In the following, some of these molecular parameters will be discussed, while the influence of morphological and other structural parameters will be ignored.

Based on equation 1, high charge-transfer rate-constants (k_{CT}) need minimal values of the reorganization energy (λ) and large values of the electronic coupling parameter (t). In order to compare compounds **7–10**, we have calculated some of these parameters and collected them in Table 4.9.

Table 4.9. Hole- and electron intramolecular reorganization energies for the model compounds **M7**–**M10** computed at the B3LYP/6-31G(d,p) level

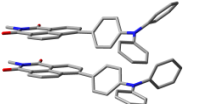
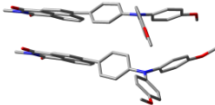
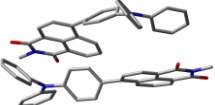
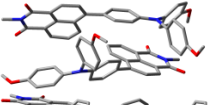
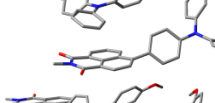
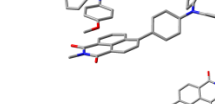
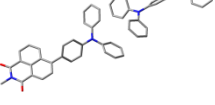
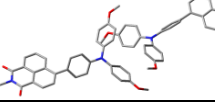
Compound	λ_i^h , (eV)	λ_i^e , (eV)
M7	0.139	0.399
M8	0.258	0.422
M9	0.138	[a]
M10	0.136	[a]

^a Similar reorganization energy values as compared to **M7** can be assumed for **M9** and **M10**. See text for details.

The hole reorganization energies (λ_i^h) of model compounds **M7**, **M9**, and **M10** are almost identical, which is due to the identical spatial distribution of the HOMO orbitals in these compounds (Fig. 4.9). The electron reorganization energies (λ_i^e) are also supposed to remain similar for **M7**, **M9**, and **M10** despite the increasing number of naphthalimide arms. Indeed, the coupling between the arms in **M10** (~ 0.023 eV) is much smaller than the reorganization energy of a single naphthalimide arm (0.399 eV for **M7**, Table 4.9), suggesting localization of the LUMO orbital in **M10** (and **M9**). Concerning the compound **M8**, both values are larger than for the other compounds. The much larger λ_i^h value for **M8** as compared to **M7** could be due to the additional contribution inherent to the relaxation of the C-OMe bonds. Indeed, the local anti-bonding contributions in the HOMO orbital at the C-OMe bonds (Fig. 4.9) are released in the cationic state, as indicated by the bond-length reduction of ~ 0.02 Å. As for λ_i^e , much smaller difference between **M8** and **M7** is found, which is mostly due to the space separation between the naphthalimide groups and the methoxy substituents in **M8**.

However, the main observation in Table 4.9 is that λ_i^e values are more important than the hole analogues, suggesting that this parameter cannot account for the larger electron mobilities found experimentally. Similarly, both λ_i^e and λ_i^h values for **M8** are larger than for the other compounds, which is in opposite agreement with the largest mobility values found for this compound. Consequently, in order to obtain better understanding of the experimental observations, we focus on the influence of the electronic coupling parameter (t). The calculation of the electronic couplings is based on the assumption that, despite the irregular packing between adjacent molecules in the amorphous materials, dimers of different geometries can be established. The t values calculated for two special dimers of compounds **7** and **8** (Dim-**M7**-HH and Dim-**M7**-HH, Fig. 4.14a-c), are given in Table 4.10 (lines 1–2).

Table 4.10. Electronic couplings (t) and dissociation energies (E_D , corrected for BSSE and ZPE) for some selected dimers of model compounds M7 and M8. The electronic couplings are calculated at the B3LYP/6-31G(d,p)//CPCM//wB97XD/6-31G(d,p) level. The dissociation energies are calculated at the CPCM/wB97XD/6-31G(d,p) level. Negative dissociation energies mean repulsive state (higher level calculations would slightly modify these values, however, the trends are expected to remain unchanged)

Model dimer	t^h , (eV)	t^e , (eV)	E_D , (kcal.mol ⁻¹)
Dim-M7-HH 	0.055	-0.032	13.9
Dim-M8-HH 	0.045	-0.027	15.7
Dim-M7-HT 	-0.007	0.052	8.5
Dim-M8-HT 	-0.028	-0.001	10.3
Dim-M7-DA 	0.014	-0.001	3.4
Dim-M8-DA 	0.024	-0.004	3.9
Dim-M7-DD 	0.048	0.001	-1.9
Dim-M8-DD 	0.001	0.001	1.8

In both cases, simultaneous donor-to-donor and acceptor-to-acceptor packing is assumed, which is similar to the packing reported in polymers containing naphthalimide and bi-thiophene alternated cores [248]. The results given in Table 4.10 indicate larger t values for the holes, suggesting faster hole transfer, which, again, can not account for the higher electron mobility found experimentally.

However, the static description provided so far considers only idealized dimer geometries, ignoring the displacements between molecules in the real materials. We suspect that this last factor may constitute a possible explanation for the above disagreements, as it has been pointed out in a recent similar study [249]. In order to

give more insight in this respect, we firstly consider parallel displacements between adjacent molecules in the model dimer Dim-**M7**-HH shown in Fig. 4.14b. A detailed analysis of the LUMO orbital of compound **7** (Fig. 4.9), indicates absence of nodal planes along the long axes, suggesting that the LUMO–LUMO overlap would be very little affected by small displacements between adjacent molecules in this direction. Similar analysis with respect to the HOMO orbital indicates the presence of nodes in the longitudinal direction, suggesting much more sensitivity of the HOMO–HOMO overlap to the displacements in this direction. A similar conclusion has been reached also by Wetzelaer *et al.* [249] by calculating the LUMO–LUMO and HOMO–HOMO couplings for different reciprocal positions between molecules containing naphthalene diimide and bithiophene moieties. As for the transversal displacements (along the short axes of Dim-**M7**-HH), both HOMO and LUMO orbitals exhibit nodal surfaces, making the corresponding overlaps very sensitive to the displacements. However, the transversal displacements seem to be mostly limited by the steric hindrance between the long alkyl chains of naphthalimide groups on the one hand, and between the TPA phenyl groups on the other hand. One can thus suppose that, due to this kind of displacements, the overall variation in the orbital overlap should be larger for the HOMO orbitals. Larger disorder in the electronic couplings should be than expected for the hole transfer, which, in terms of disorder models [250] would result in smaller hole mobilities.

As for compound **8**, additional coupling schemes can be supposed, similar to those proposed previously [224]. Briefly, due to the presence of the methoxy groups, different types of C-H... π (Ph) or C-H...N,O hydrogen-bond interactions between TPA-OMe moieties of adjacent molecules have been assumed [224], resulting in strengthening of inter-molecular interactions. Stronger interactions between the TPA-OMe groups can be thus expected in the case of compound **8**, as suggested by the stronger dissociation energy found for Dim-**M8**-HH as compared to Dim-**M7**-HH (15.7 kcal.mol⁻¹ and 13.9 kcal.mol⁻¹, Table 4.10).

Consequently, in the case of Dim-**M8**-HH, reduced geometry disorder and reduced disorder in the HOMO–HOMO coupling would be expected as compared to Dim-**M7**-HH, resulting in enhanced hole mobility. Results for other dimer geometries, based on **M7** and **M8**, are also shown in Table 4.10. One can observe that the HOMO–HOMO couplings are generally larger for dimers containing no OMe groups, which seem to contradict the experimental trend of hole mobilities between **7** and **8**. However, systematically stronger interactions are found in the case of OMe-containing dimers, again suggesting that the disorder in HOMO–HOMO couplings should be strongly reduced for this compound as compared to **7**. Concluding this analysis, we suggest that the enhanced hole mobility and the ambipolar CT character of **8** result from the stronger interactions between adjacent molecules, making possible to maintain the hole transport rate at a comparable level as the electron one.

Admittedly, this semi-quantitative analysis can not provide thorough explanations, but aims only to point on some possible mechanisms allowing to better understand the difference between the hole and electron transport in these materials. Interestingly, packing patterns between naphthalimide moieties similar to those

presented in Fig. 4.14a-c have been reported in polymers containing naphthalimide and bi-thiophene alternated cores [249] which comforts the validity of the above analysis.

In conclusion, a series of ambipolar materials containing electron accepting 1,8-naphthalimide moieties and electron-donating triphenylamino groups were obtained via Suzuki cross-coupling reaction. Their 5% weight loss temperatures range from 429 to 483 °C. All the synthesized compounds are capable of glass formation. Their glass transition temperatures are in the range from 45 to 84 °C. The lowest ionization potentials and the best charge-transporting properties were observed for the amorphous layers of 4-(4'-(di-(4''-methoxyphenyl)amino)phenyl)-*N*-(2-ethylhexyl)-1,8-naphthalimide (**8**). Electron mobilities of $7.5 \cdot 10^{-4} \text{ cm}^2 \cdot \text{V}^{-1} \cdot \text{s}^{-1}$ and hole mobilities of $1.1 \cdot 10^{-4} \text{ cm}^2 \cdot \text{V}^{-1} \cdot \text{s}^{-1}$ were recorded for this compound at an electric field of $1 \cdot 10^6 \text{ V/cm}$. Compounds containing no methoxy groups exhibit electron mobilities by 2–3 order of magnitude higher than the hole mobilities. The comparison between compounds **7** and **8** shows that the methoxy groups increase the hole mobility by ~3 orders of magnitude.

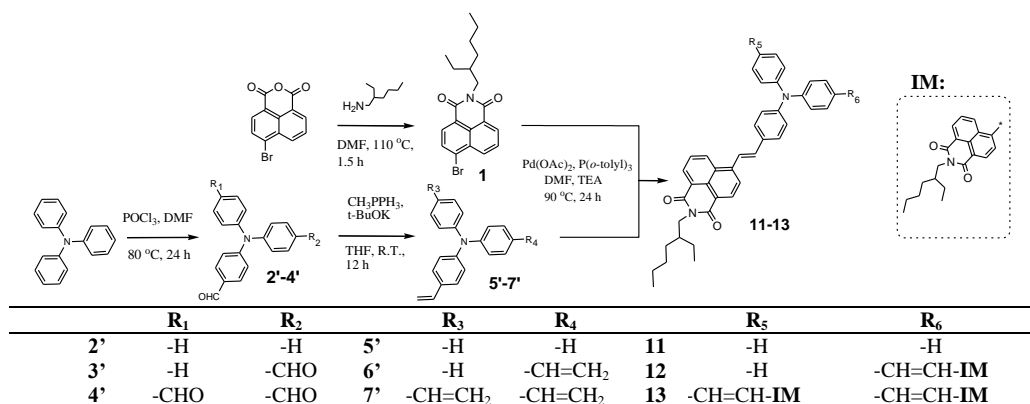
4.1.3. Synthesis and properties of glass-forming derivatives with triphenylamino and 1,8-naphthalimide moieties linked via ethenyl-containing linkages

In this chapter, new solution-processable donor-acceptor organic molecules with TPA and 1,8-naphthalimide moieties linked via ethenyl-containing linkages which were synthesized by palladium-catalyzed Heck reaction are reported. It is expected that the absorption of these molecules will be extended to longer wavelengths due to intramolecular charge transfer between the donor and the acceptor units. The double bond linkage between TPA and 1,8-naphthalimide fragments will enhance the extent of conjugation degree which is also expected to result in the shift of absorption to longer wavelength region.

Joint experimental and theoretical approaches are employed in order to characterize the synthesized compounds and to better understand the structure-property relationships. In order to get some more insight in the hole-transport properties of these amorphous compounds, Marcus theory is applied by means of a comparative analysis of some molecular parameters involved in the calculation of charge-transfer rate-constants (k_{HT}) [219–222].

Synthesis and characterization

The synthetic route to derivatives (**11–13**) is shown in Scheme 4.4.



Scheme 4.4. Synthetic route to **11–13**

The first step was condensation of 4-bromo-1,8-naphthalic anhydride with 2-ethylhexylamine in DMF to obtain 4-bromo-*N*-(2-ethylhexyl)-1,8-naphthalimide (**1**). Aldehydes (**2'–4'**) were obtained under the conditions of Vilsmeier reaction. Compounds **5–7** were prepared by the reaction of aldehydes (**2'–4'**) with methyltriphenylphosphonium bromide. The final step was Heck reactions of bromide **1** with 4-vinyltriphenylamine (**5'**), 4,4'-divinylphenylamine (**6'**) and tris-(4-vinyl-phenyl)amine (**7'**) in the presence of palladium(II) acetate and tri-*o*-tolylphosphine to obtain the target compounds **11–13**.

The chemical structures of the synthesized compounds were confirmed by ¹H NMR, ¹³C NMR, IR, mass spectrometries and elemental analysis. Compounds **11–13** were readily soluble in common organic solvents like DCM, chloroform, THF, acetonitrile, toluene.

DFT calculations, geometries and frontier orbitals

The geometries of **M11**, **M12**, and **M13** model compounds (containing methyl groups instead of longer-chain alkyl groups) are presented in Fig. 4.22.

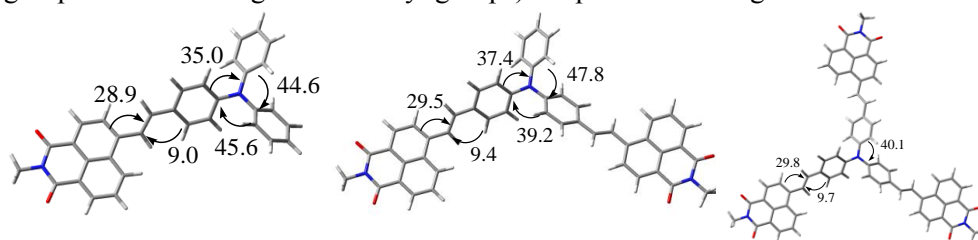


Figure 4.22. Optimized geometries of **M11** (left), **M12** (center), and **M13** (right) model compounds, obtained at the B3LYP/6-31G(d,p) level¹⁰. Some relevant dihedral angles (absolute values in degrees) are shown

Some relevant geometrical parameters are also indicated. In the three molecules the geometry around the central N atom is planar (“N-plane”), due to the

¹⁰ DFT calculations have done at the Laboratoire de Physicochimie des Polymères et des Interfaces, Université de Cergy-Pontoise by dr. G. Sini.

π -conjugation between the phenyl groups and the lone pair of the central N atom. The dihedral angles of each phenyl group with the “N- plane” are approximately 44–47° for the un-substituted phenyl rings and 35–40° for the substituted ones (angles increasing with the number of 1,8-naphthalimide fragments in the arms). The frontier orbitals for the three molecules are given in Fig. 4.23.

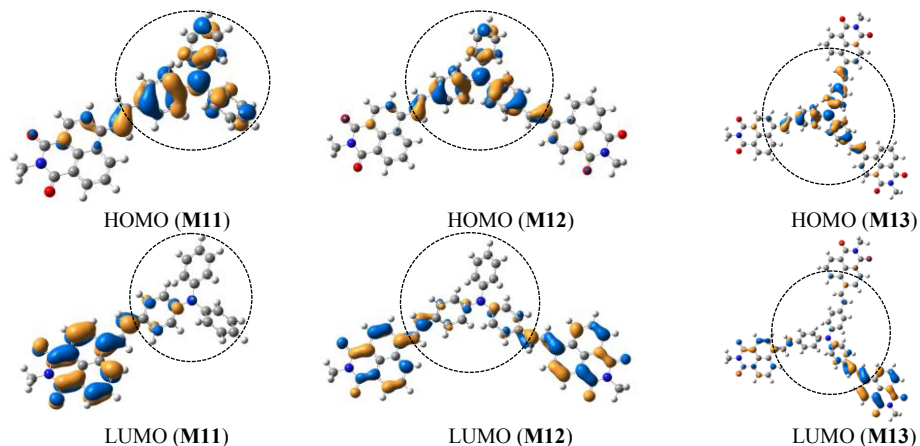


Figure 4.23. Pictograms of frontier orbitals for the model compounds **M11**, **M12**, and **M13**. The encircled parts delimit the TPA moiety

The three HOMO orbitals are very similar, being localized almost entirely on the TPA core, containing only small antibonding contributions from the ethylene moieties. Similar HOMO energies should be then expected for these compounds suggesting similar electronic and optical properties.

Thermal properties

The thermal behavior of compounds **11–13** was studied by TGA. The 5% weight loss temperatures ($T_{ID-5\%}$) were found to be in the range of 431–448 °C (Table 4.11). The thermal stability of the synthesized donor-acceptor derivatives increased with increase of the number of 1,8-naphthalimide arms.

Table 4.11. Thermal characteristics of compounds **11–13**

Molecule	T_g (°C) (2 nd heating)	T_m (°C)	$T_{ID-5\%}$ (°C)
11	55	163	431
12	90	185	445
13	107	222	448

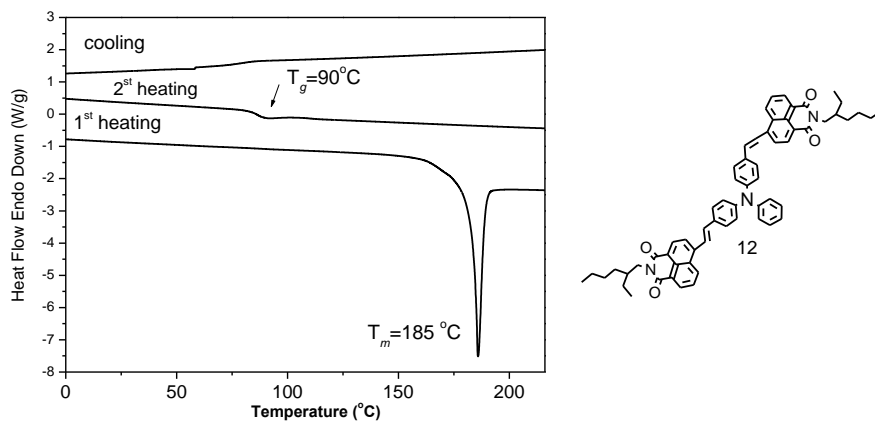


Figure 4.24. DSC thermograms of compound **12** (scan rate of 10 °C/min, N₂ atmosphere)

Compounds **11–13** were isolated after the synthesis as crystalline materials. Their behaviour in DSC experiments was similar, therefore DSC curves of only one compound are given in Fig. 4.24.

Temperatures of thermal transitions of compounds **11–13** are summarized in Table 4.11. The first run heating scans revealed only melting endotherms. No crystallization was observed during the cooling scans. In the second heating scans compounds **11**, **12** and **13** showed glass transitions at 55 °C, 90 °C and 107 °C, respectively and no crystallization was observed in the following heating and cooling scans. Both T_g and melting points increased with the increase of the number of 1,8-naphthalimide arms. This observation can apparently be explained by the enhancement of intermolecular interaction.

Optical properties

Absorption and FL spectra of dilute solutions in THF of compounds **11–13** are shown in Fig. 4.25. The wavelengths of the absorption and fluorescence maxima and Φ_F are summarized in Table 4.12.

Table 4.12. Optical and fluorescence characteristics of **11–13**

Compound	Solution λ_{max} , (nm)		Film λ_{max} , (nm)		Stokes shift, (nm) sol/film	Φ_F sol/film
	UV	FL	UV	FL		
11	455	641	470	624	186/154	0.64/0.18
12	469	643	489	643	174/154	0.45/0.14
13	474	646	490	652	172/162	0.48/0.09

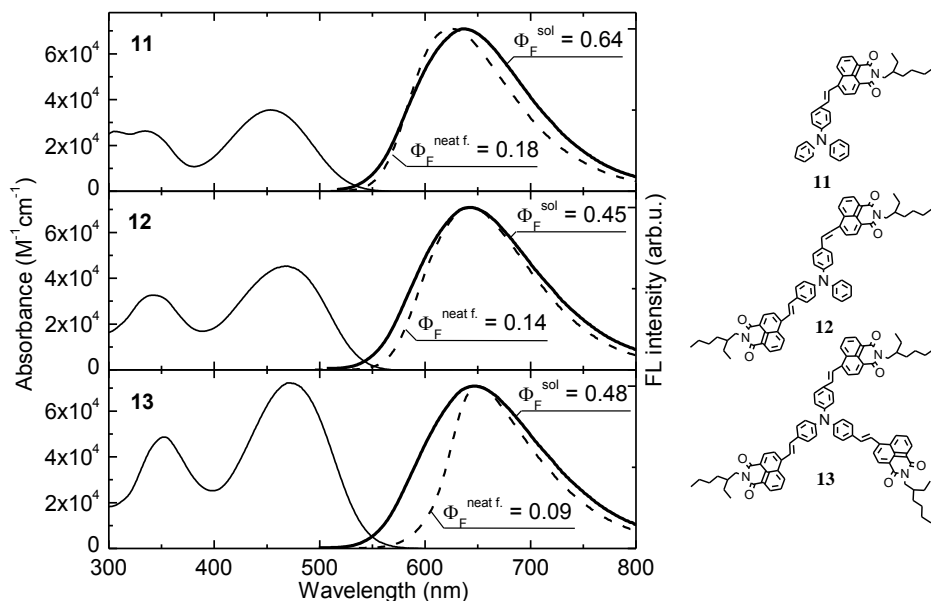


Figure 4.25. UV-Vis and FL ($\lambda_{\text{ex}} = 365 \text{ nm}$) spectra of the dilute THF solutions (10^{-5} M) and of solid films of compounds **11–13**¹¹

The lowest energy absorption bands of these compounds which can be ascribed to the charge transfer exhibit bathochromic and hyperchromic shifts with the increase of the number of 1,8-naphthalimide arms. All compounds show a broad structureless long wavelength absorbance band with strongly Stokes shifted broad fluorescence typical for intramolecular charge-transfer states. The solutions of all the compounds (**11–13**) also show absorption bands peaking at ca. 350 nm. These absorption bands can be assigned to $\pi\text{-}\pi^*$ transition of naphthalimide groups [230]. The dilute solutions of these compounds emit orange light peaking in the range of 641–646 nm when excited with the ultraviolet radiation. Incorporation of additional 1,8-naphthalimide arms weakly affects the emissive states. The spectra of the solid samples of compounds **11–13** exhibit small red shifts with respect of those of the dilute solutions, probably due to the smaller dihedral angles in solid state, thus giving rise to more efficient π -conjugation and decreased HOMO–LUMO gap. The TDDFT calculations also support the charge-transfer nature of the lowest energy band. The theoretical UV-Vis spectra for the model compounds **M11–M13** are shown in Fig. 4.26.

¹¹ *Optical and fluorescence properties were studied in collaboration with Institute of Applied Research, Vilnius University by dr. A. Miasojedovas.*

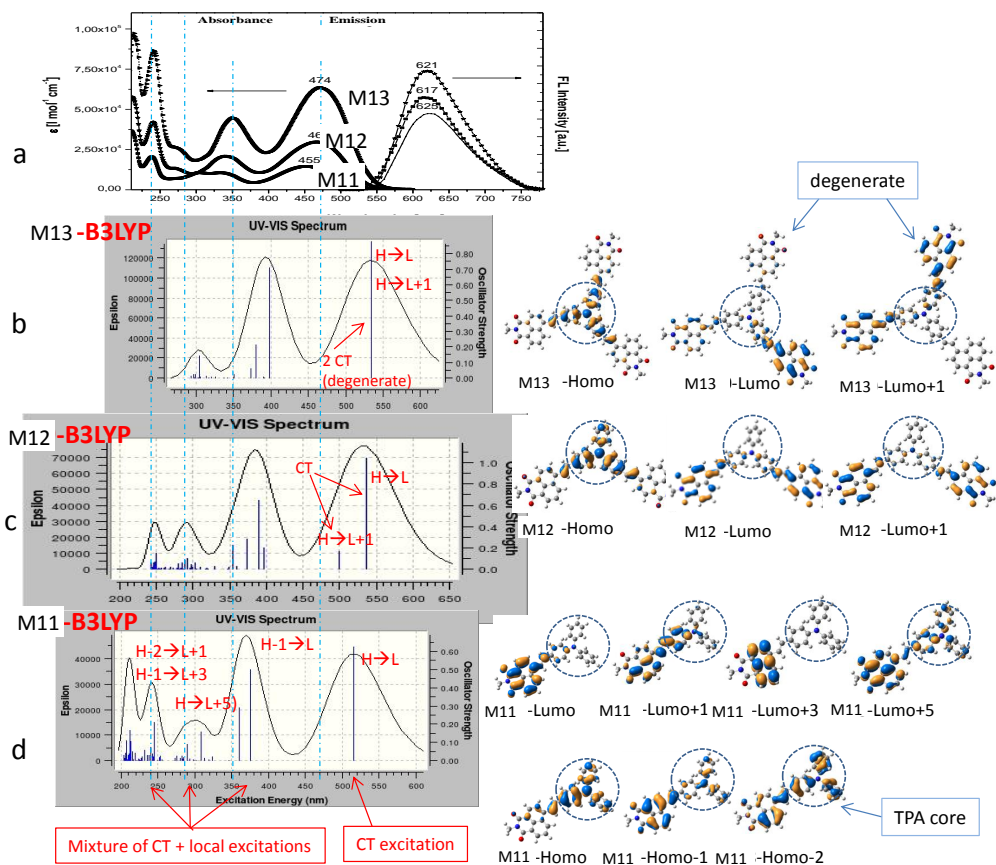


Figure 4.26. UV-Vis experimental (a) and theoretical spectra of **M13**, **M12**, and **M11** model compounds (b, c, and d, respectively) obtained by mean of TDDFT calculations at B3LYP/6-31G(d,p) level. The absorption bands are obtained by considering peak half-widths at half height of 0.2 eV. Some relevant MOs are also presented (see Fig. 4.27 for more clear pictograms)

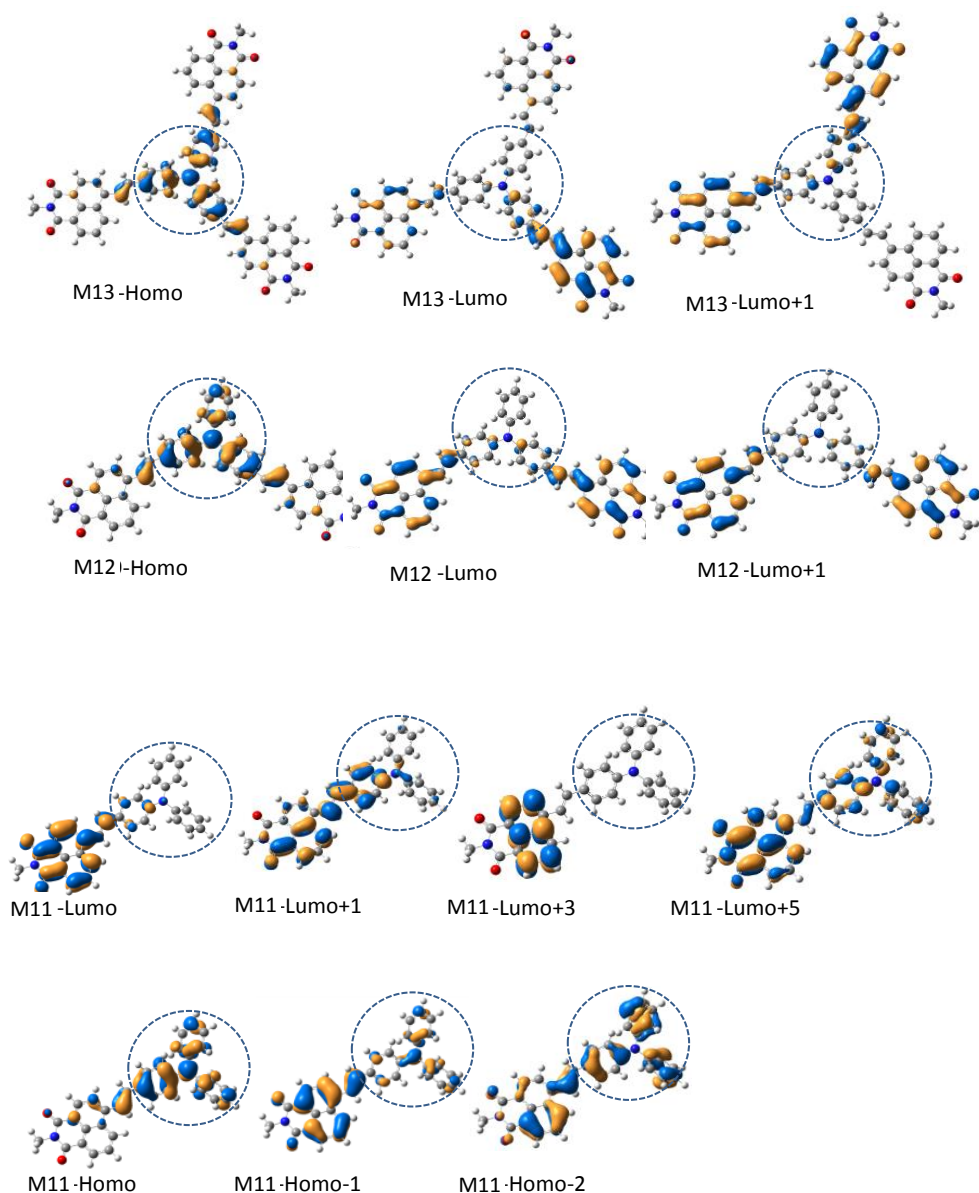


Figure 4.27. Pictograms of some relevant orbitals for the neutral model compounds **M11**–**M13**

The $S_0 \rightarrow S_1$ excitation in compound **11** is entirely due to HOMO \rightarrow LUMO electronic transition, with HOMO and LUMO orbitals being almost entirely localized on the donor and acceptor moieties, respectively (Fig. 4.23). In the case of compound **12**, a second CT excitation ($S_0 \rightarrow S_2$) of smaller oscillator strength (0.163 as compared to 1.044 for $S_0 \rightarrow S_1$) is present in the CT band (Fig. 4.26). The $S_0 \rightarrow S_2$ excitation corresponds to HOMO \rightarrow LUMO+1 electronic transition. It is worth of pointing out that LUMO and LUMO+1 orbitals of compound **12** (containing two

1,8-naphthalimide arms) are the in-phase and out-of-phase combinations of the local LUMO orbitals of each 1,8-naphthalimide arm. The similar observations can be done in the case of compound **13**, with the difference that the two CT electronic transitions (HOMO→LUMO, LUMO+1) are degenerate, hence corresponding to identical oscillator strengths (0.876). The roughly linearly increasing intensity of the charge transfer bands from **11** to **13** is thus related to the presence (in the compounds **12** and **13**) of a second CT transition ($S_0 \rightarrow S_2$) of increasing intensity in the same order.

The other bands seem to contain some mixing of CT and local excitations. The important Stokes shifts observed for all compounds (Table 4.12) can also be traced back to the large geometrical reorganizations happening after HOMO→LUMO(LUMO+1) transitions, which is suggested by the totally different space localization of the HOMO and LUMO orbitals for each compounds.

Φ_F of the dilute solutions of **11–13** range from 0.64 to 0.45, while those of the films are considerably lower and range from 0.09 to 0.18. The highest Φ_F both for solution and for the solid sample were observed for compound **11**.

Electrochemical properties

We used CV for the investigation of the redox behavior of compounds **11–13** and for the estimation of their IP_{CV} and EA_{CV} values. The CV curves of **11–13** are shown in Fig. 4.28, Table 4.13 summarizes the relevant data.

Table 4.13. IP_{CV}/EA_{CV} , optical and electrochemical band-gap energies and IP_{EP} of **11–13**

Molecule	IP_{CV} , (eV) ^a	EA_{CV} , (eV) ^a	E_g^{elc} , (eV) ^c	E_g^{opt} , (eV) ^d	IP_{EP} , (eV) ^e
11	5.18 (5.17) ^f	-3.06 (-2.45) ^f	2.12	2.34	5.75 (6.33) ^f
12	5.24 (5.29) ^f	-3.07 (-2.63) ^f	2.17	2.28	5.78 (6.28) ^f
13	5.25 (5.39) ^f	-3.08 (-2.72) ^f	2.17	2.27	5.80 (6.26) ^f

^a Ionization potentials and electron affinities estimated according to $IP_{CV} = (E_{onset}^{ox} + 4.8)$ (eV), $EA_{CV} = -(E_{onset}^{red} + 4.8)$ (eV). E_{onset}^{ox} and E_{onset}^{red} of Fc/Fc⁺ measured in DCM solution containing 0.1 M Bu₄NPF₆ was 0.27 V vs. ferrocene/ferrocenium). ^c $E_g^{elc} = |IP_{CV}| - |EA_{CV}|$. ^d The optical band gap estimated from the onset wavelength of optical absorption in dilute solution according to the formula: $E_g^{opt} = 1240/\lambda_{edge}$. ^e Established from electron photoemission in air spectra. ^f Corresponding to the model compounds **M11**, **M12**, and **M13** calculated at the B3LYP/6-31G(d,p) level.

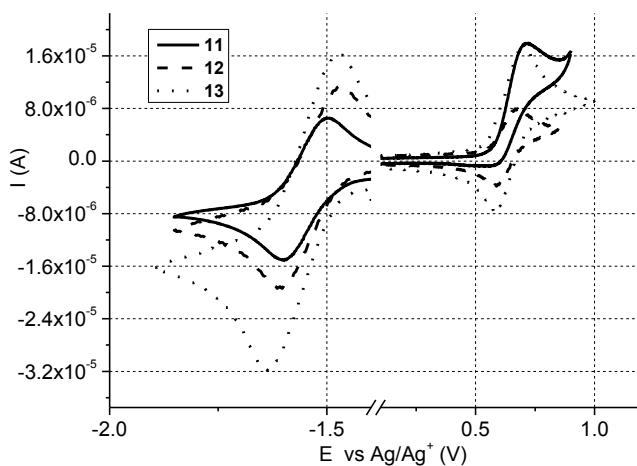


Figure 4.28. Cyclic voltammograms of **11–13** (10^{-5} M solutions, scan rate of $50 \text{ mV}\cdot\text{s}^{-1}$ vs Ag/Ag^+) in 0.1 M solution of Bu_4NPF_6 in DCM

Compounds **11–13** were found to be electrochemically stable. Their cyclic voltammograms showed one quasi-reversible oxidation and reduction couple waves. The shapes of CV curves were found to be similar for all the compounds (**11–13**). Oxidation part of CV curves is principally related to the oxidation of triphenylamino group and reduction part is related to the reduction of imido group, which is also suggested from the shape of the HOMO and LUMO orbitals (see pictograms in Fig. 4.23).

On the basis of the onset potentials, we estimated IP_{CV} values of **11**, **12** and **13** to be 5.18 eV , 5.24 eV , 5.25 eV , respectively, with EA_{CV} values of -3.06 eV , -3.07 eV , -3.08 eV , respectively, according to the energy level of the ferrocene reference (-4.8 eV) [251]. The small range of the IP_{CV} values (0.07 eV) is due to their similar shape for the three compounds (almost total localization of this orbital on the TPA core, Fig. 4.23). The slight decrease of the IP_{CV} values from **11–13** is related to the electron withdrawing nature of 1,8-naphthalimide arms. The similar arguments can explain the small range and the trend of the LUMO energies.

The band-gap value is one of the most useful characteristics for materials used in optoelectronic devices. E_g^{elc} of **11–13** were $2.12\text{--}2.17 \text{ eV}$ and they were slightly lower than corresponding E_g^{opt} ($2.27\text{--}2.34 \text{ eV}$, Table 4.13), but within the range of error ($0.2\text{--}0.5 \text{ eV}$) [252].

Photoelectrical properties

Amorphous thin films on substrates could be prepared by casting or spin coating techniques from the materials reported in this chapter. Fig. 4.29 shows electron photoemission spectra of the layers of compounds **11–13** recorded in air.

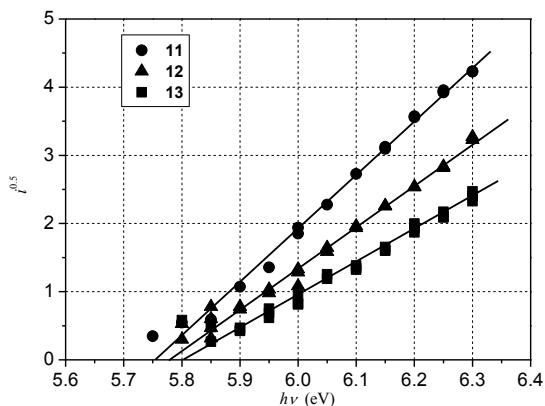


Figure 4.29. Electron photoemission spectra¹² of the layers of **11–13**

The values of ionization potentials obtained by extrapolation of the straight parts of the spectra to the X-axis are given in Table 4.13. The values of IP_{EP} of the films of compounds **11–13** range from 5.75 eV to 5.80 eV. These values are very close and comparable to those of TPA derivatives [224,253]. It seems that the introduction of 1,8-naphthalimide arms and the increase of the number of these arms has a negligible effect on the ionization potentials of the TPA derivatives. In the frame of Koopmans' theorem (relating in this case the first IP_{EP} values to the HOMO energies) these observations can be explained by the similarity between the HOMO orbitals of compounds **11–13** on the one hand and the HOMO (TPA) on the other hand (Fig. 4.23).

The slightly increasing experimental IP_{EP} values (from 5.75 eV to 5.80 eV) can be explained at first sight in a straightforward manner: on the bases of Koopmans' theorem, the decreasing HOMO energies from **11–13** (Table 4.13) can explain the increasing experimental IP_{EP} values in the same order. However, the theoretical results indicate that the picture is slightly different: while the theoretical HOMO (and LUMO) energies decrease from **M11–M13** (in line with the above explanation), the theoretical IP_{EP} values decrease (from 6.33 to 6.26 eV) instead of increasing. This result is intriguing as it is at odds with the trends deduced from the Koopmans' theorem and the experimental results. In order to check for possible bad performances in the applied theoretical methods, medium effects, different DFT methods, and different basis sets were considered. However, the similar results were obtained in all cases. It is worth of pointing out that the ranges of the experimental and theoretical IP_{EP} values are both very small (0.05 and 0.07 eV, respectively). The discrepancies reported so far might then be due to the influence of other factors such as: (i) the fact that the orbital-relaxation energy terms between the neutral and cationic species are ignored in the Koopmans' theorem („frozen orbital“ approximation), which can be on the origin of the different IP_{EP} trends deduced from the Koopmans' theorem and from the direct calculations. (ii) the quite different T_g

¹² IP_{EP} was measured at the Department of Solid State Electronics, Vilnius University.

values between **11** and **12** or **13** (Table 4.11) indicate different molecular packing, which also might influence the trend of the IP_{EP} values.

We conclude this point by underlying that the relevant result to retain here is the very small range of the IP_{EP} values obtained (experimentally and theoretically) for the three compounds **11–13**, which is principally due to the similar nature of their HOMO orbitals. Time-of-flight technique was used to study charge-transporting properties of the derivatives (**11–13**). Fig. 4.30 shows the electric field dependencies of the hole-drift mobilities of the amorphous layers of **11–13**.

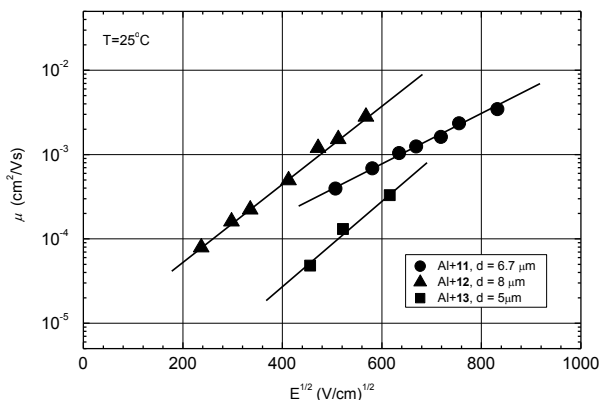


Figure 4.30. Electric field dependencies of hole-drift mobilities¹³ in the layers of **11–13**

The layers of compounds **11–13** demonstrated hole-drift mobility values in the range from 10^{-4} to 10^{-3} $\text{cm}^2 \cdot \text{V}^{-1} \cdot \text{s}^{-1}$ at moderate electric fields at the room temperature. Hole mobilities in the layers of compounds **11** and **12** having one and two 1,8-naphthalimide moieties well exceeded 10^{-3} $\text{cm}^2 \cdot \text{V}^{-1} \cdot \text{s}^{-1}$ at high electric fields. The charge transporting properties of the amorphous layers of pure **11** and **12** are good enough for many practical applications [254,255]. Dispersive hole-transport was observed for the layers of compounds **11–13**. For the illustration of this statement representative TOF transients of holes for compound **11** are shown in Fig. 4.31.

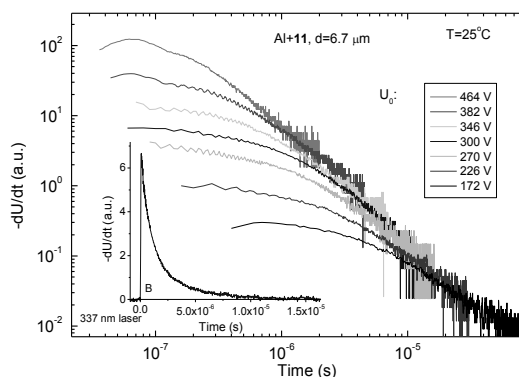


Figure 4.31. Representative TOF transients of the layer of compound **11**

¹³ Hole mobilities were measured at the Department of Solid State Electronics, Vilnius University by dr. V. Jankauskas.

In every case, the short initial spike, limited by the time resolution of the measurement setup, is followed first by a clear constant current plateau and then by a drop. In order to get some more insight in the hole-transport properties of these compounds, a qualitative discussion of charge-transfer rate-constants (k_{HT}) based on the Marcus theory can be helpful [219–222].

In the case of amorphous materials, the rate-constant of a hole-transfer reaction between two adjacent molecules can be described by the “hopping” mechanism and calculated mean of the following equation [219–222]:

$$k_{HT} = \frac{4\pi^2}{h} \frac{1}{\sqrt{4\pi\lambda k_B T}} t^2 \exp\left[\frac{-(\Delta G^\circ + \lambda)^2}{4k_B \lambda T}\right], \quad (4.2)$$

In this equation, t is the electronic coupling between two adjacent molecules, ΔG° is the free energy of the hole-transfer reaction, and λ is the reorganization energy. This last parameter is the sum of two terms: (i) λ_s , containing the contribution from the medium polarization energy. (ii) λ_i , representing the energetic effort due to the intra-molecular geometric relaxations related to the hole transfer between two adjacent molecules.

Equation 2 indicates that in order to obtain high hole-transfer rate-constants (k_{HT}), the reorganization energy (λ) should be small whereas the electronic coupling parameter (t) should be large. In the following only these two molecular parameters will be discussed, whereas the influence of morphological and other structural parameters will be ignored.

The internal reorganization energy (λ_i) values of model compounds **11–13** (0.18, 0.14, and 0.11 eV, respectively, B3LYP/6-31G(d,p) level) are small and vary in a narrow range. The relatively small λ_i values for the three compounds suggest good hole-transfer properties, which seems in line with the high hole mobilities measured for compounds **11** and **12**. On the other hand, the trend of λ_i values (**11** > **12** > **13**) suggests increasing hole-transfer rate-constants (k_{HT}) in the order **11** < **12** < **13** which seems in disagreement with the experimental trend of the hole mobilities (**13** < **11** < **12**). This discrepancy along with the narrow range of λ_i values (0.07 eV), indicates that from the microscopical viewpoint, the hole transfer in these compounds should be dominated by the electronic coupling between the HOMO orbitals of adjacent molecules.

The electronic coupling parameter is strongly dependent on the overlap between the HOMO orbitals of adjacent molecules. The HOMO pictograms in Fig. 4.23 suggest that in order for these compounds to exhibit good hole-transfer properties, a sufficient spatial overlap should be established between the TPA cores. In the case of compound **13**, the TPA core is hindered by three 1,8-naphthalimide arms, which prevent from efficient approach of the TPA cores of two adjacent molecules. In the case of **11** and **12**, there are still one or two phenyl rings non substituted by 1,8-naphthalimide arms, thus suggesting less hindered overlap between adjacent HOMO orbitals. However, while this observation might give ideas on why compound **13** exhibits lower hole mobilities than **11** and **12**, the higher mobility of **12** as compared to **11** seems in disagreement with the above argument.

Other factors should consequently dominate in the comparison of hole mobilities between **11** and **12**. We suspect that the different packing manners between **11** and **12**, as suggested by the very different T_g values (Table 4.11), indicate stronger intermolecular interactions in **12** as compared to compound **11**, which might result in smaller mean intermolecular distances, hence larger electronic coupling in compound **12**.

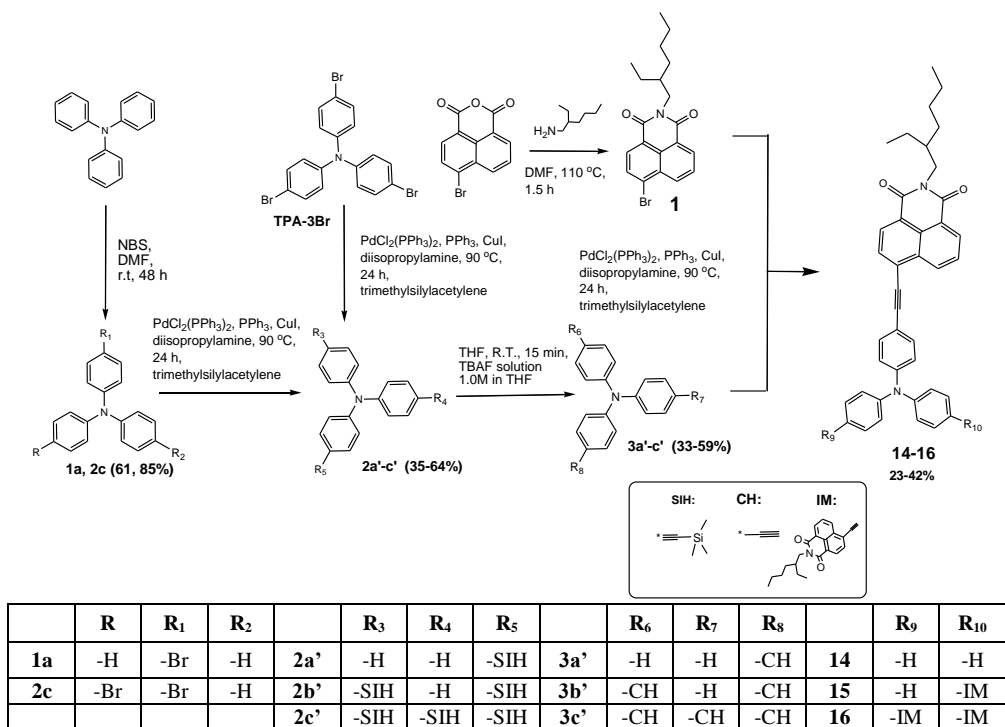
In conclusion, three new donor–acceptor glass-forming derivatives with triphenylamine core and 1,8-naphthalimide arms were synthesized and characterized. Their thermal, optical, electrochemical, and photoelectrical properties were studied and discussed in terms of correlation with their chemical structures. The 5% weight loss temperatures ranging from 431 to 448 °C. The compounds form glasses with glass-transition temperatures being in the range of 55–107 °C. Electron photoemission spectra of the amorphous films of the materials revealed ionization potentials similar to those of the derivatives of triphenylamine (5.75–5.80 eV) with no evidence of dependence of ionization potentials on the number of 1,8-naphthalimide arms. Hole mobilities in the layers of the compounds having one and two 1,8-naphthalimide moieties well exceeded $10^{-3} \text{ cm}^2 \cdot \text{V}^{-1} \cdot \text{s}^{-1}$ at high electric fields at room temperature.

4.1.4. Synthesis and properties of glass-forming derivatives with triphenylamino and 1,8-naphthalimide moieties linked via ethynyl-containing linkages

In this chapter, the synthesis of three new derivatives with the TPA moiety as a core and 1,8-naphthalimide fragments as arms with the ethynyl linkages between electrophores are presented. The triple bond containing linkage between TPA and 1,8-naphthalimide moieties is expected to enhance the extent of conjugation which in turn is expected to result in the improved photoelectrical properties. Another aim of this work was characterization of the three new compounds for the better understanding of the structure-property relationship of the electroactive materials with the donor-acceptor structure.

Synthesis and characterization

Palladium/copper-catalyzed Sonogashira cross-coupling reaction was used as a key reaction to obtain compounds with ethynyl linkages. Scheme 4.5 illustrates the synthetic routes to the intermediates and the target compounds. The first step was condensation of 4-bromo-1,8-naphthalic anhydride with 2-ethylhexylamine in DMF which gave 4-bromo-*N*-(2-ethylhexyl)-1,8-naphthalimide (**1**). Compounds **1a**, **2c** were prepared by bromination of TPA with NBS. Intermediates **3a'-c'** were prepared by coupling **2a'-c'** with ethynyltrimethylsilane in the presence of Pd/Cu and subsequently base-promoted deprotection. The treatment of **3a-c** with compound **1** by a Sonogashira cross-coupling reaction gave the desired compounds **14**, **15** and **16**. All these derivatives were characterized by ^1H and ^{13}C NMR, mass spectrometries and elemental analysis. The target compounds (**14–16**) are soluble in common organic solvents such as DCM, chloroform, THF, chlorobenzene, toluene etc.



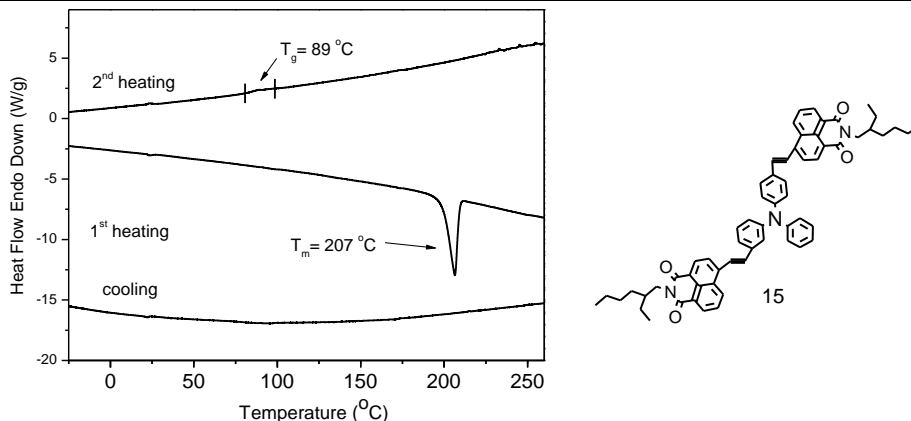
Scheme 4.5. The synthetic routes to **14–16**

Thermal properties

The thermal properties of compounds **14–16** were investigated by TGA and DSC under a nitrogen atmosphere. The values of T_g , T_m and 5% weight loss temperatures ($T_{ID-5\%}$) are summarized in Table 4.14. The T_{ID} are in the range of 396–462 °C. These data indicate that all derivatives have high thermal stabilities. The thermal stability of the synthesized donor-acceptor derivatives increases with increase of the number of naphthalimide arms (**14** < **15** < **16**). These results are in agreement the previously reported data on the thermal stability of the other derivatives of naphthalimide and TPA [71,256]. Compounds **14–16** were isolated after the synthesis as crystalline materials. Their behaviour in DSC experiments was similar, therefore DSC curves of only one compound are given in Fig. 4.32. The first heating scan revealed only one endothermic melting peak. No crystallization was observed during the cooling scan. In the second heating scans compounds **14**, **15** and **16** showed glass transitions at 73 °C, 89 °C and 96 °C, respectively and no crystallization was observed in the following heating and cooling scans. These T_g values are higher than those earlier reported for the derivatives of naphthalimide and TPA with the single bond linkages between the chromophores [256]. T_m of the synthesized compounds also increased with the increase of the number of naphthalimide arms. These observations can apparently be explained by the enhancement of intermolecular interaction.

Table 4.14. Thermal characteristics of compounds **14–16**

Compound	T_g (°C) (2 nd heating)	T_m (°C)	$T_{ID-5\%}$ (°C)
14	73	181	396
15	89	207	454
16	96	216	462

**Figure 4.32.** DSC thermograms of compound **15** (scan rate of $10^\circ\text{C}/\text{min}$, N_2 atmosphere)

Optical and fluorescence properties

Absorption and FL spectra of the dilute solutions (10^{-5} M) in toluene and of the thin solid films of the derivatives (**14–16**) are shown in Fig. 4.33. The wavelengths of the absorption maxima, molar extinction coefficients (ϵ), the wavelengths of fluorescence maxima, Φ_F , Stokes shifts of the dilute solutions in different organic solvents are summarized in Table 4.15.

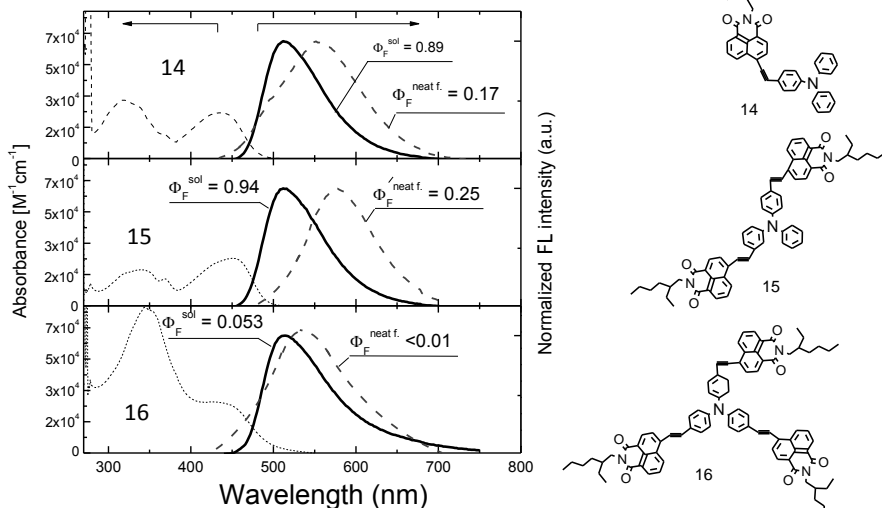
**Figure 4.33.** UV-Vis (dashed thin line) spectra of 10^{-5} M solutions of compounds **14–16** and normalized FL spectra of the dilute solutions in toluene (thick, solid line), and of the solid films (solution spin-coated on quartz, dashed grey line). Fluorescence quantum yields are indicated. Absorption maxima wavelengths were used as excitation wavelengths

Table 4.15. Optical and fluorescence characteristics of the solutions in the different solvents and of thin solid films of compounds **14–16**

Solvent	Compound								
	14			15			16		
	λ_{abs} , nm ($\epsilon/M^{-1}cm^{-1}$)	λ_{em} , nm (Φ_F)	$\Delta\nu$, nm	λ_{abs} , nm ($\epsilon/M^{-1}cm^{-1}$)	λ_{em} , nm (Φ_F)	$\Delta\nu$, nm	λ_{abs} , nm ($\epsilon/M^{-1}cm^{-1}$)	λ_{em} , nm (Φ_F)	$\Delta\nu$, nm
Toluene	438 (2.43)	512 (0.89)	74	452 (2.56)	514 (0.94)	62	446 (2.46)	516 (0.053)	70
Cyclohexane	422, 441 (1.19, 1.21)	462, 491 (0.66)	50	430, 453 (1.22, 1.27)	472, 505 (0.93)	52	424, 444 (1.34, 1.07)	474, 502 (0.064)	58
Chloroform	450 (2.21)	582 (0.51, 0.96 ^a)	132	466 (2.24)	587 (0.44, 0.82 ^a)	122	453 (2.33)	588 (0.041, 0.054 ^a)	134
THF	434 (2.26)	621 (0.62)	187	451 (2.53)	631 (0.85)	180	447 (2.21)	633 (0.027)	186
ACN	433 (1.76)	547 (0.026)	114	456 (1.44)	549 (0.012)	93	454 (1.41)	612 (0.111)	158
Solid film	460	554 (0.17)	94	486	576 (0.25)	90	470	549 (0.011)	79

^a upon deoxygenation; $\Delta\nu$ (Stokes shift) = $\lambda_{em} - \lambda_{abs}$.

The absorption bands in the range between 321 and 346 nm can be assigned to $\pi-\pi^*$ transition of naphthalimide groups [230], while the lowest energy absorption bands between 438 and 452 nm can be ascribed to the ICT of compounds **14–16** (Fig. 4.33 and Table 4.15). Such ICT absorption bands were observed for the earlier described derivatives of TPA and naphthalimide [71,256]. Molar extinction coefficients of the ICT bands of the dilute toluene solutions of compounds **14–16** were $2.43 \times 10^{-4} M^{-1} \cdot cm^{-1}$, $2.56 \times 10^{-4} M^{-1} \cdot cm^{-1}$ and $2.46 \times 10^{-4} M^{-1} \cdot cm^{-1}$, respectively.

The absorption maxima of the solid films of compounds **14** and **16** show blue shifts of 26 and 16 nm, respectively compared to the wavelength of absorption maximum compound **15** apparently owing to the smaller dihedral angle, thus giving rise to more efficient π -conjugation in molecule **15**. At the same time the absorption maxima of the solid films of compounds **14–16** show red shifts of 22, 34 and 24 nm, respectively with respect of those of dilute toluene solutions. This observation indicates that there are significant conformational changes of compounds **14–16** in the solid state with respect of those characteristic of the dilute solutions. The absorption edges E_g^{opt} of the thin films of compounds **14–16** were estimated as 2.38, 2.33, and 2.21 eV, respectively. The values of E_g^{opt} observed for the dilute solutions were found to be by ca. 0.1 eV higher.

The emission intensity maxima of the dilute toluene solutions of compounds **14–16** were found to be in the close range of 512–516 nm (Fig. 4.33). The FL spectra of the solid films of **14–16** were broadened with the intensity maxima at 554, 576 and 549 nm, respectively. They were without vibronic features and exhibited considerable red shifts with respect to the spectra of the dilute solutions. The considerable red shifts of the fluorescence spectra of the films of compounds **14–16** with respect of those of the solutions can apparently be explained by the formation

of excited complexes (exciplexes) in the solid state [257]. These results are consistent with the results obtained by UV spectrometry for the same compounds. The Stokes shifts of 94 nm, 90 nm and 79 nm were observed for the solid films of compounds **14**, **15** and **16**, respectively. They decreased with the increased number of naphthalimide arms. For the dilute toluene solutions no decrease of the Stokes shifts with the increase of the number of naphthalimide arms was observed.

To investigate in detail the effect of solvatochromism of compounds **14–16**, the spectral changes induced by solvent polarity are exemplified by comparison of the absorption and FL spectra of each compound using several different polar solvents with dielectric constants ranging from 2.02 to 37.50, including cyclohexane (dipole moment = 0 D), toluene (0.36 D), chloroform (1.04 D), THF (1.75 D) and acetonitrile (ACN, 3.92 D).

The influence of solvent polarity on the absorption wavelengths was negligible, however considerable red shifts were observed for the emission bands of all the studied compounds. Fig. 4.34 shows the effect of solvent polarity on FL spectra of compounds **14–16**. FL spectra of the dilute solutions of compounds **14–16** in cyclohexane show two peaks which can be associated with the transitions from the lowest vibrational state to two different vibrational states. As the solvent polarity increased, the FL spectra of all the studied compounds exhibited only one broad band. Compounds **14–16** showed a blue shifted FL maxima in non-polar solvent (cyclohexane and toluene) and red shifted FL maxima in polar solvent (THF and chloroform). This suggests ICT occurring from the less polar ground state to the more polar excited state [258]. The Stokes shifts increased with the increase in the solvent polarity (>100 nm for the solutions in chloroform, ACN and THF) which indicates that the polar excited state is more stabilized in the polar solvent.

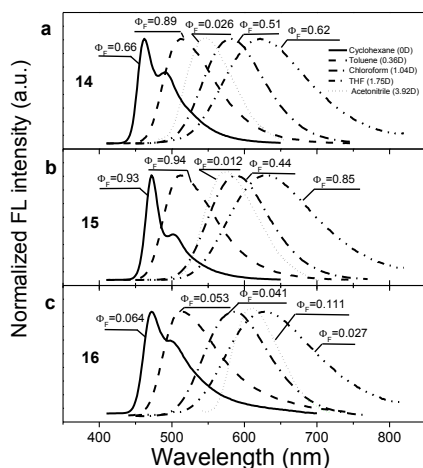


Figure 4.34. FL spectra of the solutions (10^{-5} M) of compounds **14** (a), **15** (b) and **16** (c) in dilute cyclohexane (solid line), toluene (dashed line), chloroform (dashed dot line), THF (dashed dot dot line), and acetonitrile (short dot line). Absorption maxima wavelengths were used as excitation wavelengths

The spectral dependency on the solvent polarity was studied on the basis of the Lippert-Mataga model. The Lippert-Mataga polarity parameter (Δf) was considered

as the measure of the polarity of different solvents used. It was calculated according to the following equation [259]:

$$\begin{aligned} \nu_A - \nu_F &= 2/hc \times \Delta\mu^2 \times \Delta f \times a^{-3} + const. \\ \Delta f &= (\epsilon - 1)/(2\epsilon + 1) - (n^2 - 1)/(2n^2 + 1), \quad \Delta\mu = \mu_E - \mu_G, \\ (\nu_A - \nu_F)/\Delta f &= 11307.6\Delta\mu^2 \times a^{-3} + const. \end{aligned} \quad (4.3)$$

where ν_A and ν_F are the wavenumbers (cm^{-1}) of the absorption and emission maxima, respectively, $h = 6.6256 \times 10^{-27}$ erg·s (Planck's constant); $c = 2.9979 \times 10^{10}$ $\text{cm}\cdot\text{s}^{-1}$ (the speed of light); a is the radius of the cavity in which the fluorophore resides; μ_G and μ_E refer to the ground state and excited state dipole moments, respectively. The slope of the Lippert plot reflects the solvent sensitivity of a fluorophore.

Therefore, the Lippert-Mataga plot has to be linear, provided the solvent-solute interactions are dipolar. However, as it can be seen from Fig. 4.35a, there is a poor linear correlation between the Stokes shift of derivative **14** and the solvent orientation polarizability. Poor linear correlations are also observed for compounds **15** and **16**, suggesting that strong solute-solvent interaction other than dipole-dipole interaction occurs in the excited states of compounds **14–16**.

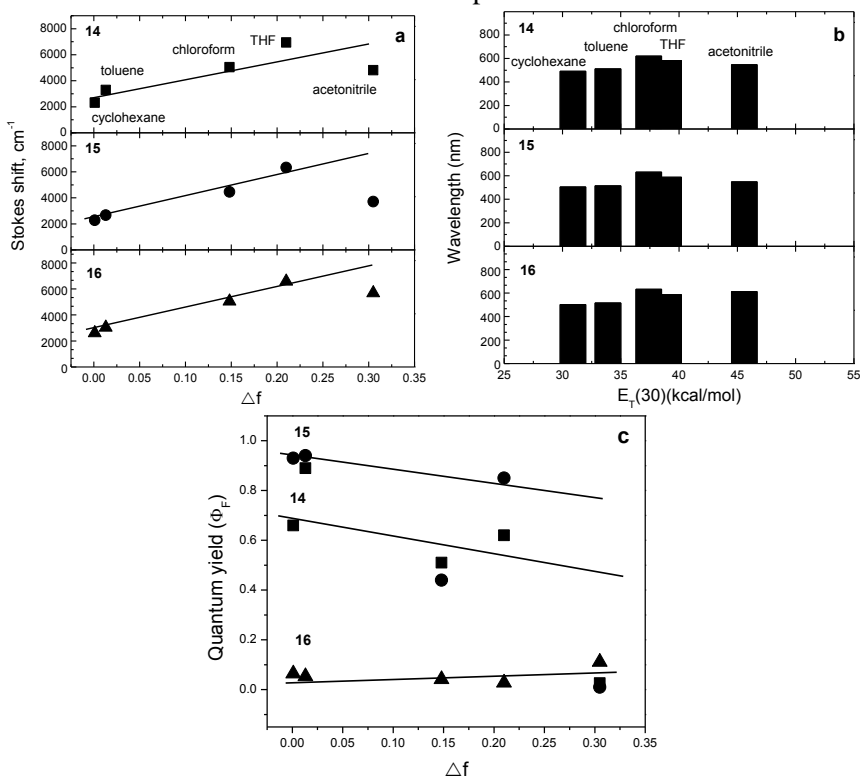


Figure 4.35. (a) Dependences of Stokes shifts $\Delta\nu$ of compounds **14–16** ($c = 10^{-5}$ M) on the orientation polarizability Δf . Solid lines were obtained from the linear fits. (b) plots of the wavelengths of fluorescence intensity maxima of **14–16** versus the $E_T(30)$ polarity parameter of the different solvents. (c) fluorescence quantum yields of the solutions **14–16** versus the solvent polarity $\Delta f(\epsilon, n)$

In order to get a deeper understanding on the solvatochromism of compounds **14–16**, the Reichardt-Dimroth equation was used [260]:

$$\nu_A - \nu_F = m_4 \cdot E_T^N + const., \quad (4.4)$$

where E_T^N , the normalized solvent polarity of Reichardt is a solvatochromic parameter based on the absorption wavenumber of a standard betaine dye in the corresponding solvent.

A linear correlation between the position of the emission maxima and empirical solvent polarity parameter ($E_T(30)$) is observed for the solutions of compounds **14–16** in aprotic solvents (Fig. 4.35b), revealing the involvement of solvent polarity dependent ICT emissive states. The values of Φ_F of the solutions of the synthesized compounds in different solvents were also estimated. They are summarized in Table 4.15. For the solution in chloroform the largest Φ_F of 0.51 was found for the derivative **14** containing one naphthalimide moiety. The solutions of compounds **15** and **16** showed Φ_F values of 0.44 and 0.041, respectively. Thus higher fluorescence quantum efficiencies were observed for the solutions in non-polar solvents compared to those in polar solvents (Fig. 4.35c). The fluorescence quenching in most of the polar solvents was accounted for exciplex or cluster formation [232]. Compounds **14–16** showed very low emission intensity in ACN, which is in accordance with the low Φ_F observed (Table 4.15). This is probably due to the ICT from the TPA to the naphthalimide moieties through the ethynyl spacers. ICT normally reduces the quantum yield due to more pronounced relaxation and nonradiative decay of the excited state [261]. To study the effect of an increased number of naphthalimide moieties on Φ_F , the Φ_F of the three compounds in dilute toluene solutions was estimated. It is known that the triplet excitons of thermally activated delayed fluorescence materials are inactivated by included triplet oxygen molecules (3O_2) [262]. Therefore Φ_F were measured after deoxygenation of the dilute solutions by bubbling nitrogen through them. The Φ_F of the three compounds increased from 0.041–0.51 to 0.054–0.96 upon deoxygenation. These results showed that **14–16** might be useful as emitters for new generation organic light emitting diodes [263,264].

To reveal the delayed fluorescence of the dilute solutions and solid films of compounds **14–16** in toluene solutions (10^{-5} M) and solid films we recorded time resolved fluorescence spectra (Fig. 4.36). The spectra of the delayed fluorescence of the solutions and the layers of compounds **14, 15** are identical to those of the prompt fluorescence. The resemblance between the prompt and delayed fluorescence spectra of the compounds with donor-acceptor structure can be explained by the effective ICT [265,266].

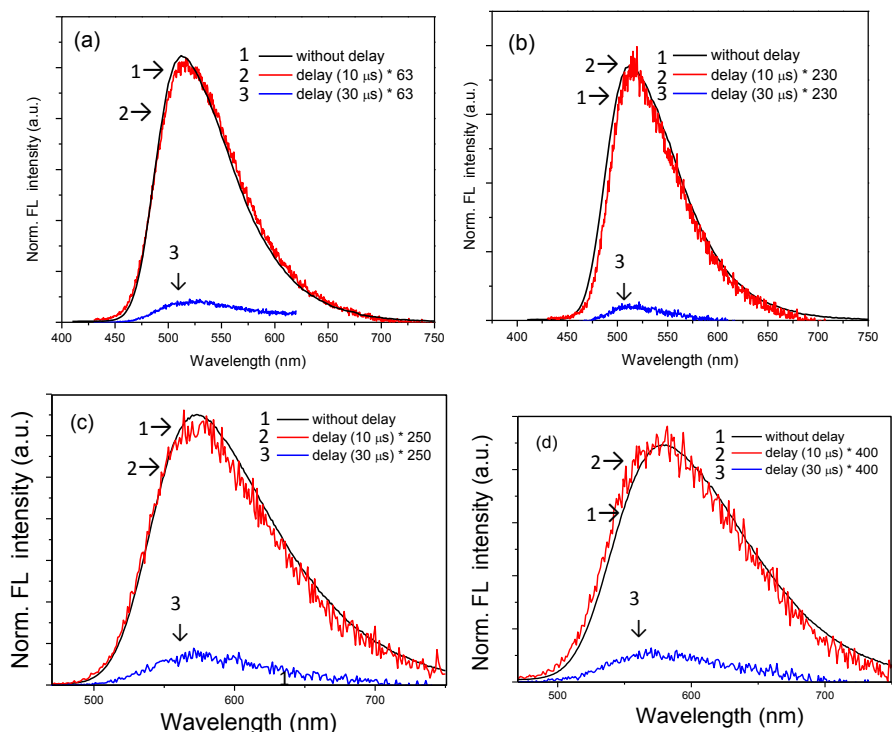


Figure 4.36. Normalized prompt and delayed fluorescence spectra of the toluene solutions (10^{-5} M) of **14** (a) and **15** (b) and of the solid films of **14** (c) and **15** (d)

Electrochemical properties

The results of the electrochemical measurements are listed in Table 4.16. Fig. 4.37 shows that the shapes of CV curves are similar and compounds **14–16** showed ambipolar redox behavior. One irreversible n-doping/dedoping (reduction/reoxidation) process in the negative potential range (related to the reduction of naphthalimide group) and one irreversible p-doping/dedoping (oxidation/rereduction) process in the positive potential range (related to the oxidation of triphenylamino group) were observed for all the compounds (**14–16**). The onsets of the oxidation potential (E_{onset}^{ox}) were found to be 0.76 V for compound **14**, 0.68 V for **15** and 0.81 V for **16**. Derivative **15** possesses the lowest onset oxidation potential, which means that the electron-donating ability of compound **15** containing two naphthalimide moieties is the strongest among these three compounds. In the reductive potential region, the onset reduction potentials (E_{onset}^{red}) were found to be -1.62 V for **14**, -1.65 V for **15** and -1.51 V for **16**. The electrochemically estimated band gaps (E_g^{elc}) of **14–16** were in the range of 2.31–2.38 eV (Table 4.16). They were found to be slightly lower than the corresponding optical band gaps (E_g^{opt}) observed for the solutions of **14–16** (2.32–2.53 eV), but within the range of error (0.2–0.5 eV) [252]. The values of E_g^{elc} of these compounds

were smaller than the corresponding values of E_g^{opt} . Such relatively small differences between E_g^{opt} and E_g^{elc} were also observed for the other derivatives of TPA and naphthalimide [71,256]. The solid state ionization potentials (IP_{CV}) and electron affinities (EA_{CV}) were also estimated by CV (Table 4.16). The values of IP_{CV} for compounds **14–16** ranged from 5.48 to 5.61 eV. They are comparable to those of the other derivatives of TPA and naphthalimide [71,256].

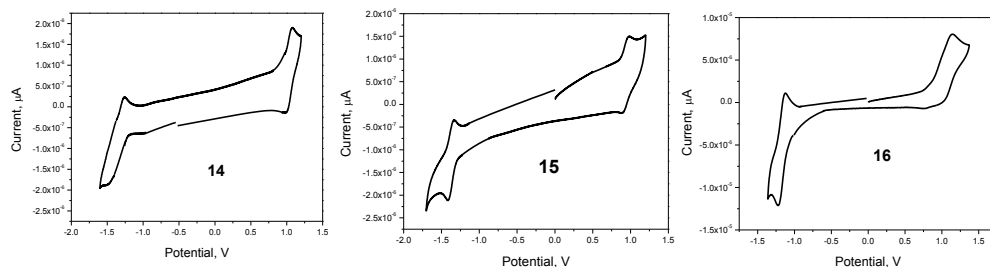


Figure 4.37. Cyclic voltammograms of **14–16** (10^{-5} M solutions, scan rate of $50 \text{ mV} \cdot \text{s}^{-1}$ vs Ag/Ag^+) in 0.1 M solution of Bu_4NPF_6 in CH_2Cl_2

Table 4.16. Electrochemical characteristics of **14–16**

Compound	E_{onset}^{ox} vs Fc/V^a	E_{onset}^{red} vs Fc/V^a	IP_{CV} , (eV) ^b	EA_{CV} , (eV) ^b	E_g^{elc} , (eV) ^c	E_g^{opt} , (eV) ^d	E_g^{opt} , (eV) ^e
14	0.76	-1.62	5.56	-3.18	2.38	2.53	2.38
15	0.68	-1.65	5.48	-3.16	2.32	2.44	2.33
16	0.81	-1.51	5.61	-3.29	2.31	2.32	2.21

^a E_{onset}^{ox} and E_{onset}^{red} are measured vs. ferrocene/ferrocenium. ^b Ionization potentials and electron affinities estimated according to $IP_{CV} = (E_{onset}^{ox} + 4.8)$ (eV). $EA_{CV} = -(E_{onset}^{red} + 4.8)$ (eV) (where, E_{onset}^{ox} and E_{onset}^{red} are the onset reduction and oxidation potentials versus the Fc/Fc^+). E_{onset}^{ox} and E_{onset}^{red} of Fc/Fc^+ measured in DCM solution containing 0.1 M Bu_4NPF_6 was 0.275 V vs. ferrocene/ferrocenium). ^c $E_g^{elc} = |IP_{CV}| - |EA_{CV}|$, where E_g^{elc} is the electrochemical band gap. ^d The optical band gap estimated from the onset wavelength of optical absorption of dilute solution, according to the formula: $E_g = 1240/\lambda_{edge}$, in which the λ_{edge} is the onset value of absorption spectra in long wave direction. ^e The optical band gap estimated from the onset wavelength of optical absorption of the solid film.

Photoelectrical properties

The electron photoemission spectra of the amorphous films of compounds **14–16**, taking the square root of the photocurrent i versus the light irradiation energy $h\nu$ are plotted in Fig. 4.38. The values of ionization potentials were obtained by extrapolation of the straight parts of the spectra to $i=0$. The ionization potential values of 5.70, 5.65 and 5.61 eV observed for compounds **14**, **15** and **16**. They are comparable and slightly higher than those estimated by CV. The ionization potentials of **14**, **15** and **16** are slightly lower than those of the earlier reported

derivatives of TPA and 1,8-naphthalimide moieties linked via single and double linkages [71,256].

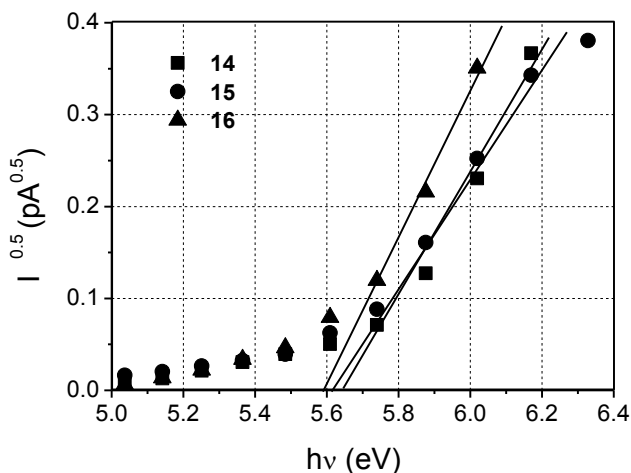


Figure 4.38. Electron photoemission spectra of the films of compounds **14–16**

To investigate the effect of attaching of the different number of naphthalimide acceptor units to a triphenylamine donor core on the charge-transporting properties of compounds **14–16**, we used the method of charge extraction by linearly increasing voltage (CELIV) [129,130]. Fig. 4.39 shows dark-CELIV and photo-CELIV transients recorded respectively in the dark and under illumination at various applied electric fields, which were changed by increasing the maximum voltage of the pulse while keeping its duration constant, in a 285 nm thick sample of the amorphous layer of **14**. The dark-CELIV curves show a purely capacitive response in case of the absence of photoexcitation. At 20 V the dark injection from the electrodes is beginning to occur as evidenced by the tail observed in the transient. The shape of the photo-CELIV transients resemble the typical case for the extraction of photogenerated charge carriers from the layer. As it is seen from photo-CELIV curves, the time of the maximum extraction current (t_{max}) shifts to the smaller values at high voltages. For the layer of compound **15** the extraction of photogenerated charge carriers in photo-CELIV transients was seen only at high voltage (20 V). In case photo-CELIV of the layer of compound **16** we did not obtain the signal for the extraction of photogenerated charge carriers. This observation shows that the recombination of charge carriers in the layers of the compound is faster than the allowed range of the photo-CELIV method (the range from μ s to ms).

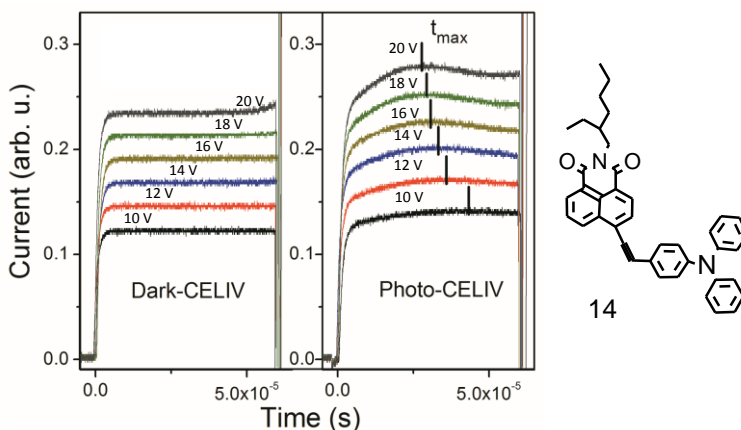


Figure 4.39. Dark CELIV and photo-CELIV curves for compound the layer of **14** as a function of an applied triangle-shaped voltage pulse with amplitude from 10 to 20 V. The maximum extraction time was marked in photo-CELIV curves when the maximum in the current transients was observed

Hole mobilities were calculated at 20 V by the formula $\mu = 2d^2/3At_{max}^2$, where d is the sample thickness, $A = U(t)/t$ is the voltage rise rate, t_{max} is extraction time when the maximum in the current transients is observed (marked in Fig. 4.39). For the layers of compounds **14** and **15** they were found to be $2.23 \times 10^{-6} \text{ cm}^2/\text{V}\cdot\text{s}$ at $3.2 \times 10^5 \text{ V/cm}$, and $4.1 \times 10^{-6} \text{ cm}^2/\text{V}\cdot\text{s}$ at $1.2 \times 10^5 \text{ V/cm}$, respectively. It was not possible to calculate charge mobilities for derivative **16** since the maximum in the current transients for its layer was not observed. The values of hole mobility for **14** and **15** are lower compared to those of the other compounds consisting of triphenylamine core and 1,8-naphthalimide arms [71,256].

In conclusion, three new donor–acceptor glass-forming derivatives with triphenylamine core and 1,8-naphthalimide arms were synthesized and characterized. Their thermal, optical, electrochemical, and photoelectrical properties were studied and discussed. The 5% weight loss temperatures ranging from 396 to 462 °C. The compounds form glasses with glass-transition temperatures being in the range of 73–96 °C. The values of IP_{CV} for compounds **14–16** ranged from 5.48 to 5.61 eV. They are comparable to those of the other derivatives of TPA and naphthalimide. The Φ_F of the three compounds increased from 0.041–0.51 to 0.054–0.96 upon deoxygenation. These results showed that **14–16** might be useful as emitters for new generation organic light emitting diodes.

4.1.5. Comparison of properties of glass-forming derivatives with triphenylamino and 1,8-naphthalimide moieties

Three groups of the synthesized compounds containing triphenylamine and naphthalimide moieties are shown in Fig 4.40. These groups differ in terms of the linking topology of the chromophores: in the first group triphenylamino and naphthalimido moieties are linked via the single bonds, in the second and in the third groups – the same species are linked via ethenyl- or ethynyl-containing bridges.

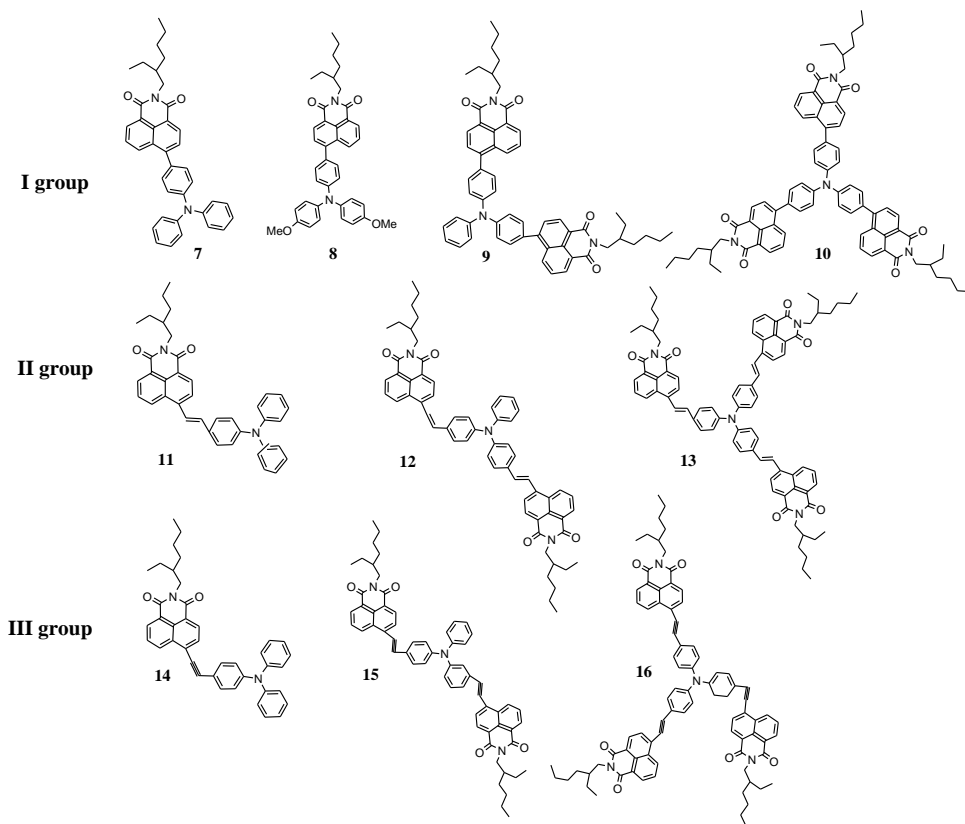


Figure 4.40. Molecular structures of 7–16

TGA revealed that first group of compounds 7–10 exhibit excellent thermal stabilities. Their 5% weight loss temperatures range from 429 to 483 °C. It was established that increase of the number of 1,8-naphthalimide moieties leads to the increase of the thermal stability of the derivatives. Molecules 9, 10 having two and three 1,8-naphthalimide moieties showed higher 5% weight loss temperatures than molecules 7 and 8 containing one 1,8-naphthalimide moiety. Compounds 7, 9 and 10 were obtained as crystalline substances. However in the second DSC heating scans, the glass transitions of 7–10 were observed in the range of 45–84 °C. DSC revealed that the compounds of the second (11–13) and the third (14–16) groups can also exist in the glassy state. The glass transition range from 55 to 107 °C for the compounds of the second group and from 73 to 96 °C for the compounds of the third

group. The linking topology of the chromophores has significant effect on the glass transition temperature of the synthesized derivatives. The highest glass transition temperature was observed for compound **13** in which the chromophores are linked via the bridge containing double bonds. The lowest T_g was recorded for compound **8** in which the chromophores are linked via the single C-C bond.

The lowest-energy absorption bands of compounds **7–10** are shifted to the longer wavelengths in respect to the absorbance bands of the compounds having electronically isolated 1,8-naphthalimide or triphenylamine moieties. FL spectra of compounds **7, 9, 10** dissolved in cyclohexane exhibit efficient molecular emission with Φ_F of 0.63–0.78. FL spectra of the solid films of compounds **7–10** are broad, unstructured and red shifted with respect to those of the dilute solutions and molecular dispersions in PS matrixes.

The dilute solutions of compounds **11–13** emit orange light with the intensities peaking in the range of 641–646 nm. The spectra of the solid samples of compounds **11–13** exhibit small red shifts with respect to those of the dilute solutions. Φ_F of the dilute solutions of **11–13** range from 0.64 to 0.45, while those of the films are considerably lower and range from 0.09 to 0.18.

The lowest energy absorption bands between 438 and 452 nm can be ascribed to the ICT of compounds **14–16**. The absorption maxima of the solid films of compounds **14–16** show red shifts of 22, 34 and 24 nm, respectively with respect to those of dilute toluene solutions. Interestingly, that the absorption spectra of the solid films of compounds **14–16**, are red-shifted with respect to those of **7–10** and **11–13**, in which donor and acceptor units are linked through the single and double bonds. For the dilute toluene solutions of **14–16** no decrease of the Stokes shifts with the increase of the number of 1,8-naphthalimide arms was observed. The FL spectra of the solid films of **14–16** were broadened as well as for compounds **7–10** and **11–13**. The considerable red shifts of the fluorescence spectra of the films of compounds **14–16** with respect to those of the solutions are observed. The same bathochromic effects are observed for the fluorescence spectra of the films of compounds **7–10** and **11–13** with respect to those of the solutions in which donor and acceptor units are linked through the single and double bonds.

The values of ionization potential of the compounds **7–10** range from 5.57 to 6.01 eV. Compounds **9** and **10** with two and three 1,8-naphthalimide moieties, respectively, demonstrated a little higher of ionization potential values with respect to those of **7** and **8** with one 1,8-naphthalimide moiety. The similar electrochemical properties were observed for the compounds of the second (**11–13**) and the third groups (**11–16**).

Compound **8** showed comparable mobilities of holes and electrons. This is a valuable property with respect of the possible application in organic light emitting diodes. Hole mobilities in the layers of compounds **11** and **12** having one and two 1,8-naphthalimide moieties well exceeded $10^{-3} \text{ cm}^2 \cdot \text{V}^{-1} \cdot \text{s}^{-1}$ at high electric fields.

In conclusion, thermal, optical, fluorescence, electrochemical, photoelectrical properties of glass-forming derivatives with triphenylamino and naphthalimide moieties linked via the single bonds, ethenyl- or ethynyl-containing linkages are

summarized in Table 4.17 (for more details see in the Chapters 4.1.2, 4.1.3 and 4.1.4).

Table 4.17. Properties of glass-forming derivatives 7–16

Compound	7	8	9	10	11	12	13	14	15	16
T _g , (°C) (2 nd heating) ^a	47	45	76	84	55	90	107	73	89	96
T _m , (°C) ^b	134	–	136	141	163	185	222	181	207	216
T _{ID-5%} , (°C) ^c	437	429	448	483	431	445	448	396	454	462
Φ _F sol/film ^d	0.78 ^(in cyclohexane) / 0.11	0.68 ^(in cyclohexane) / 0.10	0.68 ^(in cyclohexane) / 0.16	0.63 ^(in cyclohexane) / 0.23	0.64 ^(in THF) / 0.18	0.45 ^(in THF) / 0.14	0.48 ^(in THF) / 0.09	0.89 ^(in toluene) / 0.17	0.94 ^(in toluene) / 0.25	0.053 ^(in toluene) / 0.01
μ _e , (cm ² /V·s) ^e	10 ⁻⁴	10 ⁻⁴	10 ⁻⁵	10 ⁻⁵	–	–	–	–	–	–
μ _h , (cm ² /V·s) ^f	10 ⁻⁷	10 ⁻⁴	10 ⁻⁷	10 ⁻⁸	10 ⁻³	10 ⁻³	10 ⁻⁴	10 ⁻⁶	10 ⁻⁶	–
IP _{EP} , (eV) ^g	5.79	5.57	5.93	6.01	5.75	5.78	5.80	5.70	5.65	5.61
E _{onset} ^{ox} vs Fc/V ^h	0.54	0.25	0.57	0.58	0.38	0.44	0.45	0.76	0.68	0.81
E _{onset} ^{red} vs Fc/V ⁱ	-1.83	-1.84	-1.84	-1.80	-1.74	-1.73	-1.72	-1.62	-1.65	-1.51
IP _{CV} , (eV) ^j	5.34	5.05	5.37	5.38	5.18	5.24	5.25	5.56	5.48	5.61
EA _{CV} , (eV) ^k	-2.97	-2.96	-2.96	-3.00	-3.06	-3.07	-3.08	-3.18	-3.16	-3.29
E _g ^{elc} , (eV) ^l	2.34	2.26	2.49	2.60	2.12	2.17	2.17	2.38	2.32	2.31
E _g ^{opt} , (eV) ^m	2.55	2.40	2.57	2.58	2.34	2.28	2.27	2.53	2.44	2.32

^a T_g – glass transition temperature; ^b T_m – melting transition temperature; ^c T_{ID-5%} – 5% weight loss temperature; ^d Φ_F – fluorescence quantum yield in solution/solid film; ^e hole drift mobility value; ^f electron drift mobility value; ^g established from electron photoemission in air spectra; ^{h,i} E_{onset}^{ox} and E_{onset}^{red} are measured vs. ferrocene/ferrocenium; ^{j,k} ionization potentials and electron affinities estimated according to IP_{CV} = (E_{onset}^{ox} + 4.8) [eV]. EA_{CV} = -(E_{onset}^{red} + 4.8) [eV] (where, E_{onset}^{ox} and E_{onset}^{red} are the onset reduction and oxidation potentials versus the Fc/Fc⁺). E_{onset}^{ox} and E_{onset}^{red} of Fc/Fc⁺ measured in DCM solution containing 0.1 M Bu₄NPF₆; ^l E_g^{elc} = |IP_{CV} – |EA_{CV}|, where E_g^{elc} is the electrochemical band gap; ^m the optical band gap estimated from the onset wavelength of optical absorption of dilute solution, according to the formula: E_g = 1240/λ_{edge}, in which the λ_{edge} is the onset value of absorption spectra in long wave direction.

4.2. Synthesis and properties of electron-transporting derivatives of fluorene and 1,8-naphthalimide

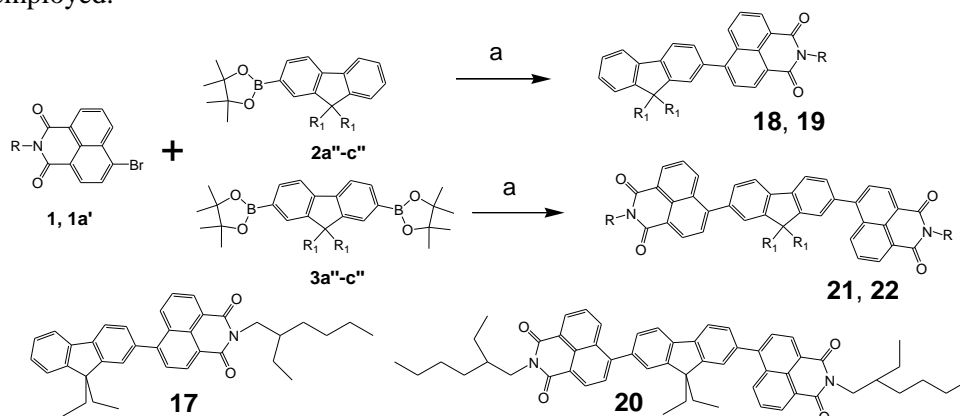
It is known that absorption, emission, electrochemical and/or photoelectrical properties of naphthalimides and their analogues can be varied by extending the π -conjugation at the carbocyclic core using electron-donor chromophores which affect the electronic structure of the derivatives [178,218,267–269]. However, the substitutions at the imide position have little or no influence on the electronic properties of the derivatives [178,218,267–270].

Fluorene and its derivatives are proven to be useful building blocks for the preparation of luminescent and charge-transporting materials [236,271,272]. They are applied extensively in the design and synthesis of polymers, low-molar-mass compounds, and dendrimers for electronic and optoelectronic applications [236,271–274]. The possibility of functionalization at 2, 7 and 9 positions, of fluorene moiety not only improves the solubility of its derivatives but also influences the molecular properties like glass transition, absorption or emission.

In this chapter, the synthesis and thermal, fluorescence, electrochemical, and charge-transporting properties of naphthalimide-substituted fluorene derivatives containing different alkyl substituents are reported.

Synthesis and characterization

Compounds **18**, **19**, **21** and **22** were synthesized by Suzuki-Miyaura coupling reactions as shown in Scheme 4.6. For the comparison compounds **17** and **20** also were synthesized as described in literature [174]. For the preparation of simple D-A compounds (**18**, **19**) containing naphthalimide acceptor and fluorene donor, mono-1,3,2-dioxaborolanyl derivatives of fluorene were used. For the synthesis of D-A-D hybrid compounds (**21**, **22**), 2,7-di-1,3,2-dioxaborolanyl derivatives of fluorene were employed.



	R		R ₁		R ₁	R
1	2-ethylhexyl	2a'' , 3a''	-ethyl	17 ^[154] , 20 ^[154]	-ethyl	2-ethylhexyl
1a'	-octyl	2b'' , 3b''	2-ethylhexyl	18 , 21	2-ethylhexyl	2-ethylhexyl
		2c'' , 3c''	-octyl	19 , 22	-octyl	-octyl

Scheme 4.6. Synthesis of compounds **17**–**22**. Reagents and conditions: (a) Pd(Ph₃)₂Cl₂, K₂CO₃, THF/H₂O, 80 °C, 12–16 h

The synthesized compounds were purified by silica gel column chromatography and characterized by ^1H NMR, ^{13}C NMR and IR and mass spectrometries, as well as by elemental analysis. The spectral and elemental analysis data are in good agreement with their chemical structures.

Thermal properties

The values of T_g , T_m , T_{cr} and 5% weight loss temperatures ($T_{ID-5\%}$) are summarized in Table 4.18. The derivatives demonstrate high thermal stability. The $T_{ID-5\%}$ occurred at the temperatures higher than 304 °C, as confirmed by TGA with a heating rate of 20 °C/min. The thermal stability of disubstituted fluorene derivatives (**20–22**) was found to be higher in comparison to that of monosubstituted compounds **17–19**.

All fluorene derivatives synthesized in this work except compound **19** were isolated after the synthesis as crystalline materials. DSC thermograms of compound **18** are shown in Fig. 4.41. When the crystalline sample of **18** was heated, the endothermic peak due to melting was observed at 61 °C. When the melted sample was cooled down and heated again, the glass transition was observed at 50 °C. On further heating, no peaks due to crystallization and melting appeared. The crystalline samples of compounds of **17**, **20** and **21** demonstrated the similar behaviour. They melted on the first heating scan at 143 °C (for **17**), 145 (for **20**) and 142 °C (for **21**), and formed glasses upon cooling at 30 °C, 76 °C and 49 °C, respectively. Compound **22** demonstrated different behaviour in the DSC experiments. The crystalline sample of **22** melted at 169 °C on the first heating and formed glass upon cooling. When the amorphous sample was heated again, the glass transition was observed at 59 °C. On further heating, an exothermic peak due to crystallization was observed at 84 °C to give the crystals which melted at 167 °C. Compound **19** having linear octyl chains was isolated after the synthesis as viscous liquid. In the second DSC heating scan it showed glass transition at -19 °C. The values of T_g of naphthalimide-substituted derivatives of fluorene can be modified by the attachment of the different alkyl chains to the fluorene and naphthalimide moieties.

Table 4.18. Thermal characteristics of compounds **17–22**

Compound	T_g (°C) (2 nd heating)	T_m (°C)	T_{cr} (°C)	$T_{ID-5\%}$ (°C)
17	30	143	–	392
18	50	61	–	304
19	-19	–	–	360
20	76	145	–	457
21	49	124	–	422
22	59	169, 167 ^b	84	441

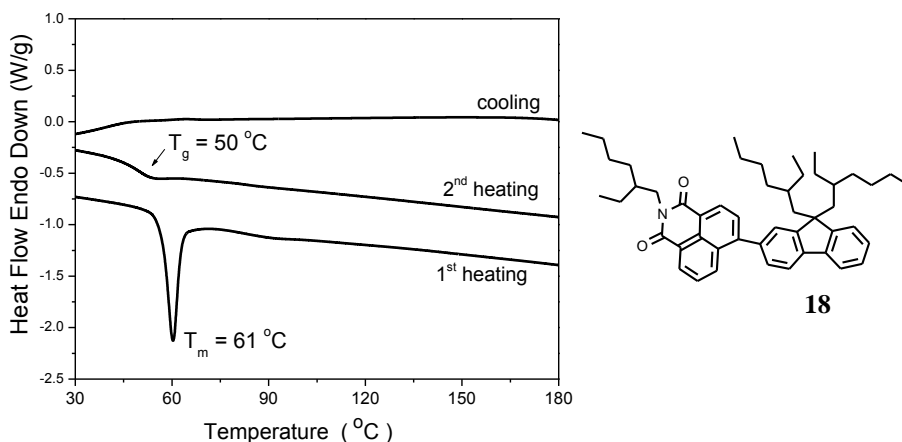


Figure 4.41. DSC curves of compound **18** (heating/cooling rate 10 °C/min, N₂)

Fluorescence properties

UV-Vis absorption spectra and fluorescence spectra of dilute solutions in cyclohexane and of solid films of the synthesized naphthalimide mono- and disubstituted fluorenes are shown in Fig. 4.42. The details of the optical and fluorescence properties of the compounds are summarized in Table 4.19.

Table 4.19. Optical and fluorescence properties¹⁴ of the dilute cyclohexane solutions and solid films of compounds **17–22**

Compound	Dilute solution in cyclohexane						Solid film			
	λ_{abs} , (nm) (ϵ , L mol ⁻¹ cm ⁻¹)	λ_{em} , (nm)	Φ_{F}	τ , (ns)	$\tau_{\text{R}}^{\text{a}}$ (ns)	$\tau_{\text{NR}}^{\text{a}}$ (ns)	λ_{abs} , (nm)	λ_{em} , (nm)	Φ_{F}	τ , (ns)
17	363 (20505)	423	0.50	1.42	2.84	2.84	380	474	0.23	2.18 (51%), 0.55 (31%), 6.84 (18%)
18	355 (24709)	423	0.53	1.42	2.68	3.02	378	495	0.17	2.03 (44%), 7.01 (29%), 0.54 (27%)
19	357 (18505)	423	0.47	1.45	3.09	2.74	393	477	0.25	2.41 (55%), 0.64 (28%), 8.29 (17%)
20	374 (42867)	425	0.69	1.22	1.77	3.94	392	489	0.14	1.95 (49%), 0.57 (41%), 8.42 (9%)
21	369 (47535)	424	0.64	1.23	1.92	3.42	406	469	0.07	0.26 (49%), 0.91 (40%), 3.40 (11%)
22	373 (42974)	424	0.65	1.24	1.91	3.54	410	480	0.25	0.42 (49%), 1.04 (44%), 4.05 (7%)

^a Radiative and non-radiative decay time constants calculated as τ/Φ_{F} and $\tau/(1-\Phi_{\text{F}})$, respectively.

¹⁴ Optical and fluorescence properties were obtained at the Institute of Applied Research, Vilnius University by dr. A. Miasojedovas.

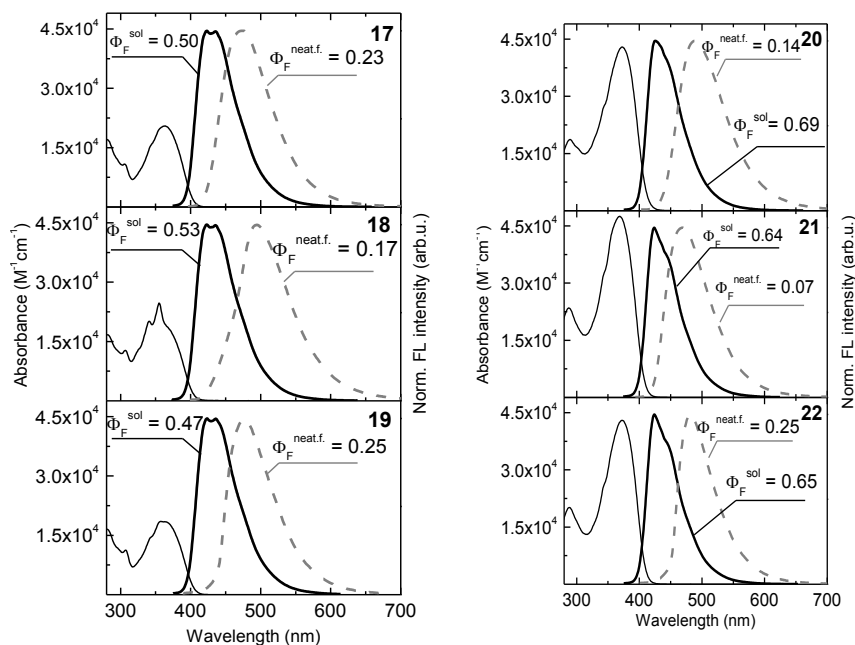


Figure 4.42. Absorption (thin solid line) and fluorescence spectra of the solutions (10^{-6} M) of **17–22** in cyclohexane (thick solid line) and of solid films (dashed grey line). Fluorescence quantum yields are indicated. Absorption maxima wavelengths were used as excitation wavelengths

The lowest-energy absorption bands of the mono- as well as of the disubstituted compounds are located at 355–374 nm. These bands are shifted to the longer wavelengths in respect to the absorbance band of the naphthalimide moiety (344 nm) [71,183,275] implying extended conjugation. The less pronounced absorbance band peaked at 306 nm can be attributed to fluorene moiety [276]. Oscillator strength of the lowest-energy transitions of the disubstituted compounds **20–22** is nearly twice as large as that of the monosubstituted compounds **17–19** as a result of extended π -conjugation on two naphthalimide moieties. Absorption spectra of the solid films of the investigated compounds were broader and red-shifted by ca. 17–37 nm indicating on excitonic coupling.

Excitation at 365 nm of dilute cyclohexane solutions of the synthesized compounds resulted in a highly efficient fluorescence in the blue spectral region with bands peaked at 423–425 nm. FL spectra of the dilute solutions of **17–22** in nonpolar solvents showed vibronic structure. Monosubstituted compounds exhibited more intense 0–1 vibronic transition (at 435 nm) in respect to the disubstituted derivatives. FL spectra of the solid films of naphthalimide derivatives **17–22** are broadened and shifted to the long wavelengths by 45–72 nm as compared to those of dilute solutions. Φ_F of the dilute cyclohexane solutions of the compounds were found to be 0.47–0.53 for the monosubstituted compounds (**17–19**), whereas a higher value of Φ_F (0.64–0.69) was obtained for the disubstituted compounds (**20–22**). Higher values of Φ_F obtained for the disubstituted compounds are consistent with the enhanced oscillator strength of the lowest electron transitions revealed by

the absorption measurements. Φ_F of the solid films was estimated to be in the range of 0.07–0.25.

It is known that fluorescence properties of naphthalimide derivatives are strongly dependent on the solvent polarity [71,183]. Significant variation of the excited state properties on the solvent polarity indicates on pronounced charge-transfer character of the lowest excited states. The normalized fluorescence spectra of the dilute solutions of compound **17** in the solvents of different polarities are shown in Fig. 4.43. The fluorescence characteristics of the solutions of compound **17** in the different solvents are summarized in Table 4.20.

Table 4.20. Fluorescence properties of the dilute solutions of compound **17** in the solvents of the different polarity

Solvent	Dielectric constant, (ϵ)	λ_{abs} , (nm)	λ_{em} , (nm)	FWHM, (nm)	Φ_F	τ , (ns)	τ_R , (ns)	τ_{NR} , (ns)
Cyclohexane	2.02	363	423	66	0.50	1.42	2.84	2.84
Toluene	2.4	369	444	70	0.44	1.33	3.02	2.38
Chloroform	4.8	375	477	78	0.62	2.25	3.63	5.92
DCM	9.08	374	481	82	0.63	2.71	4.30	7.32
Acetone	20.7	369	490	90	0.68	3.36	4.94	10.5
Acetonitrile	37.5	368	506	97	0.76	4.07	5.35	16.96
DMSO	46.7	376	517	102	0.84	4.32	5.14	27

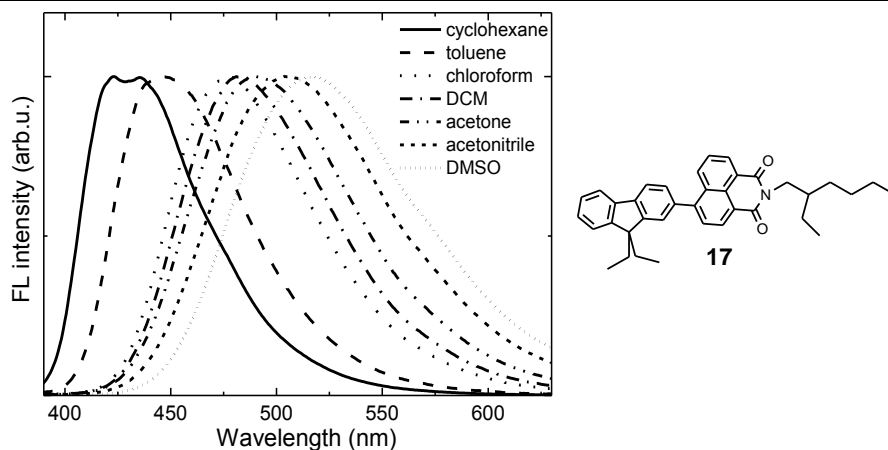


Figure 4.43. Fluorescence spectra of the dilute cyclohexane, toluene, chloroform, dichloromethane, acetone, acetonitrile and dimethylsulfoxide solutions (10^{-6} M) of compound **17**

Batochromic shift of 94 nm, broadening and the change of the shape of FL spectra was observed with increasing solvent polarity. At the same time solvatochromic shift of the absorbance band was found to be only 13 nm. Such behavior is typical for compounds possessing small dipole moment in the ground state and significantly larger dipole moment in the excited state. The most interesting solvation property is enhancement of Φ_F with the increase of the solvent

polarities. Φ_F of compound **17** increased linearly from 0.55 to 0.84 with the increasing solvent polarity (Fig. 4.44a).

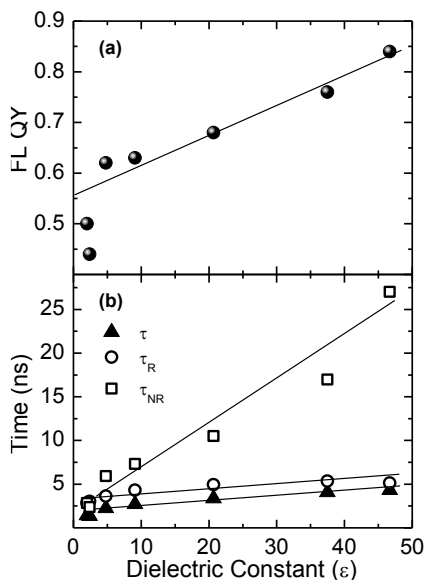


Figure 4.44. a) FL quantum yield and b) FL decay time (triangles), radiative (circles) and non-radiative (squares) decay times *versus* dielectric constants of the solvents. Lines are showing the trends

Fluorescence enhancement was also reported for other naphthalimide compounds dissolved in protic solvents [71,183,267,268,277]. Enhancement of Φ_F was accounted to the decrease in the intersystem crossing because of the hydrogen bond formation [109]. In our case increase in Φ_F in nonprotic solvents was observed as compared with Φ_F in non-polar solvents. However the similar impact of the polarity on the energy of the resonant singlet and triplet levels can be expected. The analysis of variation of radiative and nonradiative decay pathways with solvent polarity supports this assumption (see Fig. 4.44b). Nonradiative decay rate decreases by almost 10 times with increasing solvent polarity, while the radiative decay rate increases by less than 2 times. This observation is in agreement with modulation of the intersystem crossing rate by solvent polarity.

Reduction of the rate of nonradiative recombination rate of such molecules comprising singly bonded two polar aromatic moieties can be also explained by solvent polarity impact on the intramolecular twisting [278–280]. However in such a case the twisting rate should be highly sensitive to the solvent viscosity. There is minor correlation of the nonradiative decay rate with the solvent viscosity. Compounds dissolved in a solid polystyrene matrix show the values of Φ_F slightly lower than those obtained for the solutions in nonpolar solvents. The fluorescence decay time parameters of the solid molecular dispersions are similar to those obtained for the liquid solutions in nonpolar solvents. Rigid matrix restricts possible intramolecular twisting of the singly bonded naphthalimide and fluorene moieties, thus the impact of twisting effect is minor.

Electrochemical properties

Electrochemical investigation of the solutions of compounds **17–22** in DCM were carried out in order to elucidate the reduction redox processes and thereby EA_{CV} . The CV profiles of compounds **17–22** are given in Fig. 4.45. The reduction potentials, and the values of IP_{CV} and EA_{CV} are collected in Table 4.21.

Table 4.21. Electrochemical characteristics of compounds **17–22**

Compound	E_{red} , (V)	E_{ox} , (V)	E_n , (V) ^a	E_g^{opt} , (eV)	EA_{CV} , (eV)	IP_{CV} , (eV)
17	-1.81	-1.61	-1.46	3.04	-3.34	6.38
18	-1.79	-1.70	-1.37	3.04	-3.43	6.47
19	-1.60	-1.48	-1.28	3.03	-3.52	6.55
20	-1.79	-1.61	-1.43	2.98	-3.37	6.35
21	-1.82	-1.71	-1.51	3.00	-3.29	6.29
22	-1.58	-1.47	-1.28	3.00	-3.52	6.52

^a First reduction potential onset vs Fc/Fc^+ .

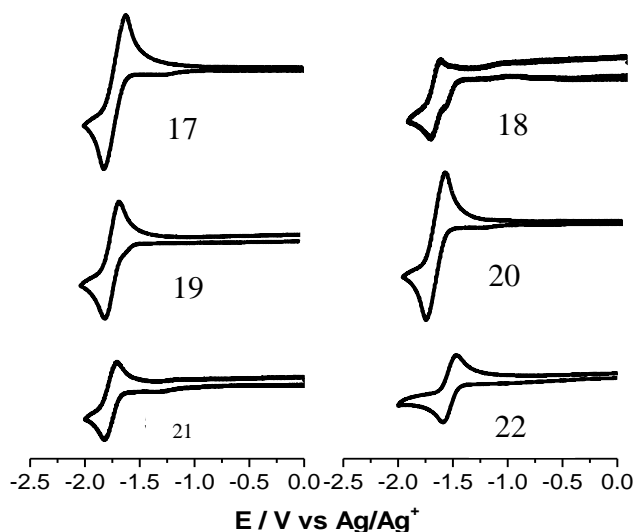


Figure 4.45. Cyclic voltammograms of compounds **17–22**

EA_{CV} were calculated by referencing with ferrocene/ferrocenium (Fc/Fc^+) redox couple according to the established relationship: EA_{CV} (eV) = $-4.8 - E_n$, where E_n is the first reduction potential onset *versus* Fc/Fc^+ . The values of IP_{CV} were calculated according to the relationship: $IP_{CV} = EA_{CV} - E_g^{opt}$, where E_g^{opt} is the optical band gap calculated from the solution absorption onset.

All the naphthalimide-substituted derivatives of fluorene exhibited reversible reduction processes corresponding to the reduction of naphthalimide moieties to radical anions (Fig. 4.45). This reduction behaviour clearly demonstrates the electron deficient nature of these derivatives. The reduction potentials range between -1.58 V and -1.81 V. No substantial influence of the number of naphthalimide moieties in the molecules on the reduction potentials were observed.

The values of EA_{CV} of compounds **17–22** range from -3.29 to -3.52 eV with respect to the vacuum level. These values are in agreement with those of naphthalimide-containing hydrazones [109]. The values of IP_{CV} of disubstituted fluorenes (**20–22**) are lower than those of monosubstituted compounds (**17–19**).

Charge-transporting properties

Xerographic time-of-flight measurements were used to characterize the charge-transporting properties of the selected compounds. Dispersive electron-transport was observed in the layers of compounds **17**, **18**, **21**, **22** coated on aluminium plated glass by solution processing technique. The representative dU/dt transients for the solid film of **21** are shown in Fig. 4.46.

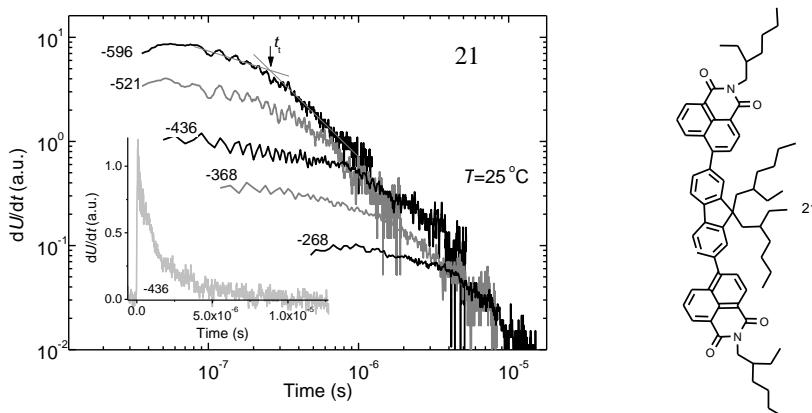


Figure 4.46. XTOF transients for the solid film of **21**. Arrow mark indicate transit time of electrons at the respective surface voltage

They clearly demonstrate dispersive electron-transport. The electron-transit times (t_t) needed for the estimation of electron mobilities were established from the intersection points of two asymptotes of the double-logarithmic plots.

The electric field dependencies of electron-drift mobilities of the layers of naphthalimide derivatives are shown in Fig. 4.47.

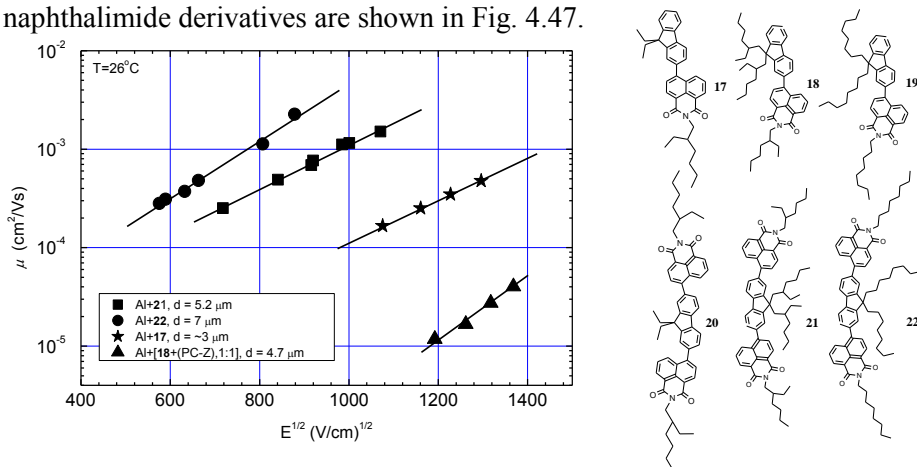


Figure 4.47. Electric field dependencies of electron-drift mobilities of the amorphous layers of **17**, **21**, **22** and of the molecular mixture of **18** with PC-Z (1:1)

Compound **18** did not form good amorphous film. Therefore the layer of its 1:1 molecular mixture with a PC-Z was prepared. For the amorphous films of compounds **17**, **21** and **22** and for the 1:1 blend of **18** with PC-Z, the linear dependencies of electron drift-mobility on the square root of the electric field were observed at room temperature.

The room temperature electron drift-mobility values in the amorphous layer of fluorene containing naphthalimides were $3.8 \times 10^{-5} \text{ cm}^2 \cdot \text{V}^{-1} \cdot \text{s}^{-1}$ for **17**, $4 \times 10^{-4} \text{ cm}^2 \cdot \text{V}^{-1} \cdot \text{s}^{-1}$ for **21** and $1.2 \times 10^{-3} \text{ cm}^2 \cdot \text{V}^{-1} \cdot \text{s}^{-1}$ for **22**, respectively, at an electric field of $6.4 \times 10^5 \text{ V} \cdot \text{cm}^{-1}$ in air. Since the concentration of chromophores was considerably lower in the 1:1 blend (**18**+PC-Z) compared to the amorphous films of neat compounds, the electron drift mobility observed was lower (in the order of $10^{-5} \text{ cm}^2 \cdot \text{V}^{-1} \cdot \text{s}^{-1}$ at $6.4 \times 10^5 \text{ V} \cdot \text{cm}^{-1}$). The highest electron mobilities were observed for compounds **22** and **21**. Compound **22** with longer linear alkyl chains both in the imide region and in C-9 position of fluorene moiety showed higher electron mobilities than compound **21** possessing branched and shorter alkyl chains. This observation can apparently be attributed to the influence π -stacking or intermolecular distance in the amorphous films of these compounds. Electron mobilities of the naphthalimide-substituted derivatives of fluorene are comparable and somewhat higher to that of electron transporting amorphous materials of organic semiconductors ($\mu_e = 10^{-5} - 10^{-4} \text{ cm}^2 \cdot \text{V}^{-1} \cdot \text{s}^{-1}$) [245,281].

In conclusion, we have synthesized a series of naphthalimide substituted derivatives of fluorene which exhibit high thermal stability with the 5% weight loss temperatures ranging from 304 to 457 °C. Most of the synthesized compounds can be attributed to molecular glasses with glass transition temperatures ranging from 30 to 76 °C. Dilute solutions of the fluorenyl substituted naphthalimide compounds in nonpolar solvents were found to emit in the blue region with high fluorescence quantum yield ranging from 0.47 to 0.69. Fluorenyl substituted naphthalimides exhibited pronounced positive solvatochromic behaviour in polar solvents indicating on charge-transfer character of the lowest excited states. The electron drift mobilities of the layer of 2,7-di(*N*-octyl-1,8-naphthalimide)-4-yl)-9,9-dioctyl-9H-fluorene reached $1.2 \times 10^{-3} \text{ cm}^2 \cdot \text{V}^{-1} \cdot \text{s}^{-1}$ at an electric field of $6.4 \times 10^5 \text{ V} \cdot \text{cm}^{-1}$.

5. THE MAIN RESULTS AND CONCLUSIONS

1. Hydrazones containing electron-accepting 1,8-naphthalimide species and electron-donating triphenylamino moieties were synthesized; the investigation of their thermal, optical, electrochemical and fluorescence properties revealed the following observations:
 - 1.1. The hydrazones exhibit high moderate stabilities with 5% weight loss temperatures in the range of 268–348 °C and can form glasses with glass transition temperatures in the range of 46–142 °C.
 - 1.2. Room temperature time-of-flight hole mobilities in the solid solutions of the alkylated derivatives in bisphenol-Z polycarbonate (50%) exceeded 10^{-5} cm²/V·s at high applied electric fields.
 - 1.3. The ionization potentials of the hydrazones, measured by electron photoemission technique were 5.45 eV. The presence of electron accepting 1,8-naphthalimide species has minor effect on the ionization potentials of the compounds.
2. A series of derivatives of 1,8-naphthalimide and triphenylamine in which the chromophores are linked via the single bonds were synthesized by Suzuki condensation reactions and their properties were studied. It was established that:
 - 2.1. They exhibit very high thermal stabilities with 5% weight loss temperatures ranging from 429 °C to 483 °C and are capable to form molecular glasses with glass transition temperatures ranging from 45 °C to 84 °C. Increase of the number of 1,8-naphthalimide moieties leads to the increase of the thermal stability as well as glass transition temperatures of the derivatives.
 - 2.2. The dilute solutions of the compounds in nonpolar solvents and in rigid polystyrene solutions show fluorescence quantum yields from 0.58 to 0.78, while emission yields of the solid films are in the range of 0.10–0.23.
 - 2.3. The ionization potentials of the solid samples of the compounds established by electron photoemission spectrometry in air ranged from 5.57 to 6.01 eV. 4,4'-(Di(*N*-(2-ethylhexyl)-1,8-naphthalimide-4-yl)phenyl)benzenamine and 4,4',4''-(tris(*N*-(2-ethylhexyl)-1,8-naphthalimide-4-yl)phenyl)benzenamine with two and three 1,8-naphthalimide moieties, respectively, demonstrated a little higher ionization potential values with respect to those of 4-(4'-diphenylaminophenyl)-*N*-ethylhexyl-1,8-naphthalimide and 4-(4'-(di-(4''-methoxyphenyl)amino)phenyl)-*N*-(2-ethylhexyl)-1,8-naphthalimide with one 1,8-naphthalimide moiety.
 - 2.4. 4-(4'-(Di-(4''-methoxyphenyl)amino)phenyl)-*N*-(2-ethylhexyl)-1,8-naphthalimide containing methoxy groups was found to show ambipolar charge transport in air with the mobilities of charges exceeding 10^{-4} cm²·V⁻¹·s⁻¹ at high electric fields.
3. A series of derivatives of 1,8-naphthalimide and triphenylamine in which the chromophores are linked via the ethenyl-containing linkages were synthesized by palladium-catalyzed Heck reactions and their properties were studied in terms of correlation with their chemical structures. It was established that:

- 3.1. The compounds showed high thermal stability with 5% weight loss temperatures ranging from 431 °C to 448 °C and the ability to form glasses with glass-transition temperatures being in the range of 55–107 °C. The thermal stability as well as glass transition temperatures of the donor-acceptor derivatives increases with increase of the number of 1,8-naphthalimide arms.
- 3.2. Fluorescence quantum yields of dilute solutions of the synthesized materials range from 0.45 to 0.64 while those of the solid samples are in the range of 0.09–0.18.
- 3.3. Electron photoemission spectra of the amorphous films of the materials revealed ionization potentials similar to those of the derivatives of triphenylamine (5.75–5.80 eV) with no evidence of dependence of ionization potentials on the number of 1,8-naphthalimide arms. DFT calculations show that HOMO and LUMO orbitals are almost entirely localized on the donor and acceptor moieties, respectively. The frontier orbital energies for the three synthesized compounds are similar and practically do not depend on the number of 1,8-naphthalimide moieties.
- 3.4. Hole mobilities in the layers of the compounds having one and two 1,8-naphthalimide moieties well exceed $10^{-3} \text{ cm}^2 \cdot \text{V}^{-1} \cdot \text{s}^{-1}$ at high electric fields at room temperature.
4. A series of derivatives of 1,8-naphthalimide and triphenylamine in which the chromophores are linked via the ethynyl-containing bridges were synthesized by palladium/copper-catalyzed Sonogashira cross-coupling reactions; investigation of their properties revealed the following observations:
 - 4.1. The synthesized compounds showed high thermal stability with 5% weight loss temperatures ranging from 396 to 462 °C and formed molecular glasses with glass transition temperatures ranging from 73 °C to 96 °C. The thermal stability as well as glass transition temperatures of the donor-acceptor derivatives increases with increase of the number of 1,8-naphthalimide arms.
 - 4.2. Dilute solutions of the compounds in nonpolar solvents showed fluorescence quantum yields from 0.063 to 0.94, while fluorescence quantum yields of the solid films were in the range of 0.011–0.25.
 - 4.3. The synthesized compounds revealed the delayed fluorescence. The fluorescence quantum yields of these compounds increased from 0.041–0.51 to 0.054–0.96 upon deoxygenation.
 - 4.4. Cyclic voltammetry measurements revealed close values of the solid state ionization potentials ranging from 5.48 to 5.61 eV and electron affinities ranging from –3.29 to –3.16 with no evidence of dependence of ionization potentials on the number of 1,8-naphthalimide arms.
5. Naphthalimide-substituted derivatives of fluorene were synthesized by Suzuki cross-coupling reaction and their properties were studied. It was established that:
 - 5.1. The compounds exhibit high thermal stability with 5% weight loss temperatures ranging from 304 to 457 °C, most of them form molecular glasses with glass transition temperatures ranging from 30 to 76 °C. The

thermal stability of disubstituted fluorene derivatives was found to be higher in comparison to that of monosubstituted compounds.

- 5.2. Dilute solutions of the compounds in nonpolar solvents were found to emit in the blue region with high quantum yields ranging from 0.47 to 0.69, while in the solid state fluorescence quantum yields were found to be in the range of 0.06–0.25. A higher value of quantum yields was obtained for the disubstituted compounds compared to the monosubstituted compounds.
- 5.3. Time-of-flight electron drift mobilities of the layer of 2,7-di(*N*-octyl-1,8-naphthalimide)-4-yl)-9,9-dioctyl-9*H*-fluorene with longer linear alkyl chains both in the imide region and in C-9 position of fluorene moiety in air at 25 °C approached $1.2 \times 10^{-3} \text{ cm}^2 \cdot \text{V}^{-1} \cdot \text{s}^{-1}$ at an electric field of $6.4 \times 10^5 \text{ V} \cdot \text{cm}^{-1}$.

REFERENCES

1. Liu, C. L., *et al.* New dibenzothiophene-containing donor-acceptor polyimides for high performance memory device applications. *Journal of Physical Chemistry C*, 2011, vol. 115, p. 5930–5939.
2. Kucheryavy, P., *et al.* Electronic properties of 4-substituted naphthalimides. *Journal of Physical Chemistry A*, 2009, vol. 113, p. 6453–6461.
3. Dhar, S., *et al.* Tunable solvatochromic response of newly synthesized antioxidative naphthalimide derivatives: Intramolecular charge transfer associated with hydrogen bonding effect. *Journal of Physical Chemistry A*, 2011, vol. 115, p. 2216–2224.
4. Jin, R. F.; Tang, S. S.; Sun, W. D. Rational design of donor- π -acceptor n-butyl-1,8-naphthalimide cored branched molecules as charge transport and luminescent. *Tetrahedron*, 2014, vol. 70, p. 47–53.
5. Alexiou, M. S., *et al.* The UV-visible absorption and fluorescence of some substituted 1,8-naphthalimides and naphthalic anhydrides. *Journal of the Chemical Society, Perkin Transactions 2*, 1990, p. 837–842.
6. Srikun, D., *et al.* An ICT-based approach to ratiometric fluorescence imaging of hydrogen peroxide produced in living cells. *Journal of American Chemical Society*, 2008, vol. 130, p. 4596–4597.
7. Alexiou, M. The synthesis of novel naphthyl-1,8-imides and naphthyl-1,8-anhydride and a study of their fluorescent properties. *PhD thesis*, Brunel University, U.K. 1983, p. 214–220, 223–230.
8. Shirota, Y.; Kageyama, H. Charge carrier transporting molecular materials and their applications in devices. *Chemical Reviews*, 2007, vol. 107, p. 953–1010.
9. Ding, G. H.; Xu, Z. W.; Zhong, G. Y. Synthesis, photophysical and electroluminescent properties of novel naphthalimide derivatives containing an electron transporting unit. *Research on Chemical Intermediates*, 2008, vol. 34, p. 299–308.
10. Liu, J., *et al.* Blue electroluminescent polymers with dopant-host systems and molecular dispersion features: polyfluorene as the deep blue host and 1,8-naphthalimide derivative units as the light blue dopants. *Journal of Materials Chemistry*, 2008, vol. 18, p. 1659–1666.
11. Aveline, B.; Matsugo, S.; Redmond, R. W. Photochemical mechanisms responsible for the versatile application of naphthalimides and naphthalidimides in biological systems. *Journal of American Chemical Society*, 1997, vol. 119, p. 11785–11795.
12. Takada, T., *et al.* Effects of interaction of photosensitizer with DNA and stacked G bases on photosensitized one-electron oxidation of DNA. *Journal of Physical Chemistry B*, 2004, vol. 108, p. 761–766.
13. Cacialli, F., *et al.* Naphthalimide side-chain polymers for organic light-emitting diodes: band-offset engineering and role of polymer thickness. *Journal of Applied Physics*, 1998, vol. 83, p. 2343–2356.
14. Zhu, W. H., *et al.* Novel luminescent carbazole-naphthalimide dyads for single-layer electroluminescent device. *Synthetic Metals*, 2001, vol. 119, p. 547–548.
15. Tian, H., *et al.* Electroluminescent property and charge separation state of bis-naphthalimides. *Optical Materials*, 2000, vol. 14, p. 91–94.

-
16. Yang, J. X., *et al.* The synthesis and spectral properties of novel 4-phenylacetylene-1,8-naphthalimide derivatives. *Dyes and Pigments*, 2005, vol. 66, p. 83–87.
 17. Sarma, R. J., *et al.* Role of π -interactions in solid state structures of a few 1,8-naphthalimide derivatives. *Journal of Molecular Structure*, 2007, vol. 829, p. 29–36.
 18. Gharanjig, K., *et al.* Synthesis, spectral properties and application of novel monoazo disperse dyes derived from *N*-ester-1,8-naphthalimide to polyester. *Dyes and Pigments*, 2008, vol. 76, p. 684–689.
 19. Sali, S., *et al.* Atomic spectroscopy selective sensors for Zn^{2+} cations based on new green fluorescent poly(amidoamine) dendrimers peripherally modified with 1,8-naphthalimides. *Spectrochimica Acta Part B*, 2006, vol. 65, p. 591–597.
 20. Patrick, L. G. F.; Whiting, A. Synthesis and application of some polycondensable fluorescent dyes. *Dyes and Pigments*, 2002, vol. 52, p. 137–143.
 21. Martin, E.; Weigand, R.; Pardo, A. Solvent dependence of the inhibition of intramolecular charge-transfer in *N*-substituted 1,8-naphthalimide derivatives as dye lasers. *Journal of Luminescence*, 1996, vol. 68, p. 157–164.
 22. Tao, Z. F.; Qian, X. Naphthalimide hydroperoxides as photonucleases: substituent effects and structural basis. *Dyes and Pigments*, 1999, vol. 43, p. 139–145.
 23. Stewart, W. Synthesis of 3,6-disulfonated 4-aminonaphthalimides. *Journal of American Chemical Society*, 1981, vol. 103, p. 7615–7620.
 24. Bouche, C. M., *et al.* Side-chain electroluminescent polymers. *Synthetic Metals*, 1996, vol. 81, p. 191–195.
 25. Tian, H., *et al.* Positive and negative fluorescent imaging induced by naphthalimide polymers. *Journal of Materials Chemistry*, 2002, vol. 12, p. 1262–1276.
 26. Gunnlaugsson, T., *et al.* Towards the development of controllable and reversible ‘on-off’ luminescence switching in soft-matter; synthesis and spectroscopic investigation of 1,8-naphthalimide-based PET (photoinduced electron transfer) chemosensors for pH in water-permeable hydrogels. *ARKIVOC*, 2003, vol. 7, p. 216–228.
 27. Zhu, W., *et al.* A novel family of twisted molecular luminescent materials containing carbazole unit for single-layer organic electroluminescent devices. *Journal of Photochemistry and Photobiology A: Chemistry*, 2003, vol. 154, p. 169–177.
 28. Grabchev, I., *et al.* New unsaturated 1,8-naphthalimide dyes for use in nematic liquid crystals. *Naturforsch*, 1996, vol. 51a, p. 1185–1191.
 29. Veale, E. B., *et al.* 4-Amino-1,8-naphthalimide-based Tröger’s bases as high affinity DNA targeting fluorescent supramolecular scaffolds. *Organic Letters*, 2009, vol. 11, p. 4040–4043.
 30. Cosnard, F.; Wintgens, V. A new fluoroionophore derived from 4-amino-*N*-methyl-1,8-naphthalimide. *Tetrahedron Letters*, 1998, vol. 39, p. 2751–2754.
 31. Grabchev, I.; Dumas, S.; Chovelon, J. M. Studying the photophysical properties of a polymerizable 1,8-naphthalimide dye and its copolymer with styrene as potential fluorescent sensors for metal cations. *Polymers for Advanced Technologies*, 2008, vol. 19, p. 316–321.
 32. Alcalá, M. A., *et al.* Luminescence targeting and imaging using a nanoscale generation 3 dendrimer in an in vivo colorectal. *Journal of Nanomedicine: Nanotechnology, Biology and Medicine*, 2011, vol. 7, p. 249–258.

-
33. Grabchev, I., *et al.* A new colorimetric and fluorimetric sensor for metal cations based on poly(propylene amine) dendrimer modified with 1,8-naphthalimide. *Journal of Photochemistry and Photobiology A: Chemistry*, 2009, vol. 201, p. 75–80.
 34. Grabchev, I.; Dumas, S.; Chovelon, J. M. A polyamidoamine dendrimer as a selective colorimetric and ratiometric fluorescent sensor for Li⁺ cations in alkali media. *Dyes and Pigments*, 2009, vol. 82, p. 336–340.
 35. Grabchev, I.; Staneva, D.; Chovelon, J. M. Photophysical investigations on the sensor potential of novel, poly(propylenamine) dendrimers modified with 1,8-naphthalimide units. *Dyes and Pigments*, 2010, vol. 85, p. 189–193.
 36. Georgiev, N. I.; Bojinov, V. B.; Marinova, N. Novel PAMAM light-harvesting antennae based on 1,8-naphthalimide: Synthesis, energy transfer, photophysical and pH sensing properties. *Sensors and Actuators B: Chemical*, 2010, vol. 150, p. 655–666.
 37. Georgiev, N. I.; Bojinov, V. B.; Nikolov, P. S. Design and synthesis of a novel pH sensitive core and peripherally 1,8-naphthalimide-labeled PAMAM dendron as light harvesting antenna. *Dyes and Pigments*, 2009, vol. 81, p. 18–26.
 38. McKenna, M. D.; Grabchev, I.; Bosch, P. The synthesis of a novel 1,8-naphthalimide based PAMAM-type dendron and its potential for light-harvesting. *Dyes and Pigments*, 2009, vol. 81, p. 180–186.
 39. Tang, J. G., *et al.* Ln³⁺-enhanced blue fluorescence from novel excimer of 1,8-naphthalimide-conjugated PAMAM. *Optical Materials*, 2010, vol. 32, p. 1417–1422.
 40. Rogers, J. E.; Kelly, L. A. Nucleic acid oxidation mediated by naphthalene and benzophenone imide and diimide derivatives: Consequences for DNA redox chemistry. *Journal of American Chemical Society*, 1999, vol. 121, p. 3854–3861.
 41. Islam, A., *et al.* Aminonaphthalic anhydrides as red-emitting materials: electroluminescence, crystal structure, and photophysical properties. *Journal of Physical Chemistry B*, 2005, vol. 109, p. 5509–5517.
 42. Yang, J. X., *et al.* Studies on the synthesis and spectral properties of novel 4-benzofuranyl-1,8-naphthalimide derivatives. *Dyes and Pigments*, 2005, vol. 67, p. 27–33.
 43. Magalhaes, J. L., *et al.* Solvent effect on the photophysical properties of 4-phenoxy-*N*-methyl-1,8-naphthalimide. *Journal of Photochemistry and Photobiology A: Chemistry*, 2006, vol. 183, p. 165–170.
 44. Cao, Z.; Nandhikonda, P.; Heagy, M. D. Highly water-soluble monoboronic acid probes that show optical sensitivity to glucose based on 4-sulfo-1,8-naphthalic anhydride. *Journal of Organic Chemistry*, 2009, vol. 74, p. 3544–3546.
 45. Barros, T. C., *et al.* Photophysical characterization of a 1,4,5,8-naphthalenediimide derivative. *Journal of Photochemistry and Photobiology A: Chemistry*, 1997, vol. 111, p. 97–104.
 46. Jiang, W., *et al.* Synthesis and photochemical properties of novel 4-diarylamine-1,8-naphthalimide derivatives. *Dyes and Pigments*, 2008, vol. 77, p. 125–128.
 47. Jung, S. O., *et al.* A new orange-light-emitting materials based on (naphthyl)-1,8-naphthalimide for OLED applications. *Molecular Crystals and Liquid Crystals*, 2009, vol. 514, p. 45–54.
 48. Wang, L., *et al.* “Push–pull” 1,8-naphthalic anhydride with multiple triphenylamine

-
- groups as electron donor. *Journal of Molecular Structure*, 2014, vol. 1056-1057, p. 339–346.
49. Ferreira, R., *et al.* Photophysical study of bis(naphthalimide)–amine conjugates: Toward molecular design of excimer emission switching. *Journal of Physical Chemistry A*, 2011, vol. 115, p. 1092–1099.
 50. Hanit, M., *et al.* Toward the development of the direct and selective detection of nitrates by a bioinspired Mo–Cu system. *Organic Letters*, 2011, vol. 13, p. 5532–5535.
 51. Yawei, L., *et al.* Synthesis and properties of starburst amorphous molecules: 1,3,5-tris(1,8-naphthalimide-4-yl)benzenes. *Synthetic Metals*, 2010, vol. 160, p. 2055–2060.
 52. Xiaomei, H., *et al.* Novel dyes based on naphthalimide moiety as electron acceptor for efficient dye-sensitized solar cells. *Dyes and Pigments*, 2011, vol. 90, p. 297–303.
 53. Weihong, Z., *et al.* A novel family of twisted molecular luminescent materials containing carbazole unit for single-layer organic electroluminescent devices. *Journal of Photochemistry and Photobiology A: Chemistry*, 2003, vol. 154, p. 169–177.
 54. Koyuncu, F. B., Koyuncu, S.; Ozdemira, E. A new donor–acceptor carbazole derivative: Electrochemical polymerization and photo-induced charge transfer properties. *Synthetic Metals*, 2011, vol. 161, p. 1005–1013.
 55. Jiang, W., *et al.* The synthesis, crystal structure and photophysical properties of three novel naphthalimide dyes. *Dyes and Pigments*, 2009, vol. 80, p. 11–16.
 56. Bardajee, G. R., *et al.* The synthesis and spectroscopic properties of novel, functional fluorescent naphthalimide dyes. *Dyes and Pigments*, 2008, vol. 79, p. 24–32.
 57. Koyuncu, F. B.; Koyuncu, S.; Ozdemir, E. A novel donor–acceptor polymeric electrochromic material containing carbazole and 1,8-naphthalimide as subunit. *Electrochimica Acta*, 2010, vol. 55, p. 4935–4941.
 58. Wang, Y., *et al.* The synthesis and photoluminescence characteristics of novel blue light-emitting naphthalimide derivatives. *Dyes and Pigments*, 2010, vol. 86, p. 190–196.
 59. Zheng, M., *et al.* Structure-property relationships in light-emitting polymers: optical, electrochemical, and thermal studies. *Macromolecules*, 2000, vol. 33, p. 7426–7430.
 60. Ulla, H., *et al.* Blue organic light emitting materials: Synthesis and characterization of novel 1,8-naphthalimide derivatives. *Optical Materials*, 2014, vol. 36, p. 704–711.
 61. Marinova, N. V.; Georgiev, N. I.; Bojinov, V. B. Facile synthesis, sensor activity and logic behaviour of 4-aryloxy substituted 1,8-naphthalimide. *Journal of Photochemistry and Photobiology A: Chemistry*, 2013, vol. 254, p. 54–61.
 62. Bag, S. S., *et al.* Highly solvatochromic fluorescent naphthalimides: Design, synthesis, photophysical properties and fluorescence switch-on sensing of ct-DNA. *Bioorganic & Medicinal Chemistry Letters*, 2013, vol. 23, p. 96–101.
 63. Segura, J. L.; Herrera, H.; Bäuerle, P. Oligothiophene-functionalized naphthalimides and perylene imides: design, synthesis and applications. *Journal of Materials Chemistry*, 2012, vol. 22, p. 8717–8733.
 64. Frisch, M. J., *et al.* Gaussian 03, revision C.02; Gaussian, Inc.: Wallingford, CT, 2004.
 65. McAdam, C. J., *et al.* Ferrocenyl-naphthalimide donor-acceptor dyads with aromatic spacer groups. *Organometallics*, 2010, vol. 29, p. 2474–2483.
 66. Jones, R. N. The ultraviolet absorption spectra of anthracene derivatives. *Chemical*

Reviews, 1947, vol. 41, p. 353–371.

67. McAdam, C. J., *et al.* Tunable donor–acceptor interactions in 4-ene/yne-ferrocenyl and 4-enamine naphthalimides with ferrocenyl headgroups. *Organometallics*, 2003, vol. 22, p. 5126–5136.
68. Lee, S., *et al.* Dependence of the two-photon absorption cross section on the conjugation of the phenylacetylene linker in dipolar donor-bridge-acceptor chromophores. *Journal of Physical Chemistry A*, 2005, vol. 109, p. 9767–9774.
69. Jin, R. Theoretical study on optical and electronic properties of bis-dipolar 1,8-naphthalimide derivatives. *Molecular Physics*, 2013, vol. 111, p. 3793–3800.
70. Xiao, H., *et al.* A novel fluorescent molecule based on 1,8-naphthalimide: synthesis, spectral properties, and application in cell imaging. *Research on Chemical Intermediates*, 2010, vol. 36, p. 1021–1026.
71. Gudeika, D., *et al.* Structure properties relationship of donor–acceptor derivatives of triphenylamine and 1,8-naphthalimide. *Journal of Physical Chemistry C*, 2012, vol. 116, p. 14811–14819.
72. Ren, W., *et al.* Enhancing the coplanarity of the donor moiety in a donor-acceptor molecule to improve the efficiency of switching phenomenon for flash memory devices. *Dyes and Pigments*, 2014, vol. 100, p. 127–134.
73. Mikroyannidis, J. A.; Yeb, S.; Liu, Y. Electroluminescent divinylene- and trivinylene-molecules with terminal naphthalimide or phthalimide segments. *Synthetic Metals*, 2009, vol. 159 p. 492–500.
74. Santos, L. F., *et al.* Optical, electrochemical and electrogravimetric behavior of poly(1-methoxy-4-(2-ethyl-hexyloxy)-p-phenylene vinylene) (MEH-PPV) films. *Electrochimica Acta*, 2007, vol. 52, p. 4299–4304.
75. Wang, Y., *et al.* An efficient guest/host fluorescent energy transfer pair based on the naphthalimide skeleton, and its application in heavily-doped red organic light-emitting diodes. *Dyes and Pigments*, 2014, vol. 100, p. 87–96.
76. Jiang, W., *et al.* An experimental and computational study of intramolecular charge transfer: Diarylamino derivatives of 7H-benzimidazo(2,1-a)benz(d,e)isoquinolin-7-ones. *Dyes and Pigments*, 2009, vol. 80, p. 279–286.
77. Ren, W., *et al.* Enhancing the coplanarity of the donor moiety in a donor-acceptor molecule to improve the efficiency of switching phenomenon for flash memory devices. *Dyes and Pigments*, 2014, vol. 100, p. 127–134.
78. Ye, G. J., *et al.* The synthesis and NLO properties of 1,8-naphthalimide derivatives for both femtosecond and nanosecond laser pulses. *Dyes and Pigments*, 2012, vol. 94, p. 271–277.
79. Gan, J. A., *et al.* 1,8-Naphthalimides for non-doping OLEDs: the tunable emission color from blue, green to red. *Journal of Photochemistry and Photobiology A: Chemistry*, 2004, vol. 162, p. 399–406.
80. Fengrui, L., *et al.* Synthesis of 4-aziridino[C₆₀]fullerene-1,8-naphthalimide(C₆₀-NI dyads) and their photophysical properties. *Tetrahedron*, 2010, vol. 66, p. 5467–5471.
81. Lu, B., *et al.* Synthesis, electrochemistry, and photophysical properties of pyrazolino[60]fullerene-1,8-naphthalimide fluorescent derivatives. *Tetrahedron*, 2012, vol. 68, p. 8924–8930.

-
82. Perez, L., *et al.* Comparison between the photophysical properties of pyrazolo- and isoxazolo[60]fullerenes with dual donors (ferrocene, aniline and alkoxyphenyl). *Journal of Organic Chemistry*, 2007, p. 2175–2185.
 83. Ivaylo, P., *et al.* Synthesis, structural analysis and application of a series of solid-state fluorochromesdaryl hydrazones of 4-hydrazino-*N*-hexyl-1,8-naphthalimide. *Tetrahedron*, 2013, vol. 69, p. 712–721.
 84. Ruifa, J.; Tang, S. Theoretical investigation into optical and electronic properties of 1,8-naphthalimide derivatives. *Journal of Molecular Modeling*, 2013, vol. 19, p. 1685–1693.
 85. Lin, B. C., *et al.* Charge transport properties of tris(8-hydroxyquinolino)aluminum(III): Why it is an electron transporter. *Journal of American Chemical Society*, 2005, vol. 127, p. 66–67.
 86. Gruhn, N. E., *et al.* The vibrational reorganization energy in pentacene: Molecular influences on charge transport. *Journal of American Chemical Society*, 2002, vol. 124, p. 7918–7919.
 87. Sun, F.; Jin, R. Optical and charge transport properties of *N*-butyl-1,8-naphthalimide derivatives as organic light-emitting materials: A theoretical study. *Journal of Luminescence*, 2014, vol. 149, p. 125–132.
 88. Zhengneng, J., *et al.* Synthesis and fluorescence property of some novel 1,8-naphthalimide derivatives containing a thiophene ring at the C-4 position. *Dyes and Pigments*, 2013, vol. 96, p. 204–210.
 89. Cao, Z., *et al.* *N*-Aryl arenedicarboximides as tunable panchromatic dyes for molecular solar cells. *International Journal of Photoenergy*, 2010, vol. 2010, p. 1–7.
 90. Xiao, H., *et al.* Synthesis and optoelectronic properties of a series of novel spirobifluorene derivatives starting from the readily available reagent 4,4'-bisalkylated biphenyl. *Organic Electronics*, 2012, vol. 13, p. 1553–1564.
 91. Poriel, C., *et al.* Dispirofluorene-indenofluorene derivatives as new building blocks for blue organic electroluminescent devices and electroactive polymers. *Chemistry - A European Journal*, 2007, vol. 13, p. 10055–10069.
 92. Zhengneng, J., *et al.* Novel fluorescent 1,8-naphthalimide derivatives containing thiophene and pyrazole moieties: Synthesis by direct C–H arylation and evaluation of photophysical and electrochemical properties. *Spectrochimica Acta Part A: Molecular and Biomolecular Spectroscopy*, 2014, vol. 117, p. 527–534.
 93. Wanga, H. Y., *et al.* Synthesis, spectroscopic characteristic of novel fluorescent dyes of pyrazoline Compounds. *Spectrochimica Acta Part A*, 2012, vol. 93, p. 343–347.
 94. Chen, G., *et al.* The synthesis and characterisation of novel pyrazoline derivatives containing triphenylamine. *Dyes and Pigments*, 2010, vol. 85, p. 194–200.
 95. Zhou, X., *et al.* One- and two-photon absorption properties of a series of derived pyrazolines. *Optical Materials*, 2004, vol. 27, p. 315–321.
 96. Zhang, X. H., *et al.* Photoluminescence and electroluminescence of pyrazoline monomers and dimers. *Chemical Physics Letters*, 2000, vol. 320, p. 77–80.
 97. Marinova, N. V.; Georgiev, N. I.; Bojinov, V. B. Design, synthesis and pH sensing properties of novel 1,8-naphthalimide-based bichromophoric system. *Journal of Photochemistry and Photobiology A: Chemistry*, 2011, vol. 222, p. 132–140.

-
98. Bojinov, V.; Georgiev, N.; Nikolov, P. Synthesis and photophysical properties of fluorescence sensing ester- and amidoamine-functionalized 1,8-naphthalimides. *Journal of Photochemistry and Photobiology A: Chemistry*, 2008, vol. 193, p. 129–138.
 99. Li, Z., *et al.* N-Heteroaryl-1,8-naphthalimide fluorescent sensor for water: Molecular design, synthesis and properties. *Dyes and Pigments*, 2011, vol. 88, p. 307–314.
 100. Saha, S.; Samanta, A. Influence of the structure of the amino group and polarity of the medium on the photophysical behavior of 4-amino-1,8-naphthalimide derivatives. *Journal of Physical Chemistry A*, 2002, vol. 106, p. 4763–4771.
 101. Panchenko, P. A., *et al.* Comparative analysis of the PET and ICT sensor properties of 1,8-naphthalimides containing aza-15-crown-5 ether moiety. *Dyes and Pigments*, 2013, vol. 98, p. 347–357.
 102. Formica, M., *et al.* New fluorescent chemosensors for metal ions in solution. *Coordination Chemistry Reviews*, 2012, vol. 256, p. 170–172.
 103. Bardajee, G. R., *et al.* Microwave-assisted solvent-free synthesis of fluorescent naphthalimide dyes. *Dyes and Pigments*, 2013, vol. 99, p. 52–58.
 104. Becke, A. D. A new mixing of Hartree-Fock and local density-functional theories. *Journal of Chemical Physics*, 1993, vol. 98, p. 1372–1377.
 105. Perdew, J. P.; Burke, K.; Ernzerhof, M. Generalized gradient approximation made simple. *Physical Review Letters*, 1997, vol. 78, p. 1396–1396.
 106. Miao, L., *et al.* A TDDFT and PCM-TDDFT studies on absorption spectra of N-substituted 1,8-naphthalimides dyes. *Journal of Molecular Structure: THEOCHEM*, 2008, vol. 865, p. 79–87.
 107. Khosravi, A., *et al.* Synthesis and spectroscopic studies of some naphthalimide based disperse azo dyestuffs for the dyeing of polyester fibres. *Dyes and Pigments*, 2006, vol. 69, p. 79–92.
 108. Ruifa, J.; Shanshan, T. Theoretical study on optical and electronic properties of bipolar molecules with 1,8-naphthalimide and triphenylamine moieties as organic light-emitting materials. *Journal of Molecular Graphics and Modelling*, 2013, vol. 42, p. 120–128.
 109. Gudeika, D., *et al.* Hydrazones containing electron-accepting and electron-donating moieties. *Dyes and Pigments*, 2011, vol. 91, p. 13–19.
 110. Lee, J. F.; Hsu, S. L. C. Efficient white polymer-light-emitting-diodes based on polyfluorene end-capped with yellowish-green fluorescent dye and blended with a red phosphorescent iridium complex. *Polymer*, 2009, vol. 50, p. 2558–2564.
 111. Tu, G., *et al.* White electroluminescence from polyfluorene chemically doped with 1,8-naphthalimide moieties. *Applied Physics Letters*, 2004, vol. 85, p. 2172–2174.
 112. Chang, Y. T., *et al.* Soluble phenanthrenyl-imidazole- presenting regioregular poly(3-octylthiophene) copolymers having tunable bandgaps for solar cell applications. *Advanced Functional Materials*, 2007, vol. 17, p. 3326–3331.
 113. Simas, E. R., *et al.* Intrachain energy migration to weak charge-transfer state in polyfluorene end-capped with naphthalimide derivative. *Journal of Physical Chemistry A*, 2010, vol. 114, p. 12384–12390.
 114. Lee, J. F.; Hsu, S. L. C. Green polymer-light-emitting-diodes based on polyfluorenes

-
- containing N-aryl-1,8-naphthalimide and 1,8-naphthoilene-arylimidazole derivatives as color tuner. *Polymer*, 2009, vol. 50, p. 5668–5674.
115. Tu, G., *et al.* Highly efficient pure-white-light-emitting diodes from a single polymer: polyfluorene with naphthalimide moieties. *Advanced Functional Materials*, 2006, vol. 16, p. 101–106.
 116. Coya, C., *et al.* Synthesis and tunable emission of novel polyfluorene co-polymers with 1,8-naphthalimide pendant groups and application in a single layer–single component white emitting device. *European Polymer Journal*, 2010, vol. 46, p. 1778–1789.
 117. Chongyu, M., *et al.* Green electroluminescent polyfluorenes containing 1,8-naphthalimide moieties as color tuner. *Polymer*, 2006, vol. 47, p. 4976–4984.
 118. Liu, J., *et al.* The first single polymer with simultaneous blue, green, and red emission for white electroluminescence. *Advanced Materials*, 2005, vol. 17, p. 2974–2978.
 119. Liu, J., *et al.* White electroluminescence from a single polymer system: Improved performance by means of enhanced efficiency and red-shifted luminescence of the blue-light-emitting species. *Advanced Materials*, 2007, vol. 19, p. 1859–1863.
 120. Lee, J. F., *et al.* A new intramolecular donor–acceptor polyfluorene copolymer for bulk heterojunction solar cells. *Solar Energy Materials & Solar Cells*, 2010, vol. 94, p. 1166–1172.
 121. Yamamoto, T. D., *et al.* Extensive studies on p-stacking of poly(3-alkylthiophene-2,5-diyl)s and poly(4-alkylthiazole-2,5-diyl)s by optical spectroscopy, NMR analysis, lights scattering analysis, and X-ray crystallography. *Journal of American Chemical Society*, 1998, vol. 120, p. 2047–2058.
 122. Huo, L., *et al.* Alternating copolymers of electron-rich arylamine and electron-deficient 2,1,3-benzothiadiazole: synthesis, characterization and photovoltaic properties. *Journal of Polymer Science Part A: Polymer Chemistry*, 2007, vol. 45, p. 3861–3871.
 123. de Mello, J. C.; Wittmann, H. F.; Friend, R. H. An improved experimental determination of external photoluminescence quantum efficiency. *Advanced Materials*, 1997, vol. 9, p. 230–232.
 124. Kirkus, M., *et al.* New indole-carbazole hybrids as glass-forming high-triplet-energy materials. *Synthetic Metals*, 2009, vol. 159, p. 729–734.
 125. Miyamoto, E.; Yamaguchi, Y.; Yokoyama, M. Ionization potential of organic pigment film by atmospheric photoelectron emission analysis. *Denshishashin Gakkai-shi (Electrography)*, 1989, vol. 28, p. 364–370.
 126. Montrimas, E.; Gaidelis, V.; Pazera, A. The discharge kinetics of negatively charged Se electrophotographic layers. *Lithuanian Journal of Physics*, 1966, vol. 6, p. 569–578.
 127. Vaezi-Nejad, S. M. Xerographic time of flight experiment for the determination of drift mobility in high resistivity semiconductors. *International Journal of Electronics*, 1987, vol. 62, p. 361–384.
 128. Grigalevicius, S., *et al.* Hole-transporting molecular glasses based on carbazole and diphenylamine moieties. *Materials Chemistry and Physics*, 2001, vol. 72, p. 395–400.
 129. Juska G., *et al.* Extraction of photogenerated charge carriers by linearly increasing voltage in the case of Langevin recombination. *Physical Review B*, 2011, vol. 84, p. 155202–155206.

-
130. Juška, G., *et al.* Extraction current transients: New method of study of charge transport in microcrystalline silicon. *Physical Review Letters*, 2000, vol. 84, p. 4946–4949.
 131. Yue, W., *et al.* Poly(oligothiophene-alt-benzothiadiazole)s: tuning the structures of oligothiophene units toward high-mobility “Black” conjugated polymers. *Macromolecules*, 2009, vol. 42, 6510–6518.
 132. Kohn, W.; Sham, L. Self-consistent equations including exchange and correlation effects. *Journal of Physical Review*, 1965, vol. 140, p. A1133–A1138.
 133. Lee, C. T; Yang, W. T.; Parr, R. G. Development of the Colle-Salvetti correlation-energy formula into a functional of the electron density. *Physical Review B*, 1988, vol. 37, p. 785–789.
 134. Becke, A. D. Density-functional thermochemistry. III. The role of exact exchange. *Journal of Chemical Physics*, 1993, vol. 98, p. 5648–5652.
 135. Gross, E. K. U.; Kohn, W. Local density-functional theory of frequency-dependent linear response. *Physical Review Letters*, 1985, vol. 55, p. 2850–2852.
 136. Runge, E.; Gross, E. K. U. Density-functional theory for time-dependent systems. *Physical Review Letters*, 1984, vol. 52, p. 997–1000.
 137. Gross, E. K. U.; Kohn, W. Time-dependent density functional theory. *Advanced Quantum Chemistry*, 1990, vol. 21, p. 255–291.
 138. Bauernschmitt, R.; Ahlrichs, R. Stability analysis for solutions of the closed shell Kohn-Sham equation. *Chemical Physics Letters*, 1996, vol. 256, p. 454–464.
 139. Casida, M. E., *et al.* Molecular excitation energies to high-lying bound states from time-dependent density-functional response theory: Characterisation and correction of the time-dependent local density approximation ionization threshold. *Journal of Chemical Physics*, 1998, vol. 108, p. 4439–4449.
 140. Zhao, Y.; Schultz, N. E.; Truhlar, D. G. Design of density functionals by combining the method of constraint satisfaction with parametrization for thermochemistry, thermochemical kinetics, and noncovalent interactions. *Journal of Chemical Theory and Computation*, 2006, vol. 2, p. 364–382.
 141. Boese, A. D.; Martin, J. M. L. Development of density functionals for thermochemical kinetics. *Journal of Chemical Physics*, 2004, vol. 121, p. 3405–3416.
 142. Chai, J. D.; Head-Gordon, M. Long-range corrected hybrid density functionals with damped atom-atom dispersion corrections. *Physical Chemistry Chemical Physics*, 2008, vol. 10, p. 6615–6620.
 143. Chai, J. D.; Head-Gordon, M. Systematic optimization of long-range corrected hybrid density functionals. *Journal of Chemical Physics*, 2008, vol. 128, p. 084106–084121.
 144. Bredas, J. L., *et al.* Charge-transfer and energy-transfer processes in pi-conjugated oligomers and polymers: A molecular picture. *Journal of Chemical Review*, 2004, vol. 104, p. 4971–4982.
 145. Frisch, M. J., *et al.* Gaussian 09, Revision B.01, Gaussian Inc., Wallingford CT, 2010.
 146. Harwood, L. M.; Moody, C. J. *Organic Chemistry. Principles and Practice*, Blackwell Science, 1989.
 147. Kurata, T., *et al.* Triarylamine-combined nitronyl nitroxide and its hole-transporting property. *Polyhedron*, 2007, vol. 26, p. 1776–1780.

-
148. El-Khouly, M. E., *et al.* Effect of dual fullerenes on lifetimes of charge-separated states of subphthalocyanine–triphenylamine–fullerene molecular systems. *Journal of Physical Chemistry B*, 2008, vol. 112, p. 3910–3917.
 149. Tan, Z., *et al.* Synthesis, characterization, and electroluminescence of new conjugated PPV derivatives bearing triphenylamine side-chain through a vinylene bridge. *Polymers for Advanced Technologies*, 2007, vol. 18, p. 963–970.
 150. Hagberg, D. P., *et al.* Symmetric and unsymmetric donor functionalization comparing structural and spectral benefits of chromophores for dye-sensitized solar cells. *Journal of Materials Chemistry*, 2009, vol. 19, p. 7232–7238.
 151. Lambert, C., *et al.* Photoinduced charge transfer processes along triarylamine redox cascades. *Journal of American Chemical Society*, 2005, vol. 127, p. 10600–10610.
 152. Chen, B. L., *et al.* Pure and saturated red electroluminescent polyfluorenes with dopant/host system and PLED efficiency/color purity trade-offs. *Advanced Functional Materials*, 2010, vol. 20, p. 3143–3153.
 153. Kim, S. W., *et al.* Synthesis and properties of novel triphenylamine polymers containing ethynyl and aromatic moieties. *Synthetic Metals*, 2001, vol. 122, p. 363–638.
 154. Nicolas, M., *et al.* Boronic ester-substituted triphenylamines as new Lewis base-sensitive redox receptors. *Journal of Electroanalytical Chemistry*, 2000, vol. 482, p. 211–216.
 155. Cremer, J.; Bäuerle, P. Star-shaped perylene–oligothiophene–triphenylamine hybrid systems for photovoltaic applications. *Journal of Materials Chemistry*, 2006, vol. 16, p. 874–884.
 156. Wang, X. M., *et al.* Two-photon pumped lasing stilbene-type chromophores containing various terminal donor groups: relationship between lasing efficiency and intramolecular charge transfer. *Journal of Materials Chemistry*, 2000, vol. 10, p. 2698–2703.
 157. Zeng, S., *et al.* D–A–D low band gap molecule containing triphenylamine and benzoxadiazole/benzothiadiazole units: Synthesis and photophysical properties. *Dyes and Pigments*, 2012, vol. 95, p. 229–235.
 158. Seok, J. H., *et al.* Photoinduced processes of newly synthesized bisferrocene- and bisfullerene-substituted tetrads with a triphenylamine central block. *Journal of Organometallic Chemistry*, 2009, vol. 694, p. 1818–1825.
 159. Sicard, L., *et al.* On-substrate preparation of an electroactive conjugated polyazomethine from solution-processable monomers and its application in electrochromic devices. *Advanced Functional Materials*, 2013, vol. 23, p. 3549–3559.
 160. Wang, H. Y., *et al.* Synthesis and characterization of triphenylaminebenzothiazole-based donor and acceptor materials. *Synthetic Metals*, 2010, vol. 160, p. 1065–1072.
 161. Yeh, K. M., *et al.* Poly(4-vinyltriphenylamine): optical, electrochemical properties and its new application as a host material of green phosphorescent Ir(ppy)₃ dopant. *Synthetic Metals*, 2008, vol. 158, p. 565–571.
 162. Holliman, P. J., *et al.* Ultra-fast co-sensitization and tri-sensitization of dye-sensitized solar cells with N719, SQ1 and triarylamine dyes. *Journal of Materials Chemistry*,

-
- 2012, vol. 22, p. 13318–13327.
163. Behl, M., *et al.* Towards plastic electronics: Patterning semiconducting polymers by nanoimprint lithography. *Advanced Materials*, 2002, vol. 8, p. 588–591.
 164. Singh, S. P., *et al.* New triphenylamine-based organic dyes with different numbers of anchoring groups for dye-sensitized solar cells. *Journal of Physical Chemistry C*, 2012, vol. 116, p. 5941–5950.
 165. Feng, J., *et al.* Hyperbranched polymer based on triphenylamine and pyridine: Fluorescent chemosensors for palladium ions. *Journal of Applied Polymer Science*, 2011, vol. 121, p. 217–225.
 166. Lee, D. H., *et al.* Organic dyes incorporating low-band-gap chromophores based on π -extended benzothiadiazole for dye-sensitized solar cells. *Dyes and Pigments*, 2011, vol. 91, p. 192–198.
 167. Fang, Z., *et al.* Triphenylamine derivatized phenylacetylene macrocycle with large two-photon absorption cross-section. *Tetrahedron Letters*, 2012, vol. 53, p. 4885–4888.
 168. Rouxel, C., *et al.* Octupolar derivatives functionalized with superacceptor peripheral groups: Synthesis and evaluation of the electron-withdrawing ability of potent unusual groups. *Chemistry - A European Journal*, 2012, vol. 18, p. 12487–12497.
 169. Niamnont, N., *et al.* Tunable star-shaped triphenylamine fluorophores for fluorescence quenching detection and identification of nitro-aromatic explosives. *Chemical Communications*, 2013, vol. 49, p. 780–782.
 170. Yang, J. S., *et al.* Synthesis and properties of a fluorene-capped isotruxene: A new unsymmetrical star-shaped π -system. *Organic Letters*, 2006, vol. 8, p. 5813–5816.
 171. Ding, J., *et al.* Synthesis and characterization of alternating copolymers of fluorene and oxadiazole. *Macromolecules*, 2002, vol. 35, p. 3474–3483.
 172. Dudek, S. P., *et al.* Synthesis and energy-transfer properties of hydrogen-bonded oligofluorenes. *Journal of American Chemical Society*, 2005, vol. 127, p. 11763–11768.
 173. Gan, J., *et al.* Synthesis and luminescence properties of novel ferrocene–naphthalimides dyads. *Journal of Organometallic Chemistry*, 2002, vol. 645, p. 168–175.
 174. Reghu, R. R. Synthesis and properties of electron-donor functionalized charge-transporting compounds containing aromatic or heteroaromatic cores. *PhD thesis*, Kaunas University of Technology, Kaunas, 2012, p. 57–58.
 175. Wintges, V.; *et al.* Spectroscopic properties of aromatic dicarboximides. Part 4. On the modification of the fluorescence and intersystem crossing processes of molecules by electron-donating methoxy groups at different positions. The case of 1,8-naphthalimides. *New Journal of Chemistry*, 1996, vol. 20, p. 1149–1158.
 176. Martin, E.; Weigand, R. A correlation between redox potentials and photophysical behaviour of compounds with intramolecular charge transfer: application to *N*-substituted 1,8-naphthalimide derivatives. *Chemical Physics Letters*, 1998, vol. 288, p. 52–58.
 177. Huang, J. H.; Su, J. H.; Tian, H. The development of anthracene derivatives for organic light-emitting diodes. *Journal of Materials Chemistry*, 2012, vol. 22, p. 10977–10989.
 178. Sakai, N., *et al.* Core-substituted naphthalenediimides. *Chemical Communications*,

-
- 2010, vol. 46, p. 4225–4237.
179. Jiang, X., *et al.* An electroluminescent device made with a new fluorescent dye containing 1,3,4-oxadiazole. *Journal of Materials Chemistry*, 1997, vol. 7, p. 1395–1398.
 180. Takahashi, S., *et al.* Photoinduced electron transfer of *N*-[(3- and 4-diarylamino)phenyl]-1,8-naphthalimide dyads: Orbital-orthogonal approach in a short-linked D-A system. *Journal of Physical Chemistry A*, 2008, vol. 112, p. 2533–2542.
 181. Gawrys, P., *et al.* Effect of *N*-substituents on redox, optical, and electronic properties of naphthalene bisimides used for field-effect transistors fabrication. *Journal of Physical Chemistry B*, 2010, vol. 114, p. 1803–1809.
 182. Schab-Balcerzaka E., *et al.* New low band gap compounds comprised of naphthalene diimide and imine units. *Synthetic Metals*, 2012, vol. 162, p. 543–553.
 183. Matsubayashi, K.; Kubo, Y. Control of photophysical properties and photoreactions of aromatic imides by use of intermolecular hydrogen bonding. *Journal of Organic Chemistry*, 2008, vol. 73, p. 4915–4919.
 184. Strohriegel, P.; Grazulevicius, J. V. Charge-transporting molecular glasses. *Advanced Materials*, 2002, vol. 14, p. 1439–1452.
 185. Van Slyke, S. A.; Tang, C. W. Organic electroluminescent devices having improved power conversion efficiencies. US Patent No. 4539507, 1985.
 186. Lo, S. C.; Burn, P. L. Development of dendrimers: Macromolecules for use in organic light-emitting diodes and solar cells. *Chemical Reviews*, 2007, vol. 107, p. 1097–1116.
 187. Hua, J. L., *et al.* Two-photon absorption properties of hyperbranched conjugated polymers with triphenylamine as the core. *Polymer*, 2004, vol. 45, p. 7143–7149.
 188. Iwan, A.; Sek, D. Polymers with triphenylamine units: Photonic and electroactive materials. *Progress in Polymer Science*, 2011, vol. 36, p. 1277–1325.
 189. Ning, Z. J.; Tian, H. Triarylamine: a promising core unit for efficient photovoltaic materials. *Chemical Communications*, 2009, vol. 37, p. 5483–5495.
 190. Jiang, Y., *et al.* Multibranching triarylamine end-capped triazines with aggregation-induced emission and large two-photon absorption cross-sections, *Chemical Communications*, 2010, vol. 46, p. 4689–4691.
 191. Pan, J. H., *et al.* Theoretical investigations of triphenylamine derivatives as hole transporting materials in OLEDs: correlation of Hammett parameter of the substituent to ionization potential and reorganization energy level. *Computational Materials Science*, 2006, vol. 38, p. 105–112.
 192. Sun, Y. D., *et al.* An ambipolar transporting naphtho[2,3-*c*][1,2,5]thiadiazole derivative with high electron and hole mobilities. *Organic Letters*, 2009, vol. 11, p. 2069–2072.
 193. Takizawa, S. Y.; Montes, V. A.; Anzenbacher, P. Phenylbenzimidazole-based new bipolar host materials for efficient phosphorescent organic light-emitting diodes. *Chemistry of Materials*, 2009, vol. 21, p. 2452–2458.
 194. Tsuji, H., *et al.* Bis(carbazolyl)benzodifuran: A high-mobility ambipolar material for homojunction organic light-emitting diode devices. *Advanced Materials*, 2009, vol. 21, p. 3776–3779.
 195. Wu, H., *et al.* Efficient single active layer electrophosphorescent white polymer light-emitting diodes. *Advanced Materials*, 2008, vol. 20, p. 696–702.

-
196. Chien, C. H., *et al.* Polyfluorene presenting dipolar pendent groups and its application to electroluminescent devices. *Polymer Science Part A: Polymer Chemistry*, 2007, vol. 45, p. 2073–2084.
 197. Grimsdale, A. C., *et al.* Synthesis of light-emitting conjugated polymers for applications in electroluminescent devices. *Chemical Reviews*, 2009, vol. 109, p. 897–1091.
 198. Burgi, L., *et al.* High-mobility ambipolar near-infrared light-emitting polymer field-effect transistors. *Advanced Materials*, 2008, vol. 20, p. 2217–2224.
 199. Ostrauskaite, J., *et al.* Synthesis and properties of glass-forming hydrazones II [1]. Hydrazones containing bicarbazolyl units. *Monatshefte Fur Chemie*, 2002, vol. 133, p. 599–607.
 200. Getautis, V., *et al.* Novel hydrazone based polymers as hole transporting materials. *Polymer*, 2005, vol. 46, p. 7918–7922.
 201. Lygaitis, R.; Getautis, V.; Gražulevičius, J. V. Hole-transporting hydrazones. *Chemical Society Reviews*, 2008, vol. 37, p. 770–788.
 202. Shen, Y., *et al.* Mobility-dependent charge injection into an organic semiconductor. *Physical Review Letters*, 2001, vol. 86, p. 3867–3870.
 203. Borsenberger, M.; Weiss, D. S. *Photoreceptors for imaging systems*, Marcel Dekker, New York, 1993.
 204. Urnikaite, S., *et al.* Organic dyes with hydrazone moieties: A study of correlation between structure and performance in the solid-state dye-sensitized solar cells. *Journal of Physical Chemistry C*, 2014, vol. 118, p. 7832–7843.
 205. Michaleviciute, A., *et al.* Glass-forming carbazolylidene-containing hydrazones as hole-transporting materials. *Synthetic Metals*, 2009, vol. 159, p. 218–222.
 206. Stanislovaityte, E., *et al.* Synthesis and properties of hole-transporting indolo[3,2-b]carbazole-based hydrazones with reactive functional groups. *Tetrahedron*, 2014, p. 1–9.
 207. Kulkarni, A. P., *et al.* Electron transport materials for organic light-emitting diodes. *Chemistry of Materials*, 2004, vol. 16, p. 4556–4573.
 208. Jung, B. J., *et al.* Molecular design and synthetic approaches to electron-transporting organic transistor semiconductors. *Chemistry Materials*, 2011, vol. 23, p. 568–582.
 209. Lei, T., *et al.* A BDOPV-based donor-acceptor polymer for high-performance n-type and oxygen-doped ambipolar field-effect transistors. *Advanced Materials*, 2013, vol. 25, p. 6589–6593.
 210. Lei, T., *et al.* Electron-deficient poly(p-phenylene vinylene) provides electron mobility over $1 \text{ cm}^2 \text{ V}(-1) \text{ s}(-1)$ under ambient conditions. *Journal of American Chemical Society*, 2013, vol. 135, p. 12168–12171.
 211. Duan, L. A., *et al.* Strategies to design bipolar small molecules for OLEDs: Donor-acceptor structure and non-donor-acceptor structure. *Advanced Materials*, 2011, vol. 23, p. 1137–1144.
 212. Lei, T., *et al.* Chlorination as a useful method to modulate conjugated polymers: balanced and ambient-stable ambipolar high-performance field-effect transistors and inverters based on chlorinated isoindigo polymers. *Chemical Science*, 2013, vol. 4, p. 2447–2452.

-
213. Chen, Z., *et al.* High performance ambipolar diketopyrrolopyrrole-thieno[3,2-b]thiophene copolymer field-effect transistors with balanced hole and electron mobilities. *Advanced Materials*, 2012, vol. 24, p. 647–652.
214. Son, K. S., *et al.* Analyzing bipolar carrier transport characteristics of diarylamino-substituted heterocyclic compounds in organic light-emitting diodes by probing electroluminescence spectra. *Chemistry of Materials*, 2008, vol. 20, p. 4439–4446.
215. Huang, J. H., *et al.* Bipolar anthracene derivatives containing hole- and electron-transporting moieties for highly efficient blue electroluminescence devices. *Journal of Materials Chemistry*, 2011, vol. 21, p. 2957–2964.
216. Zheng, C. J., *et al.* New ambipolar hosts based on carbazole and 4,5-diazafluorene units for highly efficient blue phosphorescent OLEDs with low efficiency roll-off. *Chemistry of Materials*, 2012, vol. 24, p. 643–650.
217. Castellanos, S., *et al.* Stable radical cores: a key for bipolar charge transport in glass forming carbazole and indole derivatives. *Chemical Communications*, 2010, vol. 46, p. 5130–5132.
218. Reghu, R. R., *et al.* Air stable electron-transporting and ambipolar bay substituted perylene bisimides. *Journal of Materials Chemistry*, 2011, vol. 21, p. 7811–7819.
219. Marcus, R. A. Electron transfer reactions in chemistry. Theory and experiment. *Reviews of Modern Physics*, 1993, vol. 65, p. 599–610.
220. Levich, V. G. Present state of the theory of oxidation and reduction in solution (bulk and electrode reactions). *Advances in Electrochemistry and Electrochemical Engineering*, 1966, vol. 4, p. 249–271.
221. Marcus, R. A. On the theory of oxidation-reduction reactions involving electron transfer I. *Journal of Chemical Physics*, 1956, vol. 24, p. 966–978.
222. Marcus, R. A.; Sutin, N. Electron transfers in chemistry and biology. *Biochimica et Biophysica Acta*, 1985, vol. 811, p. 265–322.
223. Goodbrand, H. B.; Hu, N. X. Ligand-accelerated catalysis of the Ullmann condensation: Application to hole conducting triarylamines. *Journal of Organic Chemistry*, 1999, vol. 64, p. 670–674.
224. Keruckas, J., *et al.* Influence of methoxy groups on the properties of 1,1-bis(4-aminophenyl)cyclohexane based arylamines: experimental and theoretical approach. *Journal of Materials Chemistry*, 2012, vol. 22, p. 3015–3027.
225. Dreuw, A.; Head-Gordon, M. Failure of time-dependent density functional theory for long-range charge-transfer excited states: The Zincbacteriochlorin–Bacteriochlorin and bacteriochlorophyll–spheroidene complexes. *Journal of American Chemistry Society*, 2004, vol. 126, p. 4007–4016.
226. Dreuw, A.; Weisman, J. L.; Head-Gordon, M. Long-range charge-transfer excited states in time-dependent density functional theory require non-local exchange. *Journal of Chemistry Physics*, 2003, vol. 119, p. 2943–2946.
227. Sobolewski, A. L.; Domcke, W. Ab initio study of the excited-state coupled electron–proton-transfer process in the 2-aminopyridine dimer. *Chemical Physics*, 2003, vol. 294, p. 73–83.
228. Dreuw, A.; Fleming, G. R.; Head-Gordon, M. Charge-transfer state as a possible signature of a zeaxanthin–chlorophyll dimer in the non-photochemical quenching

-
- process in green plants. *Journal of Physical Chemistry B*, 2003, vol. 107, p. 6500–6503.
229. Dreuw, A.; Fleming, G. R.; Head-Gordon, M. Chlorophyll fluorescence quenching by xanthophylls. *Physical Chemistry Chemical Physics*, 2003, vol. 5, p. 3247–3254.
230. McMasters, S.; Kelly, L. A. Ground-state interactions of spermine-substituted naphthalimides with mononucleotides. *Journal of Physical Chemistry B*, 2006, vol. 110, p. 1046–1055.
231. Tao, S., *et al.* Efficient blue organic light-emitting devices with a new bipolar emitter. *Organic Electronics*, 2011, vol. 12, p. 358–363.
232. Demets, G. J. F., *et al.* Solvent influence on the photophysical properties of 4-methoxy-*N*-methyl-1,8-naphthalimide. *Spectrochimica Acta Part A*, 2006, vol. 63, p. 220–226.
233. Poteau, X., *et al.* Fluorescence switching in 4-amino-1,8-naphthalimides: “on–off–on” operation controlled by solvent and cations. *Dyes and Pigments*, 2000, vol. 47, p. 91–105.
234. Ramachandram, B., *et al.* Unusually high fluorescence enhancement of some 1,8-naphthalimide derivatives induced by transition metal salts. *Journal of Physical Chemistry B*, 2000, vol. 104, p. 11824–11832.
235. Yuan, D.; Brown, R. G. Enhanced nonradiative decay in aqueous solutions of aminonaphthalimide derivatives via water-cluster formation. *Journal of Physical Chemistry A*, 1997, vol. 101, p. 3461–3466.
236. Krotkus, S., *et al.* Pyrenyl-functionalized fluorene and carbazole derivatives as blue light emitters. *Journal of Physical Chemistry C*, 2012, vol. 116, p. 7561–7572.
237. Gulbinas, V., *et al.* Charge transfer induced excited state twisting of *N,N*-dimethylaminobenzylidene-1,3-indandione in solution. *Journal of Physical Chemistry A*, 1999, vol. 103, p. 3969–3980.
238. Harrer, D.; Pilpott, M. R. In spectroscopy and excitation dynamics of condensed molecular systems; Agranovich, V. M.; Hochstrasser, R.M. Eds.; Amsterdam: North Holland, 1983, p. 27.
239. Jursenas, S., *et al.* Free and self-trapped charge-transfer excitons in crystals of dipolar molecules of *N,N*-dimethylaminobenzylidene 1,3-indandione. *Journal of Physical Chemistry B*, 1998, vol. 102, p. 1086–1094.
240. Jones, B. A., *et al.* Tuning orbital energetics in arylene diimide semiconductors. Materials design for ambient stability of n-type charge transport. *Journal of American Chemical Society*, 2007, vol. 129, p. 15259–15278.
241. Segura, J. L., *et al.* Synthesis and electronic properties of anthraquinone-, tetracyanoanthraquinodimethane-, and perylenetetracarboxylic diimide-functionalized poly(3,4-ethylenedioxythiophenes). *Chemistry of Materials*, 2006, vol. 18, p. 2834–2847.
242. Segura, J. L., *et al.* Synthesis and electropolymerization of a perylenebisimide-functionalized 3,4-ethylenedioxythiophene (EDOT) derivative. *Organic Letters*, 2005, vol. 7, p. 2345–2348.
243. Gómez, R., *et al.* Energy and electron transfer in a poly(fluorene-alt-phenylene) bearing perylenediimides as pendant electron acceptor groups. *Macromolecules*, 2007, vol. 40, p. 2760–2772.

-
244. Hsiao, S. H., *et al.* Synthesis and properties of new aromatic polyamides with redox-active 2,4-dimethoxytriphenylamine moieties. *Journal of Polymer Science Part B: Polymer Physics*, 2010, vol. 48, p. 3392–3401.
 245. Kim, J. Y., *et al.* Mobility of electrons and holes in an n-type organic semiconductor perylene diimide thin film. *Current Applied Physics*, 2005, vol. 5, p. 615–618.
 246. Borsenberger, P. M., *et al.* The role of dipole moments on hole transport in triphenylamine-doped polymers. *Journal of Polymer Science Part B: Polymer Physics*, 1996, vol. 34, p. 317–323.
 247. Maldonado, J. L., *et al.* Effect of substitution on the hole mobility of bis(diaryl amino)biphenyl derivatives doped in poly(styrene). *Chemistry of Materials*, 2003, vol. 15, p. 994–999.
 248. Rivnay, J., *et al.* Unconventional face-on texture and exceptional in-plane order of a high mobility n-type polymer. *Advanced Materials*, 2010, vol. 22, p. 4359–4363.
 249. Wetzelaer, G. J. A. H., *et al.* Asymmetric electron and hole transport in a high-mobility n-type conjugated polymer. *Physical Review B*, 2012, vol. 86, p. 165203–165221.
 250. Bassler, H. Charge transport in disordered organic photoconductors a Monte Carlo study. *Physica Status Solidi B*, 1993, vol. 175, p. 15–56.
 251. Pommerehne, J., *et al.* Efficient two layer leds on a polymer blend basis. *Journal of Advanced Materials*, 1995, vol. 7, p. 551–554.
 252. Chen, W. C., *et al.* Theoretical and experimental characterization of small band gap poly(3,4-ethylenedioxythiophene methine)s. *Macromolecules*, 2004, vol. 37, p. 5959–5964.
 253. Mimaite, V., *et al.* Efficient dye regeneration in solid-state dye-sensitized solar cells fabricated with melt processed hole conductors. *Synthetic Metals*, 2011, vol. 161, p. 1575–1581.
 254. Michaleviciute, A., *et al.* Star-shaped carbazole derivatives for bilayer white organic light-emitting diodes combining emission from both excitons and exciplexes. *Journal of Physical Chemistry C*, 2012, vol. 116, p. 20769–20778.
 255. Tomkeviciene, A., *et al.* Diphenylamino-substituted derivatives of 9-phenylcarbazole as glass-forming hole-transporting materials for solid state dye sensitized solar cells. *Synthetic Metals*, 2012, vol. 162, p. 1997–2004.
 256. Gudeika, D., *et al.* New derivatives of triphenylamine and naphthalimide as ambipolar organic semiconductors: Experimental and theoretical approach. *Dyes and Pigments*, 2014, vol. 106, p. 58–70.
 257. Sherwood, G. A., *et al.* Aggregation effects on the emission spectra and dynamics of model oligomers of MEH-PPV. *Journal of Physical Chemistry C*, 2009, vol. 113, p. 18851–18862.
 258. Gupta, V. D., *et al.* Red emitting solid state fluorescent triphenylamine dyes: Synthesis, photo-physical property and DFT study. *Dyes and Pigments*, 2013, vol. 97, p. 429–439.
 259. Bangal, P.R.; Panja, S.; Chakravorti, S. Excited state photodynamics of 4-N,N-dimethylamino cinnamaldehyde: A solvent dependent competition of TICT and intermolecular hydrogen bonding. *Journal of Photochemistry and Photobiology A: Chemistry*, 2001, vol. 139, p. 5–16.
 260. Reichardt, C.; Welton, T. Solvents and solvents effects in organic chemistry, 4th ed.,

Wiley-VCH, Weinheim, 2011.

261. Sung, J., *et al.* Characterization of ultrafast intramolecular charge transfer dynamics in pyrenyl derivatives: Systematic change of the number of peripheral *N,N*-dimethylaniline substituents. *Journal of Physical Chemistry Letters*, 2011, vol. 2, p. 818–823.
262. Tanaka, H., *et al.* Twisted intramolecular charge transfer state for long-wavelength thermally activated delayed fluorescence. *Chemistry of Materials*, 2013, vol. 25, p. 3766–3771.
263. Uoyama, H., *et al.* Highly efficient organic light-emitting diodes from delayed fluorescence. *Nature*, 2012, vol. 492, p. 234–238.
264. Volyniuk, D., *et al.* Highly efficient blue organic light-emitting diodes based on intermolecular triplet–singlet energy transfer. *Journal of Physical Chemistry C*, 2013, vol. 117, p. 22538–22544.
265. Endo, A., *et al.* Thermally activated delayed fluorescence from Sn⁴⁺–porphyrin complexes and their application to organic light emitting diodes – a novel mechanism for electroluminescence. *Advanced Materials*, 2009, vol. 21, p. 4802–4806.
266. Dias, F. B., *et al.* Triplet harvesting with 100% efficiency by way of thermally activated delayed fluorescence in charge transfer OLED emitters. *Advanced Materials*, 2013, vol. 25, p. 3707–3714.
267. Guo, X., *et al.* Naphthalene diimide-based polymer semiconductors: synthesis, structure–property correlations, and n-channel and ambipolar field-effect transistors. *Chemistry of Materials*, 2012, vol. 24, p. 1434–1442.
268. Chen, J., *et al.* Solvatochromism of *N*-[2-(2-hydroxyethylamino)-ethyl]-1,8-naphthalimide in protic solvent. *Journal of Molecular Structure*, 2009, vol. 917, p. 170–175.
269. Huang, C.; Barlow, S.; Marder, S. R. Perylene-3,4,9,10-tetracarboxylic acid diimides: synthesis, physical properties, and use in organic electronics. *Journal of Organic Chemistry*, 2011, vol. 76, p. 2386–2407.
270. Cho, D. W., *et al.* Intramolecular excimer formation and photoinduced electron-transfer process in bis-1,8-naphthalimide dyads depending on the linker length. *Journal of Physical Chemistry A*, 2008, vol. 112, p. 7208–7213.
271. Xie, L. H., *et al.* Polyfluorene-based semiconductors combined with various periodic table elements for organic electronics. *Progress in Polymer Science*, 2012, vol. 37, p. 1192–1264.
272. Kamtekar, K. T.; Monkman, A. P.; Bryce, M. R. Recent advances in white organic light-emitting materials and devices (WOLEDs). *Advanced Materials*, 2010, vol. 22, p. 572–582.
273. Han, S. C.; Jin, S. H.; Lee, J. W. Synthesis of dendrimer containing dialkylated-fluorene unit as a core chromophore via click chemistry. *Bulletin of the Korean Chemical Society*, 2012, vol. 33, p. 137–141.
274. Lin, T. C., *et al.* Synthesis and two-photon properties of small dendritic chromophores with symmetrical and unsymmetrical substituted skeletons. *Chemistry - A European Journal*, 2012, vol. 2012, p. 1737–1745.
275. Jacquemin, D., *et al.* Absorption and emission spectra of 1,8-naphthalimide fluorophores: A PCM-TD-DFT investigation. *Chemical Physics*, 2010, vol. 372, p. 61–66.

-
276. Ramart-Lucas, M.; Matti, M. J.; Guilmart, T. Structure, absorption et comportement chimique dans la serie du phenanthrene. *Bulletin de la Societe Chimique de France*, 1948, vol. 15, p. 1215–1225.
 277. Hrdlovic, P., *et al.* Influence of polarity of solvents on the spectral properties of bichromophoric coumarins. *Molecules*, 2010, vol. 15, p. 8915–8932.
 278. Czerwieńiec, R., *et al.* Radiative electron transfer in planar donor-acceptor quinoxaline derivatives. *Journal of Physical Chemistry Letters*, 2000, vol. 325, p. 589–598.
 279. Zachariasse, K. A. Comment on “Pseudo-Jahn–Teller and TICT-models: a photophysical comparison of meta-and para-DMABN derivatives” [Chemical Physics Letters, 1999, vol. 305, p. 8]: The PICT model for dual fluorescence of aminobenzonitriles. *Chemical Physics Letters*, 2000, vol. 320, p. 8–13.
 280. Grabowski, Z. R.; Rotkiewicz, K.; Rettig, W. Structural changes accompanying intramolecular electron transfer: Focus on twisted intramolecular charge-transfer states and structures. *Chemical Reviews*, 2003, vol. 103, p. 3899–4032.
 281. Vajiravelu, S., *et al.* Effect of substituents on the electron transport properties of bay substituted perylene diimide derivatives. *Journal of Materials Chemistry*, 2009, vol. 19, p. 4268–4275.
-



LIST OF PUBLICATIONS

Publications on the theme of the dissertation in the journals included into the Thomson Reuters Web of Science (ISI) database

1. Gudeika, D.; Lygaitis, R.; Mimaitė, V.; Grazulevicius, J. V.; Jankauskas, V.; Lapkowski, M.; Data, P. Hydrazones containing electron-accepting and electron-donating moieties. *Dyes and Pigments*, 2011, vol. 91, p. 13–19.
2. Gudeika, D.; Michaleviciute, A.; Grazulevicius, J. V.; Lygaitis, R.; Grigalevicius, S.; Jankauskas, V.; Miasojedovas, A.; Jursenas, S.; Sini, G. Structure properties relationship of donor-acceptor derivatives of triphenylamine and 1,8-naphthalimide. *Journal of Physical Chemistry C*, 2012, vol. 116, p. 14811–14819.
3. Gudeika, D.; Reghu, R. R.; Grazulevicius, J. V.; Buika, G.; Simokaitiene, J.; Miasojedovas, A.; Jursenas, S.; Jankauskas, V. Electron-transporting naphthalimide-substituted derivatives of fluorene. *Dyes and Pigments*, 2013, vol. 99, p. 895–902.
4. Gudeika, D.; Grazulevicius, J. V.; Bucinskas, A.; Sini, G.; Jankauskas, V.; Miasojedovas, A.; Jursenas, S. New derivatives of triphenylamine and naphthalimide as ambipolar organic semiconductors: experimental and theoretical approach. *Dyes and Pigments*, 2014, vol. 106, p. 58–70.
5. Dudok, T. H.; Krupych, O. M.; Savaryn, V. I.; Cherpak, V. V.; Fechan, A. V.; Gudeika, D.; Grazulevicius, J. V.; Pansu, B.; Nastishin, Y. A. Lasing in a cholesteric liquid crystal doped with derivative of triphenylamine and 1,8-naphthalimide, and optical characterization of the materials. *Ukrainian Journal of Physical Optics*, 2014, vol. 15, p. 162–172.

List of the presentations on the theme of the dissertation at the local and international conferences

1. Gudeika, D.; Grazulevicius, J. V. Impact of linking topology on the properties of the derivatives of triphenylamine and naphthalimide // International Conference On “Balticum Organicum Syntheticum” (BOS), July 6-9, 2014, Vilnius, p. 156.
2. Gudeika, D.; Grazulevicius, J. V.; Jankauskas, V. Donor- π -acceptor derivatives with triphenylamino core and 1,8-naphthalimide arms // The 11th International Symposium on Functional π -electron systems (F π -11), June 2-7, 2013, Arcachon, Aquitaine, France.
3. Savaryn, V. I.; Krupych, O. M.; Dudok, T. G.; Cherpak, V. V.; Gudeika, D.; Grazulevicius, J. V.; Nastishin, Y. A. Optical characterization of a cholesteric liquid crystal doped with the derivative of triphenylamine and 8-naphthalimide for laser generation // 11th International Conference on Correlation Optics, 18–21 September 2013, Chernivtsi, Ukraine.
4. Miasojedovas, A.; Jankauskas, V.; Sini, G.; Gudeika, D.; Michaleviciute, A.; Lygaitis, R.; Grigalevicius, S.; Grazulevicius, J. V.; Jursenas, S. Triphenylamine and naphthalimide derivatives as multicolor emitters // The 10th International Conference on Optical Probes of Conjugated Polymers and Organic Nanostructures, July 14-19, 2013, Durham, United Kingdom.
5. Jursenas, S.; Miasojedovas, A.; Jankauskas, V.; Sini, G.; Gudeika, D.; Michaleviciute, A.; Lygaitis, R.; Grigalevicius, S.; Grazulevicius, J. V. Triphenylamine and naphthalimide derivatives for optoelectronic Applications // 2013 Optics+Photonics, 25 – 29 August 2013, Proceedings of SPIE, vol. 8831B, p. 8831–227.
6. Gudeika, D.; Grazulevicius, J. V.; Jankauskas, V. Triphenylamine- and 1,8-naphthalimide-based materials for potential electronic devices // 6th International Meeting on Molecular Electronics (ELECTMOL'12), December 3-7, 2012, Grenoble, France, p. 183.
7. Gudeika, D.; Grazulevicius, J. V.; Lygaitis, R.; Miasojedovas, A.; Jursenas, S. Synthesis and properties of glass-forming 1,8-naphthalimide derivatives // Baltic Polymer Symposium 2011: Pärnu, Estonia, 2011: program and abstracts / Tallinn University of Technology. ISBN: 978-9955-25-838-4, p. 87.

Other publications in the journals included into the Thomson Reuters Web of Knowledge database

1. Gudeika, D.; Lygaitis, R.; Grazulevicius, J. V.; Kublickas, R. H.; Rubeziene, V.; Vedegyte, J. Synthesis and properties of dimeric naphthalene diimides. *Chemija*, 2012, vol. 23, p. 233–238.
2. Lukstaite, J.; Gudeika, D.; Grazulevicius, J. V.; Grigalevicius, S.; Zhang, B.; Xie, Z. Copolymers containing electronically isolated indolyl fragments as materials for optoelectronics. *Reactive and Functional Polymers*, 2010, vol. 70, p. 572–577.
3. Juskelyte, E.; Lygaitis, R.; Buika, G.; Ostrauskaite, J.; Gudeika, D.; Grazulevicius, J. V.; Jankauskas, V. Glass-forming hole-transporting carbazole-based hydrazone monomers, polymers, and twin compounds. *Reactive and Functional Polymers*, 2010, vol. 70, p. 81–87.
4. Lygaitis, R.; Gudeika, D.; Grazulevicius, J. V.; Jankauskas, V. Electron-transporting naphthalenetetracarboxy diimide based monomers and polymers. *Synthetic Metals*, 2013, vol. 81, p. 56–63.
5. Mimaite, V.; Ostrauskaite, J.; Gudeika, D.; Grazulevicius, J. V.; Jankauskas, V. Structure-properties relationship of hydrazones containing methoxy-substituted triphenylamino groups. *Synthetic Metals*, 2011, vol. 161, p. 1575–1581.
6. Zilinskaite, V.; Gudeika, D.; Grazulevicius, J. V.; Sidaravicius, J. Synthesis and properties of 1,3-indandione-disubstituted derivatives of carbazole, phenothiazine and phenoxazine. *Molecular Crystals and Liquid Crystals*, 2014, vol. 590, p. 80–89.
7. Dainyte, A.; Gudeika, D.; Buika, G.; Grazulevicius, J. V. Synthesis and properties of 2,4,6-tris(phenoxy)-1,3,5-triazine. *Molecular Crystals and Liquid Crystals*, 2014, vol. 590, p. 73–79.
8. Zilinskaite, V.; Gudeika, D.; Grazulevicius, J. V.; Volyniuk, D.; Buika, G.; Jankauskas, V.; Juska, G.; Rutkis, M.; Tokmakov, A. Derivatives of indandione and differently substituted triphenylamine with charge-transporting and NLO properties. *Dyes and Pigments*, 2015, vol. 113, p. 38–46.
9. Gudeika, D.; Grazulevicius, J. V.; Volyniuk, D.; Juska, G.; Butkute, R.; Miasojedovas, A.; Gruodis, A.; Jursenas, S. Structure-properties relationship of the derivatives of carbazole and 1,8-naphthalimide. *Dyes and Pigments*, 2014, accepted.

List of the presentations in other local and international conferences

1. Sini, G.; Grazulevicius, J. V.; Keruckas, J.; Gudeika, D.; Mimaite, V.; Jankauskas, V. Hydrogen-bonding versus dipole-moment disorder in charge-transporting properties: experimental and theoretical approach // Synthetic metals guiding the future (ICSM), June 30-July 5, 2014, Turku, Finland.
2. Volyniuk, D.; Cherpak, V.; Stakhira, P.; Tomkeviciene, A.; Simokaitiene, J.; Dabulienė, A.; Gudeika, D.; Grazulevicius, J. V. Photoelectrical studying of carbazol and triphenylamine based materials for organic electroluminescent devices // Baltic Polymer Symposium 2014: Laulasmaa, Estonia, September 24-26, 2014: program and abstracts/ Tallinn University of Technology, p. 32.
3. Gudeika, D.; Grazulevicius. Synthesis and properties of naphthalimide based derivative with reactive vinyl functional group // Baltic Polymer Symposium 2014:

-
- Laulasmaa, Estonia, September 24-26, 2014: program and abstracts/ Tallinn University of Technology, p. 71.
4. Zilinskaite, V.; Gudeika, D.; Grazulevicius. Synthesis and properties of polymers containing indandione moiety // Baltic Polymer Symposium 2014: Laulasmaa, Estonia, September 24-26, 2014: program and abstracts/ Tallinn University of Technology, p. 102.
 5. Zilinskaite, V.; Tomkeviciene, A.; Gudeika, D.; Grazulevicius, J. V. Synthesis and properties of arylene-1,3-indandione based monomers // Baltic Polymer Symposium 2013: Trakai, Lithuania, September 19-21, 2013: program and abstracts/ Kaunas University of Technology, p. 119.
 6. Sini, G.; Grazulevicius, J. V.; Keruckas, J.; Gudeika, D.; Mimaite, V.; Jankauskas, V. Hydrogen-bonding versus dipole-moment disorder in charge-transporting properties: experimental and theoretical approach // Baltic Polymer Symposium 2013: Trakai, Lithuania, September 19-21, 2013: program and abstracts/ Kaunas University of Technology, p. 63.
 7. Dainyte, A.; Gudeika, D.; Grazulevicius, J. V. Synthesis and properties of differently substituted derivatives of cyanuric acid // Baltic Polymer Symposium 2013: Trakai, Lithuania, September 19-21, 2013: program and abstracts/ Kaunas University of Technology, p. 73.
 8. Gudeika, D.; Grazulevicius, J.V. Synthesis and characterization of bipolar (2),7-functionalized carbazoles // 10th International Conference on Electroluminescence and Optoelectronic Devices (ICEL-10), August 31-September 3, 2014, Cologne, Germany, p. 41.
 9. Žilinskaitė, V.; Gudeika, D.; Gražulevičius, J. V. Elektronų donorines ir akceptorines grupes turinčių junginių sintezė ir savybių tyrimas // Chemija ir cheminė technologija, 2014 m. gegužės 23 d., Kaunas. ISBN 978-609-02-1071-0, p. 107–109.
 10. Gudeika, D.; Grazulevicius, J.V.; Jankauskas, V. Naphthalimide-functionalized fluorene and carbazole derivatives // Solar energy for world peace : book of abstracts, 17-19 August 2013, Stambul, Turkey, 2013, p. 167.
 11. Gudeika, D.; Grazulevicius, J. V.; Miasojedovas, A.; Jursenas, S. Synthesis and properties of glass-forming Naphthalimide compounds containing Carbazole moieties // Baltic Polymer Symposium 2013: Trakai, Lithuania, September 19-21, 2013: program and abstracts/ Kaunas University of Technology, p. 81.
 12. Kalnina, Z.; Tokmakovs, A.; Rutkis, M.; Grazulevicius, J. V.; Zilinskaite, V.; Gudeika, D. Triphenylamino indanedione type structures research as nonlinear optical actine materials // Developments in Optics and Communications 2013, Riga, April 10-12, 2013, p. 124.
 13. Gudeika, D.; Grazulevicius, J. V.; Jankauskas, V. Carbazole-functionalized benzothiadiazole derivatives // 9-th International Conference “Electronic processes in organic materials” (ICEPOM-9), May 20-24, 2013, Lviv, Ukraine, p. 181.
 14. Gudeika, D.; Grazulevicius, J. V.; Jankauskas, V. Synthesis and characterization of donor-acceptor type 2,1,3-benzothiadiazole-based compounds // Chemistry and Chemical Technology, Kaunas University of Technology, 30 May 2013 / Kaunas University of Technology. Kaunas: Technologija. ISSN 2029-2457, 2013.
 15. Žilinskaitė, V.; Gudeika, D. 1,3-Indandiono fragmentus turinčių polimerų sintezė ir

-
- savybės // Studentų moksliniai tyrimai 2012-2013, 2013 m, spalio 9-10 d., Vilnius. ISBN 978-9955-613-63, p. 264–266.
16. Bistrickas, M.; Gudeika, D. 1,3,6,8-tetrapakeistų karbazolo junginių sintezė ir savybės // Studentų moksliniai tyrimai 2013-2014, 2014 m, spalio 9-10 d., Vilnius. ISBN 978-609-417-091-1, p. 92–93.
 17. Krupych, O. M.; Savaryn, V. I.; Dudok, T. G.; Cherpak, V. V.; Gudeika, D.; Grazulevicius, J. V.; Nastishin, Y. A. Cholesteric liquid crystal doped with new dye for laser generation. Materials of international scientific and technical conference laser technologies. Lasers and their application, June 25–27, 2013, Truskavets, Ukraine.
 18. Dainytė, A.; Gudeika, D.; Gražulevičius, J. V. Triazino branduolį turinčių junginių sintezė ir tyrimas, Chemija ir cheminė technologija, 2013 m. gegužės 31 d., Vilnius.
 19. Gudeika, D.; Grazulevicius, J. V.; Buika, G. Ambipolar Perylene Bisimide Containing Polymers for Optoelectronics // Advanced Materials and Technologies: book of abstracts of the 14-th international conference-school, 27-31 August 2012, Palanga, Lithuania. 2012. ISSN 1822-7759. p. 119.
 20. Žilinskaitė, V.; Gudeika, D. 1,3-Indandiono fragmentą turinčių junginių sintezė ir savybės // Chemija ir cheminė technologija, 2012 m. gegužės 4 d., Klaipėda. ISBN 978-9955-18-651-9, p. 227.
 21. Žilinskaitė, V.; Gudeika, D. Indandionilfragmentus turinčių junginių sintezė ir tyrimas // Studentų moksliniai tyrimai 2011-2012, 2012 m. birželio 28-29 d., Vilnius. ISBN 978-9955-786-61-0, p. 289.
 22. Dainytė, A.; Gudeika, D. Nekonjuguotų 3D tipo molekulių sintezė ir savybės // Studentų moksliniai tyrimai 2012, 2012 m. spalio 18-19 d., Vilnius. ISBN 978-9955-786-79-5, p. 77.
 23. Gudeika, D.; Grazulevicius, J. V.; Buika, G. Synthesis and characterization of polymers based on perylene diimide // Baltic Polymer Symposium 2012 : Liepaja, Latvia, September 19-21, 2012: program and abstracts / Rigas University of Technology. p. 133.
 24. Gudeika, D.; Gražulevičius, J. V. Trifenilamino ir 1,8-naftalimido dariniai organiniams puslaidininkiams // Medžiagų inžinerija 2012: respublikinė konferencija: konferencijos pranešimų santrauka, 2012 m. lapkričio 16 d., Kaunas, 2012. ISBN 9786090207505, p. 34.
 25. Gudeika, D.; Grazulevicius, J. V.; Buika, G. Synthesis and properties of polymers based on perylene diimide // Physical and technological problems of radio engineering devices, telecommunication, nano-and microelectronics proceedings of the II International Scientific-Practical Conference 2012 : Chernivtsy, Ukraine, October 25-27, 2012: program and abstracts / Chernivtsy National University, UDK 621.37/39(06), p. 196.
 26. Gudeika, D.; Grazulevicius, J. V.; Lygaitis, R. Substituent effect on the photophysical properties of 1,8-naphthalimide // Advanced Materials and Technologies: book of abstracts of the 13-th international conference-school, Palanga, Lithuania, 2011. ISSN: 1822-7759, p. 101.
 27. Gudeika, D.; Lygaitis, R.; Gražulevičius, J. V. Synthesis and characterization of electron transporting polymers // Baltic Polymer Symposium 2010 conference abstracts, Palanga, Lithuania, 2010. ISBN: 978-9955-25-838-4, p. 127.

-
28. Gudeika, D.; Lygaitis, R.; Grazulevicius, J. V.; Jankauskas, V. Bipolar organic semiconductors based on naphthalene-imide // ICEPOM-8 2010 conference abstracts, Kyiv: Ivano-Frankivs'k region, 2010. ISBN: 978-966-675-629-2, p. 234.
 29. Gudeika, D.; Lygaitis, R.; Grazulevicius, J. V. New electron-transporting naphthalene diimide containing polymers // Advanced materials and technologies and European doctorate in physics and chemistry of advanced materials: book of abstracts of the Joint International Summer School-Conference. Palanga, Lithuania, 2010. ISSN: 1822-7759, p. 127.
 30. Gudeika, D.; Lygaitis, R.; Gražulevičius, J. V. Naftalenimido chromoforą turintys bipoliniai ir elektronus pernešantys organiniai puslaidininkiai // Chemija ir cheminė technologija, Kaunas, 2010. ISSN: 978-9955-25-804-9, p. 31.
 31. Gudeika D. Aromatic imides and hydrazones synthesis, properties, applications // Scientific summer camp smithy of ideas 2010, steading Trakšalis, Katyšių village, Trakai district, June 17-20, 2010.
 32. Gudeika, D.; Lygaitis, R.; Gražulevičius, J. V. Bipolinių organinių puslaidininkių sintezė ir savybės // Studentų moksliniai darbai 2008–2010 konferencijos medžiaga. ISBN: 978-609-420-069-4, Vilnius, 2010, p. 109.

Publications in other refereed scientific journals

1. Gudeika, D.; Grazulevicius, J. V.; Ivanauskaite, A. Synthesis and properties of ambipolar 1,8-naphthalimide based compounds. *Polymer chemistry and technology : proceedings of scientific conference Chemistry and Chemical Technology*, 2014, p. 329–332.
2. Gudeika, D.; Grazulevicius, J. V. Synthesis and properties of 1,8-naphthalene imide-based derivative with reactive vinyl group. *Polymer chemistry and technology : proceedings of scientific conference Chemistry and Chemical Technology*, 2014, p. 332–335.
3. Gudeika, D.; Peculyte, L.; Grazulevicius, J. V. Synthesis and properties of differently substituted naphthalimide twin compounds. *Polymer chemistry and technology : proceedings of scientific conference Chemistry and Chemical Technology*, 2014, p. 336–339.
4. Zilinskaite, V.; Gudeika, D.; Grazulevicius, J. V.; Buika, G. Synthesis and properties of 1,3-indandione based monomer and polymer. *Polymer chemistry and technology : proceedings of scientific conference Chemistry and Chemical Technology*, 2014, p. 230–233.
5. Gudeika, D.; Grazulevicius, J. V. Synthesis and properties of star-shaped naphthalimide-triphenylamine based compound. *Polymer chemistry and technology : proceedings of scientific conference Chemistry and Chemical Technology*, 2014, p. 339–342.
6. Gudeika, D.; Grazulevicius, J. V.; Buika, G.; Vedegyte, J. Synthesis and properties of polymers containing perylene diimide moieties. *Polymer chemistry and technology : proceedings of scientific conference Chemistry and Chemical Technology*, 2012, p. 5–9.
7. Gudeika, D.; Gražulevičius, J. V.; Lygaitis, R. Differently substituted derivatives of 1,8-naphthalene imide. *Polymer Chemistry and Technology : proceedings of scientific conference Chemistry and Chemical Technology*, 2011, p. 34–36.

ACKNOWLEDGEMENTS

I am grateful to many people who have been very helpful to me. Primarily, foremost gratitude goes to my supervisor prof. habil. dr. Juozas Vidas Gražulevičius for giving me the opportunity to do the PhD.

Thanks to dr. R. Lygaitis, prof. A. Žemaitaitis, prof. S. Grigalevičius, prof. G. Buika, prof. J. Liesienė, dr. T. Malinauskas, dr. S. Urnikaitė, prof. V. Getautis, dr. A. Tomkevičienė, dr. A. Dabulienė, dr. R. R. Reghu and dr. J. Keruckas (KTU), prof. W. Dehaen (Katholieke Universiteit Leuven) for their help with the teaching assignments.

Dr. V. Gaidelis and dr. V. Jankauskas (Vilnius University), dr. D. Volyniuk (KTU) are thanked for the measurements of ionization potentials and charge carrier mobilities.

Prof. S. A. Juršėnas and dr. A. Miasojedovas (VU) are sincerely thanked for the measurements of fluorescence quantum efficiencies.

Dr. P. Data (Silesian University of Technology) are thanked for electrochemical measurements.

Dr. G. Sini (University of Cergy-Pontoise, France) is thanked for computational quantum mechanical modelings and exhaustive interpretations of theoretical results.

Dr. J. Simokaitienė, E. Stanislovaitytė, E. Valančienė and dr. L. Pečiulytė (KTU), dr. A. Šakalytė (Departament d'Enginyeria Química, Universitat Rovira i Virgili) are sincerely thanked for DSC and TGA measurements.

Dr. M. Krenevičienė (VU), dr. B. Barvainienė, dr. I. M. Liutvinienė, dr. A. Pukalskas, A. Ivanauskaitė, A. Bučinskas and G. Bagdžiūnas (KTU) are acknowledged for ^1H NMR, ^{13}C NMR and IR spectroscopy, X-ray structure analysis and elemental analysis.

I am thankful to all faculties of my department for providing me a healthy atmosphere. I am grateful to all of them.

I wish to express my deepest thanks to my family members, Jūratė, Vakarė, Deimantė, mother, father, sister, grandmothers and grandfather for their love and support.

CURRICULUM VITAE

Name, Surname Dalius Gudeika
E-mail dalius.gudeika@gmail.com

Education:

2010–2014 m. Kaunas University of Technology (KTU), Faculty of Chemical Technology, Department of Polymer Chemistry and Technology, Materials engineering.
2008–2010 m. Kaunas University of Technology (KTU), Faculty of Chemical Technology, Department of Organic Technology, now (Department of Polymer Chemistry and Technology), Master of Chemical Technology Engineering.
2004–2008 m. Kaunas University of Technology (KTU), Faculty of Chemical Technology, Department of Organic Technology, now (Department of Polymer Chemistry and Technology), Bachelor of Applied Chemistry.

Experience:

2010 m. – now Kaunas University of Technology (KTU), Faculty of Chemical Technology, Department of Polymer Chemistry and Technology, project junior researcher.

Social activities:

Kaunas University of Technology (KTU), the folk art ensemble of „Nemunas”.

Fields of interest:

Synthesis, analysis and application of new organic semiconductors.